Optimization of Microbiologically Induced Calcium Carbonate Precipitation (MICP) for Biocementation: Influence of Process Parameters and Particle Size

Vom Fachbereich Maschinenbau und Verfahrenstechnik der Rheinland-Pfälzischen Technischen Universität Kaiserslautern Landau zur Erlangung des akademischen Grades

Doktor-Ingenieur (Dr.-Ing.)

genehmigte

Dissertation

vorgelegt von

Herr

M. Sc. Niklas Julian Erdmann

aus Köln

Dekan:	Prof. Dr. Roland Ulber
Prüfungsvorsitzender:	Prof. Dr.-Ing. Eberhard Kerscher
Berichterstatter:	Prof. Dr. Roland Ulber
	Prof. Dr.-Ing. Kristin de Payrebrune
Datum der mündlichen Prüfung:	16.06.2025

Kaiserslautern, 2025

D 386

Abstract

Microbiologically induced calcium carbonate precipitation (MICP) is an emerging technology with applications in geotechnical engineering and construction. This dissertation investigates the ureolytic MICP process, focusing on optimizing its efficiency and applicability for biocementation of granular materials such as sand. The study systematically examines key influencing factors, biomass concentration, temperature, the composition of the cementation solution and particle size distribution. Experiments were conducted using the ureolytic bacterium *Sporosarcina pasteurii* to induce calcium carbonate precipitation under controlled conditions. The research explores the kinetics of ureolysis and its impact on the efficiency of calcium carbonate precipitation. A particular focus is placed on the influence of sand particle size on the mechanical properties and pore structure of MICP-treated sand. Variations in particle size affect the distribution and bonding of calcium carbonate, impacting overall compressive strength and durability. Following this, the study employs response surface methodology (RSM) to optimize compressive strength by systematically varying and analyzing multiple parameters to enhance biocementation outcomes.

Despite the advantages of MICP as a sustainable alternative to conventional cement-based materials, challenges remain. The production of ammonium as a by-product and the energy-intensive synthesis of urea present environmental concerns that require further optimization. This work contributes to a deeper understanding of MICP and provides a framework for improving its efficiency and scalability in construction and soil stabilization applications. The findings highlight the potential of MICP to enhance the durability of built environments while identifying key areas for future research in microbial mineralization processes.

Kurzzusammenfassung

Die mikrobiologisch induzierte Calciumcarbonatfällung (MICP) ist eine aufkommende Technologie mit Anwendungen im geotechnischen Ingenieurwesen und Bauwesen. Die vorliegende Dissertation untersucht den ureolytischen MICP-Prozess mit dem Fokus der Effizienz-Optimierung und Anwendbarkeit für die Biozementierung von mineralischer Partikel wie Sand. Die Studie untersucht systematisch die wichtigsten Einflussfaktoren, wie Biomassekonzentration, Temperatur, die Zusammensetzung der Calcinierungslösung (Harnstoff, Calcium) und die Partikelgrößenverteilung des Sandes. Der ureolytische Mikroorganismus *Sporosarcina pasteurii* wurde genutzt, um Calciumcarbonat unter kontrollierten Bedingungen zu fällen. Die Forschung untersucht die Kinetik der Ureolyse und deren Einfluss auf die Effizienz der Calciumcarbonat-Präzipitation. Ein Schwerpunkt liegt auf dem Einfluss der Partikelgröße des Sandes auf die mechanischen Eigenschaften und die Porenstruktur von MICP-behandeltem Sand. Eine Verringerung in der Partikelgröße beeinflusst die Verteilung und Bindung von Calciumcarbonat, was sich positiv auf die Druckfestigkeit auswirkt. Im Anschluss daran wird die Methode der Antwortflächenmethodik (RSM) eingesetzt, um die Druckfestigkeit durch systematische Variation und Analyse mehrerer Parameter zu optimieren, um die Ergebnisse der Biozementierung zu verbessern.

Trotz der Vorteile von MICP als nachhaltige Alternative zu herkömmlichen zementbasierten Materialien bestehen weiterhin große Herausforderungen für die Technologie. Die Produktion von Ammonium als Nebenprodukt und die energieintensive Synthese von Harnstoff stellen Umweltbelastungen dar, die weiterer Optimierung bedürfen. Diese Arbeit trägt zu einem tieferen Verständnis von MICP bei und bietet einen Rahmen für die Verbesserung seiner Effizienz und Skalierbarkeit in Bau- und Bodenstabilisierungsanwendungen. Die Ergebnisse zeigen das Potenzial der MICP zur Verbesserung der Haltbarkeit bebauter Umgebungen auf und identifizieren zentrale Bereiche für zukünftige Forschungen in mikrobiologisch induzierten Mineralisierungsprozessen.

List of Publications

This list contains publications that are part of this thesis. Publications that were not within scope of this thesis can be found in section VIII-2

Peer-reviewed:

N. Erdmann, K. Aldabbousi, D. Strieth (2025)
Influencing factors on ureolytic microbiologically induced calcium carbonate precipitation for biocementation, *Discover Applied Sciences 7, 696*

N. Erdmann, S. Schaefer, T. Simon, A. Becker, U. Bröckel, D. Strieth (2024) MICP treated sand: Insights into the impact of particle size on mechanical parameters and pore network after biocementation, *Discover Materials,* Volume 4, Article Number 45

N. Erdmann, S. Schaefer, T. Simon, A. Becker, U. Bröckel, D. Strieth (2024) Optimizing compressive strength of sand treated with MICP using response surface methodology, *SN Applied Sciences* 4, 282

N. Erdmann, D. Strieth (2023) Influencing factors on ureolytic microbiologically induced calcium carbonate precipitation for biocementation, *World Journal of Microbiology and Biotechnology* Volume 39, Article 61

N. Erdmann, S. Schaefer, T. Simon, A. Becker, U. Bröckel, D. Strieth (2022) *Sporosarcina pasteurii* can be used to print a layer of calcium carbonate, *Engineering in Life Sciences 22(12):760-768*

Table of contents

I General Introduction

1 Challenges of Portland Cement

The construction industry is one of the most resource-intensive sectors globally, with Portland cement being the primary binding material [1] for concrete, the most commonly used construction material [2]. Despite its widespread use, Portland cement presents several significant challenges, particularly in terms of environmental impact, resource consumption, and long-term durability.

One of the most critical challenges associated with Portland cement is its environmental impact. Cement production accounts for approximately 8 % of global CO_2 emissions [3], making it one of the largest industrial contributors to climate change. The manufacturing process involves the calcination of limestone ($CaCO_3$) at high temperatures (~1450 °C), which releases large amounts of CO_2 [4]. Additionally, fossil fuels are heavily used to achieve the necessary heat levels, further exacerbating emissions. These environmental concerns have driven the search for alternative materials and processes that can reduce the construction industry's carbon footprint.

Portland cement production is not only highly energy-intensive, but requires substantial amounts of raw materials, including limestone, clay, and gypsum. The mining and transportation of these materials contribute to environmental degradation and resource depletion [5]. Additionally, as demand for cement increases worldwide, especially in developing economies [5], concerns regarding the long-term availability of high-quality raw materials are growing. Reducing reliance on traditional cement-based construction materials is therefore a key priority in sustainable development.

While concrete is valued for its strength and versatility, its long-term durability remains a concern. Over time, concrete structures are prone to cracking due to mechanical stress, shrinkage, thermal expansion, and chemical attack. Cracking impairs the functionality of concrete, accelerates its degradation, and shortens its service life, thus further reducing its sustainability [6]. Autogenous crack healing, an intrinsic mechanism in cement-based materials, can contribute to the partial or complete self-healing of cracks. In this process, unhydrated cement grains continue

to hydrate through chemical processes, resulting in the formation of calcium carbonate, the main component of cement. However, autogenous crack healing is limited, which is why various methods have been developed to support crack healing [7].

Beyond concrete structures, soil stabilization presents another significant challenge in construction. Weak and loose soils pose risks to the stability of foundations, roads, and embankments, while also increasing susceptibility to soil erosion [8, 9]. Traditional soil stabilization methods based on calcium include lime and cement are considered costly and not environmental friendly due to the CO_2 emissions [10–12]. Nontraditional stabilizers include salts, acids and enzymes [13, 11]. But these nontraditional approaches often come with environmental drawbacks, including soil and groundwater contamination due to the leaching of chemical additives.

Given the challenges associated with Portland cement and conventional soil stabilization methods, researchers and engineers are increasingly exploring sustainable alternatives that offer both environmental benefits and enhanced material performance. One promising biotechnological approach is Microbiologically Induced Calcium Carbonate Precipitation (MICP), a natural process that utilizes microbial activity to induce the precipitation of calcium carbonate ($CaCO_3$). This innovative technique has garnered significant attention as a potential solution for reducing the carbon footprint of construction materials, enhancing the durability of concrete, and providing an eco-friendly method for soil stabilization and erosion protection. By binding soil particles and increasing cohesion, MICP not only improves load-bearing capacity but also minimizes the risk of surface runoff and sediment displacement, making it an effective tool for sustainable land management.

2 Microbiologically Induced Calcium Carbonate Precipitation (MICP)

MICP is a biomineralization process wherein microorganisms induce the precipitation of calcium carbonate ($CaCO_3$), leading to the binding of granular materials. MICP can occur via both autotrophic (photosynthesis, non-methylotrophic methanogenesis) and heterotrophic metabolic pathways (sulfur cycle, nitrogen cycle) [14–16]. The most extensively studied mechanism is ureolysis (nitrogen cycle), which is based on

ureolytic microorganisms like *Sporosarcina pasteurii*, which hydrolyze urea into ammonia and carbonate, increasing local pH and facilitating $CaCO_3$ precipitation.

In ureolytic MICP, one mole of urea is catalytically hydrolyzed intracellularly by urease (EC 3.5.1.5) to one mole of ammonia and one mole of carbamic acid (Eq. 1) [17].

$$CO(NH_2)_2 + H_2O \rightarrow NH_2COOH + NH_3 \quad \text{(Eq. 1)}$$

$$NH_2COOH + H_2O \rightarrow H_2CO_3 + NH_3 \quad \text{(Eq. 2)}$$

$$2NH_3 + 2H_2O \leftrightarrow 2NH^{4+} + 2OH^- \quad \text{(Eq. 3)}$$

$$2OH^- + H_2CO_3 \leftrightarrow CO_3^{2-} + 2H_2O \quad \text{(Eq. 4)}$$

$$Ca^{2+} + CO_3^{2-} \rightarrow CaCO_3 \quad \text{(Eq. 5)}$$

$$CO(NH_2)_2 + 2\,H_2O + Ca^{2+} \rightarrow 2NH_4^+ + CaCO_3 \quad \text{(Eq. 6)}$$

The calcium carbonate precipitates as crystals. These crystals can fill gaps between particles, binding and cementing the materials together (Figure 1). The carbamic acid is then spontaneously hydrolyzed to ammonia and carbonic acid (Eq. 2). The ammonia formed diffuses out and dissociates outside the cell, forming hydroxide ions (Eq. 3-4) [18].

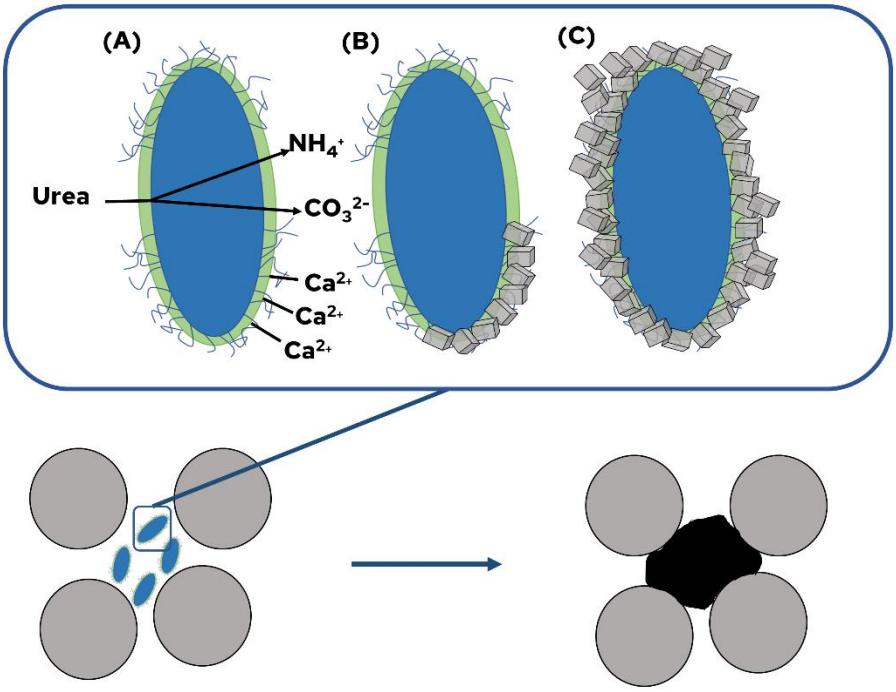

Figure 1: Process during the ureolytic calcium carbonate precipitation that leads to the precipitation of calcium carbonate (black) between mineral particles (grey circles). (A) Urea is enzymatically degraded to ammonium and carbonate ions. (B) Calcium carbonate crystals begin to form in proximity of the cells. (C) The bacteria eventually encapsulate themselves in calcium carbonate crystals. Modified from Muynck et al. [6].

By increasing the pH value, the position of the lime-carbonic acid equilibrium is shifted towards carbonate ions, leading to calcium carbonate precipitation outside the cells (Eq. 5).

These bridges between particles ensure that the material is consolidated, which increases mechanical parameters such as compressive strength and shear resistance [19]. **Chapter 2** describes this process in more detail while highlighting the key factors influencing calcium carbonate precipitation efficiency, such as bacterial strain selection, nutrient availability, pH, temperature, and calcium source.

The possibility of precipitating calcium carbonate in several different matrixes like existing construction material, soil and sand results in various areas of application for MICP in the construction industry. The ability to precipitate calcium carbonate in various matrices, such as existing construction materials, soil, and sand, opens numerous application areas for MICP in the construction industry. These areas are discussed in the following chapter. It is important to note that precipitating other bivalent ions, such as lead or copper, as carbonates is possible. This process offers possibilities of various other applications, particularly for treating heavy metal-contaminated soil and water. However, these applications are beyond the scope of this thesis.

3 Applications for MICP in construction industry

Various approaches to apply MICP in construction have been researched. As described in the previous chapter, these applications rely on the ability of calcium carbonate crystals from MICP to act as a cementing agent like regular Portland cement. The main application in scope of this thesis is the consolidation of loose mineral particles (i.e. sand) to produce novel construction materials and for soil stabilization. However, some of the results give us a better understanding of the MICP process and can help to optimize processes involving MICP like strengthening of already existing construction materials for example sandstone or concrete. The main applications of MICP in the construction industry are:

- Improving the mechanical properties of concrete. At the beginning of the millennium, Ramachandran et al. demonstrated that the compressive strength of concrete cubes could be increased from 55±1 to 65±1 MPa by adding *S. pasteurii* [20]. Since then, various studies have shown the positive impact of

ureolytic MICP on concrete [21–23]. This improvement can be attributed to the reduction of porosity and permeability in the concrete through calcium carbonate precipitation, which reduces weak points and makes it more difficult for corrosive agents to penetrate [24, 25].

- External treatment of cracks using MICP, known as microbially enhanced crack remediation, was described by Ramachandran et al. [20] and Bang et al. [26]. In this process, a suspension containing ureolytic microorganisms is applied to the cracks, followed by a solution containing urea and a calcium source. Through this method, Jongvivatsukul et al. increased the compressive strength of cracked mortar specimens by 43 % after 20 days of treatment with ureolytic MICP [27]. This application seems to be limited in depth, as the high pH values in the concrete matrix (11~12) can hinder bacterial activity, especially in deeper cracks [28].
- Self-healing concrete can be achieved by mixing alkali-tolerant bacteria directly into the concrete matrix, either as spores or encapsulated. Additionally, urea, a calcium source, and a carbon source can be mixed into the mortar or encapsulated. Once cracks form in the concrete and water encounters the bacteria and nutrients, the MICP process forms calcium carbonate and seals the cracks [29]. Self-healing concrete was one of the first MICP products brought to market maturity by Evonik through the Wallcraft project and has been marketed under the name "SITREN® Self-Heal" since 2021 [30] and by Basilisk under the name "Self-Healing Repair Mortar MR3" [31].
- The production of novel construction materials based on MICP is an approach aimed at substituting concrete and other construction materials in certain areas. These materials are called “bio-bricks” [28], BioZEment [4], or biocement [32, 33]. The production process is like the surface treatment for crack remediation of concrete. It involves a suspension of ureolytic bacteria and a solution containing at least urea and a calcium source. These components are applied to a matrix of mineral particles and possibly additional components like fly ash, silica fume, and rice husk ash [23, 34–36]. This process is the main field of application for the research conducted in this

thesis. Details of the production process of bio-bricks and possible influencing factors are described in **Chapter 2**.

Soil stabilization, a critical aspect of construction, is essential for ensuring the structural integrity and longevity of infrastructure projects. Soil stabilization encompasses various applications, each facing its own challenges, presenting an opportunity for MICP to provide an innovative technological solution. Traditional methods of soil stabilization, such as compaction, preloading, vibration, and chemical consolidation, while effective, are resource-intensive and contribute to environmental pollution. The search for more environmentally friendly and cost-effective alternatives has led to increased research in the field of MICP. There are several areas of soil stabilization where MICP shows promising applications:

- Improving the bearing capacity of soil is crucial for infrastructure projects, such as road pavement subgrades. The bearing capacity is closely linked to the unconfined compressive strength (UCS) of soils. MICP treatment has been shown to enhance both the UCS and the bearing capacity of soil. For instance, Meng et al. increased the bearing capacity of soil in the Ulan Buh desert in China to a maximum of 459.9 kPa within three days of MICP treatment [37]. Similarly, Kulkarni et al. reported a 2.95 to 5.8-fold increase in the bearing capacity of sand treated with MICP [38]. Although field studies on soil strengthening are still limited [39], MICP offers a promising solution for soil stabilization by increasing bearing capacity.
- Soil erosion by water and wind is a global environmental threat that leads to land loss, water quality degradation, and sedimentation. MICP can be applied to bind the upper layers of sand and soil, increasing the forces required to detach particles. Field tests in the Chinese desert by Meng et al. demonstrated that after 90 and 180 days, the wind erosion depth of MICP-treated sand was only 4.5 and 5.1 % of that of untreated sand, respectively [37]. Nasir et al. conducted wind tunnel experiments that showed a sixfold decrease in soil erosion 28 days after MICP treatment compared to control soil [40]. Liu et al. demonstrated the feasibility of using MICP to treat clay and reduce erosion during simulated rainfall, observing a decrease in the erosion rate from 16 g/min in untreated clay to just 1 g/min in MICP-treated clay [41].

- Soil liquefaction, typically caused by earthquakes or sudden stress changes, poses a significant risk to geotechnical structures. It occurs in loose, sandy soils below the water table when seismic waves exert cyclic shear forces, increasing pore water pressure and decreasing shear strength [42]. This risk is particularly relevant for areas like the Fraser River region in Canada, which is prone to earthquakes and has deposits of loose Fraser River sand [43]. Riveros et al. conducted experiments on Fraser sand treated with a solution of 0.5 M urea and 0.75 M calcium chloride. They demonstrated a 67 % increase in liquefaction resistance, measured as cyclic resistance in shear tests [43].

4 Aim of this study

Ureolytic MICP has proven to be particularly promising in research due to its simple handling and fast process [44]. Despite the growing research interest and the technology's potential, MICP faces two major challenges that need to be addressed before it can become a serious alternative to conventional methodologies.

Firstly, ureolytic MICP will always produce the toxic by-product ammonium. This by-product may either leach from biosandstone and other artificial construction materials based on MICP or form directly in soil during soil stabilization treatment, thus being present in the environment. The strength of building materials and soils stabilized with MICP correlates with the amount of calcium carbonate in the final product [45–47]. The stronger the material, the more calcium carbonate must be precipitated, leading to increased ammonium production (eq. 1.2).

The second challenge is the energy demand of urea production. Many studies claim that MICP is more energy-efficient compared to Portland cement, which requires significant energy for clinker burning. For instance, Myhr et al. state that the global warming potential of one ton of BioZEment is 70 - 83 % lower than that of conventional concrete [48]. However, the synthetic urea used in most MICP studies is produced via the Haber-Bosch process, which is highly energy-intensive, producing 890 kg CO_2 for each ton of urea in Europe [49]. This makes it crucial to achieve high efficiency in MICP, meaning the highest possible strength per ton of urea/calcium source/bacteria.

To achieve higher efficiency in MICP, it is necessary to increase our understanding and optimize the MICP process. **Chapter 2** provides a detailed overview of the

biological, chemical, and physical parameters that influence the efficiency of MICP. Understanding these parameters can help identify areas for process improvement. **Chapters 3 and 4** further investigate some of these parameters. **Chapter 3** explores the reaction kinetics of MICP based on parameters such as pH, temperature, cell density, and the amount of calcium source. Most MICP processes require multiple applications of cell suspension and calcination solution. The results should help improve resource efficiency concerning the incubation time between these applications, balancing feasible production times and high conversion rates of urea/calcium to calcium carbonate. **Chapter 4** investigates the impact of sand particle size to determine if waste sand from a local quarry near Kaiserslautern could be a suitable source for MICP. **Chapter 5** optimizes the MICP of industrial sand using a design of experiments approach. Finally**, Chapter 6** demonstrates an alternative approach to the established method of percolation for MICP, exploring the possibility of applying MICP in a process similar to powder-bed 3D printing as a proof of concept.

5 References

1. imarc group (2024) Cement Market Size, Share, Trends and Forecast by Type, End Use, and Region, 2025-2033. https://www.imarcgroup.com/cement-manufacturing-plant?utm_source=chatgpt.com. Accessed 16 Feb 2025
2. Gartner EM, Macphee DE (2011) A physico-chemical basis for novel cementitious binders. Cement and Concrete Research 41:736–749. https://doi.org/10.1016/j.cemconres.2011.03.006
3. Lippiatt N, Ling T-C, Pan S-Y (2020) Towards carbon-neutral construction materials: Carbonation of cement-based materials and the future perspective. Journal of Building Engineering 28:101062. https://doi.org/10.1016/j.jobe.2019.101062
4. Røyne A, Phua YJ, Balzer Le S et al. (2019) Towards a low CO2 emission building material employing bacterial metabolism (1/2): The bacterial system and prototype production. PLoS ONE 14:e0212990. https://doi.org/10.1371/journal.pone.0212990
5. Ige OE, Olanrewaju OA, Duffy KJ et al. (2022) Environmental Impact Analysis of Portland Cement (CEM1) Using the Midpoint Method. Energies 15:2708. https://doi.org/10.3390/en15072708
6. Belie N de, Gruyaert E, Al-Tabbaa A et al. (2018) A Review of Self-Healing Concrete for Damage Management of Structures. Adv Materials Inter 5. https://doi.org/10.1002/admi.201800074
7. Rooij M de, van Tittelboom K, Belie N de et al. (2013) Self-Healing Phenomena in Cement-Based Materials, vol 11. Springer Netherlands, Dordrecht
8. Moghal AAB, Vydehi KV (2021) State-of-the-art review on efficacy of xanthan gum and guar gum inclusion on the engineering behavior of soils. Innov Infrastruct Solut 6. https://doi.org/10.1007/s41062-021-00462-8
9. Wang Y, Sun X, Miao L et al. (2024) State-of-the-art review of soil erosion control by MICP and EICP techniques: Problems, applications, and prospects. Sci Total Environ 912:169016. https://doi.org/10.1016/j.scitotenv.2023.169016

10. Pooni J, Giustozzi F, Robert D et al. (2019) Durability of enzyme stabilized expansive soil in road pavements subjected to moisture degradation. Transportation Geotechnics 21:100255. https://doi.org/10.1016/j.trgeo.2019.100255
11. Behnood A (2018) Soil and clay stabilization with calcium- and non-calcium-based additives: A state-of-the-art review of challenges, approaches and techniques. Transportation Geotechnics 17:14–32. https://doi.org/10.1016/j.trgeo.2018.08.002
12. Imbabi MS, Carrigan C, McKenna S (2012) Trends and developments in green cement and concrete technology. International Journal of Sustainable Built Environment 1:194–216. https://doi.org/10.1016/j.ijsbe.2013.05.001
13. Tingle JS, Newman JK, Larson SL et al. (2007) Stabilization Mechanisms of Nontraditional Additives. Transportation Research Record: Journal of the Transportation Research Board 1989-2:59–67. https://doi.org/10.3141/1989-49
14. Castanier S, Le Métayer-Levrel G, Perthuisot J-P (1999) Ca-carbonates precipitation and limestone genesis — the microbiogeologist point of view. Sedimentary Geology 126:9–23. https://doi.org/10.1016/s0037-0738(99)00028-7
15. Mondal S, Ghosh A (2019) Review on microbial induced calcite precipitation mechanisms leading to bacterial selection for microbial concrete. Construction and Building Materials 225:67–75. https://doi.org/10.1016/j.conbuildmat.2019.07.122
16. Castanier S, Le Métayer-Levrel G, Perthuisot J-P (2000) Bacterial Roles in the Precipitation of Carbonate Minerals. In: Riding RE, Awramik SM (eds) Microbial Sediments, vol 5. Springer Berlin Heidelberg, Berlin, Heidelberg, pp 32–39
17. Anbu P, Kang C-H, Shin Y-J et al. (2016) Formations of calcium carbonate minerals by bacteria and its multiple applications. Springerplus 5:250. https://doi.org/10.1186/s40064-016-1869-2
18. Jahns T (1996) Ammonium/urea-dependent generation of a proton electrochemical potential and synthesis of ATP in Bacillus pasteurii. J Bacteriol 178:403–409. https://doi.org/10.1128/jb.178.2.403-409.1996

19. Fu T, Saracho AC, Haigh SK (2023) Microbially induced carbonate precipitation (MICP) for soil strengthening: A comprehensive review. Biogeotechnics 1:100002. https://doi.org/10.1016/j.bgtech.2023.100002
20. SK Ramachandran (2001) Ramachandran SK, Ramakrishnan V, Bang SS (2001) Remediation of concrete using micro-organisms. ACI Mater J 98:3–9. ACI Mater J 98:3
21. Al-Salloum Y, Abbas H, Sheikh QI et al. (2017) Effect of some biotic factors on microbially-induced calcite precipitation in cement mortar. Saudi J Biol Sci 24:286–294. https://doi.org/10.1016/j.sjbs.2016.01.016
22. Achal V, Pan X, Özyurt N (2011) Improved strength and durability of fly ash-amended concrete by microbial calcite precipitation. Ecological Engineering 37:554–559. https://doi.org/10.1016/j.ecoleng.2010.11.009
23. Chahal N, Siddique R, Rajor A (2012) Influence of bacteria on the compressive strength, water absorption and rapid chloride permeability of fly ash concrete. Construction and Building Materials 28:351–356. https://doi.org/10.1016/j.conbuildmat.2011.07.042
24. Muynck W de, Cox K, Belie N de et al. (2008) Bacterial carbonate precipitation as an alternative surface treatment for concrete. Construction and Building Materials 22:875–885. https://doi.org/10.1016/j.conbuildmat.2006.12.011
25. Muynck W de, Debrouwer D, Belie N de et al. (2008) Bacterial carbonate precipitation improves the durability of cementitious materials. Cement and Concrete Research 38:1005–1014. https://doi.org/10.1016/j.cemconres.2008.03.005
26. Bang SS, Galinat JK, Ramakrishnan V (2001) Calcite precipitation induced by polyurethane-immobilized Bacillus pasteurii. Enzyme and Microbial Technology 28:404–409. https://doi.org/10.1016/s0141-0229(00)00348-3
27. Jongvivatsakul P, Janprasit K, Nuaklong P et al. (2019) Investigation of the crack healing performance in mortar using microbially induced calcium carbonate precipitation (MICP) method. Construction and Building Materials 212:737–744. https://doi.org/10.1016/j.conbuildmat.2019.04.035
28. Zhang K, Tang C-S, Jiang N et al. (2023) Microbial-induced carbonate precipitation (MICP) technology: a review on the fundamentals and engineering

applications. Environ Earth Sci 82:229. https://doi.org/10.1007/s12665-023-10899-y
29. Lee YS, Park W (2018) Current challenges and future directions for bacterial self-healing concrete. Appl Microbiol Biotechnol 102:3059–3070. https://doi.org/10.1007/s00253-018-8830-y
30. Evonik Industries AG (2021) Grauer Star - Wie Beton nachhaltiger wird. ELEMENTS Forschen. Wissen. Zukunft 2021
31. Basilisk Products. https://basiliskconcrete.com/en/products/. Accessed 2.2.25
32. Whiffin VS (2004) Microbial CaCO3 Precipitation for the Production of Biocement. PhD Thesis, Murdoch University
33. Whiffin VS, van Paassen LA, Harkes MP (2007) Microbial Carbonate Precipitation as a Soil Improvement Technique. Geomicrobiology Journal 24:417–423. https://doi.org/10.1080/01490450701436505
34. Siddique R, Singh K, Kunal et al. (2016) Properties of bacterial rice husk ash concrete. Construction and Building Materials 121:112–119. https://doi.org/10.1016/j.conbuildmat.2016.05.146
35. Chahal N, Siddique R (2013) Permeation properties of concrete made with fly ash and silica fume: Influence of ureolytic bacteria. Construction and Building Materials 49:161–174. https://doi.org/10.1016/j.conbuildmat.2013.08.023
36. Li P, Liu C, Zhou W (2015) Influence of Bacterial Carbonate Precipitation on the Compressive Strength and Water Absorption of Fly Ash Concrete. In: Proceedings of the 3rd International Conference on Mechatronics, Robotics and Automation. Atlantis PressParis, France
37. Meng H, Gao Y, He J et al. (2021) Microbially induced carbonate precipitation for wind erosion control of desert soil: Field-scale tests. Geoderma 383:114723. https://doi.org/10.1016/J.GEODERMA.2020.114723
38. Kulkarni PB, Nemade PD, Chavan R et al. (2021) Development of Single-Phase Microbial Cementation Method and to Investigate its Efficacy on Bearing Capacity, UCS, and Permeability of Sandy Soils. J Eng Technol Sci 53:210602. https://doi.org/10.5614/j.eng.technol.sci.2021.53.6.2
39. Portugal CRMe, Fonyo C, Machado CC et al. (2020) Microbiologically Induced Calcite Precipitation biocementation, green alternative for roads – is this the

breakthrough? A critical review. Journal of Cleaner Production 262:121372. https://doi.org/10.1016/j.jclepro.2020.121372

40. Nasir SS, Mohammadi Torkashvand A, Khakipour N (2022) An experimental investigation of bacteria-producing calcareous cement in wind erosion prevention. Int J Environ Sci Technol 19:2107–2118. https://doi.org/10.1007/s13762-021-03207-3
41. Liu B, Xie Y-H, Tang C-S et al. (2021) Bio-mediated method for improving surface erosion resistance of clayey soils. Engineering Geology 293:106295. https://doi.org/10.1016/j.enggeo.2021.106295
42. Lirer S, Mele L (2019) On the apparent viscosity of granular soils during liquefaction tests. Bull Earthquake Eng 17:5809–5824. https://doi.org/10.1007/s10518-019-00706-0
43. Riveros GA, Sadrekarimi A (2020) Liquefaction resistance of Fraser River sand improved by a microbially-induced cementation. Soil Dynamics and Earthquake Engineering 131:106034. https://doi.org/10.1016/j.soildyn.2020.106034
44. Dhami NK (2013) Biomineralization of Calcium Carbonate Polymorphs by the Bacterial Strains Isolated from Calcareous Sites. Journal of Microbiology and Biotechnology 23:707–714. https://doi.org/10.4014/jmb.1212.11087
45. Yang D, Xu G, Duan Y (2020) Effect of Particle Size on Mechanical Property of Bio-Treated Sand Foundation. Applied Sciences 10:8294. https://doi.org/10.3390/app10228294
46. Chu J, Ivanov V, Naeimi M et al. (2014) Optimization of calcium-based bioclogging and biocementation of sand. Acta Geotech 9:277–285. https://doi.org/10.1007/s11440-013-0278-8
47. Zhao Q, Li L, Li C et al. (2014) Factors Affecting Improvement of Engineering Properties of MICP-Treated Soil Catalyzed by Bacteria and Urease. Journal of Materials in Civil Engineering, 26(12), 04014094. https://doi.org/10.1061/(ASCE)MT.1943-5533.0001013
48. Myhr A, Røyne F, Brandtsegg AS et al. (2019) Towards a low CO2 emission building material employing bacterial metabolism (2/2): Prospects for global warming potential reduction in the concrete industry. PLoS ONE 14. https://doi.org/10.1371/journal.pone.0208643

49. Brentrup F, Hoxha A, Christensen B (2016) Carbon footprint analysis of mineral fertilizer production in Europe and other world regions. https://irees.de/wp-content/uploads/2020/04/180716_IREES_AP4_Prozessemissionen.pdf. Accessed 15 February 2025

II Influencing factors on ureolytic microbiologically induced calcium carbonate precipitation for biocementation

N. Erdmann[1] D. Strieth[1]

[1]Technical University of Kaiserslautern, Chair of Bioprocess Engineering, Kaiserslautern, Germany

*World Journal of Microbiology and Biotechnol*ogy Volume 39, Article 61 (2023). https://doi.org/10.1007/s11274-022-03499-8

Author Contribution:

N. Erdmann	Project administration, visualization, writing, investigation (Literature review)
D. Strieth	Funding acquisition, supervision, review&editing

Keywords: biocementation, biosandstone, microbiologically induced calcium carbonate precipitation (MICP), ureolytic activity,

1 Abstract

Microbiologically induced calcium carbonate precipitation (MICP) is a technique that has received a lot of attention in the field of geotechnology in the last decade. It has the potential to provide a sustainable and ecological alternative to conventional consolidation of minerals, for example by the use of cement. From a variety of microbiological metabolic pathways that can induce calcium carbonate ($CaCO_3$) precipitation, ureolysis has been established as the most commonly used method. To better understand the mechanisms of MICP and to develop new processes and optimize existing ones based on this understanding, ureolytic MICP is the subject of intensive research. The interplay of biological and civil engineering aspects shows how interdisciplinary research needs to be to advance the potential of this technology. This paper describes and critically discusses, based on current literature, the key influencing factors involved in the cementation of sand by ureolytic MICP. Due to the complexity of MICP, these factors often influence each other, making it essential for researchers from all disciplines to be aware of these factors and its interactions. Furthermore, this paper discusses the opportunities and challenges for future research in this area to provide impetus for studies that can further advance the understanding of MICP.

2 Introduction

With more than 10 km^3 per year, concrete is the most used building material [1]. A main component of concrete is cement (CaO), which is produced from limestone ($CaCO_3$) at high temperatures [2]. During the so-called burning of cement clinker, the temperatures reach about 1,450 °C. The energy required for this process is about 2.6 % of global energy demand [3]. Due to resource limitation and a rethinking of ecological issues, there are efforts worldwide to find alternatives to the use of cement. Microbiologically induced calcium carbonate precipitation (MICP) has become an increasingly important research topic in recent years as a possible technology for the consolidation of sand (see Figure 1).

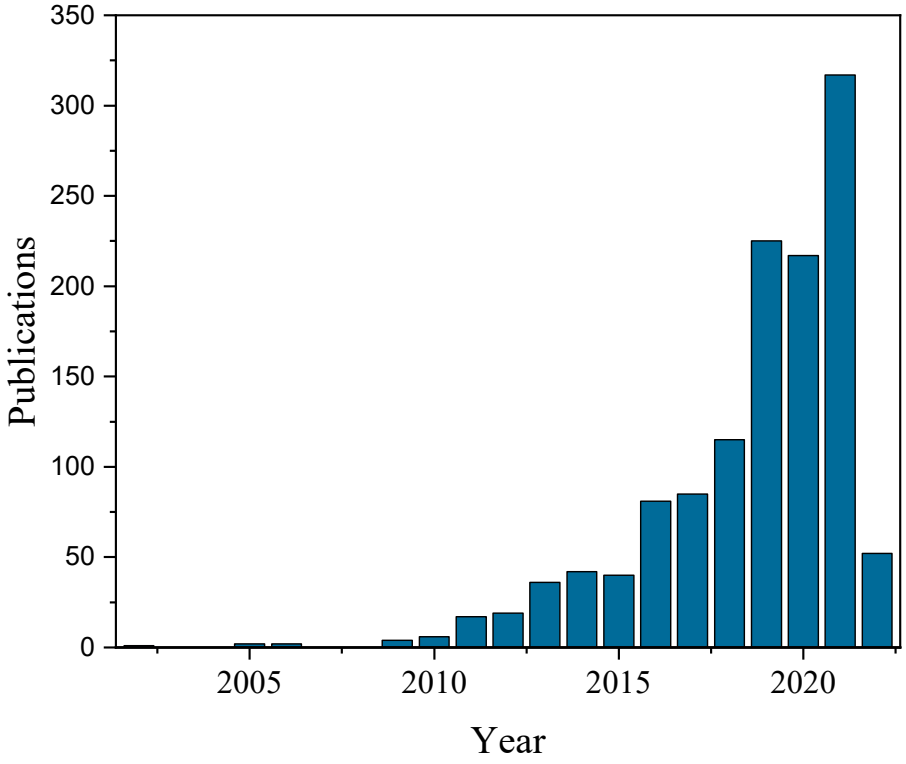

Figure 1: Number of publications per year for the terms "microbi* induced calcium carbonate precipitation", "microbi* induced calcite precipitation" and "microbi* induced carbonate precipitation. The data was collected from Scopus in August 2022.

MICP is a process in which, through the use of microorganisms, carbonate ions (CO_3^{2-}) are formed via various metabolic pathways, which are precipitated as $CaCO_3$ in the presence of calcium ions (Ca^{2+}) (see eq. 1). Precipitation occurs when the ion activity product exceeds the solubility constant of $CaCO_3$, i.e. the saturation coefficient Ω ≥ 1 (see eq. 2) [4].

$$Ca^{2+} + CO_3^{2-} \leftrightarrow CaCO_3 \qquad \text{eq. 1}$$

$$\Omega = [Ca^{2+}][CO_3^{2-}]/K_{S,calcium\ carbonate} \qquad \text{eq. 2}$$

If the precipitation occurs in cavities between mineral particles, they can be connected and strengthened. MICP can occur via both autotrophic and heterotrophic metabolic pathways [5]. Autotrophic photosynthetic organisms (cyanobacteria, microalgae) and heterotrophic organisms that use the nitrogen cycle (ureolytic organisms, nitrate-reducing organisms) have the greatest potential for MICP (see Table 1).

Table 1: Overview of the MICP metabolic pathways that have the greatest potential to consolidate sand.

Metabolic pathway	Strains	Pro	Contra	References
Oxygenic photosynthesis	• *Gloeocapsa sp.* PCC 73106 [19] • *Synechococcus* pevalekii BDHKU 35101 [20]	• Tolerance of most strains to alkaline environment • No toxic by-products • Cheap media for cultivation	• CO_2 limitation in sand • Light dependent • Slow growth rates during phototrophic cultivation	[21, 22]
Ureolysis	• Sporosarcina pasteurii [23, 24] • Bacillus sphaericus [16] • Bacillus cereus[25] • Bacillus megaterium [26]	• Easy to control • Cheap media components • High calcium carbonate precipitation rates • High tolerance of strains to alkaline enviroment	• Toxic ammonia as by-product • Production of urea coupled to CO_2 emissions	[9, 6, 27]
Denitrification	• Castellianelle denitrificans [28] • Pseudomonas denitrificans [29]	• By-products calcium formiate and calcium nitrate are commercial additives for cement • Nitrite ions can inhibit corrosion	• Usage of carriers for alkaline environments necessary	[30]

Due to its advantages such as low-cost cultivation in complex media and easy-to-control metabolism, ureolytic MICP is the most widely used mechanism for MICP [6, 7]. During this mechanism, one mole of urea is catalytically hydrolyzed intracellularly by urease (EC 3.5.1.5) to one mole of ammonia and one mole of carbamic acid (see eq. 3) [8]. The carbamic acid is then spontaneously hydrolyzed to ammonia and carbonic acid (see eq. 4). The ammonia diffuses out of the cell and dissociates, forming hydroxide ions. This raises the pH in the area surrounding the cell, which shifts the carbonic acid balance, resulting in the formation of carbonate ions (see eq. 5,6).

$$CO(NH_2)_2 + H_2O \rightarrow NH_2COOH + NH_3 \quad \text{eq. 3}$$

$$NH_2COOH + H_2O \rightarrow H_2CO_3 + NH_3 \quad \text{eq. 4}$$

$$^{-}2NH_3 + 2H_2O \leftrightarrow 2NH^{4+} + 2OH^{-} \quad \text{eq. 5}$$

$$2OH^{-} + H_2CO_3 \leftrightarrow CO_3^{2-} + 2H_2O \quad \text{eq. 6}$$

Beyond the urea metabolism of the microorganisms, the calcium metabolism also has an influence on the MICP (see Figure 2). Due to an alkaline environment and a high calcium concentration outside the cell, an electrochemical gradient leads to the passive influence of Ca^{2+} with a simultaneous outflow of protons from the cell.

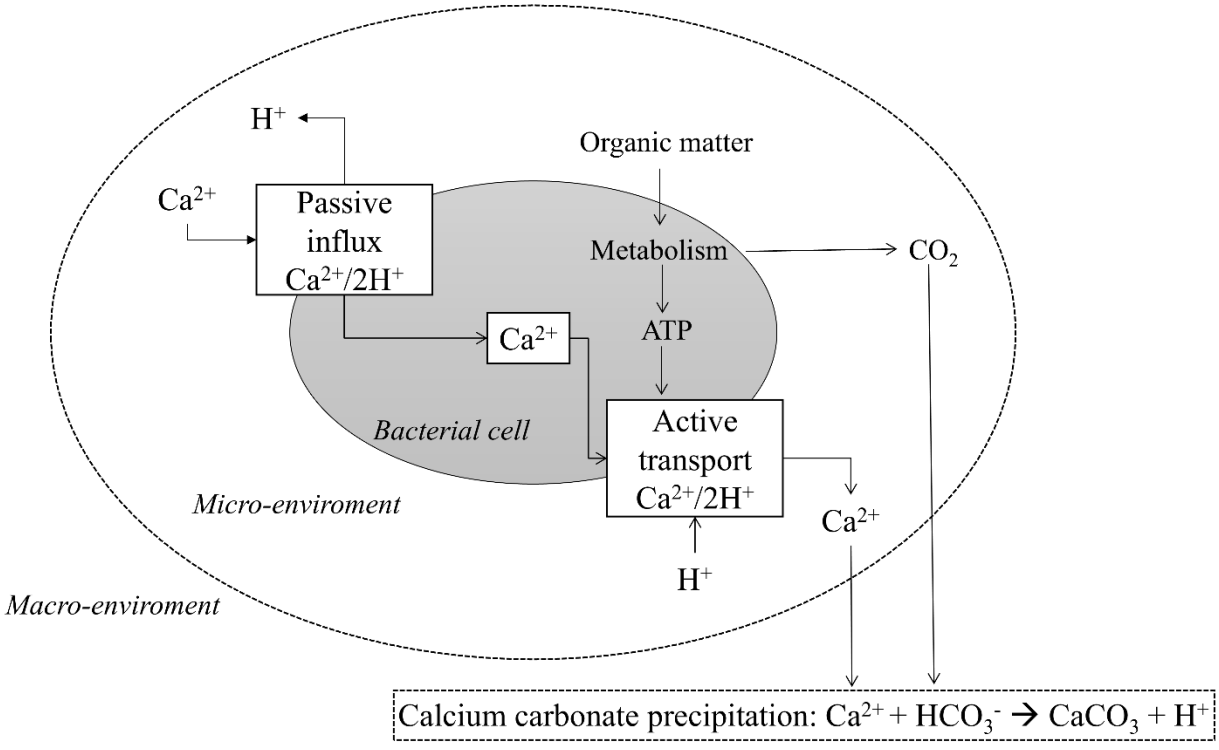

Figure 2: Schematic representation of a proposed calcium metabolic pathway leading to calcium carbonate precipitation modified from Hammes et al. [9].

Due to the decrease in intracellular proton concentration, the internal pH increases. The high calcium concentration can disrupt several bacterial physiological processes like chemotaxis, cell differentiation and membrane transport as well as signaling processes [10, 11]. In order to survive under these circumstances, most bacteria export Ca^{2+} by Ca^{2+} exchangers, Ca^{2+}/H^{+} or Ca^{2+}/Na^{+} antiporters. This process is coupled to an influx of protons and is ATP dependent [10]. As a result of the transport, the concentration of protons in the laminar boundary layer decreases and the concentration of calcium ions increases. A high pH value in combination with high calcium concentration is the optimal basis for $CaCO_3$ precipitation. The creation of the advantageous microenvironment results in the formation of crystals on the cell surface, ensuing in the encapsulation of the cell [6].

Although ureolytic MICP is the subject of intensive research, many relationships concerning the interaction of individual influencing parameters during MICP are not fully understood. Various studies have been able to show that MICP has the potential to improve the strength and water permeability of existing construction materials, such as cement mortar and sandstone [12]. It also shows the potential to repair cracks in construction materials [13, 14] and to produce materials that could be a more sustainable and ecological alternative to conventional building materials [4, 15]. MICP can also be used to improve the properties of soils for example its liquefaction resistance [16] or resilience against wind erosion [17]. Although some of the influencing factors presented in this study have a general impact of MICP regardless of the application some factors specifically apply to the consolidation of loose sand. Most research in this area uses protocols to consolidate sand in cubic or cylindric moulds. During this process a suspension of ureolytic bacteria and a solution containing a calcium salt and urea are fed into the mould and during curing time $CaCO_3$ crystals are formed (see Figure. 3). This review summarizes the current research results regarding biological, chemical and physical influencing factors of the ureolytic MICP with regard to the consolidation of sand and highlights the interaction of these parameters. Furthermore, open research gaps as well as limitations and challenges of the technology are discussed. These findings can give impulses for future research projects in the field of ureolytic MICP.

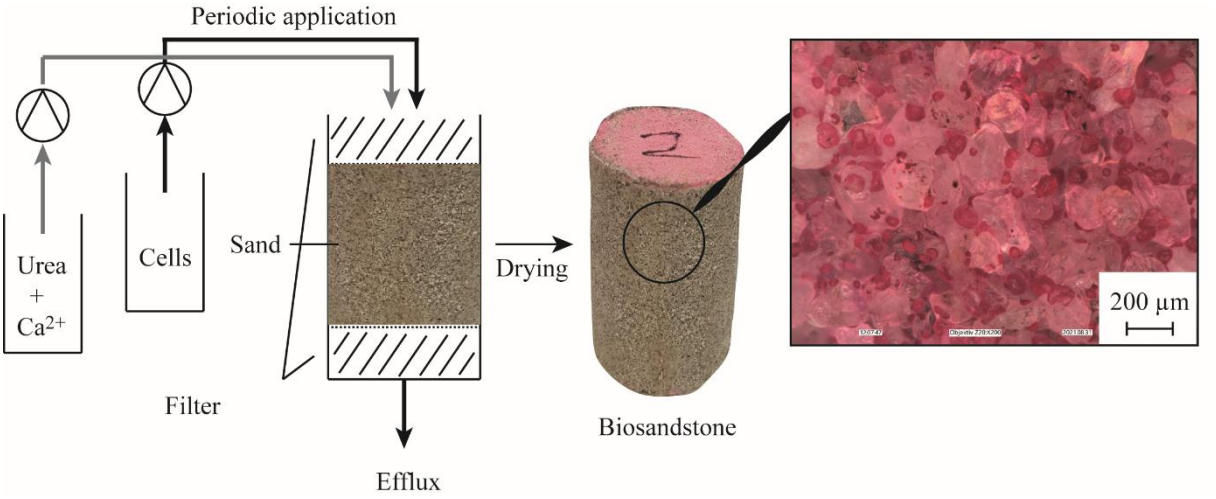

Figure 3: Process for the production of biosandstone modified after Strieth [18]. Right side: Microscopic image of biosandstone after staining calcium carbonate crystals with alizarin red S.

Ureolytic MICP is a process that can be influenced by a large number of parameters. In order to improve the process, a basic understanding of these parameters is necessary. A large number of studies have been carried out to identify influencing factors on ureolytic MICP. For calcination of sand, the following influencing factors can be categorized. (i) bacterial strain, (ii) cultivation parameters (iii) biomass and ureolytic activity, (iv) pH, (v) temperature, (vi) concentration of urea and calcium, (vii) calcium source, (viii) sand properties and (ix) grouting protocol (see Figure 4).

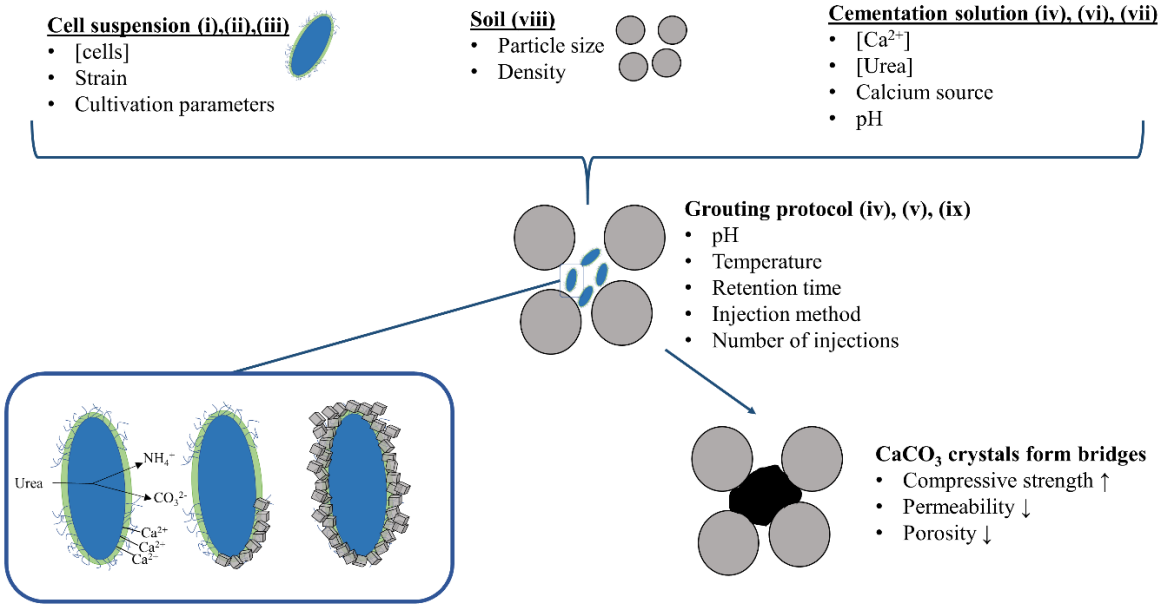

Figure 4: Overview of the influencing parameters during ureolytic MICP for the consolidation of sand. Modified from Muynck [43]

In literature different ureolytic organisms were investigated for their ability to consolidate sand. *Bacillus* and *Sporosarcina* are the most commonly used strains of MICP [31]. In general, the choice of organism has an influence on the ureolytic activity which again impacts the morphology of formed crystals. These factors, in turn, have an influence on the result of consolidation of sand. Therefore, the choice of a suitable organism is of great interest for the MICP process. Regarding ureolytic activity, it should be noted that both the choice of organism and the cell concentration influence ureolytic activity during MICP. The influence of biomass concentration will be considered in a separate chapter. Dhami et al. [7] studied the morphology of formed $CaCO_3$ crystals of different isolates from calcereous sand from Anantapur district, India by SEM, EDX and CLSM. They found that depending on the microorganism, there were differences in the size and structure of the $CaCO_3$ crystals formed (see Table 2). The authors of the study concluded, based on the results, that the morphology and nature of the $CaCO_3$ polymorph are strain-specific.

Table 2: Overview of Calcium carbonate morphology and polymorphs of different ureolytic strains. Data collected from Dhami et al. [32].

Strain	Urease activity in $U \cdot mL^{-1}$	Crystal Size in µm	Calcium carbonate polymorph	Appearance
Bacillus megaterium	690	30-50	Calcite major form Few vaterites	Spherical, oval, rhombohedral, triangular. Smooth and rough surfaces
Bacillus cereus	587	15-40	Calcite Major form Very few vaterites	Needle-like, layer-flake structures, irregular square morphology
Bacillus subtilis	515	10-50	Calcite Major form Very few vaterites	Spherical, ellipsoidal, very smooth
Bacillus thuringiensis	620	2-15	Vaterite major form Few calcite	Round, circular rings, rectangular
Lysinbacillus fusiformis	525	2-10	Pure vaterite	Flaky needle like mesh, very rough surface

In a recent study the morphology of $CaCO_3$ crystals precipitated from locally isolated strains *Curvibacter sp*. SP-1 and *Arthrobacter sp*. MF-2 were compared [33]. For this purpose both strains were cultivated for 50 days in complex medium containing 0.05 M calcium acetate and 0.075 M magnesium acetate. They found an influence of the strain used on the morphology of the crystals. During the cultivation of *Curvibacter sp.* SP-1, mainly dumbbell-shaped crystals were formed within the first days of cultivation, which aggregated into spherical particles during the course of cultivation. *Arthrobacter sp.*MF-2, on the other hand, formed long rod-shaped crystals during the initial phase of cultivation, which also aggregated into spherical particles. However, the surface of spherical particles of *Arthrobacter sp*. MF-2 remained rougher than that of *Curvibacter sp*. SP-1. Calcite was formed by both strains as the main polymorph of $CaCO_3$. Crystals formed by *Curvibacter sp*. SP-1 also had an aragonite content of about 20 %. Also, amorphous $CaCO_3$ formed during the first days of cultivation was converted to crystalline form more slowly in the presence of *Curvibacter sp*. SP-1. These differences in the formation of $CaCO_3$ crystals are assumed by Zhang et al. to be due to the different composition of the surface and therefore the surface charge of the strains. How exactly surface proteins or the surface charge influence the polymorphs of $CaCO_3$ remains unanswered. Future studies could investigate MICP of genetically modified ureolytic strains which specifically alter the zeta potential or certain knocked out surface proteins. The results could lead to a better understanding of which surface characteristics of microbiological strains have a positive influence on MICP. In follow up studies it will be of interest if tailoring the surface characteristics of these strains can help to achieve certain crystal sizes and therefore different compressive strengths of MICP treated sand.

In addition to its influence on the morphology of the $CaCO_3$ crystals, the strain used also has an influence on the tolerance of the organism to temperature, salinity and alkalinity during MICP. In order to find an ureolytic organism with a high tolerance for the conditions during MICP and a high yield of $CaCO_3$ crystals, a large number of studies in recent years have investigated different ureolytic organisms regarding MICP. For this purpose, not only organisms from strain collections, but also local isolates were investigated in several studies [34–36]. These studies usually select

strains with ureolytic activity comparable to commonly used microorganisms for MICP like *Sporosarcina pasteurii* DSM 33. It appears that halotolerant alkaliphilic ureolytic microorganisms are common in a lot of climate zones with 99 % of phylogenic similarity [36]. Although some of these isolates grow faster than *Sporosarcina pasteurii* [34], or could achieve 17 % higher compressive strengths of biocemented samples than *Sporosarcina pasteurii* DSM 33 there is still no isolate that appears to have a significantly higher potential for MICP than the commonly used strains. However these strains might an impact on local acceptance of the MICP technology. These strains could find more acceptance with local communities and authorities when releasing these strains into the environment while still maintaining similar potential for MICP as *Sporosarcina pasteurii*.

Besides the search for organisms that offer advantages over other strains due to their natural environment, few studies have modified strains to investigate the process of MICP. Konstantinou et al. [37] developed a method to adjust the urease activity of *Sporosarcina pasteurii*. They inoculated *Sporosarcina pasteurii* in nutrient broth liquid containing no urea and stored this solution at 4 °C. After 3-5 days, fresh nutrient broth liquid was inoculated from this generation and stored at 4 °C. This procedure was repeated until day 42. The authors were able to detect a decrease in urease activity and expression of the Ure-C gene, which encodes for the largest subunit of urease. They compared generations with three urease activities (294, 66 and 19 $mmol \cdot L^{-1} \cdot h^{-1}$) for consolidation of sand. When using the generation with high urease activity, a highly non-uniform distribution of $CaCO_3$ was observed in the samples. Also, clogging of the samples was observed whereby only the upper parts of the samples were consolidated. When strains with lower urease activity were used, an almost homogeneous distribution of $CaCO_3$ was observed over the entire sample. The authors emphasize the potential of this method to precisely adjust the ureolytic activity of *Sporosarcina pasteurii* to the application, as they have different requirements for MICP. Furthermore, these results show that ureolytic activity directly impacts the result of MICP which is most likely due to different shapes and sizes of calcium carbonate crystals depending on ureolytic activity.

Another way to adapt a microorganism to the needs of MICP application is genetic engineering. However, large-scale application of genetically modified organisms

(GMO) outside of controlled laboratories seems unlikely due to local regulatory constraints. However, genetically modified organisms may help to better understand the fundamental mechanisms of MICP. For example did Liang et al. [38] design 13 plasmids with the urease gene cluster from *Sporosarcina pasteurii* (ATCC 11859) and transformed these plasmids into *Escherichia coli* HB101. They investigated the influence of 4 genes outside the urease gene cluster by deleting these genes resulting in different urease activities and calcium uptake rates for all strains. Therefore, the authors hypothesize that $CaCO_3$ precipitation is controlled by more factors of a strain than just its urease activity and that the genes outside the urease gene cluster also have an influence on $CaCO_3$ productivity.

In a follow-up study Heveran et al. [39] showed that the morphology and nanomechanical properties of $CaCO_3$ can be manipulated by the use of genetic engineering. They compared wild-type *Sporosarcina pasteurii* (ATCC 11859) with two engineered *Escherichia coli* strains HB101/ure-integration and HB101/pBU11 from the study of Liang et al. [38]. *Escherichia coli* HB101/pBU11 was adapted to have urease activity similar to *Sporosarcina pasteurii*, whereas *Escherichia coli* HB101/ure-integration had lower urease activity. During precipitation experiments, only calcite was detected by XRD for all three strains after 7 days. However, for *Sporosarcina pasteurii*, vaterite appeared after 12 h as a transition polymorph. In comparison, for the two *Escherichia coli* strains, no metastable polymorph was observed at any time point. Since *Escherichia coli* HB101, unlike *Sporosarcina pasteurii*, does not form extracellular polymeric substances the authors hypothesized that these stabilized vaterite. They also observed significant differences in the size of $CaCO_3$ crystals formed among the strains. While *Sporosarcina pasteurii* crystals had an area of 72 µm², *Escherichia coli* HB101/pBU11 and *Escherichia coli* Hb101/ure-integration reached 16.8 and 340 µm², respectively. The authors concluded that the difference in crystal size is due to the low urease activity, which favors slower crystal growth and thus larger crystals. However, the significant difference in crystal size with similar urease activity of *Sporosarcina pasteurii* and *Escherichia coli* HB101/pBU11 shows that other factors besides urease activity influence MICP. Investigation of the influence of other genes in the region surrounding the urease gene clusters and the composition of extracellular polymeric

substances and their influence on crystal formation require more research to advance the understanding of the mechanism of ureolytic MICP. The use of modified ureolytic strains in the recent past has shown that not all mechanisms and influences of MICP can be studied by using wild types such as *Sporosarcina pasteurii*.

There is a need in future studies to investigate the influence of individual properties of microorganisms on MICP to better understand the process in detail. Thus, with progressing knowledge of MICP mechanisms, strains can be specifically adapted to meet requirements for the application of MICP. For example, to achieve the highest compressive strength of a construction material, a strain will have to be developed that produces $CaCO_3$ in a morphology that creates optimal contact points between individual sand particles to achieve the best consolidation. For the treatment of cracks in existing building materials or for the use of MICP as a natural water barrier, the highest possible decrease in permeability of the treated material would be of importance. Regardless of the application, the use of genetically modified organisms does not appear to be a viable approach for industrial use. Often MICP depends on the application of the organism or a product produced by ureolytic organisms directly in the environment. Large-scale sterilization of artificially produced construction material would be associated with additional energy consumption and would make the application of this technology difficult and less environmentally friendly. The search for suitable wild types and the random mutagenesis of these strains seems to be the more suitable way for an industrial application of MICP.

3 Biomass concentration and ureolytic activity

For the application of *Sporosarcina pasteurii* and other ureolytic microorganisms with intracellular urease, the biomass concentration and the urease activity are parameters that cannot influence MICP separately from each other. A higher biomass concentration and thus urease activity, leads to an increased degradation of urea and thus to a faster formation of carbonate ions, which in turn favors a faster $CaCO_3$ precipitation [40]. However, the use of higher urease activities promotes the formation of smaller $CaCO_3$ crystals, which in turn may have a negative effect on the consolidation of sand [41, 42]. There are strong indicators that ureolytic organisms serve the MICP process not only as source of urease but also as initial nucleation sites for crystal growth [43, 8, 44]. Positively charged calcium ions in the environment

of the microorganisms are attracted by negatively charged carboxy and phosphoryl groups on the cell surface through electrostatic interactions [45]. This increases the calcium concentration in the micro environment of the cells.

Also, calcium metabolism causes an increase in pH near the cells, which promotes the formation of carbonate ions and thus $CaCO_3$ precipitation (see Figure 2). This is subsequently carried out at this nucleation site in the liquid phase around the cell. Recently it was shown that during MICP nanometer sized crystals are formed at the cell surface for *Sporosarcina pasteurii,* which were confirmed as $CaCO_3$ by Energy dispersive X-Ray spectroscopy and X-ray powder diffraction. These results are a further indicator for the role of ureolytic microorganisms as nucleation sites [44].

The influence of these nucleation sites becomes clear by comparing MICP and enzymatically induced calcium carbonate precipitation (EICP). Zhao et al. [46] were able to show that in aqueous solution for *Sporosarcina pasteurii*, the efficiency of MICP is higher than for EICP regarding the amount of precipitated $CaCO_3$. In addition, they found that when comparing the two methods for consolidation of sand, MICP had higher unconfined compressive strength (UCS) in relation to $CaCO_3$ content than EICP (see Table 3).

Table 3: $CaCO_3$ content and unconfined compressive strength (UCS) of samples treated with urease and *Sporosarcina pasteurii*. Modified after Zhao et al. [46].

	Sporosarcina pasteurii		**Urease**	
Cementation Media concentration (1 M Urea)	**$CaCO_3$ content in %**	**UCS (MPa)**	**$CaCO_3$ content in %**	**UCS (MPa)**
0.25 M Ca	1.90 - 2.02	0.08 - 0.18	-	-
0.5 M Ca	7.21 - 7.88	1.28 - 1.43	5.12 - 5.55	0.58 - 0.62
1.0 M Ca	9.56 - 11.12	1.60 - 2.10	6.03 - 7.02	0.57 - 0.76
1.5 M Ca	12.14 - 13.39	2.04 - 2.13	7.36 - 8.90	0.79 - 0.81

The cell concentration and thus the amount of nucleation sites available for formation of new nuclei influence the size of the crystals formed. The formation of new crystals at nucleation sites competes with the growth of already existing crystals. An increase in cell concentration and thus in urease activity leads to a higher number of

nucleation sites and thus to smaller crystals, whereas at lower cell concentrations the growth of pre-existing crystals predominates and thus larger crystals occur. In recent studies, Cheng et al. [42] and Wang et al. [41] investigated the influence of biomass concentration on crystal size. Cheng et al. found that small $CaCO_3$ crystals of about 2 - 5 µm were formed during calcination of silica sand when a biomass concentration of about OD_{600} 10 was used. At OD_{600} 1, agglomerates of crystals were formed that ranged in size from 20-50 µm. Wang et al. also observed an increase in crystal sizes with a decrease in the cell concentrations used. For a cell suspension with OD_{600}=0.15 they found the largest crystals with a volume of 8000 µm³, for a cell suspension of OD_{600}=1.3 only crystals with a volume of 400 µm³.

These results are in accordance with the findings of Konstantinou et al. [37], Heveran et al. [39] and Murugan [40] all of whom found an antiproportional relationship between the urease activity and therefore the OD of an organism and the size of $CaCO_3$ crystals formed. Except the study of Konstantinou et al. [37] these studies did not differentiate between biomass concentration and ureolytic activity. Since an increase of biomass concentration will lead to an increase of the ureolytic activity and the number of nucleation sites, future research on this topic should try to separate the effects. This could be achieved by mutagenesis of the investigated strain as described by Konstantinou et al. [37] or through the utilization of GMO´s. Research with these organisms might help to increase the knowledge especially on the role of the bacteria as nucleation sites which is still not fully understood. This knowledge will help to shape further studies concerning the correlation of morphology and size of $CaCO_3$ crystals and mechanical parameters of biocemented sand.

4 pH value

The pH of the environment can influence MICP. For example, pH affects the growth of ureolytic microorganisms, urease activity, and $CaCO_3$ precipitation. Ureolytic microorganisms in the presence of urea increase the pH in the environment to about 9.25 which is both the optimal pH for growth of *Sporosarcina pasteurii* [47] and at the same time promotes the formation of carbonate supersaturated conditions in the environment of the cells [23]. Furthermore ureolytic activity is pH dependent. Most ureases reach their optimal activity at around pH 8 [27]. Above pH 8, urease activity decreases. However, since the urease of *Sporosarcina pasteurii* is not

extracellular [48], the pH of the environment plays a minor role for this strain. When using ureolytic microorganisms with extracellular urease, the pH should be considered during MICP to avoid limiting the efficiency of the urease too much. The major influence of pH during MICP is mainly related to $CaCO_3$ precipitation itself. $CaCO_3$ precipitation is favored by a high concentration of CO_3^{2-} ions. CO_3^{2-} ions are in equilibrium with hydrogen carbonate ions and carbonic acid, the so-called lime-carbonic acid equilibrium (see eq. 7-9).

$$CO_2 + H_2O \leftrightarrow H^+ + H_2CO_3 \quad \text{eq. 7}$$

$$H_2CO_3 \leftrightarrow H^+ + HCO_3^- \quad \text{eq. 8}$$

$$HCO_3^- \leftrightarrow CO_3^{2-} + H^+ \quad \text{eq. 9}$$

The balance of this equilibrium, and thus the ratios between the carbonic acid species, is dependent on the pH of the environment. Above pH 10.3 ($pH > pK_a$) carbonate ions begins to dominate, favoring $CaCO_3$ precipitation. Cheng et al. [49] investigated the influence of the pH of the calcination solution on the conversion rate of calcium ions to $CaCO_3$. They found that the efficiency of MICP remains approximately the same for pH values of 4 - 8.1, because the degradation of urea increased the pH in the environment, allowing $CaCO_3$ precipitation. However, for pH values below 4, there is a rapid decrease in conversion efficiency to 60 % (pH 3.5), 10 % (pH 3.0) and no $CaCO_3$ precipitation could be observed for pH values of 2.5 and lower.

In a similar study Lai et al. [50] investigated the precipitated $CaCO_3$ during MICP with *Sporosarcina pasteurii* DSM 33. They also describe a pH value which acts as a deactivation threshold for MICP. For pH values lower than this threshold no $CaCO_3$ precipitation occurs. They found that this threshold is dependent on the cell density. Between cell densities of $0.06 \cdot 10^8$ to $10 \cdot 10^8$ cells $\cdot$ ml^{-1} the pH threshold rises from pH 2.5 up to pH 4. They also describe that the threshold can be lowered by suspending the bacterial cells into fresh medium before MICP.

It is theorized that the cells need adequate nutrients to overcome the severe acidic environment. Which nutrients this might be could not be investigated due to the nature of the complex medium that was used during cultivation of *Sporosarcina pasteurii*. Since initial pH values impacts the initial flocculation time and $CaCO_3$ conversion rate [49, 50]. Based on this knowledge Cheng et al. [49] developed a

grouting protocol that utilizes low pH cementation solutions. Further information on this topic will be given in a later chapter. To improve this novel injection method future studies should investigate what nutrients are required to achieve lower pH thresholds. This will help to improve the delay that can be forced until flocculation occurs and thereby give possibilities of injection strategies that were in the past limited due to clogging.

5 Temperature

Like other enzymatic reactions MICP is temperature-dependent. The temperature optimum of most ureases lies between 20 and 37 °C [47] but during MICP the rate of ureolysis is not only dependent on the enzyme activity but also other factors like urea uptake, the release of CO_3^{2-} and the precipitation kinetics. In the past available kinetic studies on MICP focused on a single step reaction. They described the kinetic of MICP either through Michaelis-Menten [51], zero order [40], or first order kinetics [52, 51, 47]. While these studies could describe the perceived precipitation rate or urea depletion rate during MICP the kinetic models did not incorporate that the process of MICP has multiple reaction steps staring with urea uptake and ending with the precipitation of $CaCO_3$.

In a recent study Sridhar et al. [53] investigated the kinetics of ureolysis of *Sporosarcina pasteurii* DSM 33. They developed a simple structured kinetic model that incorporated urea transport into the cells, hydrolysis of urea, ammonium assimilation and the transport of ammonium out of the cells. It was found urea uptake follows a first order kinetic with a rate constant of $9.8 \cdot 10^{-2} \cdot d^{-1}$ which suggests active transport of urea into cells. They describe the ammonium excretion as free diffusion with a permeability coefficient of $9.2 \cdot 10^{3}$ m $\cdot$ d^{-1}. None of these studies did incorporate the influence of temperature into the kinetic model. Investigations of temperature on each single aspect of ureolysis during MICP will be of interest to develop kinetic models that can be used in the future to predict the exact reaction time based on local ambient temperatures In addition to urease activity, temperature also has an effect on the morphology of calcium carbonate crystals.

Cheng et al. [42] were able to show that at a temperature of 50 °C, three times more $CaCO_3$ crystals were formed in sand samples during MICP than at 25 °C. However, these had a smaller diameter (2-5 µm) than crystals formed at 25 °C (15-20 µm),

resulting in a 60 % reduction in the strength of the consolidated sand. Kim et al. [54] studied the relative $CaCO_3$ precipitation for temperatures between 20 and 50 °C. They obtained the maximum precipitated amount of $CaCO_3$ for a temperature of 30 °C. As the temperature increased to 50 °C, the amount of precipitated $CaCO_3$ decreased by about 50 %. While these studies investigated the crystal size directly in the sand bed and the total amount of by $CaCO_3$ weight the development of a microfluidic chip [55] allowed the observation of crystal growth during different stages of the MICP process in pore spaces. While investigating the $CaCO_3$ crystal growth in the temperature range of 4 °C to 50 °C the correlation between temperature and crystal size was found to be dependent on two phenomena.

As described earlier the crystal growth is dependent on ureolytic activity. Temperature can therefore impact the crystal morphology indirectly by impacting ureolytic activity. Temperature can also have a direct impact on crystal dissolution behavior following the Ostwald law [56]. Usually the least dense phase of a crystal is formed first and transformed into the next dense phase. Therefore low temperatures favor the formation of vaterite while high temperatures lead to the formation of the denser and more stable calcite. During this study the average crystal size was the highest for temperatures of 35 °C. The authors of the study state that this is most likely due to higher temperatures reducing cell dennsity and bacterial specific urease activity in their experimental setup and lower temperatures leading to lower chemical transformation efficiency. The potential of this microfluidic chip for the investigation of crystal growth in an environment close to a field of application seem promising. The different findings of temperature influence on the efficiency of MICP might also be dependent on different ureolytic strains. Therefore, it will not only be necessary to find suitable strains depending on ureolytic activity, pH tolerance or the ability to achieve high biomass concentrations during cultivation. Overall temperature is a parameter that is easy to control during MICP and can be altered to achieve certain goals like a faster reaction time or the production of different crystal sizes.

However, there is still a need for research on how these effects mutually affect the crystal size and strength of consolidated sand. Furthermore, the contrary results of some of the studies concerning efficiency of the conversion rate of MICP depending on temperature show that it is difficult to investigate certain influencing parameters of

MICP independently. For example, while conducting a study on crystal precipitation of MICP not only temperature will impact the results through impact of the observed ureolytic activity and crystal dissolution but also the type of strain that was used and its specific ureolytic activity and mass transport phenomena. Furthermore, the cell density will also impact the results by altering the number of nucleation sites and ureolytic activity during the experiment. It is therefore difficult to compare results of different laboratory setups during these studies. Studies that can truly investigate single influencing factors by disconnecting a factor could help to make these results comparable and increase the overall knowledge of MICP.

6 Composition of the calcination solution

Most calcination solutions contain urea, a calcium salt, and are dissolved in either water or a cultivation medium [57, 23, 58]. The urea and calcium concentrations affect the metabolism of ureolytic microorganisms, the efficiency of $CaCO_3$ formation, and the morphology of the formed crystals. Since the stoichiometry of $CaCO_3$ formation ideally requires an equimolar amount of urea and calcium, most studies are conducted with equimolar concentrations of urea and a calcium salt [42, 24, 59, 23]. Optimization of these concentrations has been a central aspect of many studies dealing with MICP. Qabany et al. [60] investigated the influence of different equimolar concentrations of urea and calcium in the range between 0.25 and 1 M on MICP. They were able to show that with increasing concentration of the calcination solution, the size of the $CaCO_3$ crystals increased from 3-5 µm to up to 35 µm, while the uniformity of the distribution of the crystals and the permeability of the sample decreased. Zhao et al. [46] treated silica sand with cell suspension of *Sporosarcina pasteurii* and equimolar calcination solutions in the range 0.25 to 1.5 M urea/Ca^{2+}. Above a concentration of 0.5 M, they observed a consolidation of the silica sand. The strength of the samples increased with increasing concentration of the calcination solution from 0.6 MPa (0.5 M) to 0.8 MPa (1.5 M) which corresponds to a small increase with a much higher input of resources. However, the authors of the study state that the low concentration of microorganisms with OD_{600}=0.6 may have limited a higher efficiency at a calcination solution of 1.5 M.

In comparison to equimolar calcination solutions, various studies were able to find an improvement in calcination with non-equimolar ratios (see Table 4). For example,

Sotoudehafar et al. [61] found an optimum compressive strength of sand at a ratio of urea to calcium chloride of 3 M to 1.5 M. Muynck et al. [6] also investigated the influence of different concentrations of urea and calcium on MICP. Based on their results, they postulated that an optimum of urea and calcium exists for a certain amount of retained cells in sand samples. Up to this optimum, desired effects (consolidation of sand by increasing the concentrations of urea and calcium) outweigh the harmful effects (accumulation of salt and urea in the pores, discoloration of the sand). Han et al. [62] obtained the best results with an almost equimolar ratio of 0.73 M $CaCl_2$ and 0.75 M urea.

Table 4: Optimization approaches of calcination solutions with non-equimolar ratios.

Strain	Varied parameters	Target parameter	Optimum (mM Urea/Ca^{2+})	Source
Sporosarcina pasteurii	[Urea] [$CaCl_2$] Ratio of Cells/Calcination solution	Compressive strength	1492 mM Urea 1391 mM CaCl2 7,47 mL cell suspension 7,53 mL cementation solution	[66]
Sporosarcina pasteurii	[Urea] [$CaCl_2$] NiCl2	Calcium carbonate precipitation rate (h^{-1})	63 mM $CaCl_2$ 700 mM Urea 6,9 mM Nickel	[65]
Sporosarcina pasteurii	[Urea] [$CaCl_2$]; Reaction time; Flow rate; Cell concentration (OD_{600})	UCS (kPa)	3000 mM Urea 1500 mM $CaCl_2$ 20 mL/min OD 4 Curing time 21 d	[61]
Sporosarcina pasteurii	[Urea] [$CaCl_2$]	Rate of ureolysis (h^{-1})	666 mM Urea 250 mM $CaCl_2$	[47]
Lysinbacillus sphaericus	[Urea] [$CaCl_2$]	Weight gain of sandstone, Permeability	167 mM Urea 227 mM $CaCL_2$	[6]
Sporosarcina pasteurii	[Urea] [$CaCl_2$] [Temperatur]	$CaCO_3$ precipitated ($g \cdot L^{-1}$)	0.73 mol/l $CaCl_2$ 0.75 mol/l Urea 45 °C	[62]

However, they did not consider the compressive strength of treated sand but the amount of $CaCO_3$ that could be precipitated from an aqueous solution.

These studies vary in the absolute values of optimum concentrations of the calcination solution but it is apparent that high concentrations above 0.5 M urea and calcium ions are necessary to achieve high compressive strength. This is especially true since compressive strength of biocemented soil correlates with the amount of $CaCO_3$ [63] after treatment and the amount of precipitated $CaCO_3$ during MICP is directly dependent on the initial concentration of urea and calcium ions and the number of treatment cycles of cell suspension and cementation solution. Compressive strength is not always the most important factor during MICP, for example when environmental impact through high concentrations of the by-product ammonium are a concern. This is true for example for when treating of coastal sand. Ashraf et al. [64] optimized the cementation solution towards the compressive strength of coastal sand under low concentrations of urea (< 0.1 M) and calcium (< 0.05 M) and achieved compressive strengths up to 154.5 kPa which is described as suitable to strengthen coastal sand into resilient yet habitable ecosystems. While it seems that for MICP it is generally suitable to apply higher concentrations of urea and calcium ions to achieve high strengths there is still more research necessary to understand this process. Especially the correlation between compressive strength, the size of precipitated crystals and homogeneity of samples after treatment are factors that all seem to be influenced by the concentrations of the cementation solution.

While these studies were concerned with the compressive strength or the amount of precipitated $CaCO_3$, others investigated the influence on the speed of the MICP itself in order to make a statement about the efficiency of the MICP. Okwadha et al. [47] found the highest rates of ureolysis for MICP at concentrations of 666 mM urea and 250 mM calcium. Okyay et al. [65] reported the highest $CaCO_3$ precipitation rate for a calcination solution with a $CaCl_2$ concentration of 63 mM and an urea concentration of 700 mM. For all these studies, there are large variations in the $CaCO_3$ and urea concentrations described as optimal for MICP. These findings are largely dependent on which parameter is set as the target parameter for MICP. While $CaCO_3$ precipitation is fast for low calcium concentrations, since calcium ions inhibit urease

activity, MICP stops completely at high concentrations [48]. In this case a large number of treatment cycles must be performed to precipitate a sufficient amount of $CaCO_3$, which would not be time and resource efficient. Therefore, in order to make statements about the optimal parameters of the calcination solution, a compromise must always be found between speed and efficiency in terms of the amount of $CaCO_3$. Past research could show that the choice of calcium source has an impact on the morphology of calcium carbonate crystals and on mechanical parameters like UCS of treated samples [67, 68]. In these studies, $CaCl_2$ was found to be the optimal calcium source. Since chloride ions have little impact on sandy soil and its low cost, $CaCl_2$ is still the preferred calcium source for MICP [69]. Samples treated with calcium acetate achieved higher carbonate content than samples treated with calcium chloride or calcium nitrate [70]. The mechanical strength however is lower which is most likely due to more calcite crystals produced with calcium chloride and calcium nitrate compared to the vaterite that was formed during treatment with calcium acetate [70].

Although calcium acetate seems to be inferior as a calcium source regarding strength of treated samples Xiang et al. [69] showed that acetate ions react with NH_3 during MICP which leads to 54.2 % and 51.4 %, respectively reduced NH_3 emission in comparison with calcium chloride and calcium nitrate. It should be noted that the utilization of calcium acetate in a seawater environment might be preferable due to less NH_3 emission, but Peng et al. [71] found that in seawater environment calcium chloride showed 2 % less calcium carbonate production compared to freshwater environment. In comparison calcium acetate showed 7 % and calcium nitrate 20 % less carbonate production in seawater environment. Nonetheless both environments lead to high strength of the treated coral sand columns. The authors of the study attributed this loss in efficiency to magnesium ions in seawater. These ions promoted the formation of acicular aragonite while in freshwater massive calcite crystals were the main morphology

These results show that during the choice of a suitable calcium source the application and environment in which the MICP will be carried out should always be of concern. Although there are still questions regarding the exact mechanisms on the morphology of $CaCO_3$ depending on the composition it appears that the composition of the

cementation solution is easy to change during MICP and also has one of the biggest impacts on the efficiency of the process. Since the compressive strength of biocemented sand positively correlates with the amount of precipitated $CaCO_3$ in the sample [63] there will always be the necessity for multiple cycles of treatment to achieve high $CaCO_3$ contents. To keep the number of individual cycles low it will be beneficial to have the highest concentration of urea and calcium in the cementation solution as possible while still maintaining high conversion efficiency of the ureolysis. If ureolytic strains can be found or designed that tolerate high concentrations of calcium during MICP the limitation of the amount of $CaCO_3$ precipitated by each treatment cycle would in this case be the solubility of urea and the corresponding calcium salt. This limit can be extended by using higher temperatures of the cementation solution since the solubility of urea and calcium chloride rises with higher temperature.

7 Sand properties

While the factors discussed so far have a universal influence on the MICP, different applications of the MICP have additional influences that need to be considered. Regarding the cementation of sand, the particle size and the density of the material impact the result of the MICP. In order to achieve the most homogeneous distribution of $CaCO_3$ possible during biocementation, it is necessary for the microorganisms to be able to distribute themselves freely in the matrix before they come into contact with calcination solution. The transport and retention of bacteria in a porous network is dependent on the relative pore throat volume in comparison to the size of individual cells and electrostatic interactions between cells and the particles [72]. Since the pore throat volume is directly dependent on the size of the particles, the size of the particles has an influence on the MICP. Most ureolytic organisms used for MICP have a size in the range of 1-5 µm. If particles smaller than this are used, this can prevent the free distribution of bacteria and thus a homogeneous result of the MICP [72]. Too large particles, on the other hand, have fewer contact points between particles, which does not prevent coarse particles from being consolidated, but increases the effort and amount of resources needed to form a $CaCO_3$ layer sufficient to consolidate these particles [73].

Several studies have investigated the influence of particle size on the efficiency of MICP cementation of sand. Dhami et al. [74] investigated the consolidation of different sand fractions with grain sizes between 0.1 and 2 mm by *Bacillus megaterium*. For this purpose, they considered the decrease in flow rate through a 76 mm sand bed. For all grain sizes, they observed a decrease in flux rate after 10 days compared to untreated sand. They achieved a larger percent decrease in flow rate for smaller particle sizes compared to larger particle sizes. The largest decrease (88% reduction) occurred for a particle size of 0.5 mm, while only a 66 % reduction was observed for particle sizes of 0.2 mm. However, since the initial flow rate at 0.2 mm was 70 % lower than at 1.5 mm, because smaller grain sizes have a higher resistance to flow, it is not clear in this study whether these results can also be applied to other parameters that allow statements to be made about the efficiency of the MICP.

Cheshomi et al. [75] compared two silica sands with particle sizes of 0.075-2 mm (S1) and 0.12-0.85 mm (S2). They found that S1 had a higher permeability than S2. As a consequence, S1 showed a homogeneous distribution of $CaCO_3$ after MICP, while S2 showed clogging, resulting in an inhomogeneous $CaCO_3$ distribution of the samples. The authors concluded that these results were due to the fact that cells were able to move more easily through S1 and thus achieved a better distribution in the sample. In addition to the homogeneity of the distribution, a higher shear strength of 380.6 kPa was also observed in this study compared to S2 (140.2 kPa). Konstantinou et al. [76] compared the compressive strength of a fine and a coarse quartz sand with average particle diameters of 0.18 mm and 1.82 mm, respectively, after consolidation by MICP. While for a low degree of calcination (5.5 % $CaCO_3$) the compressive strengths of the specimens were still close to each other with 500 kPa for fine and 450 kPa for coarse sand, a compressive strength of 2500 kPa was achieved for fine sand and 1600 kPa for coarse sand at a degree of calcination of 10 %. Mahawish et al. [77] investigated the compressive strength of fine (D_{50} = 0.37 mm) and coarse (D_{50} = 9.90 mm) aggregate as well as different blends with 75, 50 and 25 % of fine aggregate. Lower compressive strengths were obtained for both pure fine and pure coarse aggregate compared to blends of the aggregates. For a fine aggregate content of 25 %, the authors of the study achieved the highest

compressive strength of 575 kPa. Further research into the optimum composition of the grain sizes has the potential to make the MICP more efficient without investing in more biomass or urea and calcium ions. Especially interactions between the grain size and density of the soil with the size of precipitated $CaCO_3$ crystals during MICP might lead to a better understanding of the overall process and therefore to a reduction in resources used for MICP while maintaining high compressive strength. In addition to particle size, the relative density of the soil also has an effect on the cementation effect of MICP. The relative density D_R describes how dense sandy soils are. 0 % and 100 % indicate the loosest and densest states a sand can assume. Rowshanbakht et al. [78] and Gao et al. [79] measured the compressive strength of silica sand after MICP and observed not only a positive correlation between the relative density of the sand and the compressive strength, but also a simultaneous lower $CaCO_3$ content of the denser specimens.

All of these studies conclude the improved mechanical parameters of the specimens to the fact that compacting the sand brings the particles closer together and thus $CaCO_3$ crystals have to bridge shorter distances to consolidate in order to bond the sand particles. Regardless of the choice and particle size of the sand, it therefore seems advantageous to compact the sand before treating the MICP in order to achieve the most efficient increase in mechanical properties. In recent years a transparent microfluidic chip was designed [55]. The chip allows for a 2D visualization and investigation of processes during MICP. The authors of the study could therefore observe processes like the detachment of bacterial cells from sand grains during flushing with cementation solution and the growth of $CaCO_3$ crystals during sequential injections. In future research concerning MICP it will be important to combine these findings of 2D small scale experiments with results obtained in classic column experiments to further develop the knowledge of the multifactorial interactions during MICP.

8 Biocementation protocol

In early studies of MICP, sand was mixed with ureolytic organisms, filled into molds and then treated with calcination solution by gravity feed, or cell suspension and calcination solution were mixed and immediately applied to a sand bed under pressure. [27, 48]. However, these methods often lead to a clogging of the sample at

the entry point of the calcination solution due to the decrease in permeability, which resulted in an uneven consolidation of the samples [80, 27]. Since then, various methods have been developed over the years to perform MICP more efficiently (see Figure 5). In 2007, Whiffin et al. [80] developed a 2-phase injection protocol. Phase 1 is the placement step in which the cell suspension is applied to the sand and fixed. For this purpose, the cell suspension is applied until the mould is completely filled and bacterial cells are observed at the exit point. Then, a pore volume of 50 mM calcium chloride solution is applied to increase the ionic strength and thus increase the adsorption of cells on the surface of sand particles. Immediately after the placement step, a calcination solution is applied under uniform flow. Over the length of a 5 m column of sand, they were able to demonstrate the formation of $CaCO_3$ over the full length using this method without causing a complete clogging during the process. However, complete homogeneity was not achieved in terms of compressive strength and $CaCO_3$ content of individual sections. With increasing distance from the injection point, the $CaCO_3$ content decreased from 85 $kg \cdot m^{-3}$ sand to about 3 $kg \cdot m^{-3}$ sand. From a distance of 2.5 m from the injection point, they could not detect any increase in the compressive strength of the sand in contrast to untreated samples.

Cheng et al. [81] developed a simple surface percolation method for MICP consisting of four steps. (i) percolation of the cell suspension (50 % water retention capacity), (ii) percolation of a fixation solution (50 % water retention capacity), (iii) incubation for 12 h to allow diffusion processes, and (iv) percolation of the calcination solution (100 % water retention capacity).Using this method, they were able to achieve nearly uniform consolidation over a length of 1 m for one column. Cheng et al. [81] combined the percolation method with the two-phase injection of Whiffin et al. [80] and were able to achieve higher localized strength over the entire length of the specimen with the percolation method than with the two-phase injection. However, inhomogeneities in $CaCO_3$ content along the length of the specimen were also observed for this method. While consolidation of sand could be achieved with these methods and the problem of complete clogging could be eliminated, effluent reduces the number of bacteria in the sample and the problem of unevenly precipitated $CaCO_3$ remains. Zhao et al. [46] developed a novel method by using full contact

flexible molds made of geotextile, a polypropylene, staple fiber and needle punched nonwoven material. Sand is mixed with ureolytic bacteria for this method and filled into the molds. The molds are then completely immersed in a reactor filled with calcination solution consisting of $CaCl_2$, NH_4Cl, $NaHCO_3$ and nutrient broth [82]. Through the pores in the mold, the calcination solution can soak into the specimens and the specimens are consolidated by ureolytic MICP. Using this method, the authors were able to achieve a compressive strength of 2 MPa with nearly homogeneous $CaCO_3$ concentration in the specimens. However, a disadvantage of this method is that no further cells can be introduced into the moulds during curing and the amount of precipitated $CaCO_3$ is thus limited by the amount of cells applied, which encapsulate and die over time [43]. Wen et al. [83] were able to solve this problem by further developing the method. They took the samples after immersion, dried them for 24 h at 105 °C and then treated them again with cell suspension and calcination solution in a batch reactor. This allowed them to increase the compressive strength of the samples from 2.2 MPa to 6.4 MPa. Cheng et al. [84] were also able to achieve a uniform distribution of microorganisms by using a so-called bioslurry.

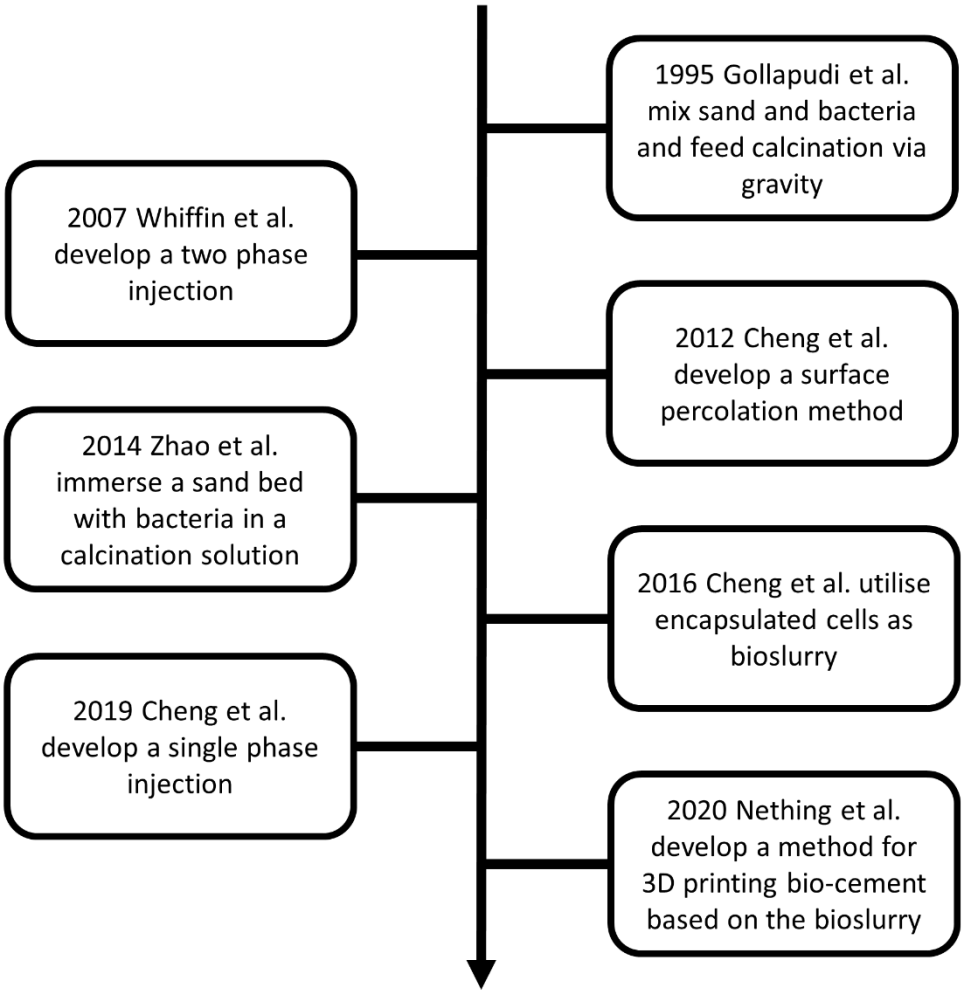

Figure 5: Overview over the development of grouting protocols for MICP.

To prepare the bioslurry, a cell suspension of *Bacillus sp.* DSM 23526 was mixed with a solution of urea and calcium chloride. The cells then precipitated $CaCO_3$ and were encapsulated. After sedimentation of the crystals, they were separated from the supernatant to harvest the bioslurry. For biocementation, sand was mixed with bioslurry at a ratio of 10:1 and placed in a PVC column. The column was flushed up to eight times with a calcination solution, resulting in a UCS of 1.1 MPa. Over a column length of 275 mm, a uniform $CaCO_3$ content of 0.055 g $CaCO_3 \cdot g^{-1}$ sand was achieved. However, this sample also has the disadvantage that the amount of cells is limited during MICP and thus no further $CaCO_3$ precipitation takes place after encapsulation of the cells. A possible approach to achieve a homogeneous distribution as well as to provide a sufficient amount of cells in a sample was

developed by Cheng et al. [49]. This approach takes advantage of the dependence of MICP on pH as described earlier. By lowering the calcination solution to pH 4, a lag phase could be generated before the ureolytic activity of microorganisms causes the pH to rise and $CaCO_3$ precipitation to occur. This allows calcination solution and cell suspension to be mixed and then immediatly be applied to a column of sand without being limited by clogging. Using this method, Cheng et al. [49] were able to consolidate silica sand to a compressive strength of 2.5 MPa using *Sporosarcina pasteurii* and achieved a nearly homogeneous distribution in a 360 mm column. An advantage of this method is that the atmospheric ammonium released was reduced by 90%. However, this method has a limitation in application at low cell concentrations and ureolytic activities, as these were not able to raise the pH of the environment to a level that allowed MICP to occur. However, this study could not answer whether the results could be transferred to other ureolytic organisms. It may be possible to extend the lag phase by using organisms that tolerate lower pH values, which could further increase the efficiency of the method.

Another approach to improve the homogeneity of the samples could be the approach of 3D printing. Nething et al. [85] combined the method of bioslurry with the method of immersion in their study on the feasibility of 3D printing using MICP. For this approach, they lyophilized the bioslurry to obtain a ureolytically active powder. A sand bed was now printed over a powder print. In the areas that were to be consolidated using MICP, the sand was mixed with the bioslurry powder via a screw thread. The entire sand bed was then immersed in a calcination solution. Via this method, the authors were able to print geometrically stable 3D structures.

This overview of grouting protocols shows that there is a steady evolution in MICP methods. This is mainly driven by the fact that the protocols often lead to non-uniform distributions of $CaCO_3$ in the samples due to blocking or washing out of cells. Especially regarding the application as sustainable building materials, suitable protocols have to be found that can reproduce the materials with high precision to not allow weak spots due to inhomogeneous samples. The development of new strains and a deeper understanding of the mechanism of MICP may allow in the future to develop new grouting protocols precisely adapted to a specific use case of MICP. The issue of clogging and homogeneity of samples in a lot of cases is still a problem

that needs to be addressed in future research. To improve these protocols, it will be necessary to understand the process of MICP in detail. Recent research on the topic of ureolytic activity can be incorporated to find the optimal curing time between treatment cycles which is often still overestimated to give the process enough time to fully degrade urea. Especially the understanding of microscopic processes during MICP through microfluidic chips could lead to the development of customized parameters. While in the past it was difficult to see and conduct research on the growth of $CaCO_3$ crystals in the sand matrix it will be possible to get visualization of this process. This will help to develop new protocols not only based on parameters of treated samples but also through understanding of the behavior of the microorganisms, especially their attachment to particles and flow through the pore spaces during injections, and the interactions of $CaCO_3$ crystals with sand grains.

9 Limitations and challenges

Although there are promising results in laboratory and even field scale application of biocementation by MICP there are some issues that need to be addressed for a widespread use and acceptance of biocement in industrial scale. During ureolytic MICP ammonium is produced in high amounts as a by-product (see eq. 3-6). Ammonium can have a serious negative impact on the environment and human health. Although this might not be a problem for laboratory scale production of biosandstone a widespread application of MICP would lead to significant waste streams containing ammonium. A promising solution for this problem lies in the utilization of the mineral struvite ($NH_4MgPO_4 \cdot 6H_2O$). Yu et al. [86, 87] demonstrated that struvite precipitation can, similar to, $CaCO_3$ be induced by ureolytic microorganisms. For the biomineralization they used *Sporosarcina pasteurii* and a solution of $MgCl_2$, $K_2HPO_4 \cdot 3H_2O$ and urea. The precipitated struvite acts similar to $CaCO_3$ as a binder between particles. Instead of precipitating struvite directly in the sand Gowthaman et al. [88] treated the effluent of MICP experiments with Mg^{2+} and PO_4^{3-} and could achieve a reduction of around 90 % of ammonium from the effluent through struvite precipitation.

Other alternatives for the treatment of ammonium rich efflux could lie in treatment of the efflux by anaerobic ammonium oxidation [89] or the usage of zeolites during MICP to reduce the ammonia leakage [90]. In any case the utilization of ammonium

will be necessary for widespread application of MICP. The treatment of efflux during production of construction materials by MICP will generally be easier to handle than in other biomineralization applications like soil remediation where the ammonium will be directly released in the environment. Additionally, to the challenge of treating the toxic by-product during MICP the environmental impact needs to be kept low for a technology that is supposed to be an ecological alternative to conventional cement. In lab scale research on MICP for the cultivation of ureolytic microorganisms mainly lab grade chemicals like yeast extract or nutrient broth are used [59]. Since these chemicals are expensive a transition to industrial scale application of MICP will only be possible if suitable alternatives to these chemicals are found.

Although expensive, these cultivations usually lead to low or medium biomass concentrations. Lapierre et al. [91] studied the nutrient requirements of *Sporosarcina pasteurii* in a defined medium in detail and published a supplemented complex medium that lead to an increase of cell density of about 400 % by only increasing the price of the medium by about 4.3 %. Another approach to obtain biomass of *Sporosarcina pasteurii* is upcycling of waste streams for example diary and brewery waste [92, 93]. By combining the knowledge of suitable waste streams and nutrient requirements of the strains, protocols for cultivation of ureolytic bacteria can be improved which will help MICP to become a truly environmentally friendly alternative to conventional cementation processes. Also for calcium ions and urea cheap and environmentally compatible alternatives have to be found. While calcium chloride is a by-product of the Solvay synthesis and therefore readily available as a waste stream, urea from Haber-Bosch synthesis is highly energy dependent.

The usage of urine as urea source is a promising approach for another step towards an ecological process of MICP. Few studies have already started to investigate the process of MICP using urine from pigs [94], cows [95] and humans [96]. Seawater appears to be a source for free calcium. Although there is only a concentration of about 10 mM calcium in seawater, Cheng et al. [97] were able to stabilize sand up to an UCS of 300 kPa with seawater as sole calcium source. Yang et al. [98] used concentrated seawater and were able to consolidate sand columns with UCS of 653 kPa over a duration of 4.5 days. While the low concentrations of calcium ions in seawater might limit the possibility to achieve high compressive strengths over a

short duration of time that might be necessary for some applications these studies show the potential that seawater as the sole calcium source can have for MICP especially in marine environment. Another possible source are calcium ions from dissolved eggshells, oysters and scallops. During the process the calcium carbonate from these sources is dissolved in acid and afterwards the pH neutralized. Liang et al. [99] consolidated poorly graded sand and achieved UCS of 649.7 kPa with dissolved eggshells as sole calcium source. While these approaches are important for the overall development of the process there is still more research necessary concerning the basic mechanisms and influences of the cementation solution composition that can then be transferred towards more environmentally friendly sources of urea and calcium.

Besides the environmental impact of MICP there is another challenge in the biocementation itself. Most protocols for biocementation of sand show clogging to some degree during the process due to $CaCO_3$ crystals forming close to the injection points. This leads to an inhomogeneous distribution of $CaCO_3$ and compressive strength of the samples to a certain degree for all developed protocols [81, 46, 83, 84, 49]. Especially for the production of novel construction materials this issue needs to be addressed in the future. Standardized production and testing protocols will be necessary to transfer this technology to a larger scale and achieve widespread acceptance and implementation of MICP in the construction industry.

10 Concluding remarks and prospects for future work

While there is a lot of knowledge about influencing factors on the results of ureolytic MICP there is still the necessity of understanding these factors on an independent level. This is especially true for the influence of ureolytic activity on the result of MICP. There is sufficient evidence that the rate of ureolysis impacts the morphology and size of $CaCO_3$ crystals which again impacts mechanical parameters of treated samples. But this knowledge often derives from studies with varying biomass concentrations, bacterial strains, temperatures and compositions of cementation solution. These parameters impact the rate of ureolysis directly or indirectly. Ureolytic activity correlates directly with the biomass in the system. The specific ureolytic activity varies between ureolytic strains for example due to differences in enzyme expressions for urease or urea transporters. Temperature impacts the rate of

ureolysis just like any other enzymatically catalyzed reaction and calcium ions in certain concentrations can inhibit the rate of ureolysis. The separation of these parameters for example by the utilization of GMO´s is certainly a topic for future research that will benefit the development of MICP as a technology. An increase in the usage of GMO´s will also benefit understanding the basic processes during MICP. While it might be sufficient for a lot of experimental studies to monitor the rate of ureolysis through conductivity measurements or colorimetric assays to determine the rate of ammonium production there is still a gap in understanding the separate steps of the ureolysis starting with urea uptake of the cells up to the precipitation kinetics of $CaCO_3$ outside of the cell. Increasing the knowledge of these fundamental mechanisms will allow researchers to develop better kinetic models for MICP instead of relying on experimental observations.

During the past decades of research concerning ureolytic driven MICP the used strains were almost exclusively cultivated in complex medium. Optimization of cultivation media therefore happened mostly through supplementing complex media with cheap nutrient sources. The publication of a few studies on the cultivation of the most commonly used strain of *Sporosarcina. pasteurii* in defined media in the past years could be the base on which future research could improve the knowledge of the necessary components during cultivation of these strains. While the production of ureolytic microorganisms for MICP in defined medium will most likely not be possible due to the higher cost of these media this will help to move to a more structured approach for media optimization for example through the supplement of complex media with certain vitamins or amino acids. The treatment of ammonium as a toxic by-product is another problem that has to be solved on the adaptation of MICP as a technology. The utilization of ammonium ions through struvite precipitation is a promising technology that gained attention in recent years and deserve a closer look in future studies.

Although the usage of zeolites during MICP and the use of low phase injection seem to be able to reduce ammonia leakage during the treatment process significantly ammonium ions will still be leaked into the environment which would not solve the problem long term these technologies might still help to mitigate the ammonia leakage which could make a treatment of ammonium containing waste streams

through oxidation easier. Although there are still challenges and problems that need to be solved, MICP is a promising technology with a wide field of possible applications like improvement of existing construction materials, improving mechanical parameters of soils or the production of novel construction material. With increasing knowledge of the fundamental mechanisms and the utilization of cheap and environmentally friendly alternative resources in the coming years MICP can overcome these challenges and get closer to a widespread industrial application of the technology.

11 Acknowledgemnts

Funding

This project was financially supported by the Deutsche Forschungsgemeinschaft (DFG, German Research Foundation) – Project-ID 172116086 – SFB 926, the TU Nachwuchsring and the “Landespotentialbereich NanoKat”.

12 Compliance with Ethical Standards

Conflict of Interest

The authors have no relevant financial or non-financial interests to disclose

13 References

1. Gartner EM, Macphee DE (2011) A physico-chemical basis for novel cementitious binders. Cement and Concrete Research 41:736–749. https://doi.org/10.1016/j.cemconres.2011.03.006
2. Røyne A, Phua YJ, Balzer Le S et al. (2019) Towards a low CO2 emission building material employing bacterial metabolism (1/2): The bacterial system and prototype production. PLoS ONE 14:e0212990. https://doi.org/10.1371/journal.pone.0212990
3. Miller SA, Horvath A, Monteiro PJM (2018) Impacts of booming concrete production on water resources worldwide. Nat Sustain 1:69–76. https://doi.org/10.1038/s41893-017-0009-5
4. Mondal S, Ghosh A (2019) Review on microbial induced calcite precipitation mechanisms leading to bacterial selection for microbial concrete. Construction and Building Materials 225:67–75. https://doi.org/10.1016/j.conbuildmat.2019.07.122
5. Castanier S, Le Métayer-Levrel G, Perthuisot J-P (2000) Bacterial Roles in the Precipitation of Carbonate Minerals. In: Riding RE, Awramik SM (eds) Microbial Sediments, vol 5. Springer Berlin Heidelberg, Berlin, Heidelberg, pp 32–39
6. Muynck W de, Verbeken K, Belie N de et al. (2010) Influence of urea and calcium dosage on the effectiveness of bacterially induced carbonate precipitation on limestone. Ecological Engineering 36:99–111. https://doi.org/10.1016/j.ecoleng.2009.03.025
7. Dhami NK, Reddy MS, Mukherjee A (2013) Biomineralization of calcium carbonates and their engineered applications: a review. Front Microbiol 4:314. https://doi.org/10.3389/fmicb.2013.00314
8. Anbu P, Kang C-H, Shin Y-J et al. (2016) Formations of calcium carbonate minerals by bacteria and its multiple applications. Springerplus 5:250. https://doi.org/10.1186/s40064-016-1869-2
9. Hammes F, Verstraete W (2002) Key roles of pH and calcium metabolism in microbial carbonate precipitation. Rev Environ Sci Biotechnol 1:3–7. https://doi.org/10.1023/A:1015135629155

10. Domínguez DC (2018) Calcium Signaling in Prokaryotes. In J. N. Buchholz, & E. J. Behringer (Eds.), Calcium and Signal Transduction. IntechOpen. https://doi.org/10.5772/intechopen.78546
11. Nava AR, Mauricio N, Sanca AJ et al. (2020) Evidence of Calcium Signaling and Modulation of the LmrS Multidrug Resistant Efflux Pump Activity by Ca2 + Ions in S. aureus. Front Microbiol 11:573388. https://doi.org/10.3389/fmicb.2020.573388
12. Nasser AA, Sorour NM, Saafan MA et al. (2022) Microbially-Induced-Calcite-Precipitation (MICP): A biotechnological approach to enhance the durability of concrete using Bacillus pasteurii and Bacillus sphaericus. Heliyon 8:e09879. https://doi.org/10.1016/j.heliyon.2022.e09879
13. Wu C, Chu J, Wu S et al. (2019) Quantifying the Permeability Reduction of Biogrouted Rock Fracture. Rock Mech Rock Eng 52:947–954. https://doi.org/10.1007/s00603-018-1669-9
14. Kulkarni PB, Nemade PD, Wagh MP (2020) Healing of Generated Cracks in Cement Mortar Using MICP. Civ Eng J 6:679–692. https://doi.org/10.28991/cej-2020-03091500
15. Mondal S, Ghosh A (2018) Microbial Concrete as a Sustainable Option for Infrastructural Development in Emerging Economies:413–423. https://doi.org/10.1061/9780784482032.042
16. Sharma M, Satyam N, Reddy KR (2022) Liquefaction Resistance of Biotreated Sand Before and After Exposing to Weathering Conditions. Indian Geotech J 52:328–340. https://doi.org/10.1007/s40098-021-00576-x
17. Dagliya M, Satyam N, Sharma M et al. (2022) Experimental study on mitigating wind erosion of calcareous desert sand using spray method for microbially induced calcium carbonate precipitation. Journal of Rock Mechanics and Geotechnical Engineering. https://doi.org/10.1016/j.jrmge.2021.12.008
18. Strieth D (2022) Nachhaltigkeit in der Bioverfahrenstechnik. Chemie Ingenieur Technik 94:1061–1070. https://doi.org/10.1002/cite.202200053
19. Zhu T, Merroun ML, Arhonditsis G et al. (2021) Attachment on mortar surfaces by cyanobacterium Gloeocapsa PCC 73106 and sequestration of CO2 by microbially induced calcium carbonate. Microbiologyopen 10:e1243. https://doi.org/10.1002/mbo3.1243

20. Sidhu N, Goyal S, Reddy MS (2022) Biomineralization of cyanobacteria Synechocystis pevalekii improves the durability properties of cement mortar. AMB Express 12:59. https://doi.org/10.1186/s13568-022-01403-z
21. Zhu T, Paulo C, Merroun ML et al. (2015) Potential application of biomineralization by Synechococcus PCC8806 for concrete restoration. Ecological Engineering 82:459–468. https://doi.org/10.1016/j.ecoleng.2015.05.017
22. Dhami NK, Reddy MS, Mukherjee A (2014) Application of calcifying bacteria for remediation of stones and cultural heritages. Front Microbiol 5:304. https://doi.org/10.3389/fmicb.2014.00304
23. Zhao Y, Xiao Z, Lv J et al. (2019) A Novel Approach to Enhance the Urease Activity of Sporosarcina pasteurii and its Application on Microbial-Induced Calcium Carbonate Precipitation for Sand. Geomicrobiology Journal 36:819–825. https://doi.org/10.1080/01490451.2019.1631911
24. Ma L, Pang A-P, Luo Y et al. (2020) Beneficial factors for biomineralization by ureolytic bacterium Sporosarcina pasteurii. Microb Cell Fact 19:12. https://doi.org/10.1186/s12934-020-1281-z
25. Oualha M, Bibi S, Sulaiman M et al. (2020) Microbially induced calcite precipitation in calcareous soils by endogenous Bacillus cereus, at high pH and harsh weather. Journal of Environmental Management 257:109965. https://doi.org/10.1016/j.jenvman.2019.109965
26. Mukherjee S, Sahu RB, Mukherjee J (2022) Effect of Biologically Induced Cementation via Ureolysis in Stabilization of Silty Soil. Geomicrobiology Journal 39:66–82. https://doi.org/10.1080/01490451.2021.2005188
27. Stocks-Fischer S, Galinat JK, Bang SS (1999) Microbiological precipitation of CaCO3. Soil Biology and Biochemistry 31:1563–1571. https://doi.org/10.1016/S0038-0717(99)00082-6
28. Jin C, Liu H, Guo M et al. (2022) Experimental study on tailings cementation by MICP technique with immersion curing. PLoS ONE 17:e0272281. https://doi.org/10.1371/journal.pone.0272281
29. Hamdan N, Kavazanjian E, Rittmann BE et al. (2017) Carbonate Mineral Precipitation for Soil Improvement Through Microbial Denitrification.

Geomicrobiology Journal 34:139–146. https://doi.org/10.1080/01490451.2016.1154117

30. Erşan YÇ, Verbruggen H, Graeve I de et al. (2016) Nitrate reducing CaCO3 precipitating bacteria survive in mortar and inhibit steel corrosion. Cement and Concrete Research 83:19–30. https://doi.org/10.1016/j.cemconres.2016.01.009
31. Jiang N, Tang C-S, Yin L et al. (2019) Applicability of Microbial Calcification Method for Sandy-Slope Surface Erosion Control. J Mater Civ Eng 31:4019250. https://doi.org/10.1061/(ASCE)MT.1943-5533.0002897
32. Dhami NK (2013) Biomineralization of Calcium Carbonate Polymorphs by the Bacterial Strains Isolated from Calcareous Sites. Journal of Microbiology and Biotechnology 23:707–714. https://doi.org/10.4014/jmb.1212.11087
33. Zhang C, Li X, Lyu J et al. (2020) Comparison of carbonate precipitation induced by Curvibacter sp. HJ-1 and Arthrobacter sp. MF-2: Further insight into the biomineralization process. J Struct Biol 212:107609. https://doi.org/10.1016/j.jsb.2020.107609
34. Farajnia A, Shafaat A, Farajnia S et al. (2022) The efficiency of ureolytic bacteria isolated from historical adobe structures in the production of bio-bricks. Construction and Building Materials 317:125868. https://doi.org/10.1016/j.conbuildmat.2021.125868
35. Ezzat SM, Ewida AYI (2021) Smart soil grouting using innovative urease-producing bacteria and low cost materials. Journal of Applied Microbiology 131:2294–2307. https://doi.org/10.1111/jam.15117
36. Stabnikov V, Jian C, Ivanov V et al. (2013) Halotolerant, alkaliphilic urease-producing bacteria from different climate zones and their application for biocementation of sand. World Journal of Microbiology and Biotechnology 29:1453–1460. https://doi.org/10.1007/s11274-013-1309-1
37. Konstantinou C, Wang Y, Biscontin G et al. (2021) The role of bacterial urease activity on the uniformity of carbonate precipitation profiles of bio-treated coarse sand specimens. Scientific reports 11:6161. https://doi.org/10.1038/s41598-021-85712-6

38. Liang L, Heveran C, Liu R et al. (2018) Rational Control of Calcium Carbonate Precipitation by Engineered Escherichia coli. ACS Synth Biol 7:2497–2506. https://doi.org/10.1021/acssynbio.8b00194
39. Heveran CM, Liang L, Nagarajan A et al. (2019) Engineered Ureolytic Microorganisms Can Tailor the Morphology and Nanomechanical Properties of Microbial-Precipitated Calcium Carbonate. Scientific reports 9:14721. https://doi.org/10.1038/s41598-019-51133-9
40. Murugan R, Suraishkumar GK, Mukherjee A et al. (2021) Insights into the influence of cell concentration in design and development of microbially induced calcium carbonate precipitation (MICP) process. PLoS ONE 16:e0254536. https://doi.org/10.1371/journal.pone.0254536
41. Wang Y, Soga K, DeJong JT et al. (2021) Effects of Bacterial Density on Growth Rate and Characteristics of Microbial-Induced CaCO3 Precipitates: Particle-Scale Experimental Study. J Geotech Geoenviron Eng 147. https://doi.org/10.1061/(ASCE)GT.1943-5606.0002509
42. Cheng L, Shahin MA, Mujah D (2017) Influence of Key Environmental Conditions on Microbially Induced Cementation for Soil Stabilization. J Geotech Geoenviron Eng 143:4016083. https://doi.org/10.1061/(ASCE)GT.1943-5606.0001586
43. Muynck W de, Belie N de, Verstraete W (2010) Microbial carbonate precipitation in construction materials: A review. Ecological Engineering 36:118–136. https://doi.org/10.1016/j.ecoleng.2009.02.006
44. Ghosh T, Bhaduri S, Montemagno C et al. (2019) Sporosarcina pasteurii can form nanoscale calcium carbonate crystals on cell surface. PLoS ONE 14:e0210339. https://doi.org/10.1371/journal.pone.0210339
45. Seifan M, Samani AK, Berenjian A (2016) Bioconcrete: next generation of self-healing concrete. Appl Microbiol Biotechnol 100:2591–2602. https://doi.org/10.1007/s00253-016-7316-z
46. Zhao Q, Li L, Li C et al. (2014) A Full Contact Flexible Mold for Preparing Samples Based on Microbial-Induced Calcite Precipitation Technology. Geotech Test J 37:20130090. https://doi.org/10.1520/GTJ20130090

47. Okwadha GD, Li J (2010) Optimum conditions for microbial carbonate precipitation. Chemosphere 81:1143–1148. https://doi.org/10.1016/j.chemosphere.2010.09.066
48. Whiffin (2004) High strength in-situ biocementation of soil by calcite precipitating locally isolated ureolytic bacteria. Dissertation, Murdoch University
49. Cheng L, Shahin MA, Chu J (2019) Soil bio-cementation using a new one-phase low-pH injection method. Acta Geotech 14:615–626. https://doi.org/10.1007/s11440-018-0738-2
50. Lai Y, Yu J, Liu S et al. (2021) Experimental study to improve the mechanical properties of iron tailings sand by using MICP at low pH. Construction and Building Materials 273:121729. https://doi.org/10.1016/j.conbuildmat.2020.121729
51. Lauchnor EG, Topp DM, Parker AE et al. (2015) Whole cell kinetics of ureolysis by Sporosarcina pasteurii. Journal of Applied Microbiology 118:1321–1332. https://doi.org/10.1111/jam.12804
52. Mitchell AC, Espinosa-Ortiz EJ, Parks SL et al. (2019) Kinetics of calcite precipitation by ureolytic bacteria under aerobic and anaerobic conditions. Biogeosciences, 16(10), 2147-2161. https://doi.org/10.5194/BG-16-2147-2019
53. Sridhar S, Bhatt N, Suraishkumar GK (2021) Mechanistic insights into ureolysis mediated calcite precipitation. Biochemical Engineering Journal 176:108214. https://doi.org/10.1016/j.bej.2021.108214
54. Kim G, Kim J, Youn H (2018) Effect of Temperature, pH, and Reaction Duration on Microbially Induced Calcite Precipitation. Applied Sciences 8:1277. https://doi.org/10.3390/app8081277
55. Wang Y, Soga K, DeJong JT et al. (2019) A microfluidic chip and its use in characterising the particle-scale behaviour of microbial-induced calcium carbonate precipitation (MICP). Géotechnique 69:1086–1094. https://doi.org/10.1680/jgeot.18.P.031
56. Wang Y, Wang Y, Soga K et al. (2022) Microscale investigations of temperature-dependent microbially induced carbonate precipitation (MICP) in the temperature range 4–50 °C. Acta Geotech. https://doi.org/10.1007/s11440-022-01664-9

57. Amini Kiasari M, Pakbaz MS, Ghezelbash GR (2019) Comparison of Effects of Different Nutrients on Stimulating Indigenous Soil Bacteria for Biocementation. J Mater Civ Eng 31:4019067. https://doi.org/10.1061/(ASCE)MT.1943-5533.0002693
58. Qian C, Ren X, Rui Y et al. (2021) Characteristics of bio-CaCO3 from microbial bio-mineralization with different bacteria species. Biochemical Engineering Journal 176:108180. https://doi.org/10.1016/j.bej.2021.108180
59. Omoregie AI, Ngu LH, Ong DEL et al. (2019) Low-cost cultivation of Sporosarcina pasteurii strain in food-grade yeast extract medium for microbially induced carbonate precipitation (MICP) application. Biocatalysis and Agricultural Biotechnology 17:247–255. https://doi.org/10.1016/j.bcab.2018.11.030
60. Qabany A, Soga K (2013) Effect of chemical treatment used in MICP on engineering properties of cemented soils. Géotechnique 63:331–339. https://doi.org/10.1680/geot.SIP13.P.022
61. Sotoudehfar AR, Mirmohammad sadeghi M, Mokhtari E et al. (2016) Assessment of the Parameters Influencing Microbial Calcite Precipitation in Injection Experiments Using Taguchi Methodology. Geomicrobiology Journal 33:163–172. https://doi.org/10.1080/01490451.2015.1025316
62. Han P-P, Geng W-J, Li M-N et al. (2021) Improvement of Biomineralization of Sporosarcina pasteurii as Biocementing Material for Concrete Repair by Atmospheric and Room Temperature Plasma Mutagenesis and Response Surface Methodology. Journal of Microbiology and Biotechnology 31:1311–1322. https://doi.org/10.4014/jmb.2104.04019
63. Rahman MM, Hora RN, Ahenkorah I et al. (2020) State-of-the-Art Review of Microbial-Induced Calcite Precipitation and Its Sustainability in Engineering Applications. Sustainability 12:6281. https://doi.org/10.3390/su12156281
64. Ashraf MS, Hassan Shah MU, Bokhari A et al. (2021) Less is more: Optimising the biocementation of coastal sands by reducing influent urea through response surface method. Journal of Cleaner Production 315:128208. https://doi.org/10.1016/j.jclepro.2021.128208
65. Onal Okyay T, Frigi Rodrigues D (2014) Optimized carbonate micro-particle production by Sporosarcina pasteurii using response surface methodology.

Ecological Engineering 62:168–174. https://doi.org/10.1016/j.ecoleng.2013.10.024
66. Erdmann N, Payrebrune KM de, Ulber R et al. (2022) Optimizing compressive strength of sand treated with MICP using response surface methodology. SN Appl Sci 4. https://doi.org/10.1007/s42452-022-05169-8
67. Achal V, Pan X (2014) Influence of Calcium Sources on Microbially Induced Calcium Carbonate Precipitation by Bacillus sp. CR2. Applied Biochemistry and Biotechnology 173:307–317. https://doi.org/10.1007/s12010-014-0842-1
68. Zhang Y, Guo HX, Cheng XH (2015) Role of calcium sources in the strength and microstructure of microbial mortar. Construction and Building Materials 77:160–167. https://doi.org/10.1016/j.conbuildmat.2014.12.040
69. Xiang J, Qiu J, Wang Y et al. (2022) Calcium acetate as calcium source used to biocement for improving performance and reducing ammonia emission. Journal of Cleaner Production 348:131286. https://doi.org/10.1016/j.jclepro.2022.131286
70. Lv C, Tang C-S, Zhang J-Z et al. (2022) Effects of calcium sources and magnesium ions on the mechanical behavior of MICP-treated calcareous sand: experimental evidence and precipitated crystal insights. Acta Geotech. https://doi.org/10.1007/s11440-022-01748-6
71. Peng J, Cao T, He J et al. (2022) Improvement of Coral Sand With MICP Using Various Calcium Sources in Sea Water Environment. Front Phys 10. https://doi.org/10.3389/fphy.2022.825409
72. Mitchell JK, Santamarina JC (2005) Biological Considerations in Geotechnical Engineering. J Geotech Geoenviron Eng 131:1222–1233. https://doi.org/10.1061/(ASCE)1090-0241(2005)131:10(1222)
73. Rebeta-Landa V (2007) Microbial Activity in Sediments: Effects on Soil Behavior. Dissertation, Georgia Institute of Technology
74. Dhami NK, Reddy MS, Mukherjee A (2016) Significant indicators for biomineralisation in sand of varying grain sizes. Construction and Building Materials 104:198–207. https://doi.org/10.1016/j.conbuildmat.2015.12.023
75. Cheshomi A, Mansouri S (2020) Study the grain size and infiltration method effects for sand soil improvement using the microbial method. Geomicrobiology Journal 37:355–365. https://doi.org/10.1080/01490451.2019.1705437

76. Konstantinou C, Biscontin G, Jiang N et al. (2021) Application of microbially induced carbonate precipitation to form bio-cemented artificial sandstone. Journal of Rock Mechanics and Geotechnical Engineering 13:579–592. https://doi.org/10.1016/j.jrmge.2021.01.010
77. Mahawish A, Bouazza A, Gates WP (2018) Effect of particle size distribution on the bio-cementation of coarse aggregates. Acta Geotech 13:1019–1025. https://doi.org/10.1007/s11440-017-0604-7
78. Rowshanbakht K, Khamehchiyan M, Sajedi RH et al. (2016) Effect of injected bacterial suspension volume and relative density on carbonate precipitation resulting from microbial treatment. Ecological Engineering 89:49–55. https://doi.org/10.1016/j.ecoleng.2016.01.010
79. Gao Y, Hang L, He J et al. (2019) Mechanical behaviour of biocemented sands at various treatment levels and relative densities. Acta Geotech 14:697–707. https://doi.org/10.1007/s11440-018-0729-3
80. Whiffin VS, van Paassen LA, Harkes MP (2007) Microbial Carbonate Precipitation as a Soil Improvement Technique. Geomicrobiology Journal 24:417–423. https://doi.org/10.1080/01490450701436505
81. Cheng L, Cord-Ruwisch R (2012) In situ soil cementation with ureolytic bacteria by surface percolation. Ecological Engineering 42:64–72. https://doi.org/10.1016/j.ecoleng.2012.01.013
82. Mortensen BM, Haber MJ, DeJong JT et al. (2011) Effects of environmental factors on microbial induced calcium carbonate precipitation. Journal of Applied Microbiology 111:338–349. https://doi.org/10.1111/j.1365-2672.2011.05065.x
83. Wen K, Li Y, Amini F et al. (2020) Impact of bacteria and urease concentration on precipitation kinetics and crystal morphology of calcium carbonate. Acta Geotech 15:17–27. https://doi.org/10.1007/s11440-019-00899-3
84. Cheng L, Shahin MA (2016) Urease active bioslurry: a novel soil improvement approach based on microbially induced carbonate precipitation. Can Geotech J 53:1376–1385. https://doi.org/10.1139/cgj-2015-0635
85. Nething C, Smirnova M, Gröning JA et al. (2020) A method for 3D printing bio-cemented spatial structures using sand and urease active calcium carbonate

powder. Materials & Design 195:109032. https://doi.org/10.1016/j.matdes.2020.109032
86. Yu X, Qian C, Xue B (2016) Loose sand particles cemented by different bio-phosphate and carbonate composite cement. Construction and Building Materials 113:571–578. https://doi.org/10.1016/j.conbuildmat.2016.03.105
87. Yu X, Qian C, Sun L (2018) The influence of the number of injections of bio-composite cement on the properties of bio-sandstone cemented by bio-composite cement. Construction and Building Materials 164:682–687. https://doi.org/10.1016/j.conbuildmat.2018.01.014
88. Gowthaman S, Mohsenzadeh A, Nakashima K et al. (2022) Removal of ammonium by-products from the effluent of bio-cementation system through struvite precipitation. Materials Today: Proceedings 61:243–249. https://doi.org/10.1016/j.matpr.2021.09.013
89. Mao N, Ren H, Geng J et al. (2017) Engineering application of anaerobic ammonium oxidation process in wastewater treatment. World journal of microbiology & biotechnology 33:153. https://doi.org/10.1007/s11274-017-2313-7
90. Su F, Yang Y, Qi Y et al. (2022) Combining microbially induced calcite precipitation (MICP) with zeolite: A new technique to reduce ammonia emission and enhance soil treatment ability of MICP technology. Journal of Environmental Chemical Engineering 10:107770. https://doi.org/10.1016/j.jece.2022.107770
91. Lapierre FM, Schmid J, Ederer B et al. (2020) Revealing nutritional requirements of MICP-relevant Sporosarcina pasteurii DSM33 for growth improvement in chemically defined and complex media. Scientific reports 10:22448. https://doi.org/10.1038/s41598-020-79904-9
92. Cuzman OA, Richter K, Wittig L et al. (2015) Alternative nutrient sources for biotechnological use of Sporosarcina pasteurii. World journal of microbiology & biotechnology 31:897–906. https://doi.org/10.1007/s11274-015-1844-z
93. Kahani M, Kalantary F, Soudi MR et al. (2020) Optimization of cost effective culture medium for Sporosarcina pasteurii as biocementing agent using response surface methodology: Up cycling dairy waste and seawater. Journal of Cleaner Production 253:120022. https://doi.org/10.1016/j.jclepro.2020.120022

94. Chen H-J, Huang Y-H, Chen C-C et al. (2019) Microbial Induced Calcium Carbonate Precipitation (MICP) Using Pig Urine as an Alternative to Industrial Urea. Waste Biomass Valor 10:2887–2895. https://doi.org/10.1007/s12649-018-0324-8
95. Comadran-Casas C, Schaschke CJ, Akunna JC et al. (2022) Cow urine as a source of nutrients for Microbial-Induced Calcite Precipitation in sandy soil. Journal of Environmental Management 304:114307. https://doi.org/10.1016/j.jenvman.2021.114307
96. Lambert SE, Randall DG (2019) Manufacturing bio-bricks using microbial induced calcium carbonate precipitation and human urine. Water Research 160:158–166. https://doi.org/10.1016/j.watres.2019.05.069
97. Cheng, L., Shahin, M., Cord-Ruwisch, R., Addis, M., Hartanto, T., Elms, C. (2014) Soil Stabilisation by Microbial-Induced Calcite Precipitation (MICP): Investigation into Some Physical and Environmental Aspects. 7th International Congress on Environmental Geotechnics:pp. 1105–1112
98. Yang S-M, Peng J, Wen Z-L et al. (2021) Application of concentrated seawater as calcium source solution in sand reinforcement using MICP. Yantu Lixue/Rock and Soil Mechanics 42:746–754. https://doi.org/10.16285/j.rsm.2020.0424
99. Liang S, Chen J, Niu J et al. (2020) Using recycled calcium sources to solidify sandy soil through microbial induced carbonate precipitation. Marine Georesources & Geotechnology 38:393–399. https://doi.org/10.1080/1064119X.2019.1575939

III Investigating the Influential Factors on Microbially Induced Calcium Carbonate Precipitation: Effects of Cell Density, Temperature, and Calcium Concentration

N. Erdmann[1], K. Aldabbousi[1], D. Strieth[1]

[1]University of Kaiserslautern-Landau, Chair of Bioprocess Engineering, Kaiserslautern, Germany

Discover Applied Sciences 7, 696 (2025)
https://doi.org/10.1007/s42452-025-06881-x

Author Contribution:

N. Erdmann	Methodology, Project administration, visualization, writing, Data acquisition for figure (2, 3, 5, 6, 8,9) and table (2, 3) Data curation and analysis (all data)
K. Aldabbousi	Methodology, Data acquisition for figure 4 and figure 7
D. Strieth	Funding acquisition, supervision, review&editing

Keywords: microbially induced calcium carbonate precipitation (MICP), ureolysis, *Sporosarcina pasteurii*, calcium concentration, cell density, temperatures,

Abstract

This study investigates the impact of key parameters—bacterial cell density, calcium ion concentration, and ambient temperature—on the kinetics and outcomes of Microbially Induced Calcium Carbonate Precipitation (MICP) using *Sporosarcina pasteurii*. By extending reaction conditions to cell density up to OD_{600}=30, urea and calcium concentrations up to 4.5 M, and a temperature range of 4 to 75 °C, this research provides insights into the boundaries of MICP's efficiency. Zero order reaction kinetics were determined by monitoring free NH_4^+ and Ca^{2+} during MICP through ion exchange chromatography and the resulting precipitate was characterized by Fourier-transform infrared spectroscopy and microscopical imaging. Reaction kinetics demonstrated a linear correlation between cell density and ureolysis (k_{urea}) and calcium carbonate precipitation ($k_{calcium}$,) with high densities driving rapid reaction rates. Optimal precipitation rates occurred at 45 °C, beyond which thermal deactivation of urease impeded MICP. High calcium concentrations increased calcium carbonate yield but required elevated cell densities to mitigate inhibitory effects of Ca^{2+}. Morphological and polymorphic shifts in calcium carbonate crystals were observed, transitioning from calcite at standard conditions to vaterite and aragonite under extreme scenarios (Cell density of OD_{600}=30 and 65 °C respectively). These findings underscore the multi-factorial dependencies of MICP and highlight upper boundaries of these parameters for process optimization.

Article Highlights

- Ureolytic activity is the primary driver of MICP reaction rates, irrespective of experimental conditions.
- Higher cell densities accelerate reaction rates, with no saturation observed up to OD_{600}=30.
- Temperature strongly influences MICP, with optimal reaction rates at 45°C and no activity above 75°C.
- Calcium chloride concentrations up to 4 $mol \cdot L^{-1}$ are effective for MICP, with cell density mitigating inhibitory effects from calcium ions.

1 Introduction

Over the past two decades, Microbially Induced Calcium Carbonate Precipitation (MICP) has become a prominent research focus, offering applications that span soil stabilization, eco-friendly construction, and environmental remediation [1]. MICP can occur via multiple biological pathways, with ureolysis being the most widely studied due to its speed and reliability [2, 3] Urease (EC 3.5.1.5) catalyses the hydrolysis of urea into ammonium and carbonate ions (Eqs. 1-4). In the presence of calcium ions (e.g., from calcium chloride) and an alkaline environment, the carbonate ions precipitate as calcium carbonate ($CaCO_3$) (Eqs. 5-6). Like cement the $CaCO_3$ crystals then act as a binder between particles, like cement.

$$CO(NH_2)_2 + H_2O \rightarrow NH_2COOH + NH_3 \quad (1)$$

$$NH_2COOH + H_2O \rightleftharpoons H_2CO_3 + NH_3 \quad (2)$$

$$2NH_3 + 2H_2O \rightleftharpoons 2NH_4^+ + 2OH^- \quad (3)$$

$$2OH^- + H_2CO_3 \rightleftharpoons CO_3^{2-} + 2H_2O \quad (4)$$

$$Ca^{2+} + CO_3^{2-} \rightarrow 2NH_4^+ + CaCO_3 \quad (5)$$

$$CO(NH_2)_2 + 2H_2O + Ca^{2+} \rightarrow 2NH_4^+ + CaCO_3 \quad (6)$$

MICP has several applications e.g. soil strengthening against erosion and liquefaction, production of novel construction materials (Bio-bricks), as self-healing concrete or for heavy metal remediation in soil and water [4, 5]. These processes often need soils or sand treated with multiple cycles of a suspension containing ureolytic microorganisms and a solution containing urea and a calcium salt to achieve carbonate precipitation. With each cycle more calcium carbonate is formed and therefore the bonds between particles get stronger and the material more durable. This phenomenon was observed in various studies which concluded that with increasing calcium carbonate content the strength of biocemented sand increases [6]. One of the most important drawbacks of ureolytic MICP is its by-product ammonium, which can pollute the environment. During the MICP it is therefore of great importance to give the reaction enough time between the cycles to achieve high conversion rates. A loss in efficiency results in more urea and calcium salts being introduced into the environment. Knowledge about the speed of ureolysis and calcium carbonate precipitation are therefore mandatory to determine correct incubation times between these cycles. The rate of ureolysis and the precipitation

process is dependent on several biological, chemical and physical factors like cell density, urea and calcium concentration, pH, temperature [1, 7]. Depending on the application of MICP these parameters can widely vary. Temperatures during soil stabilisation for example could vary between 10 °C [8] for treatment of soil in shallow seabeds in winter and temperatures of up to 50 °C in arid regions [9]. Chemical composition of the cementation solution can vary greatly depending on the environment in which MICP is conducted. Low concentrations of urea and calcium chloride between 0.01 and 0.1 $mol \cdot L^{-1}$ are necessary in environments with fragile ecosystems like coastal areas [10] while studies that focus on the highest achievable compressive strength under laboratory conditions use concentrations above 1 M urea and calcium chloride and report best results for concentrations above 2.5 $mol \cdot L^{-1}$ [11] or 3 $mol \cdot L^{-1}$ [12]. Several studies investigated MICP reaction speed for the most used ureolytic microorganism *Sporosarcina pasteurii.*

Table 1: Overview of studies on reaction rates of ureolysis and calcium carbonate precipitation during MICP with Sporosarcina pasteurii. RT=Room temperature. M-M=Michaelis-Menten

Temperature in °C	[Urea] in mM	$[Ca^{2+}]$ in mM	OD_{600}	Kinetics	Reference
30	333	25.2	0.014	First-order	Mitchell et al. 2019 [13]
20	50-500	250-500	0.07	First-order	Tobler et al. 2011[14]
30	333	0	0,1	M-M	Lauchnor et al. 2015 [15]
25	666	250	0.18	First-order	Okwadha and Li 2010[16]
20	6	0	0.07	First-order	Ferris et al. 2004 [17]
RT	500	500	0.5	Zero-order	Murugan et al. 2021[18]
30	1000	1000	1.14	M-M	Jain et al. 2024 [7]
5-70	500	750	1	Zero-order	Wang et al. 2022 [9]

For most studies that investigated MICP reactions speed, concentration of cementation solution ranges up to 1 mol·L^{-1} urea and 1 mol·L^{-1} calcium and cell densities are used at the lower end of up to OD_{600}=1.14 (Table 1). The experiments are often resembled at room temperature. Wang et al [9] being the only exception, investigating the influence of temperature on MICP kinetics of *S. pasteurii* over a wide temperature range (5-70 °C). Depending on urea concentration the order of enzyme kinetics assumed in these studies varies.

Studies of whole cell kinetics from *S. pasteurii* revealed that between an urea concentration of 300 to 400 mmol·L^{-1} the behaviour transitions from first order to zero order kinetics [15, 7]. While all these studies give us a good understanding how MICP behaves at low to medium concentrations of cementation solution, cell densities and temperatures, there is still a gap in knowledge towards the higher ends of these parameters. Due to the biological nature of MICP, it is expected that the use of higher temperatures and higher cell densities could lead to significantly faster reaction rates. High concentrations of calcium and urea are expected to result in higher mass of calcium carbonate precipitated during MICP treatment cycles subsequently decreasing the necessary number of cycles to achieve suitable degrees of cementation. In this study optical density of up to OD_{600}=30, urea and calcium concentrations up to 4.5 M and a temperature range from 4 up to 75 °C was investigated. Due to the high urea concentration's reaction rates were calculated based on zero-order kinetics.

Besides reaction rate of ureolysis and calcium carbonate precipitation, crystal size and morphology of the precipitated calcium carbonate was investigated by microscopy and Fourier transform infrared spectroscopy (FTIR). Knowledge of these process conditions will help to broaden our understanding of MICP and can be used to set the stage for future optimisation studies on MICP by providing knowledge about the boundaries of MICP.

2 Material and Methods

2.1 Preparation of Sporosarcina pasteurii cells

Sporosarcina pasteurii (DSM 33; ATCC 11859) was acquired from the German Collection of Microorganisms and Cell Cultures (DSMZ). The strain was cultivated under sterile conditions in a medium containing 20 $g \cdot L^{-1}$ yeast extract (YE) (Carl Roth, Germany), 10 $g \cdot L^{-1}$ Glucose (Carl Roth, Germany) and 20 $g \cdot L^{-1}$ Urea (Fischer Scientific, USA) in 15.75 $g \cdot L^{-1}$ TRIS Buffer pH 9.25 (Carl Roth, Germany). The medium was freshly prepared and filter sterilized (Steritop 0.22 µm, Merck, Germany) before each experiment. For cultivation 300 mL Erlenmeyer flasks were aseptically filled with 50 mL of sterile medium and inoculated with a stock of cryo preserved *S. pasteurii* cells (15 % glycerol in culture medium, OD_{600}=1.5, -80 °C). Cell density was measured as OD_{600} with an UV-Vis spectrophotometer at a wavelength of 600 nm. If an OD_{600} of 0.9 or higher was measured the samples was diluted with 0.9 % NaCl and measurement repeated. The culture was then inoculated at 30 °C and 250 rpm until late exponential phase was reached. Afterwards the cells were centrifuged (Mega Star 1.6 R, VWR, USA) at 3005 g and 4 °C for 10 minutes and subsequently washed with 0.9 % NaCl solution. This process was repeated three times to get rid of residues from cultivation media. During the third washing step the cell density was diluted in 0.9 % NaCl as necessary to achieve the desired OD_{600}.

2.2 Composition of cementation solution

During all experiments cementation solution (CS) contained urea (Fischer Scientific, USA) and calcium chloride (Carl Roth, Germany) of analytical grade quality in varying concentrations. Before each experiment the components were dissolved overnight in distilled water at 25 °C.

2.3 Gravimetrical determination of precipitation efficiency

15 mL centrifuge tubes (Greiner, Austria) were oven dried (60 °C, 24 h) and cooled down in a desiccator (30 min). The weight of the tube was noted. Afterwards the tubes were filled with 5 mL of washed cell suspension with a desired cell density and 5 mL of CS. The tubes were then incubated at 30 °C for 48 hours. After incubation, the tubes were centrifuged (3005 g, 4 °C, 10 minutes) and washed three times with

distilled water. The precipitate was then oven dried for 48 hours at 60 °C, cooled down in a desiccator (30 min) and the weight of the tube noted. By subtracting the weight of the tube, the amount of precipitated calcium carbonate was determined.

2.4 Determination of kinetic parameters of MICP

Bacterial suspension (BS) and cementation solution (CS) were prepared as described in section 2.1 and 2.2. Then 7.5 mL of BS and CS were combined in 15 mL centrifuge tubes and inoculated under varying conditions (Figure 1). During each experiment the tubes were shaken in an overhead shaker at 20 rpm. The sole exception for this being the temperature dependent experiment. During these experiments the tubes were only shaken at each sampling time 30 seconds at 20 rpm in the overhead shaker. For sampling 300 µL were extracted with a 2 mL syringe and immediately filtered (Chromafil Xtra PA-20/13 0.2 µm) to separate the catalyst (cells) from the sample and thereby stop the reaction. The filtrate was then frozen in liquid nitrogen to stop any further reaction that might occur due leaked free urease from damaged bacteria cells. After the last sampling the residue precipitate was washed and centrifuged as described in section 2.3 for microscopy and FTIR analysis.

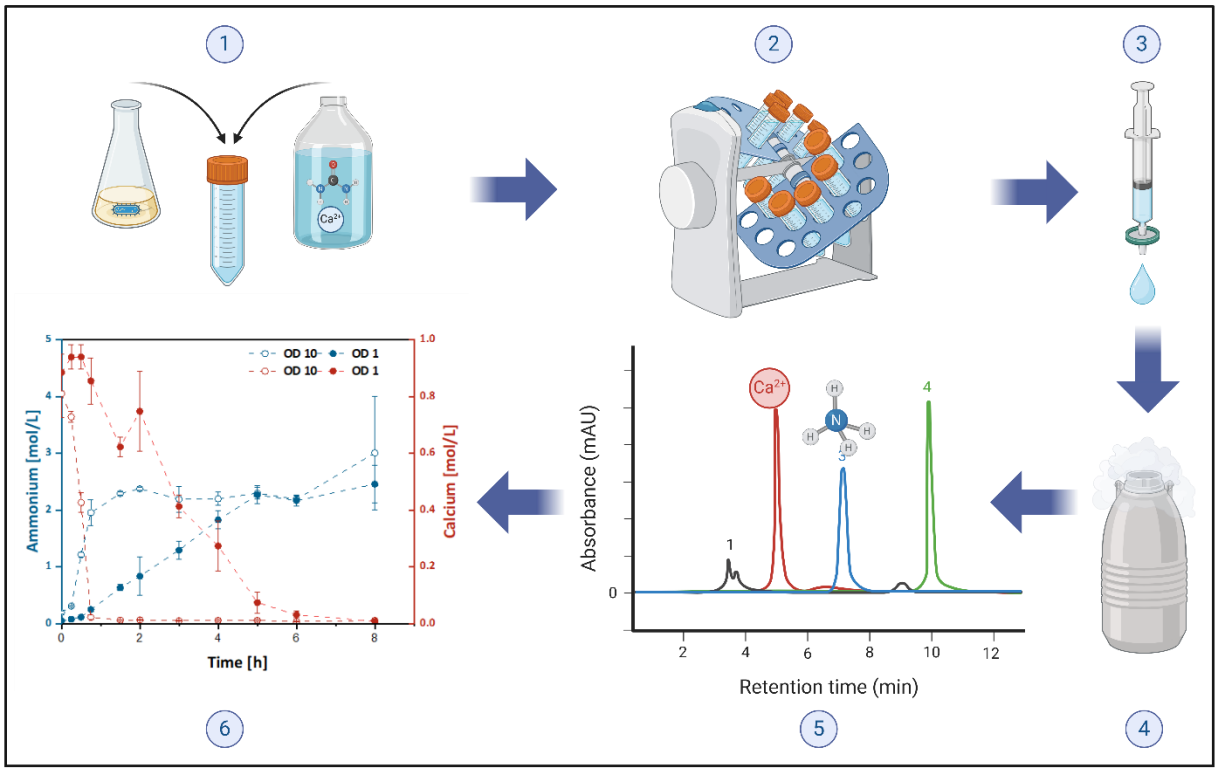

Figure 1: Overview of the determination of kinetic parameters during MICP. (1) Mixing of bacterial solution (BS) and cementation solution (CS), (2) Incubation, (3) Sampling and sterile filtration, (4) Freezing in liquid nitrogen, (5) Determination of Ca^{2+} and NH_4^+ through IEX, (6) Calculation of k values

Ammonium and calcium ions were determined by ion exchange chromatography as described in section 2.5. Zero-order reaction rate for calcium precipitation ($k_{calcium}$) were calculated from the linear part of the decline from free calcium ions over time under the assumption that a decline in free calcium ion was the result of calcium carbonate precipitation. Zero-order reaction rate for ureolysis (k_{urea}) was determined from the linear part of the ammonium increase under the assumption that two mol of formed free ammonia correspond to one mol of hydrolysed urea (Eq. 6)

2.5 Determination of ammonium and calcium ions

For ion exchange chromatography (IEX) (930 Compact IC Flex, METROHM GmbH & Co. KG) samples were diluted in 2 mM nitric acid (HNO_3). The samples passed a precolumn ((Metrosept C4 Guart/4.0) followed by the main column (Metrosept C4-250/4.0). Elution from the column was realised with 1.7 mM HNO_3 and 0.7 mM dipicolinic acid in ultrapure water at a flow rate of 0.9 mL· min^{-1}. A conductivity sensor was used, and determination of ammonium and calcium ions was realised through a standard calibration in the range of 0.1-100 mg·L^{-1} (Ammonium) and 0.5-100 mg·L^{-1} (Calcium).

2.6 Analysis of the crystal structure and determination of the polymorph

Washed and dried precipitates were distributed evenly at a glass slide and microscopic images taken with a digital reflective-light microscope (VHX 7000, KEYENCE, Japan) at different levels of magnification. For determination of the calcium carbonate polymorph Fourier-transform infrared spectroscopy was used (Spektrum 100, Perkin Elmer, USA). Characteristic peaks for Calcite, Vaterite and Aragonite were taken from literature [19, 20] and compared with the spectrograms obtained from the samples.

3 Results

3.1 Impact of bacterial density

The impact of the concentration of the catalyst (bacterial density) on the reaction speed of MICP was investigated for cell densities of BS between OD_{600}=1 and OD_{600}=30 and an equimolar concentration of 2 mol·L^{-1} urea and calcium chloride in the CS. During all experiments NH_4^+ concentration increased due to urea degradation (Figure 2 A) while simultaneously Ca^{2+} concentration decreased due to calcium carbonate precipitation (Figure 2 B). k_{urea} increased from 0.019±0.002 and 1.621±0.053 mol·L^{-1}·h^{-1} for OD_{600}=1 and 30 respectively. Similarly, $k_{calcium}$ increased from 0.022 ± 0.005 to 1.502±0.110 mol·L^{-1}·h^{-1} in the same range.

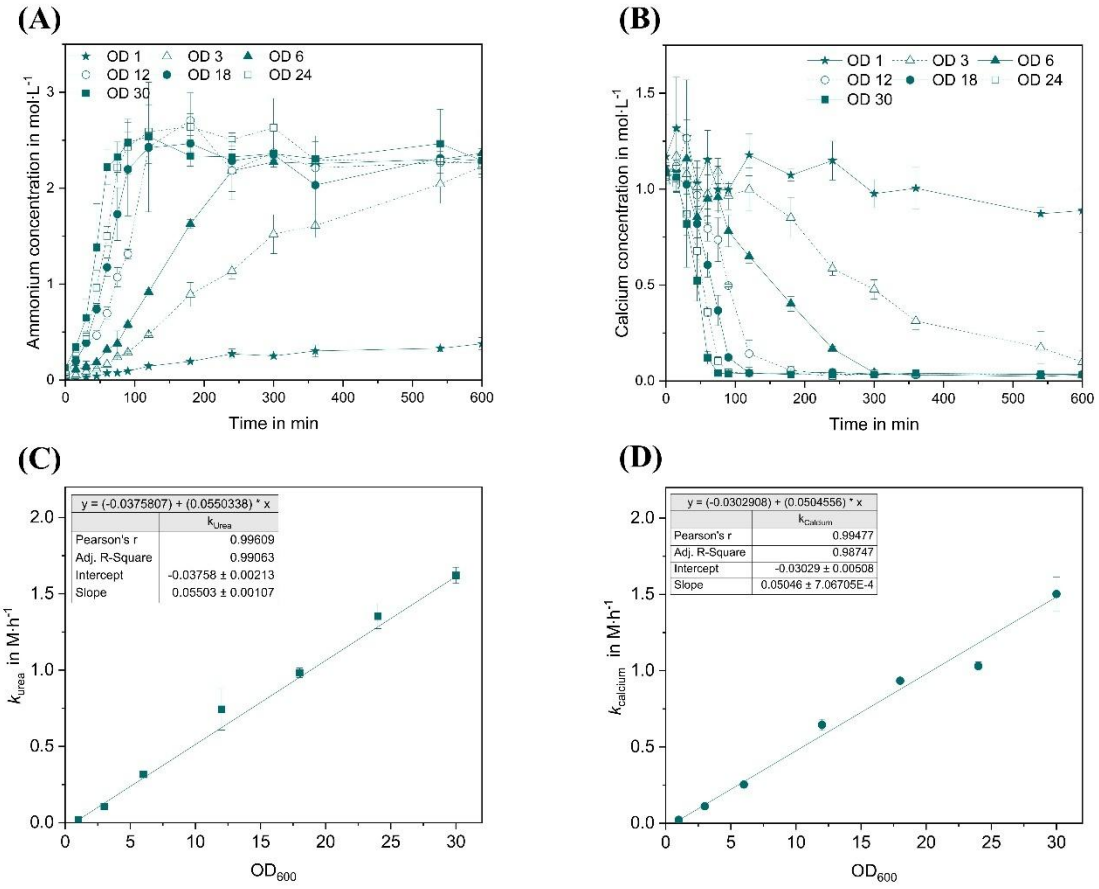

Figure 2: Impact of cell density on MICP. (A) NH_4^+ and (B) Ca^{2+} concentration during kinetics experiments. (C) k_{urea} values determined from change of NH_4^+ over time. (D) $k_{calcium}$ values determined from change of Ca^{2+} over time. Lines between data points are plotted to guide the eyes. Error bars represent standard deviation of average values from n=3 technical replicates.

For all cell densities above OD_{600}=6 a 100 % conversion rate of urea and $CaCl_2$ was observed after a reaction time of 180 minutes. After 10 hours all cell densities except OD_{600}=1 achieved a full conversion of the reactants (Figure 10). During the beginning of the experiment reaction speed for urea degradation and calcium carbonate precipitation was slower and increased after 30-80 minutes with a shorter lag phase for higher cell densities. k_{urea} (adj. R^2=0.99063) and $k_{calcium}$ (adj. R^2=0.98747) showed positive linear correlations with OD_{600} (Figure 2 C-D).

Table 2: Overview of calcium carbonate polymorphs for different cell densities during MICP as determined by Fourier-transform infrared spectroscopy.

Temperature in °C	[Urea] in mol·L^{-1}	[Calcium] in mol·L^{-1}	OD_{600}	$CaCO_3$ polymorphs
25	2	2	1	Calcite
25	2	2	3	Calcite
25	2	2	6	Calcite
25	2	2	12	Calcite
25	2	2	18	Calcite
25	2	2	24	Vaterite
25	2	2	30	Vaterite

Besides this correlation in reaction speed the cell density had an impact on the morphology and polymorph of the calcium carbonate crystals. For cell densities between OD_{600}=1 and OD_{600}=18, calcite was the only polymorph that was detected by FTIR while at OD_{600} of 24 and 30 only vaterite was detected. This shift in the polymorph could also be observed in the crystal structure under the microscope. Until the shift towards vaterite the crystals showed sharp edges and mostly uniform size (Figure 3 A-E). At cell densities above OD_{600}=24 smaller crystals with a flaky structure could be observed.

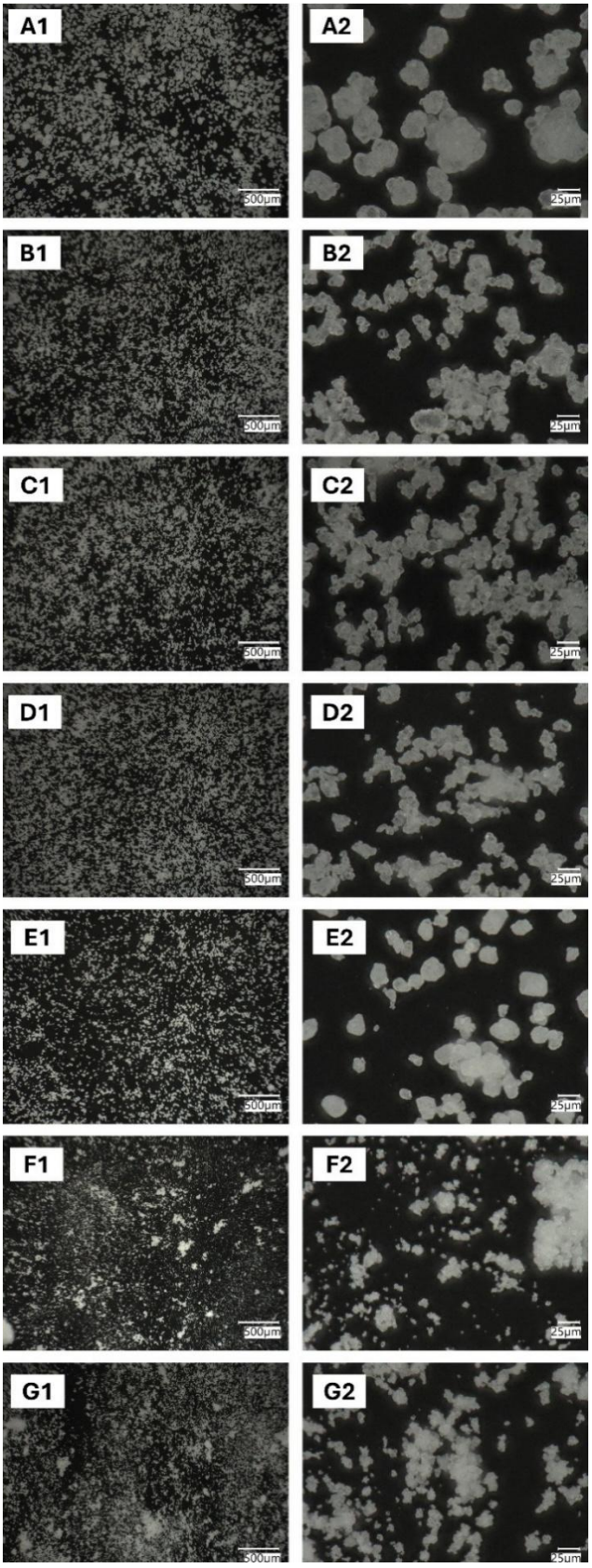

Figure 3: Microscopic images (VHX-7000) of different levels of magnification of calcium carbonate crystals after MICP at different cell densities. (A) OD_{600}=1, (B) OD_{600}=3, (C) OD_{600}=6, (D) OD_{600}=12, (E) OD_{600}=18, (F) OD_{600}=24, (G) OD_{600}=30

3.2 Impact of calcium concentration on MICP

A screening was performed to determine which ranges of calcium and cell density were suitable for determination of the reaction kinetics. The ranges for the screening were chosen for initial $CaCl_2$ concentrations between 2 and 5.4 mol·L^{-1}, resulting in 1 to 2.7 mol·L^{-1} after combining with BS. The lowest concentration of 2 mol·L^{-1} was chosen due to data from previous literature suggesting that concentrations of CS under 2 mol·L^{-1} do not negatively affect MICP [7, 21] and because higher concentration of $CaCl_2$ are necessary to achieve high mass of $CaCO_3$ per treatment cycle during MICP. The higher limit of 5.4 mol·L^{-1} was based on the solubility of $CaCl_2$ and Urea in the CS.

OD_{600} between 1 and 20 were chosen to determine which cell densities are suitable for degradation of high calcium concentrations. For all experiments initial urea concentration was kept constant at 5.4 mol·L^{-1}. conversion rate was calculated by dividing the precipitated calcium carbonate by the theoretically achievable calcium carbonate content.

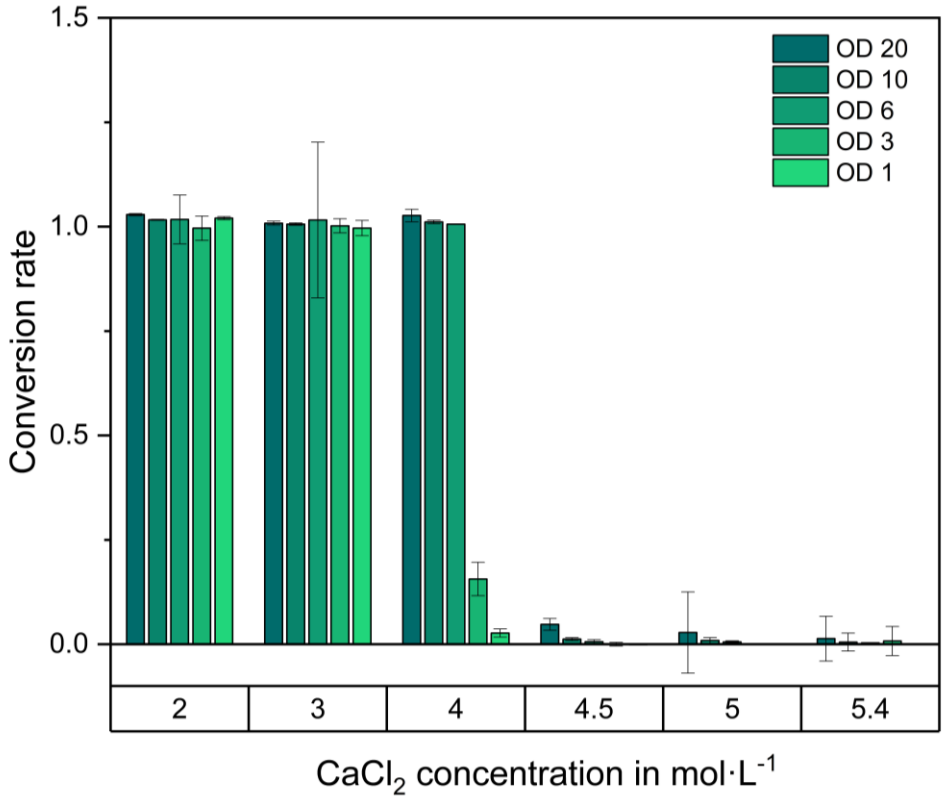

Figure 4: Conversion rate of Ca^{2+} to calcium carbonate during MICP at different initial $CaCl_2$ concentrations and cell densities. Error bars represent standard deviation of average values from n=3 technical replicates.

For $CaCl_2$ concentrations below 3 mol·L^{-1} a complete conversion could be observed regardless of cell density (Figure 4). At an initial $CaCl_2$ concentration of 4 mol·L^{-1} a sharp drop-in conversion rate from 1.01±0.01 to 0.16±0.04 mol·L^{-1}h^{-1} was observed when lowering the cell density from OD_{600}=6 to OD_{600}=3. By decreasing the cell density further to OD_{600}=1 the conversion rate dropped even further to 0.03±0.01. Above $CaCl_2$ concentrations of 4.5 mol·L^{-1} no conversion rate above 0.05±0.02 mol·L^{-1}h^{-1} could be achieved indicating that MICP comes to a complete halt at concentrations above this level of free calcium ions. Based on these findings the impact of $CaCl_2$ on the reaction rate of MICP was determined in the range of 0 - 4.5 mol·L^{-1}. The urea concentration was kept at a constant level of 4.5 mol·L^{-1} to ensure a complete precipitation of calcium carbonate for all levels of $CaCl_2$ concentration and to exclude the impact of urea concentration on reaction rates.

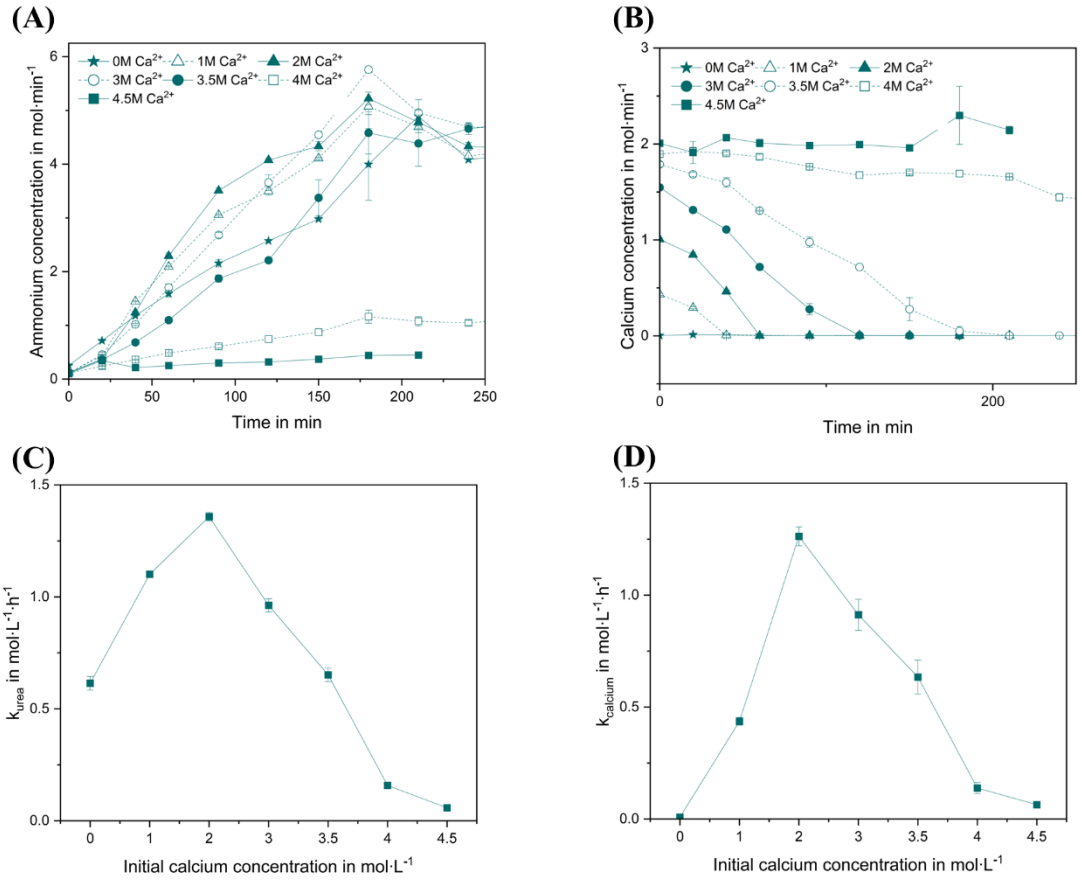

Figure 5: Impact of initial calcium concentration on MICP. (A) NH_4^+ concentration during kinetics experiments. (B) Ca^{2+} concentration during kinetics experiments. (C) k_{urea} values determined from change of NH_4^+ over time. (D) $k_{calcium}$ values determined from change of Ca^{2+} over time. Lines between data points are plotted to guide the eyes. Error bars represent standard deviation of average values from n=3 technical replicates.

During these experiments there was an increase in ammonium concentration for all initial calcium up to 4 M (Figure 5 A) with nearly no increase in ammonium concentration for an initial calcium concentration of 4.5 M. Notably k_{urea} increased from 0.61±0.03 to 1.39±0.02 with increasing initial calcium concentration from 0 to 2 mol·L^{-1} respectively. A further increase in initial calcium concentration resulted in decreasing k_{urea} with 3.5 mol·L^{-1} calcium concentration resulting in nearly the same reaction speed as 0 mol·L^{-1} calcium concentration (k_{urea}=0.65±0.03). The changes in calcium concentration showed similar trends. For all initial calcium concentrations up to 4 mol·L^{-1} all calcium ions were depleted withing the first 180 minutes of the experiment with 4 and 4.5 mol·L^{-1} calcium concentration showing slower decreases in calcium ion concentration. Calcite was the only polymorph detected by FTIR during the experiments. The visible crystals were of similar size and shape for Ca^{2+} concentrations from 1 to 4 mol·L^{-1} (Figure 6). At 4.5 mol·L^{-1} Ca^{2+} fewer and significantly larger crystals could be observed.

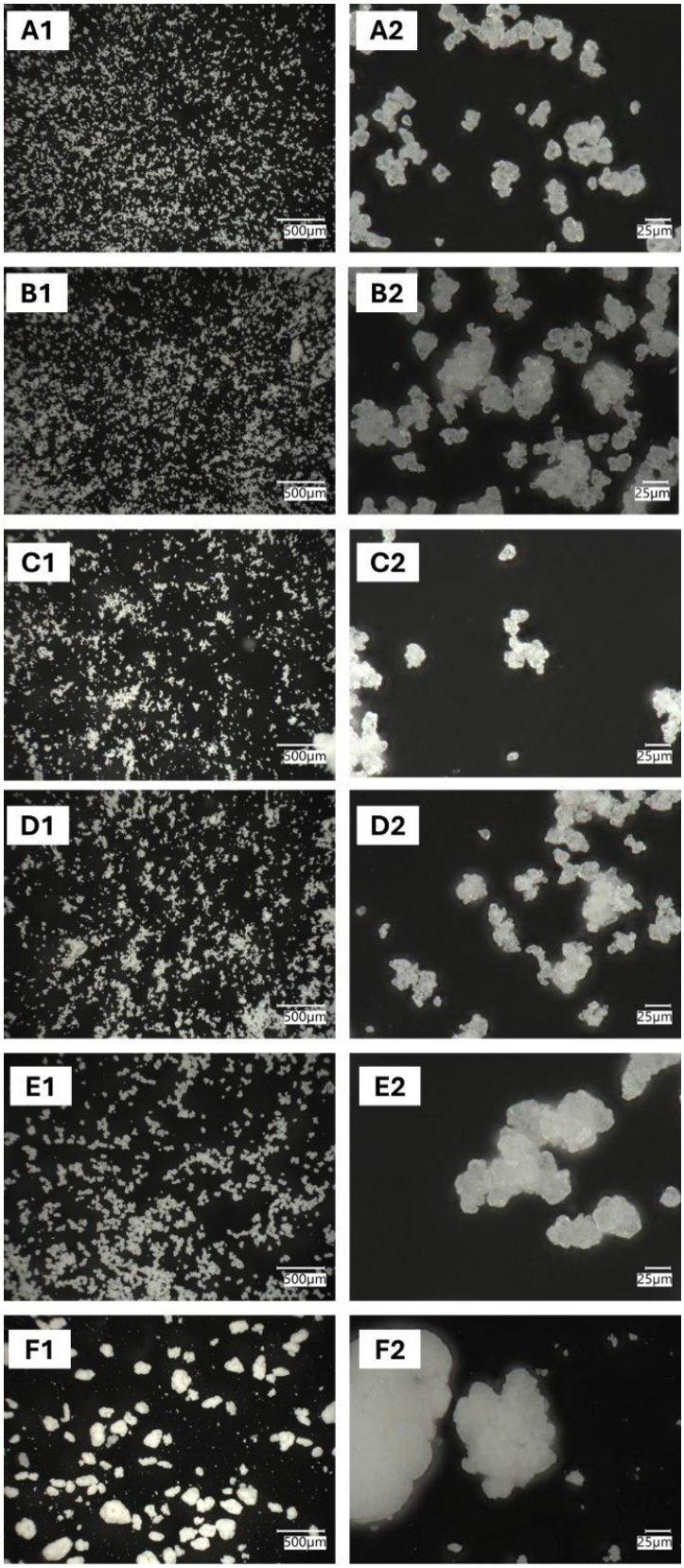

Figure 6: Microscopic images (VHX-7000) of different levels of magnification of calcium carbonate crystals after MICP at different calcium concentrations. (A) 1 mol·L^{-1}, (B) 2 mol·L^{-1}, (C) 3 mol·L^{-1}, (D) 3.5 mol·L^{-1}, (E) 4 mol·L^{-1}, (F) 4.5 mol·L^{-1}

3.3 Impact of ambient temperature on MICP

The influence of temperature on MICP was determined in a temperature range between 4 °C and 75 °C for a cell density of OD_{600}=6 and a equimolar concentration of urea and calcium chloride of 2 mol·L^{-1} based on the results in section 3.1 and 3.2. For temperatures between 4 and 55 °C ammonium concentration increased (Figure 7 A) while free calcium-ions decreased (Figure 7 B). At 65 and 75 °C there was nearly no increase in ammonium concentration or decrease in calcium concentration. Like previous results a lag phase could be observed during the initial 20 minutes of the experiment which was more pronounced for lower reaction temperatures. In the range of 4 and 45 °C k_{urea} increased tenfold from 0.13±0.03 to 1.39±0.03 mol·L^{-1}h^{-1} (Figure 7 C). At 55 °C k_{urea} decrease by 7% to 1.29±0.06 mol·L^{-1}h^{-1} in comparison to 45 °C. Between 55 and 65 °C reaction rate dropped sharply to 0.03±0.02 mol·L^{-1}h^{-1} with nearly no reaction occurring for 65 °C and higher temperatures.

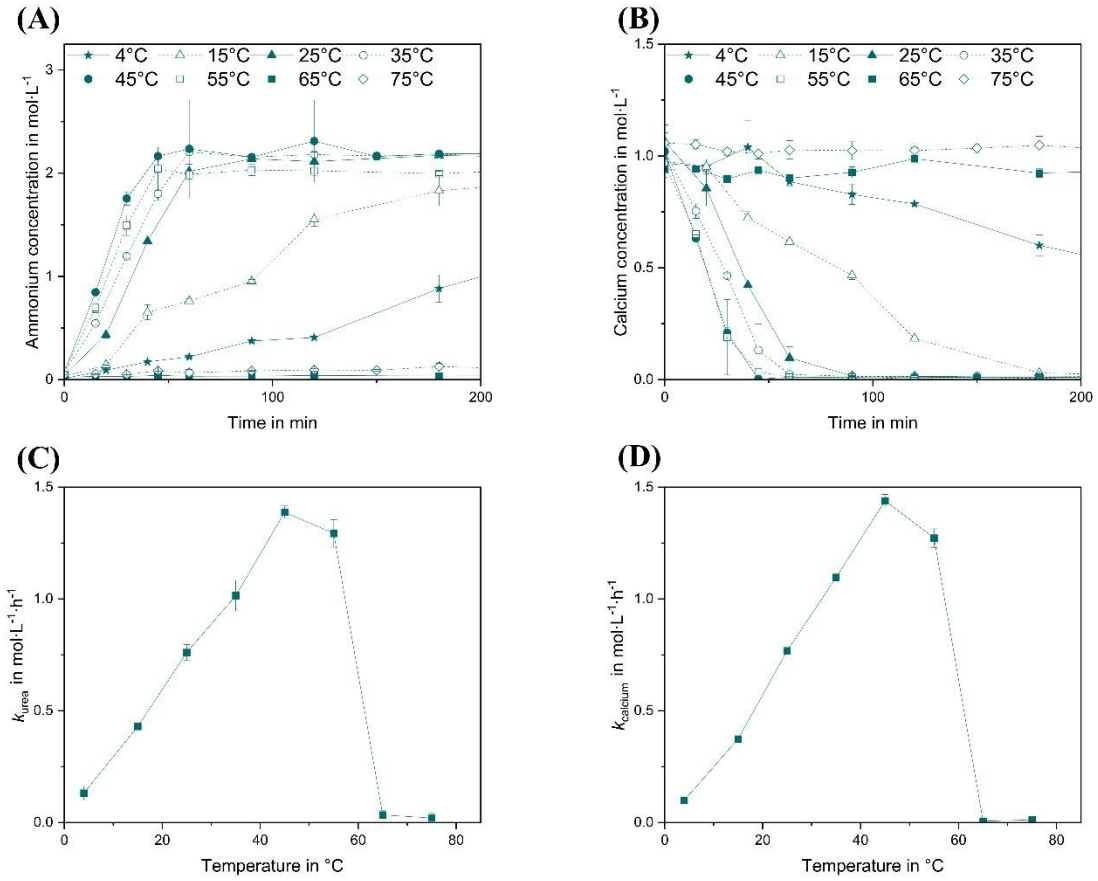

Figure 7: Impact of reaction temperature on MICP. (A) NH_4^+ and (B) Ca^{2+} concentration during kinetics experiments. (C) k_{urea} values determined from change of NH_4^+ over time. (D) $k_{calcium}$ values determined

from change of Ca^{2+} over time. Lines between data points are plotted to guide the eyes. Error bars represent standard deviation of average values from n=3 technical replicates.

The calcination process has a similar behavior with calcium concentration decreasing with various reaction speeds between 4 and 55 °C (Figure 7 B) with $k_{calcium}$ following the trends of k_{urea} with an increase from 0.10±0.00 $mol \cdot L^{-1}h^{-1}$ at 4 °C to 1.44±0.03 at 45 °C and a subsequent decrease in reaction rate to 1.27±0.04 $mol \cdot L^{-1}h^{-1}$ and 0.01±0.00 $mol \cdot L^{-1}h^{-1}$ at 55 and 65 °C respectively.

Table 3: Overview of calcium carbonate polymorphs for temperatures densities during MICP.

Temperature in °C	[Urea] in $mol \cdot L^{-1}$	[Calcium] in $mol \cdot L^{-1}$	OD_{600}	Temperature in °C	$CaCO_3$ polymorphs
25	2	2	6	4	Calcite+Vaterite
25	2	2	6	15	Calcite
25	2	2	6	25	Calcite
25	2	2	6	35	Calcite
25	2	2	6	45	Calcite
25	2	2	6	55	Calcite
25	2	2	6	65	Calcite+Aragonite

The $CaCO_3$ polymorph changed from a mixture of calcite and vaterite at 4 °C to pure calcite for the temperature range of 15 to 55 °C. At 65 °C aragonite formed in addition to calcite. These shifts in the precipitated polymorphs can also be observed in microscopic images. Only for $CaCO_3$ formed at 4 °C spherical shaped crystals could be observed (Figure 8 A) and at 65 °C characteristically needle shaped Aragonite crystals were visible (Figure 8 G).

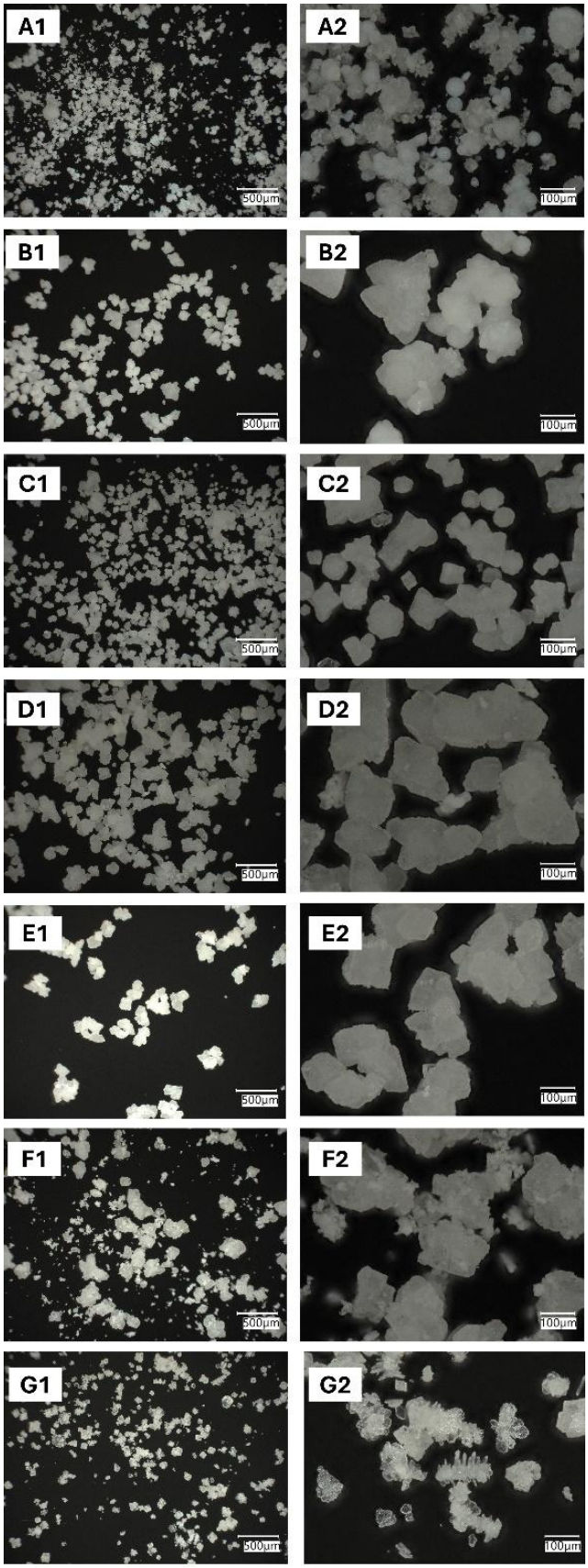

Figure 8: Microscopic images (VHX-7000) of different levels of magnification of calcium carbonate crystals after MICP at different temperatures. (A) 4 °C, (B) 15 °C, (C) 25 °C, (D) 35 °C, (E) 45 °C, (F) 55 °C, (G) 65 °C

3.4 Correlation between kurea and kcalcium

To determine the correlation between the reaction speed of ureaolysis and calcium carbonate precipitation $k_{calcium}$ was plotted as a function of k_{urea} for each datapoint of all conducted experiments with CS containing urea and calcium (Figure 9). The range for k_{urea} varied between 0.02±0.02 and 1.58±0.02 mol·L^{-1}h^{-1}. For $k_{calcium}$ the range was between 0.01±0.00 and 1.44 mol·L^{-1}h^{-1}. Regardless of the experimental setup, the calcium carbonate precipitation rate was like the speed of the ureolysis. The sole exception was the data point for a calcium concentration of 1 mol·L^{-1} (marked in red) where $k_{calcium}$ was significantly lower at 0.44±0.02 mol·L^{-1}h^{-1} in comparison to k_{urea}=1.10±0.00 mol·L^{-1}h^{-1}. A linear fit matched the data points with a slope of 0.97 (adj. R^2=0.988) which is a further indicator how closely $k_{calcium}$ and k_{urea} are correlated.

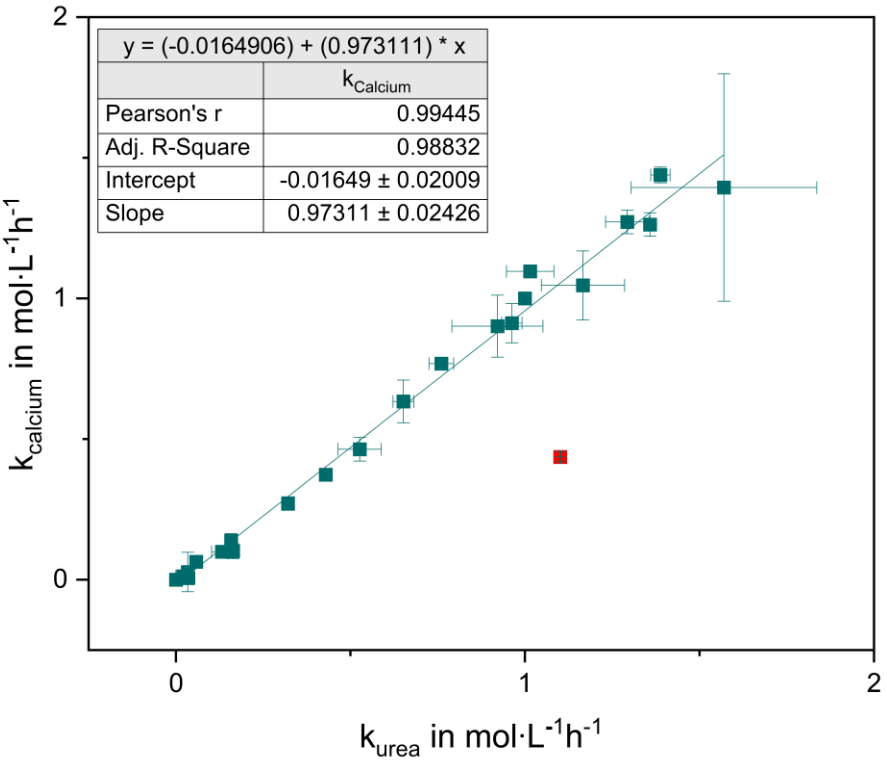

Figure 9: Correlation between $k_{calcium}$ and k_{urea} for all conducted kinetic experiments. Error bars represent standard deviation of average values from n=3 technical replicates. The red marked datapoint was excluded as an outlier from the linear fitting.

4 Discussion

Ureolytic MICP consists of multiple interlinked reactions and mass transport phenomena making it difficult to describe the process in a single model as it could be done e.g. with free urease and a Michaelis Menten model. The process involves the uptake of urea into the cells, enzymatic ureolysis, release of carbonate and NH^{4+} ions out of the bacteria cells and the precipitation of calcium carbonate. The observed increase in NH_4^+ concentration during the experiments (Figure 7 A, B; Figure 10 A, B; Figure 2 A, B) is a direct result of urea hydrolysis by *S. pasteurii*. Although the second product of the ureolysis, CO_3^{2-} was not directly measured, the decrease in Ca^{2+} was a result of CO_3^{2-} forming during ureolysis. This resulted in all cases in precipitation with the precipitate being confirmed as calcium carbonate by FTIR. The observed lag phase during the initial part of the experiments is most likely due to the organisms adjusting to the environment and initial mass transfer of urea into the cells and CO_3^{2-} out of the cell and was also observed by other researchers ranging between 1 and 6 hours depending on cell densities [7, 18, 13]. The reaction speed of the ureolysis k_{urea} that was determined in this study gives us an indicator how fast ammonia is released into the bulk medium during the reaction. The fact that calcium precipitation shows nearly the same reaction rates as ureolysis regardless of the experimental conditions (Figure 9) indicates that ureolysis is determining the overall precipitation rate during MICP. For high concentrations of Ca^{2+} (2.0-4.5 mol·L^{-1}) and high cell densities (OD_{600}=0.5-30) k_{urea} or $k_{calcium}$ are therefore suitable parameters to determine or calculate the reaction speed during different applications of MICP.

In the range from OD_{600}=1 to OD_{600}=30 we found a linear relationship between cell density, k_{urea} and $k_{calcium}$ (Figure 3 C and D). Jain et al. [7] also observed a linear correlation of the reaction rate of ureolysis from cell concentration in a range of OD_{600}=0.04 to 1.14 while Murugan et al. [18] described an exponential correlation of k_{urea} in the range between OD_{600}=0.1 to 0.4 and report no further increase in reaction speed above OD_{600}=0.5. Both authors concluded that there is a limit in cell density above which the efficiency per cells drops for MICP. In our experiment we did not observe a limit in efficiency which would manifest in a saturation curve of the reaction speed – OD_{600} curve. At what cell density such a limit would be observed could not be answered based on the results of this study. The usage of cell densities of

OD_{600}=30 is higher than most real applications of MICP could need. Most batch cultivations in MICP research achieving OD_{600} values between 0.5 and 6 [22–24] which would require an additional step in concentrating cell suspension prior to MICP application until higher cell densities during cultivation of *S. pasteurii* as described by Lapierre et al. [25, 26] become more common. Up to cell densities of OD_{600}=30 MICP reaction rate can be increased by increasing cell density. This approach would be easy to achieve but unsuitable as higher cell densities are inextricable tied to higher process cost.

High concentrations of Ca^{2+} up to 4 mol·L^{-1} could be used for MICP application but cell density must be kept at a certain level to obtain high conversion rate of urea and calcium ions towards calcium carbonate (Figure 4). All reactions up to Ca^{2+} concentrations of 3.5 mol·L^{-1} were completed within 200 minutes (Figure 5 A, B). But this comes with a loss in reaction speed when increasing the calcium concentration above 2 mol·L^{-1}. There are different explanations discussed in literature about how Ca^{2+} could negatively affect MICP. (1) encapsulation of bacteria cells [7, 13], (2) disruption of intracellular calcium-regulated signal processes of cells [27], (3) increased osmotic pressure due to high Ca^{2+} concentrations [28] and an inhibitory effect of calcium ions urease activity [29, 30]. Contrary to our results Jain et al. [7] described a negative impact of Ca^{2+} on ureolyis of *S. pasteurii* and *Proteus vulgaris* for a concentration range of 0.1 to 1 mol·L^{-1} for cell densities between OD_{600} 0.1 to 1.1. Mitchell et al. [13] described a decrease in ureolysis for cell densities of OD_{600}=0.01 in a medium containing 333 mmol·L^{-1} urea and 0.02 mmol Ca^{2+} in comparison to the same medium without Ca^{2+} and concluded that this decrease is due to encasement of cells by $CaCO_3$. Tobler et al. [14] observed no impact of Ca^{2+} concentrations between 50 and 500 mmol·L^{-1} on the ureolysis of *S. pasteurii* for even lower cell densities of OD_{600}=0.03 and OD_{600}=0.07. Okwadha et al. [16] describe a positive impact of Ca^{2+} on the ureolysis rate for *S. pasteurii* at OD_{600}=1.

The main difference between these studies and our results is the difference in cell density. In our study we used OD_{600}=6 which results in a significantly faster rate of ureolysis which results in a fast reduction of Ca^{2+} concentration due to calcium carbonate precipitation. While these studies focused on ureolyis by microorganisms (MICP) the same negative effect of calcium ions on reaction rates was observed

during Enzymatically Induced Calcium Carbonate Precipitation (EICP) by free urease from *Canavalia ensiformis* (jack bean) [30]. Zhao et al. investigated the EICP reaction rates in micro-scale environment for CS between 0.25 and 1 mol·L^{-1} urea/$CaCl_2$ and found the lowest precipitation rate for 1 mol·L^{-1} due to inhibition of the reaction through Ca^{2+} which is lower than the limit for calcium inhibition on MICP that was observed in our study. It should be noted that the tolerance of MICP to higher calcium concentrations in comparison to EICP is most likely due to intracellular urease being protected from direct contact with high calcium concentrations. The inhibitory effect of calcium on ureolysis was described by Huang et al. [31] as time dependent. A high reaction rate can help to reduce Ca^{2+} during the early part of the reaction and thereby mitigate the negative impact of Ca^{2+} ions on MICP. This interaction becomes particularly clear when the conversion rate at 4 mol·L^{-1} is considered for different cell densities (Figure 5). The conversion rate for cell densities above 6 is nearly 100 % and conversion rate drops sharply when decreasing cell density to OD_{600}=3, indicating that the inhibitory effect of calcium is dependent on cell density. Interestingly there was an initial increase in the reaction speed of ureolysis between 0 and 2 mol·L^{-1}. This phenomenon could be attributed to the ionic strength of calcium chloride impacting the membrane stability and permeability of *S. pasteurii*. This could impact the transporter that are responsible for urea uptake or the passive diffusion of ammonium ions out of the cells [32]. A release of urease into the bulk medium, which would increase k_{urea} due to improved mass transport can be ruled out. Samples were filter sterilized during several times of the experiments and filtrate tested negative for ureolytic activity (Data not shown). Other studies also observed a positive impact of low Ca^{2+} concentrations up to 50 mmol·L^{-1} on ureolysis [16, 33, 31]. An increase in reaction speed of ureolysis up to 2 mmol·L^{-1} was not described yet and could be attributed to the high cell densities utilized in our study.

Beside cell density and Ca^{2+} concentration temperature was the third factor that had a significant impact on MICP reaction rates. In the range between 4 and 45 °C we found a positive impact of temperature on k_{urea} and $k_{calcium}$ (Figure 7 C, D). All parts of MICP are somehow influenced by temperature, resulting in an overall positive trend up to a certain temperature. Urea uptake through transporters [32] increases in speed at elevated temperatures [34]. The following ureolysis is an enzymatic process

and therefore shows Arrhenius-type temperature dependence (Reaction rate increases with an increase in temperature) and temperature dependent deactivation of the intracellular enzyme (urease) above certain temperatures. Diffusion of molecules, including ammonium ions into and out of the cells [32] is also a temperature dependent process following Arrhenius law [35]. If k_{urea} was solely dependent on enzymatic ureolysis an exponential correlation between k_{urea} and the temperature should have been observable similar to experiments on the kinetics of free urease [36, 37]. We did not observe such a correlation. The increase of k_{urea} and $k_{calcium}$ with temperature seems to be linear (Figure 7 C, D). The reasoning being this observation cannot be explained solely based on our data. In future studies on the effect of temperature on MICP a closer monitoring, especially in the temperature range close to 45 °C could help to better understand these effects. Additionally, the individual uptake rate of urea, the change of local concentrations of NH_4^+ and Ca^{2+} in individual bacteria cells and in proximity of them would be valuable to provide more insight into the mechanisms behind the single steps of MICP. The decline in reaction rate for temperatures above 45 °C is most likely due to deactivation of the intracellular urease of *S. pasteurii*. The temperature optimum of several free ureases from bacteria and plants is 40 °C [38–41]. At temperatures above 40 °C activity of free urease from *S. pasteurii* drops resulting in a decrease in k_{urea} [42]. Immobilization of urease can shift the temperature optimum towards higher temperatures [37, 36] which is most likely the reason behind the slightly higher temperature optimum that was observed for the experiments that were conducted in our study. Most studies on MICP kinetics investigated MICP at a single temperature (Table 1).

To the best of our knowledge only Wang et al. [9] and Whiffin [21] conducted experiments on the influence of a wider temperature range on whole cell ureolysis of *S. pasteurii*. Wang et al. [9] described an exponential growth of ureolysis rate with temperature in the range of 5 to 70 °C. Whiffin [21] observed a stable rate of ureolysis between 15 and 25 °C followed by a linear increase up to a temperature of 70 °C. Both studies conclude that the temperature optimum of ureolysis during MICP is 70 °C. These results contrast with our own result of a temperature optimum of 45 °C. The difference between our results and results from literature is most likely due to the methodology of k_{urea} determination. Whiffin [21] and Wang et al. [9] utilized

the same conductivity method to measure only the first five minutes of ureolysis during MICP. Thermic enzyme deactivation is temperature and time dependent [43]. During our experiments we calculated k_{urea} and $k_{calcium}$ during the whole process and although we visually observed some precipitation for temperatures of 65 and 75 °C the reaction ended during the initial part of the experiment. It is therefore unlikely that temperatures of 70 °C are suitable to achieve high conversion rates during MICP with *S. pasteurii*. Cell density, calcium concentration and temperature are parameters that impact the reaction speed of MICP. This can be utilized to optimize the possible amount of calcium carbonate that can be precipitated during each cycle and the speed at which this precipitation occurs. A high conversion rate coupled with a fast reaction speed will often be desired for MICP.

The most found polymorph during our experiments was calcite (Table 1, Table 2). The less stable polymorphs vaterite and aragonite [44] were found only during extreme conditions like aragonite for high temperatures (65 °C) or vaterite for high cell densities (OD_{600}>24). During EICP the size of calcium carbonate crystals is largely dependent on urease concentration and therefore from the reaction speed [30]. The induction of different calcium carbonate polymorphs and morphologies is complex and dependent on various factors like temperature, pH, presence of other molecules and Ca^{2+}/CO_3^{2-} ratio [45]. The size and polymorph of the crystals can impact strength parameters of after MICP. For example are smaller calcium carbonate crystals less effective than larger crystals for soil strengthening [46, 47]. Smaller crystals tend to form a crust on top of soil particles or grow into void space while larger crystals can build effective contact points between particles leading to higher strength [46]. The calcium carbonate polymorph can also impact the efficiency of MICP directly: Xu et al. [48] and Hosseino et al. [49] induced aragonite formation during MICP by adding Mg^{2+} ions into the CS and achieved an increase of unconfined compressive strength after MICP treatment of 40 % respective 70 %. During our study we did not include the effect of the reaction parameters and thereby the size and polymorph of the crystals on MICP applications like soil strengthening but this is certainly an aspect that should be investigated in future studies on this topic. The results of our study can help to find the boundaries for further optimization of process parameters during MICP. We demonstrated some of the upper boundaries

for temperature and calcium concentration during possible optimization. We also showed not only reaction speed but also morphology and polymorphs can be influenced by variation of these parameters.

5 Conclusion

In conclusion, this study has provided valuable insights into the factors influencing MICP using *Sporosarcina pasteurii*. By investigating the effects of cell density, calcium concentration, and temperature on ureolysis and precipitation rates, we have contributed to the understanding of the complex mechanisms involved in MICP. Our study can help to determine boundaries for future research and parameter optimizing for efficient MICP applications, especially in areas such as soil strengthening. The main findings of this study are as follows:

- Ureolytic activity (k_{urea}) directly influences the precipitation rate ($k_{calcium}$), with ureolytic activity being the determining factor for MICP reaction rate, irrespective of experimental conditions.
- A linear relationship between cell density (OD_{600}) and both k_{urea} and $k_{calcium}$ was observed, with higher cell densities leading to faster reaction rates. We did not observe a saturation effect for cell densities up to OD_{600}=30 which is higher than necessary for most MICP applications.
- High calcium chloride concentrations (up to 4 $mol \cdot L^{-1}$) can be used effectively for MICP, but the reaction rate is sensitive to cell density, with higher cell densities mitigating calcium's inhibitory effects due to fast reduction of free calcium ions.
- Temperature significantly impacts the reaction rates, with an optimal temperature of 45°C for MICP. Above this temperature MICP reaction rates (k_{urea} and $k_{calcium}$) declined until no reaction was observed at 75 °C.
- Calcite was the most observed polymorph during all experiments. Variations in cell density, calcium concentration and temperature can impact the morphology or polymorph of precipitated calcium carbonate crystals

Due to the complexity and multi factorial influences on the MICP further studies are necessary to build up on these results, especially on the importance of reaction

parameters on crystal morphology and polymorphs and the implications of this for MICP applications. During these studies a comparison of the factorial influences on MICP the effects of these parameters on the closely related topic of EIPC should be kept in mind. Furthermore, the impact of the microenvironment in the cells (pH, concentration of reactants/ products and urease concentration) should be kept in mind to further broaden our understanding of the processes behind MICP.

6 Supplementary Materials

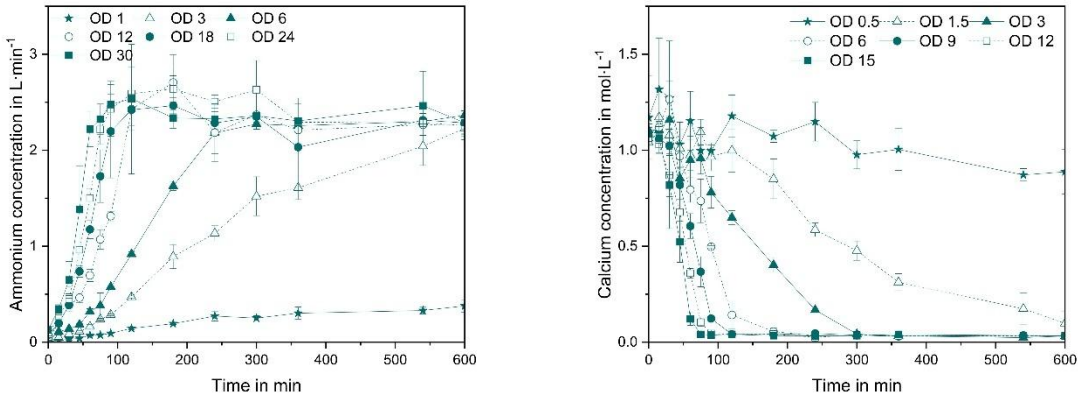

Figure 10: (A) NH_4^+ and (B) Ca^{2+} concentration during kinetics experiments. Lines between data points are plotted to guide the eyes. Error bars represent standard deviation of average values from n=3 technical replicates.

Compliance with Ethical Standards

Funding

This project was financially supported by the Deutsche Forschungsgemeinschaft (DFG, German Research Foundation) – Project-ID 172116086 – SFB 926, the TU Nachwuchsring and the “Landespotentialbereich NanoKat”.

Data availability

The data that support the findings of this study are available from the corresponding author upon reasonable request.

Conflict of Interest

The authors have no relevant financial or non-financial interests to disclose

Author Contributions

All authors contributed to the study conception and design. Material preparation, data collection and analysis were performed by Niklas Erdmann and Felix Kästner. The first draft of the manuscript was written by Niklas Erdmann and all authors commented on previous versions of the manuscript. All authors read and approved the final manuscript.

Ethical approval

This article does not contain any studies with human participants or animals performed by any of the authors.

7 References

1. Erdmann N, Strieth D (2022) Influencing factors on ureolytic microbiologically induced calcium carbonate precipitation for biocementation. World journal of microbiology & biotechnology 39:61. https://doi.org/10.1007/s11274-022-03499-8
2. DeJong JT, Mortensen BM, Martinez BC et al. (2010) Bio-mediated soil improvement. Ecological Engineering 36:197–210. https://doi.org/10.1016/j.ecoleng.2008.12.029
3. Muynck W de, Belie N de, Verstraete W (2010) Microbial carbonate precipitation in construction materials: A review. Ecological Engineering 36:118–136. https://doi.org/10.1016/j.ecoleng.2009.02.006
4. Zhang K, Tang C-S, Jiang N et al. (2023) Microbial-induced carbonate precipitation (MICP) technology: a review on the fundamentals and engineering applications. Environ Earth Sci 82:229. https://doi.org/10.1007/s12665-023-10899-y
5. Wang Y, Konstantinou C, Tang S et al. (2023) Applications of microbial-induced carbonate precipitation: A state-of-the-art review. Biogeotechnics 1:100008. https://doi.org/10.1016/j.bgtech.2023.100008
6. Rahman MM, Hora RN, Ahenkorah I et al. (2020) State-of-the-Art Review of Microbial-Induced Calcite Precipitation and Its Sustainability in Engineering Applications. Sustainability 12:6281. https://doi.org/10.3390/su12156281
7. Jain S (2024) Influence of biomass and chemicals on kinetics of ureolysis-based carbonate biomineral precipitation. Environ Earth Sci 83. https://doi.org/10.1007/s12665-023-11355-7
8. Yang J, Wang Y (2024) Efficiency and Characteristics of MICP in Environments with Elevated Salinity, Diminished Oxygen, and Lowered Temperature: A Microfluidics Investigation
9. Wang Y, Wang Y, Soga K et al. (2022) Microscale investigations of temperature-dependent microbially induced carbonate precipitation (MICP) in the temperature range 4–50 °C. Acta Geotech. https://doi.org/10.1007/s11440-022-01664-9
10. Ashraf MS, Hassan Shah MU, Bokhari A et al. (2021) Less is more: Optimising the biocementation of coastal sands by reducing influent urea through response surface method. Journal of Cleaner Production 315:128208. https://doi.org/10.1016/j.jclepro.2021.128208
11. Duo L, Kan-liang T, Hui-li Z et al. (2018) Experimental investigation of solidifying desert aeolian sand using microbially induced calcite precipitation. Construction and Building Materials 172:251–262. https://doi.org/10.1016/j.conbuildmat.2018.03.255
12. Sotoudehfar AR, Mirmohammad sadeghi M, Mokhtari E et al. (2016) Assessment of the Parameters Influencing Microbial Calcite Precipitation in Injection Experiments Using Taguchi Methodology. Geomicrobiology Journal 33:163–172. https://doi.org/10.1080/01490451.2015.1025316

13. Mitchell AC, Espinosa-Ortiz EJ, Parks SL et al. (2019) Kinetics of calcite precipitation by ureolytic bacteria under aerobic and anaerobic conditions. Biogeosciences, 16(10), 2147-2161. https://doi.org/10.5194/BG-16-2147-2019
14. Tobler DJ, Cuthbert MO, Greswell RB et al. (2011) Comparison of rates of ureolysis between Sporosarcina pasteurii and an indigenous groundwater community under conditions required to precipitate large volumes of calcite. Geochimica et Cosmochimica Acta 75:3290–3301. https://doi.org/10.1016/j.gca.2011.03.023
15. Lauchnor EG, Topp DM, Parker AE et al. (2015) Whole cell kinetics of ureolysis by Sporosarcina pasteurii. Journal of Applied Microbiology 118:1321–1332. https://doi.org/10.1111/jam.12804
16. Okwadha GD, Li J (2010) Optimum conditions for microbial carbonate precipitation. Chemosphere 81:1143–1148. https://doi.org/10.1016/j.chemosphere.2010.09.066
17. Ferris FG, Phoenix V, Fujita Y et al. (2004) Kinetics of calcite precipitation induced by ureolytic bacteria at 10 to 20°C in artificial groundwater. Geochimica et Cosmochimica Acta 68:1701–1710. https://doi.org/10.1016/S0016-7037(03)00503-9
18. Murugan R, Suraishkumar GK, Mukherjee A et al. (2021) Insights into the influence of cell concentration in design and development of microbially induced calcium carbonate precipitation (MICP) process. PLoS ONE 16:e0254536. https://doi.org/10.1371/journal.pone.0254536
19. Chakrabarty D, Mahapatra S (1999) Aragonite crystals with unconventional morphologies. J. Mater. Chem. 9:2953–2957. https://doi.org/10.1039/a905407c
20. Loftus E, Rogers K, Lee-Thorp J (2015) A simple method to establish calcite:aragonite ratios in archaeological mollusc shells. J Quaternary Sci 30:731–735. https://doi.org/10.1002/jqs.2819
21. Whiffin VS (2004) Microbial CaCO3 Precipitation for the Production of Biocement. PhD Thesis, Murdoch University
22. Cuzman OA, Richter K, Wittig L et al. (2015) Alternative nutrient sources for biotechnological use of Sporosarcina pasteurii. World journal of microbiology & biotechnology 31:897–906. https://doi.org/10.1007/s11274-015-1844-z
23. Omoregie AI, Palombo EA, Ong DE et al. (2020) A feasible scale-up production of Sporosarcina pasteurii using custom-built stirred tank reactor for in-situ soil biocementation. Biocatalysis and Agricultural Biotechnology 24:101544. https://doi.org/10.1016/j.bcab.2020.101544
24. Babakhani S, Fahmi A, Katebi H et al. (2021) Non-sterile corn steep liquor a novel, cost effective and powerful culture media for Sporosarcina pasteurii cultivation for sand improvement. Journal of Applied Microbiology 130:1232–1244. https://doi.org/10.1111/jam.14866
25. Lapierre FM, Schmid J, Ederer B et al. (2020) Revealing nutritional requirements of MICP-relevant Sporosarcina pasteurii DSM33 for growth improvement in

chemically defined and complex media. Scientific reports 10:22448. https://doi.org/10.1038/s41598-020-79904-9
26. Lapierre FM, Huber R (2024) Feeding strategies for Sporosarcina pasteurii cultivation unlock more efficient production of ureolytic biomass for MICP. Biotechnol J 19:e2300466. https://doi.org/10.1002/biot.202300466
27. Hammes F, Verstraete W (2002) Key roles of pH and calcium metabolism in microbial carbonate precipitation. Rev Environ Sci Biotechnol 1:3–7. https://doi.org/10.1023/A:1015135629155
28. Yi H, Zheng T, Jia Z et al. (2021) Study on the influencing factors and mechanism of calcium carbonate precipitation induced by urease bacteria. Journal of Crystal Growth 564:126113. https://doi.org/10.1016/j.jcrysgro.2021.126113
29. Sun X, Miao L, Wu L (2020) Applicability and Theoretical Calculation of Enzymatic Calcium Carbonate Precipitation for Sand Improvement. Geomicrobiology Journal 37:389–399. https://doi.org/10.1080/01490451.2019.1710625
30. Zhao C, Xiao Y, Liu H et al. (2024) Effects of urease and cementing solution concentrations on micro-scale enzymatic mineralisation characteristics. Géotechnique:1–15. https://doi.org/10.1680/jgeot.24.00002
31. Huang J, Yin H, Zhang H et al. (2023) Effect of Calcium and Magnesium Ions on Microbial Urease Activity in Landfill Leachate Treatment. Pol J Environ Stud. https://doi.org/10.15244/pjoes/169648
32. Sridhar S, Bhatt N, Suraishkumar GK (2021) Mechanistic insights into ureolysis mediated calcite precipitation. Biochemical Engineering Journal 176:108214. https://doi.org/10.1016/j.bej.2021.108214
33. Hammes F, Boon N, Villiers J de et al. (2003) Strain-specific ureolytic microbial calcium carbonate precipitation. Appl Environ Microbiol 69:4901–4909. https://doi.org/10.1128/AEM.69.8.4901–4909.2003
34. Spackeen JL, Sipler RE, Xu K et al. (2017) Interactive effects of elevated temperature and CO2 on nitrate, urea, and dissolved inorganic carbon uptake by a coastal California, USA, microbial community. Mar Ecol Prog Ser 577:49–65. https://doi.org/10.3354/meps12243
35. Sadoon AA, Oliver WF, Wang Y (2022) Revisiting the Temperature Dependence of Protein Diffusion inside Bacteria: Validity of the Stokes-Einstein Equation. Phys Rev Lett 129:18101. https://doi.org/10.1103/PhysRevLett.129.018101
36. Fahmy AS, Bagos VB, Mohammed TM (1998) Immobilization of Citrullus vulgaris urease on cyanuric chloride deae-cellulose ether: Preparation and properties. Bioresource Technology 64:121–129. https://doi.org/10.1016/s0960-8524(97)00174-0
37. Krajewska B, Leszko M, Zaborska W (1990) Urease immobilized on chitosan membrane: preparation and properties. J Chem Technol Biotechnol 48:337–350. https://doi.org/10.1002/jctb.280480309

38. Tetiker AT, Ertan F (2019) Optimization and immobilization of urease enzyme isolated from Proteus mirabilis on alginate beads. JEB 40:1123–1128. https://doi.org/10.22438/jeb/40/5/prn-118
39. Liu X (2018) Purification and Characterization of Urease Obtained from Thiobacillus thiooxidans. IOP Conf Ser.: Mater Sci Eng 423:12099. https://doi.org/10.1088/1757-899X/423/1/012099
40. Chouhan S, Vishnu Priya V, Gayathri R (2018) Extraction and partial purification of urease enzyme from jack fruit. International Journal of Research in Pharmaceutical Sciences 9:438–441. https://doi.org/10.26452/ijrps.v9i2.1515
41. Harrita S, Priya VV, Gayathri R (2018) Assessment of urease activity in soya bean products. Drug Invention Today 10:2045–2047
42. Ciurli S, Marzadori C, Benini S et al. (1996) Urease from the soil bacterium Bacillus pasteurii: Immobilization on Ca-polygalacturonate. Soil Biology and Biochemistry 28:811–817. https://doi.org/10.1016/0038-0717(96)00020-X
43. Illeová V, Polakovic M, Stefuca V et al. (2003) Experimental modelling of thermal inactivation of urease. Journal of Biotechnology 105:235–243. https://doi.org/10.1016/j.jbiotec.2003.07.005
44. Gorospe CM, Han S-H, Kim S-G et al. (2013) Effects of different calcium salts on calcium carbonate crystal formation by Sporosarcina pasteurii KCTC 3558. Biotechnology and Bioprocess Engineering 18:903–908. https://doi.org/10.1007/s12257-013-0030-0
45. Liendo F, Arduino M, Deorsola FA et al. (2022) Factors controlling and influencing polymorphism, morphology and size of calcium carbonate synthesized through the carbonation route: A review. Powder Technology 398:117050. https://doi.org/10.1016/j.powtec.2021.117050
46. Cheng L, Shahin MA, Mujah D (2017) Influence of Key Environmental Conditions on Microbially Induced Cementation for Soil Stabilization. J Geotech Geoenviron Eng 143:4016083. https://doi.org/10.1061/(ASCE)GT.1943-5606.0001586
47. Wang Y, Soga K, DeJong JT et al. (2021) Effects of Bacterial Density on Growth Rate and Characteristics of Microbial-Induced CaCO3 Precipitates: Particle-Scale Experimental Study. J Geotech Geoenviron Eng 147. https://doi.org/10.1061/(ASCE)GT.1943-5606.0002509
48. Xu X, Guo H, Cheng X et al. (2020) The promotion of magnesium ions on aragonite precipitation in MICP process. Construction and Building Materials 263:120057. https://doi.org/10.1016/j.conbuildmat.2020.120057
49. Hosseini SMJ, Guan D, Cheng L (2024) Ground Improvement with a Single Injection of a High-Performance All-in-one MICP Solution. Geomicrobiology Journal 41:636–647. https://doi.org/10.1080/01490451.2024.2364797

IV MICP treated sand: Insights into the impact of particle size on mechanical parameters and pore network after biocementation

N. Erdmann[1], S. Schaefer[2], T. Simon[1], A. Becker[3], U. Bröckel[2], D. Strieth[1]

[1]University of Kaiserslautern-Landau, Chair of Bioprocess Engineering, Kaiserslautern, Germany

[2]University of Applied Sciences Trier, Environmental Campus Birkenfeld, Institute of Microprocess Engineering and Particle Technology, Birkenfeld, Germany

[3]University of Kaiserslautern-Landau, Chair of Soil Mechanics and Foundation Engineering, Kaiserslautern, Germany

Discover Materials, Volume 4, Article Number 45 (2024)

https://doi.org/10.1007/s43939-024-00108-3

Author Contribution:

N. Erdmann*	Methodology, project administration, visualization, writing, data acquisition: figure (3-6), table (2, 3, 4), data curation and analysis
S. Schaefer*	Methodology, project administration, visualization, writing, data acquisition for figure (6), table (2-4), data curation and analysis
T. Simon	Methodology, data acquisition: figure (4, 5), table (1)
A. Becker	Funding acquisition, supervision, review&editing
U. Bröckel	Funding acquisition, supervision, review&editing
D. Strieth	Funding acquisition, supervision, review&editing

*Both authors contributed equally to the manuscript

Keywords: Microbiologically Induced Calcium Carbonate Precipitation (MICP); *Sporosarcina pasteurii*; X-ray microcomputed tomography (micro-CT); image analysis; Gauss filter; non-local means filter, pore network

Abstract

Microbiologically Induced Calcium Carbonate Precipitation (MICP) is a technology for improving soil characteristics, especially strength, that has been gaining increasing interest in literature during the last few years. Although a lot of influencing factors on the result of MICP are known, particle size and shape of the particles remain poorly understood. While destructive measuring of compressive strength or calcium carbonate content are important for the characterization of samples these methods give no insight into the internal structures and pore networks of the samples. X-ray microcomputed tomography (micro-CT) is a technique that is used to characterize the internals of rocks and to a certain degree MICP-treated soils. However, the impact of filtering and image processing of micro-CT data depending on the type of MICP sample is poorly described in the literature. In this study, single fractions of local quarry were treated with MICP through the ureolytic microorganism *Sporosarcina pasteurii* to investigate the influence of particle size distribution on calcium carbonate content, unconfined compressive strength and the reduction of water permeability. Additionally, micro-CT was conducted to obtain insights into the resulting pore system. The impact of the Gauss filter und non-local means filter on the resulting images and data on the pore network are discussed. The results show that particle size has a significant impact on the result of all tested parameters of biosandstone with lower particle size leading to higher strength and generally higher calcium carbonate content. Micro-CT data showed that the technology is feasible to gain valuable insights into the internal structures of biosandstone but the resolution and signal-to-noise ratio remain challenging, especially for samples with particle sizes smaller than 125 µm.

Article highlights

- Microbiologically Induced Calcium Carbonate Precipitation is more effective for smaller sand particle sizes
- Smaller particle size of sand lead to higher permeability reduction, higher compressive strength and higher calcium carbonate contents in biosandstone
- X-ray microcomputed tomography and image analysis is sufficient to characterize the pore system of biosandstone and detect uneven biocemented areas
- Usage of different digital filters influence resulting images and data from X-ray microcomputed tomography

1 Introduction

Microbiologically Induced Calcium Carbonate Precipitation (MICP) is a technology that got more and more attention in research during the last years [1]. Through different microbiological pathways calcium carbonate is precipitated. The most used pathway is still the ureolytic MICP. Ureolytic microorganisms hydrolyse urea to ammonium-ions and carbonate-ions (Eq. 1) while the latter will be precipitated in the presence of calcium-ions as calcium carbonate ($CaCO_3$) (Eq. 2).

$$CO(NH_2)_2 + 2H_2O \rightarrow CO_3^{2-} + 2\,NH_4^+ \qquad \text{Eq. 1}$$

$$CO_3^{2-} + Ca^{2+} \rightarrow CaCO_{3_{(s)}} \qquad \text{Eq. 2}$$

This $CaCO_3$ can form bridges between particles and act as a binder and can therefore improve mechanical parameters of different soil types. Researchers have shown the potential of MICP to improve compressive strength [2, 3], liquefaction resistance [4, 5] and resilience against wind erosion [6] of soils. Furthermore, it can be used to improve compressive strength and reduce water permeability [7, 8] of existing construction materials. Through this process it is also possible to produce novel, artificial sandstone like, materials. Although MICP based materials are not yet ready to be used for construction, they can be used for research purposes [9] opens up a new field of study. Regardless of the intended use case of biocemented soils, the homogeneity of calcium carbonate distribution in the sample is important to evaluate the quality of the cementation. Most studies use cyclic application of a calcination solution (Urea/Calcium salts) and Bacteria suspension (ureolytic microorganisms) to achieve biocementation. This often leads to clogging and inhomogeneous samples. It is possible to estimate sample homogeneity through measurements of calcium carbonate content or compressive strength content in different sections of the biosandstone which has been done several times in literature [10–12]. But these results are limited to sections of consolidated samples and do not yield information about small local inhomogeneities or uniformity from the outer layers of the sample to the core. Since mechanical parameters of biosandstone correlate with the calcium carbonate content in the sample [13, 14, 12], reproducible results for MICP will therefore largely depend on achieving a homogenous calcium carbonate distribution. Research has described several biological, chemical and physical

parameters that impact the final results of MICP [1, 15]. While a lot of these parameters like type and concentration of bacterial cells, temperature, composition of calcination solution, etc. can be controlled, the influence of the particle size distribution of sand dictates if the locally available sand source is suitable for MICP. Although research on the influence of particle size and shape of sand acknowledges the importance of these parameters on the result of MICP the understanding of these effects remains limited [9]. Measuring mechanical parameters and calcium carbonate content of biosandstone after MICP can only give limited insight in intrinsic effects that lead to these observed characteristics. It is therefore necessary to improve our understanding of the internal structures and the pore network of biocemented materials and their resulting influence of e.g. unconfined compressive strength (UCS) or water permeability

By using X-ray microcomputed tomography (micro-CT) it is possible to analyze materials destruction free. Therefore, X-ray images of the samples are taken based on the attenuation of X-rays due to density differences, differences in atomic numbers or phase boundaries. After reconstruction, images with distribution of grey values can be analyzed by 2D and 3D image analysis. This makes it possible to gain detailed insights into the inner structure of these samples. Scientists have analyzed different types of natural sandstone with X-ray CT [16–18] also MICP was characterized by CT [19–25]. While all these studies used X-ray CT to investigate MICP with focus on different fields and effects during MICP. Zhou et al. [23] used CT images to study the fracture behavior of single calcareous sand particles that were treated with MICP. Wang et al. [24] went to a bigger scale and focused on analyzing the aggregation patterns of $CaCO_3$ precipitates and to identify efficient cementation patterns. Roy et al. [22] and Terzis et al. [25] used CT images to gain insight into intrinsic properties like pore throats, interparticle contacts and precipitation bonds and connected these information with strength parameters of MICP treated sand. They concluded that not all calcium carbonate bonds equally contribute to the efficiency of MICP treated sand. CT imaging could therefore offer valuable insight in addition to studying only macroscale effects like strength and porosity of MICP treated sand when determining the efficiency of different MICP protocols. This study also tries to bridge CT analysis with parameters like strength, water-permeability and calcium

carbonate content of MICP treated sand to further help understanding how the intrinsic parameters are connected with the macroscopic parameters of MICP treated sand. The examinations of MICP using CT mainly comprised the sandstone structure, the pore network, the permeability [1, 22], creation of cracks and potential of crack sealing [40], or degree of calcite precipitation [1]. Various procedures for determining the aforementioned parameters based on image analysis are described in literature. There are different digital filters used to process the CT images and get better signal to noise ratios. At first, the denoising principle based on the replacing of color pixels or grey values with the average of nearby pixels [5]. Using filters, the grey values are processed e.g. with a normal distribution (Gauss filter) or a median of the grey values in the image window or section (Median filter) [24]. Because pixels with same grey value have no reason to be close at all and therefore, the non-local means filter uses the entire image for comparison of each pixel [5]. Also weighing factors are used at this filter [26].

For image analysis of CT images of sandstone or MICP sandstone Kirkland et al. [26] and Huang et al. [27] use Gauss filter, while Zhao et al. [28] and Wang et al. [24] use a Median filter. In contrast, Schlüter et al. [29], Schmitt et al. [18], Thomson et al. [30], Sun et al. [31], Peltz et al. [32] and Su et al. [33] use the non-local means filter (NLM). Gong et al. [17] show that the images look very different when Gauss, NLM, anisotropic diffusion or Mean filters are used. This research group found the NLM filter to be the most suitable and carried out the image analysis with it. What all these publications have in common is that the results without/with the use of the filter or the use of different filters are not shown in their effects on the image analysis results, but the filters are only considered as part of the image analysis. Filters have an influence of the grey value distribution in images by e.g. shifting the distribution and therefore have an impact of what remains for the subsequent image analysis. This paper gives both, an overview about the visual effects of the applied filters but also the differences in resulting pore network of the MICP sandstone.

In this work, we present the influence of different grain sizes of sand on calcium carbonate content, water permeability and unconfined compressive strength (UCS). Simultaneously utilizing micro-CT to gain insight into the biosandstone and its internal

pore network. Additionally, a comparison of different digital filters was performed to evaluate their influence on the quality of the image processing of CT images.

2 Materials and Methods

2.1 Cultivation of Sporosarcina pasteurii

During this study, *Sporosarcina pasteurii* (ATCC 11859) was used as an ureolytic microorganism for MICP. For cultivation of *S. pasteurii* the culture medium according to ATCC was used. The medium contained 20 g L^{-1} yeast extract (Carl Roth, Germany), 15.75 g L^{-1} TRIS-buffer (Carl Roth, Germany) and 10 g L^{-1} ammonium sulfate (VWR International, USA). For media preparation TRIS-Buffer was adjusted to pH 9.2 and then split into two parts: ammonium sulfate was added to one part and yeast extract to the other. The two parts were then separately autoclaved and after cooling combined under sterile conditions. *S. pasteurii* was incubated in 500 mL erlenmeyer flasks without baffles with a filling volume of 200 mL at 30 °C and at 250 rpm (Multitron S-000115689, Infors HT, Switzerland) until the cells reached late exponential phase. The cells were then harvested and washed three times with 0.9 % NaCl. Centrifugation after each washing step was performed at 10 °C for ten minutes at 4000 rpm. Cells were then resuspended in 0.9 % NaCl (Carl Roth, Germany), to an OD_{600} of 3.5 and stored at 4 °C until cementation experiments. Additional to OD_{600} the ureolytic activity of *S. pasteurii* was determined by conductivity method as described by Whiffin [34].

2.2 Sand types for cementation experiments

For cementation experiments two sands were investigated. SH (Sand Haltern) is a silica sand from Haltern (Quarzwerke Haltern GmbH, Haltern, Germany) that was used in previous studies for MICP [35]. SP (Sand Picard) is waste sand from a Sandstone Quarry (Carl Picard Natursteinwerk GmbH, Krickenbach, Germany). The particle size distribution (PSD) of 500 g of the sands was determined after wet sieving and drying for 24 h at 105 °C with sieves (Diameter 200 mm, RETSCH GmbH, Germany) with mesh size between 0.063 mm and 16.0 mm (Table 1). Each sample is named by the name of the sand type (SH, SP) and the particle size (0063, 0125, 0250, 0500, Mix) for example SP0250 is the fraction with d_{max}=0.250 mm from the sand from the Sandstone quarry Picard (SP). Additionally, the particle size

distribution (PSD) of SH was replicated from fractions of the Sands SP to compare different sand types with nearly identical PSD. This recreation is called “SPMix”.

Table 1: Overview of PSD from the Sand SH, SP, and SP after mixing to achieve the same PSD as SH. d_{min} and d_{max} give the lowest and highest range of particle size that can pass the sieves.

Particle size in mm		***Mass percentage of the particle fraction in %***		
d_{min}	d_{max}	SH	SP	SP Mix
0.0	0.063	4.61	15.28	4.61
0.063	0.125	1.87	6.40	1.87
0.125	0.25	75.81	30.41	75.81
0.25	0.5	17.7	39.31	17.7
0.5	1.0	0.01	7.56	0.01
1.0	2.0	0.00	1.03	0.00
2.0	4.0	0.00	1.18	0.00
4.0	8.0	0.00	2.25	0.00
8.0	16.0	0.00	2.33	0.00

2.3 Preparation of sand columns

Sand columns were prepared in two sizes to meet the different size requirements of the analytical methods. For unconfined compressive strength and water permeability tests sand columns were prepared from 50 mL reaction tubes, diameter 27 mm (Greiner centrifuge tubes, Sigma-Aldrich). The bottom part of the tube was cut off and five holes (diameter 6 mm) were drilled in the cap to allow liquids to flow freely through the column. Prior to filling the columns with sand, the holes were covered with filter paper (40 µm. Qualitativ Filterpapier 417, VWR International). For micro-CT smaller samples were necessary due to the size of the detector of the utilized CT device (see section 2.6). Therefore, molds were prepared from the top part of 10 mL standard Pasteur pipettes not graded 300 mm (Carl Roth, Germany). They were cut at the top and the bottom part was shortened to 1 cm to allow better handling of the columns. The outlet of the pipette was sealed with cotton. The conical part of the pipette was filled with sand SH as drainage. A non-woven all-purpose cloth (84 % viscose, 16 % polypropylene, W5, Germany) was placed on this drainage sand. The columns were filled with sand through a funnel that was placed roughly 1 cm above

the molds. 40 g sand for the big samples and 5 g sand for the small samples was poured slowly through the funnel into the mold. The sand was covered with filter paper as well to prevent disturbing the surface of the sand column during MICP. Afterwards, the columns were closed with a plug containing a hole for the application of bacteria suspension and calcination solution during MICP.

Additionally, the bulk density of the loosely filled sand was determined in 20 mL metal cylinders with a diameter of 27 mm. Therefore, sand was prepared in the same way as for the MICP molds and the excess sand from top was removed with a metal plate (N=5). After weighting the sand, the bulk density of the sand was calculated as g/cm³. The obtained bulk densities were as follows: SH (1.47±0.02 g/cm³) SPMix (1.38±0.01 g/cm³), SP0063 (1.25±0.02 g/cm³), SP0125 (1.39±0.01 g/cm³), SP0250 (1.46±0.02 g/cm³), SP0500 (1.43±0.03g/cm³). Except SP0063 all of these densities lie within 5 % of the average of 1.39 g/cm³ while SP0063 deviates 10 % from this average.

2.4 MICP Protocol for biocementation

MICP treatment was conducted as surface percolation method through sequential injection of resuspended cell suspension (OD_{600} = 3.5) and a calcination solution containing 1492 mM urea (Fisher Scientific, USA) and 1392 mM calcium chloride dihyadrate (Carl Roth, Germany).

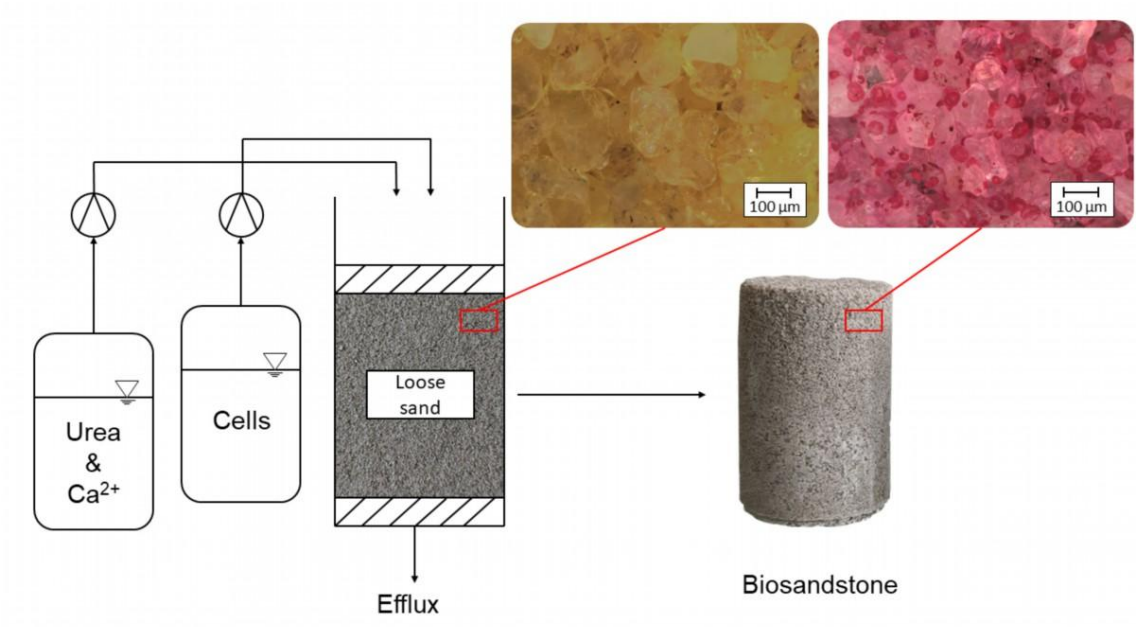

Figure 1: Schematics of biosandstone production. Microscopic images show the surface of loose sand and biosandstone after staining calcium carbonate crystals with Alizarin Red S (Carl Roth, Germany).

Initially, 50 % pore volume of cell suspension was applied on top of the column with a peristaltic pump (IPC 8, ISMATEC, Switzerland) with a flow rate of 3 $mL \cdot min^{-1}$. After 2 hours 50 % pore volume of calcination solution was applied at 3 $mL \cdot min^{-1}$. Since the percolation of liquid into the sample decreases with additional MICP cycles due to clogging this time between the applications was necessary to give the cell suspension enough time to percolate into the sample during the last cycles of the treatment. The application of calcination solution was followed by 5 hours of incubation at 25 °C to give the reaction time to form calcium carbonate. This treatment is considered as one cycle with 10 cycles in total for each column. 10 cycles were chosen because preliminary experiments showed that with 10 cycles we can achieve a reasonable strength of the samples while clogging of the samples started to occur from 10 cycles onwards which lead to uneven cementation and a wider variance of compressive strength (Supplement 7). After the last cycle columns were washed with 300 % pore volume of distilled water to flush out residual salts and cells and dried for 72 hours at 60 °C. After curing at room temperature for 14 days unconfined compressive strength and permeability tests were performed.

2.5 Determination of calcium carbonate content

For calcium carbonate determination 5 g of the sample were mixed with 20 mL of 2 M hydrochloric acid. Once no production of CO_2 gas could be visually observed the reaction was given another hour to dissolve any remaining calcium carbonate. Afterward the samples were diluted in 2 mM nitric acid and the content of soluble calcium ions was determined by ion exchange chromatography (n 930 Compact IC Flex, METROHM GmbH & Co. KG). Based on the concentration of soluble calcium ions the total amount of calcium carbonate in the sample was calculated and the content in % calculated as the quotient of calcium carbonate about the initial sample weight.

2.6 Image acquisition by X-ray microcomputed tomography

To get a better resolution on micro-CT, the smaller samples (diameter about 10 mm) were used as mentioned in section 2.3. Depending on the sample diameter, a scan resolution of 6.79 µm/pixel was achieved. With 90 kV and 110 µA as well as a 0.25 mm aluminum filter and an exposure time of 3012 ms the samples were X-rayed

at 0.3° angle steps. Scan duration was about three hours in a skyscan 1272 X-ray microtomograph (Bruker, Kontich, Belgium). To reduce noise, a frame averaging of 4 was applied. Thereafter the reconstruction was performed by using NRecon 2.0.0.5 (Bruker, Kontich, Belgium). Here postalignment was 1, no smoothing was applied, ring artefacts reduction was set to 50 although there were less to none visible. Min and max image conversion were set to 0 resp. 0.077945. Images were reconstructed as tiff 16 images.

Table 2: Overview of micro-CT samples.

Sample Label	Particle Size in mm	Weight in g	Calculated object height in Volume of Interest in mm
SP0063	> 0.063	5.01	10.054
SP0125	> 0.125	5.02	10.570
SP0250	> 0.250	5.03	10.183
SP0500	> 0.500	5.02	10.257

2.7 Determination of water permeability

Water permeability was determined as the coefficient of permeability k_f by Darcy´s law. The measurement was conducted at test station compliant with DIN EN ISO 17892-11 [36]. The test station includes a pressure-controlled tank made of polyvinyl chloride. The pressure in the pressure tank is set to a constant value of p = 0.5 bar by a compressor, which is regulated by a pressure gauge. The container is a tube that is screwed to a teflon top and bottom section using threaded rods. The samples are measured using modified centrifuge tubes. These are positioned in the centre of the pressure vessel. Filter disks made of sintered bronze with a layer thickness of 2 mm are placed above and below the sample or the loose bulk material. The centrifuge tube is screwed into a thread in the base section. The upper opening of the tube is closed using a silicone plug in which a silicone tube is positioned. The flow rate of water is set manually in the range 2 - 200 $mL \cdot min^{-1}$. Once a stationary flow regime through the sample has been established, the amount of liquid passed per time can be measured. The measurement duration of the liquid volume was five minutes with one measurement being carried out every minute. The quantity of liquid that passes through is collected in a container and the mass was determined using a

digital scale. The coefficient of permeability k_f was calculated with the equations of Darcy´s law (equation 3-5).

$$\Delta h_W = i \cdot H_P \quad \text{Eq. 3}$$

$$v = \dot{V} \cdot A^{-1} \quad \text{Eq. 4}$$

$$k_f = v \cdot i^{-1} \quad \text{Eq. 5}$$

Using the measured sample height H_P and a self-selected hydraulic gradient i, the hydraulic pressure difference Δh_W can be calculated (Eq. 3). This is required to set the pressure applied to the pressure gauge. The flow velocity v is then calculated using the volume flow $\dot{V}$, which is determined by the individual measurements, and the cross-sectional area A of the biosandstone sample (see Eq. 4). Finally, the permeability coefficient k_f is determined using the flow velocity v and the hydraulic gradient i (see Eq. 5).

3 Determination of unconfined compressive strength

Unconfined compressive strength (UCS) was determined with a universal testing stage (Compression Testing Machine Type 812, FHF Strassentest, Germany). Before measurement the top of samples were sanded flat to achieve an even surface for force application during measurement. The final height of the samples H_P were 40 ± 5 mm. Force was applied with a traverse speed of 2 mm·min^{-1} until the sample broke. From the resulting stress-strain diagrams the UCS was determined.

3.1 Image analysis

First of all, the Volume of Interest (VOI) is determined. Due to the sample setup inside the pipette with the loose sand or MICP sandstone between filter paper and non-woven cloth, the amount of images in one stack varies. The separation objects filter paper or non-woven cloth can lie in an angle and therefore, the images for image analysis have to be chosen wisely. For the analysis, only images without pipette walls, filter paper or non-woven cloth are used. Despite efforts to keep deviations as small as possible, the mean of images in one stack is about 1511 ± 28 images. This results in an object height of 10.266 ± 0.19 mm for MICP sandstone characterized with micro-CT. After the VOI determination, the image analysis can be started. Therefore, either no filter, Gauss filter or non-local means

filter were applied. No filter gives the reference, while Gauss filter is quite popular and part of many image analysis softwares. So it is a good option to compare it to other digital filter results. And non-local means filter was chosen because of the fact, it uses the entire image not just surrounding pixels for comparison of grey values and their adjustment.

The image analysis was performed with CTAnalyser V1.20 (Bruker. Kontrich, Belgium). Gauss filtering is possible with CTAnalyser (CTAn), while non-Local means (NLM) has to be performed with Fiji, an open source image processing package basing on ImageJ2. In Fiji it is possible to use the non-local means plug-in based on the work of Buades et al. [37] and Darbon et al. [38]. NLM was performed with Sigma=15. Afterward, a lot of noise, especially in sand grains, is removed. But it has to be kept in mind, that filters maybe cause artefacts, which are then part of the image analysis and results. For the image analysis with CTAn two task lists are necessary. In the first task list, sandstone volume and porosity of the object are calculated. The second task list is all about analysing pore space between sand grains. Of interest here are either the connected pores, which form a coherent pore system, or the individual pores. Both task lists can be found in supplementary material (Supplement 8-11).

Figure 2 illustrates the process of image acquisition to image analysis of sandstone and the determination of the connected pore network (CPN) and individual pores. First of all, the different filters or no filter was applied to the grey value images of the volume of interest. Then, when noise is removed, the biosandstone can be extracted by setting a threshold based on the histogram of the grey value distribution. Afterwards, the binarized images are used to calculate the sandstone volume and object porosity by creating a 3D model out of the 2D image stack using the marching cubes algorithm [39]. To extract the CPN and the individual pores (as shown on Figure 2), first a Region of Interest (ROI) shrink wrap is performed which finishes the first task list. Here, a new region of interest can be created from an existing ROI by adapting the shape of the sandstone object, which was calculated before [40]. An inversion of the sandstone images and a removal of the edge areas forms the basis of the following steps. Bitwise operations and a despeckle step are necessary to separate the CPN from the individual pores. For CPN and individual pores, the

calculation of object volume and pore diameter was also performed using marching cubes algorithm.

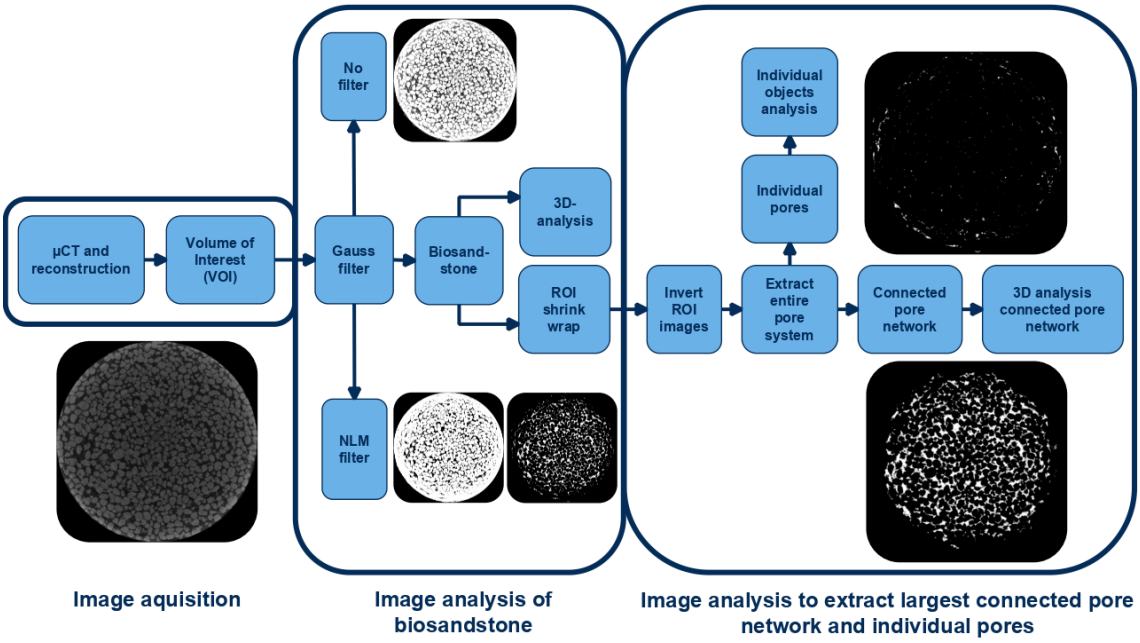

Figure 2: Scheme of image analysis procedure: The analysis is divided into two task lists where the first task list is used to analyze the sandstone object, and the second one focuses on determining the connected pore network and the individual pores.

4 Results and Discussion

4.1 Relationship between Calcium carbonate content, Water Permeability, and Unconfined Compressive Strength of biosandstone

The treatment of each sand with MICP resulted in observable calcium carbonate depositions on the sand surface (Figure 3). In the samples, effective calcium carbonate bridges as well as ineffective crystals that grew into void space could be observed. When observing the figure, the 2D nature of the microscopic image should be kept in mind. It is possible that the ineffective calcium carbonate crystals could be effective in the third dimension. The former effect is the main goal of biocementation through MICP for the improvement of mechanical soil characteristics and the reason for the observed strength of sand after biocementation. The observed quantities of calcium carbonate range from 11.60 ± 0.25 % $g \cdot g^{-1}$ to 6.69 ± 0.59 % $g \cdot g^{-1}$ of total weight with an overall trend of decreasing calcium carbonate content with increasing particle size (Figure 5).

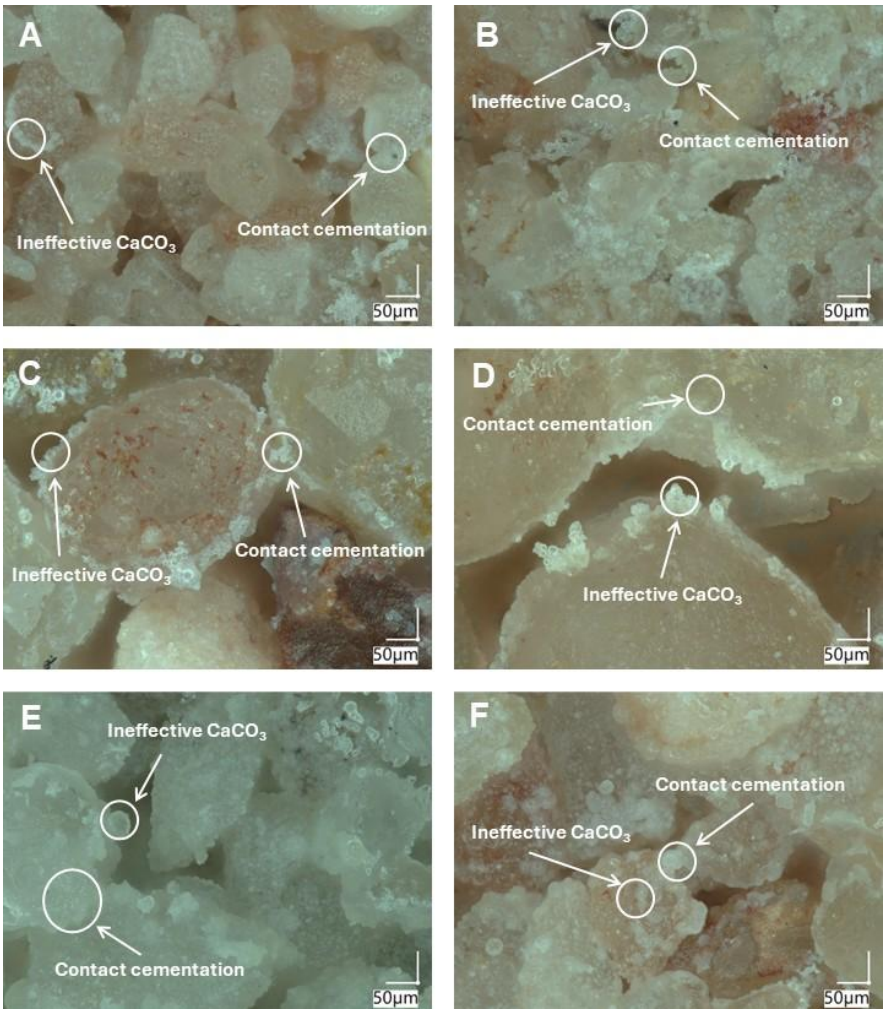

Figure 3: Microscopic images with 500x magnification (VHX-7000, Keyence, Germany) of biocemented sand. (A) SP0063; (B) SP0125; (C) SP0250; (D) SP0500; (E); SH; (F) SPMix

For each sample, there is a decrease in water permeability caused by MICP treatment. For the loose sand and samples treated with MICP, the water permeability is inversely proportional to the grain size (Figure 4). The water permeability coefficient for the loose sand fraction SP0063 – SP0500 ranges from $6.37 \cdot 10^{-5}$ m·s^{-1} to $4.55 \cdot 10^{-4}$ m·s^{-1} and decreases through MICP treatment to $2.12 \cdot 10^{-6}$ m·s^{-1} (SP0063) to $2.50 \cdot 10^{-4}$ (SP0500). The reduction of permeability ranges therefore from 96.7 % (SP0063) to 45.0 % (SP0500) and generally decreases with increasing particle size. The strongest decrease from $6.36 \cdot 10^{-5}$ m·s^{-1} to $2.12 \cdot 10^{-6}$ m·s^{-1} occurs for the smallest fraction SP0063. In contrast, the lowest decrease from $4.55 \cdot 10^{-4}$ to $2.50 \cdot 10^{-4}$ m·s^{-1} occurs for the largest fraction SP0500. Permeability coefficients of SH and SPMix lie between SP0125 and SP0250, which is because these fractions make up the largest proportion of this fill at 75.8 % and 17.7 %. Both the two sands SH and SPMix as well

as the individual fractions of SP show a reduction in water permeability after MICP treatment of 45.0 to 96.7 %. This reduction of permeability through MICP can be attributed to the blocking of flow paths through the sand. Especially large pore networks and channels through the sand get blocked by cementation and permeability is reduced with increasing degree of cementation [40]. The higher decrease for lower particle sizes is most likely attributed to this blocking effect. For smaller particles void space decreases which could lead to calcium carbonate crystals forming with a higher chance at pore throats leading to reduced permeability [9]. Furthermore, for biosandstones with smaller particle size a generally higher degree of cementation was observed (Figure 5) which also increases the chance of pore blocking. UCS shows a similar trend for sand fractions. With increasing particle size the UCS of the biocemented samples decreased from 3.04 ± 0.73 MPa (SP0063) to 0.74 ± 0.15 MPa (SP0500) (Figure 5).

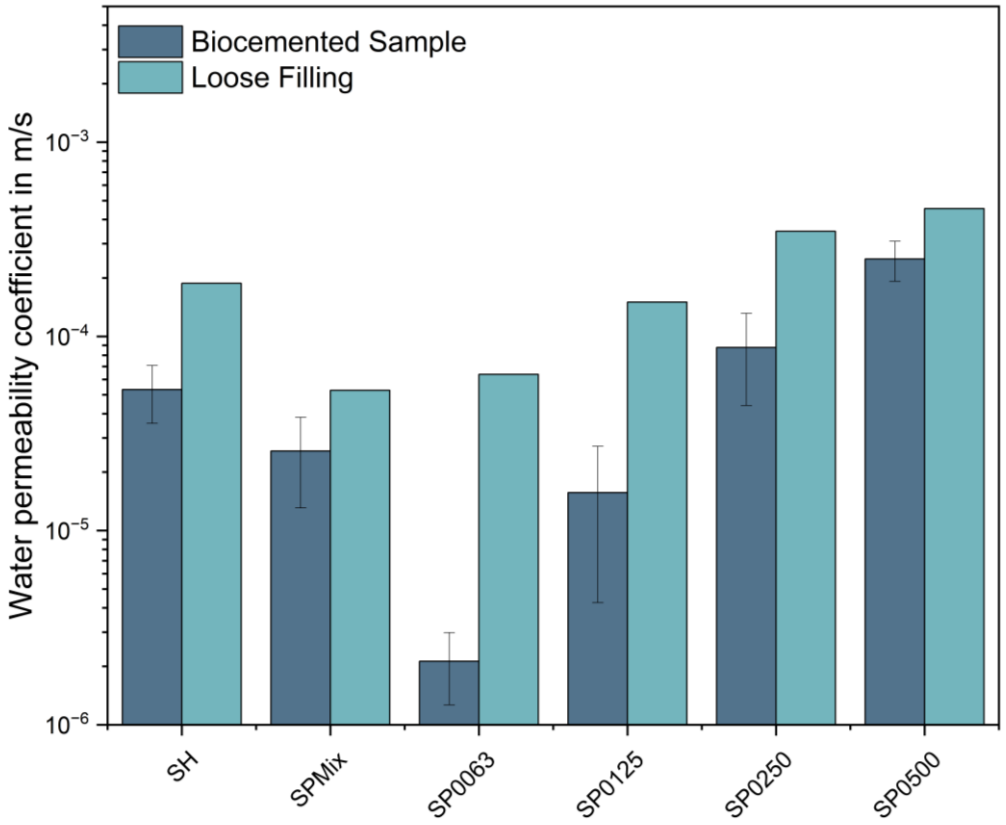

Figure 4: Water permeability coefficient of before and after MICP treatment for different sand fractions. SH = Sand Haltern, SP = Sand Picard. The sand fractions were treated with 10 cycles of *S. pasteurii* and calcination solution according to section 2.4. The error represents the standard deviation of n=6 biological replicates.

Since the void space between particles is bigger for higher particle sizes [9] the formed calcium carbonate crystals have a higher chance of growing into voids instead of forming effective bridges at contact points. SP0063 and SP0125 have nearly identical UCS with SP0125 with higher variances than samples with a bigger particle size which might be due to a higher chance of clogging in the sample which leads to a more uneven distribution of bacteria suspension and calcination solution and therefore uneven calcium carbonate distribution.

This clogging effect is a common phenomenon of MICP calcinated sand although more prominent in sand with low permeability since bacteria suspension and calcination solution can distribute more freely through the sand and therefore the reaction is more evenly distributed throughout the samples [41]. This clogging effect is also likely the reason for the higher decrease in water permeability for smaller particle sizes as the precipitated calcium carbonate blocks pores and thereby flows paths through the sand.

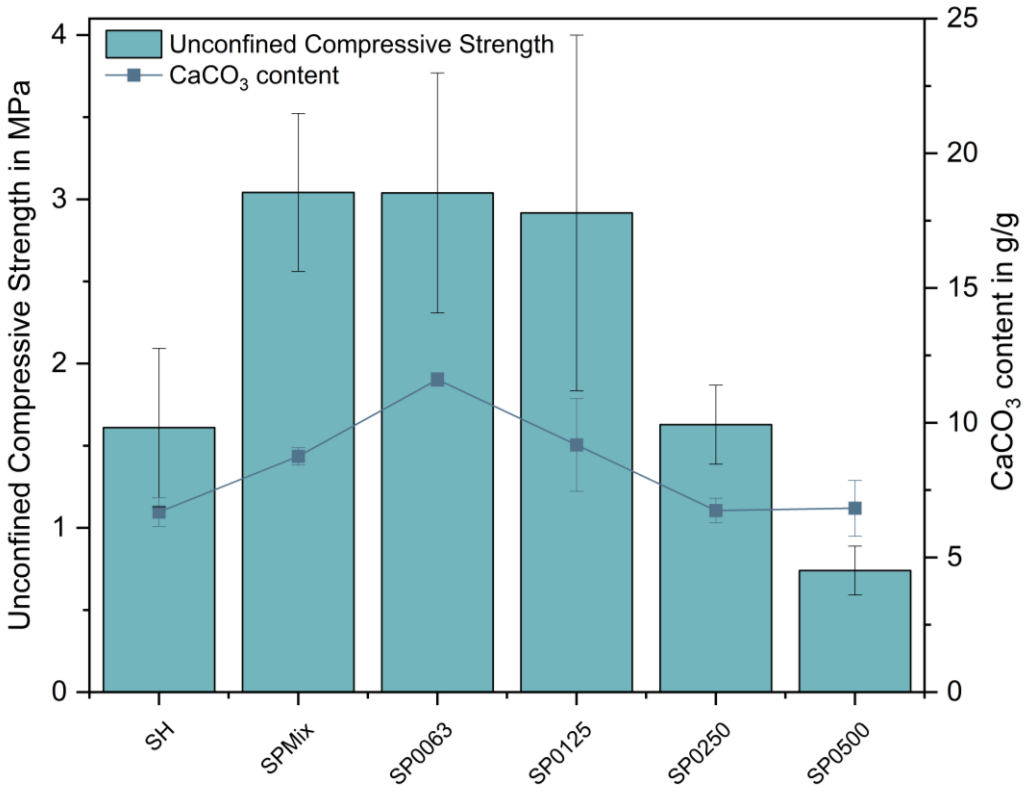

Figure 5: UCS and $CaCO_3$ content for different sands and particle fractions. SH = Sand Haltern, SP = Sand Picard. The sand fractions were treated with 10 cycles of *S. pasteurii* and calcination solution according to section 2.4. The error bars represent the standard deviation of n=6 biological replicates.

The decrease in calcium carbonate content with increasing particle size supports this. Samples with lower particle sizes withhold more calcium carbonate on throat points than samples with bigger particle sizes most likely due to flushing out calcium carbonate from big pores that could not attach to the surface of particles. This effect resulted in higher calcium carbonate content which subsequently resulted in higher UCS and greater reduction of permeability. It is notable, that by reconstructing the particle size distribution of SH with SP did not lead to similar UCS or reduction of permeability coefficient. With 3.04 ± 0.48 MPa and a reduction of permeability of 51.31 % SPMix had a significantly higher UCS compared to SH (1.61 ± 0.48 MPa) while having a lower reduction in permeability coefficient (71.60 %). This suggests that it is not solely the particle size of the sand that impacts the result but also the type of sand. Particle shape and size might be of similar importance. A study conducted by Song et al. investigated MICP-treated silica sand with different particle morphologies and gradings from three sand types sieved into four size fractions: (1.00–0.85 mm), (0.85–0.425 mm), (0.425–0.250 mm), (0.250–0.180 mm) [42]. They observed that UCS of treated spherical and near-spherical sands peaked at 5.21 MPa for particle sizes of 0.85-0.425 mm, whereas treated angular sands had increasing UCS with decreasing particle size. Similar to our findings, they observed an increase of calcium carbonate content with decreasing particle size for all tested sand types. They concluded that particle morphology and resultant bonding mechanisms exert critical controls in MICP-grouting that significantly affect the cementation structure and, as a result, the ensemble strength of the treated assemblage. Gowthaman et al. consolidated three well-graded sands Mizunami (d_{50}=1.6 mm), Mikawa (d_{50}=0.87 mm), and Toyoura (d_{50}=0.2 mm), and achieved compressive strengths of 1.82 MPa. 2.67 MPa and 3.98 MPa respectively [43]. Zhao et al. observed a notable reduction in permeability and improvement in UCS with the incorporation of different fine particle contents and pore ratios in silt [44].

Although our understanding of the mechanisms behind the impact of grain size and shape of particles on the process remains limited [9], the importance of particle size on UCS, permeability reduction, and calcium carbonate content of biocemented sand when choosing sand for MICP is clear. In summary, our research findings are in alignment with recent literature, indicating that the efficacy of MICP in improving

UCS, reducing water permeability, and influencing calcium carbonate content is significantly affected by sand particle sizes. These insights not only validate our research outcomes but also highlight the necessity of precise knowledge of the soil that will be utilized for MICP. Although the macroscopic measurements of UCS, calcium carbonate content, and permeability hold valuable information on the efficiency of the MICP process it remains important to gather information on the internal structure of biocemented sand that cannot be explained by these measurements. CT image analysis is a tool that could help extend our understanding of the internals of biocemented sand.

4.2 CT results

Images of biosandstone, created by X-ray microcomputed tomography and image analysis, were first of all processed with or without a digital filter. Afterwards, image analysis was performed with the two task lists (Supplement 8-11). Resulting images can be separated by their containing objects like sandstone, connected pore system or individual pores. A comparison of image components like sandstone, pore network, or edge areas shows: Whether or not a filter is used, the sandstone has an average proportion of about 63 % of the image, while the pores have about 13.5 % to 14.9 % as can be seen in Figure 6. The rest are edge areas, which exist due to the round sample geometry.

Figure 6 shows exemplarily 2D images the results of image analysis by displaying sandstone and pore network, consisting of connected pores and individual pores. Analysed was the entire sample in 3D, where the marching cubes algorithm, developed by Lorensen et al. [39], created a 3D Volume out of the 2D image stack. The object(s) of interest, respectively sandstone or pores, were afterwards used to determine parameters like sandstone volume, porosity or pore volumes. For a better visualization, Figure 6 presents 2D slides instead of 3D corpses, where especially the individual pores would have been difficult to be seen due to the lack of a spatial resolution in this figure. Also, the effect of different sand grain sizes on the difficulty of image analysis can be seen in the binary images. Images treated with non-local means filter show in mean the highest proportion of sandstone and the lowest proportion of pore system. Without a filter, the largest proportion of pores and the smallest proportion of sandstone are present.

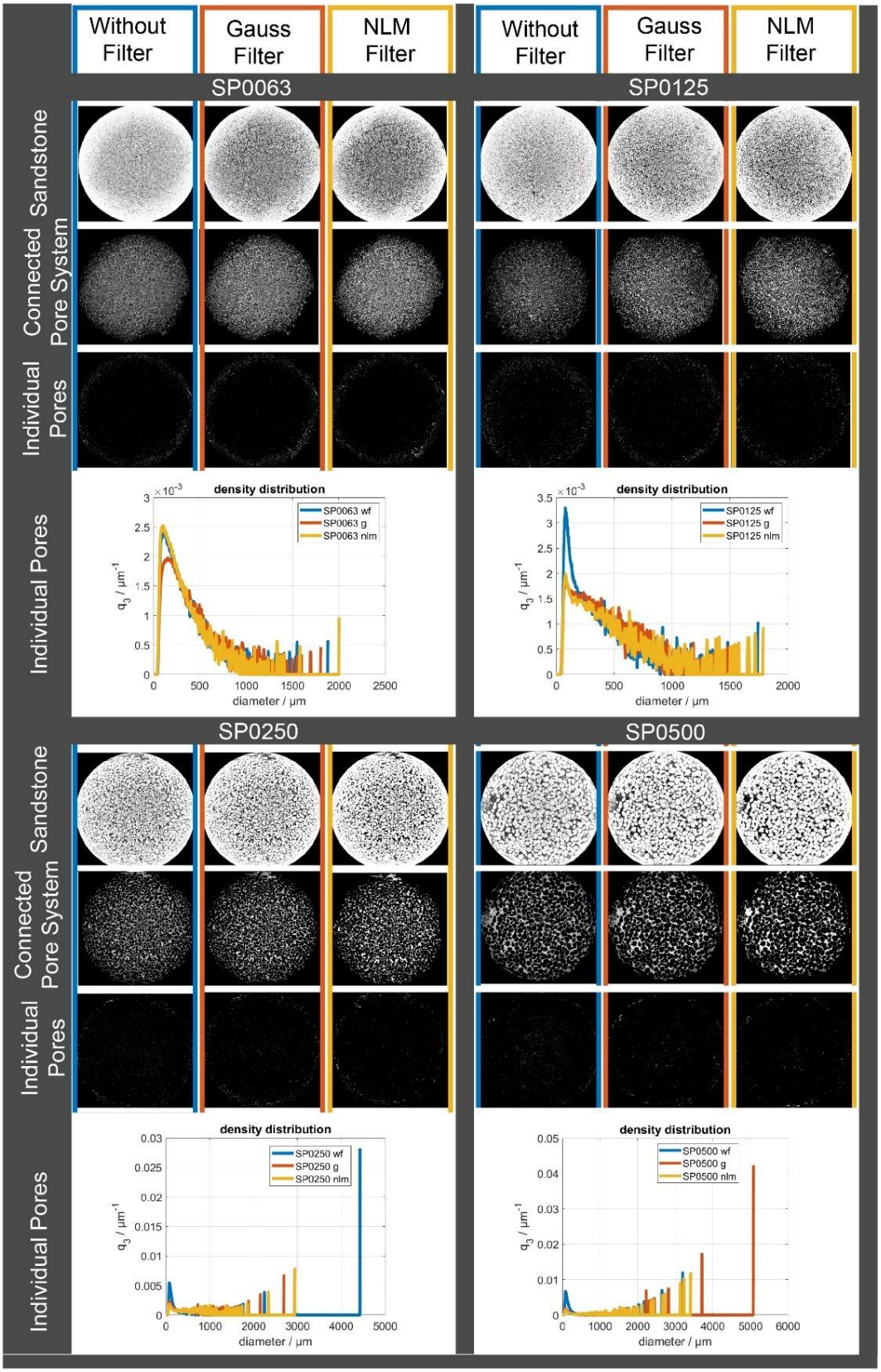

Figure 6: Results of X-ray microcomputed tomographic characterization and image analysis: Comparison of filter effects and the resulting sandstone object, connected pore network and pores and individual pores. These individual pores are also shown as density distributions of pore volume with wf = without filter, g = Gauss filter, nlm = non-local means filter.

Noise is probably still present here, which is calculated as pores after setting the threshold and analyzing the image. Table 3 shows the results of image analysis regarding the volumes of either connected pore network or biosandstone, also in comparison with used filters. It can be seen that SP0063 has always the lowest volume of CPN. The reason for this may be that the small sand grains are more densely packed than the sand grains in SP0500. The object volume of biosandstone ranges between 1963 mm^3 up to 2068 mm^3. Differences in the volume of biosandstone regarding the used filters can be recognized.

Table 3: Volumes of connected pore network and biosandstone objects calculated by CT and the image analysis

	Without filter		***Gauss filter***		***NLM filter***	
Sample Label	Connected Pore Volume in mm^3	Sandstone object volume in mm^3	Connected Pore Volume in mm^3	Sandstone object volume in mm^3	Connected Pore Volume in mm^3	Sandstone object volume in mm^3
SP0063	428	1974	446	1963	418	1981
SP0125	466	2061	466	2068	462	2068
SP0250	468	1967	452	1990	453	1998
SP0500	469	1974	453	1999	440	2010

When analyzing the pore system, it must be noted that there are two ways to achieve the results: CTAn task list 1 calculates the porosity based on the sandstone object, while there is also the possibility to characterize the pores itself to get more information. This is done by the second task list, as described in section 3.1. The detection limit for pores due to the resolution must be taken into account.

Figure 6 shows excerpts of the results of image analysis either of sandstone or CPN and individual pores. The direct characterization of the pores show that there is a large network of connected pores forming the CPN. It can be seen that the individual pores are found more frequently in the edge areas towards the pipette wall at every used sand grain fraction. Whereas the CPN is mainly at the center of the biosandstone. This is particularly interesting about a uniform flow of both, bacteria solution and calcination solution and has also an effect on solidification. Because the solutions should distribute homogeneously through the sand and not just pass

through completely. To achieve this, the reaction time must be correct so that there is sufficient time for the cementing reaction. In addition, the cementation should be as uniform as possible through the sample to achieve reproducibility. The micro-CT images provide insight in the biosandstone and enable the detection of optimization potentials. The general visualization of biosandstone can significantly enhance our understanding of the cementation process. Notably, the edges of the biosandstone show a larger amount of individual pores and a generally higher density of solid material compared to the internal part of the sample (Figure 6). This observation could be due to a higher formation of calcium carbonate at the edges of the sample which leads to more pore throats being blocked and therefore connected pores being disconnected. The reason for this could be due to a flushing-out effect of residue bacteria cells and small calcium carbonate crystals through the center of the samples with each new cycle of MICP treatment, while more bacteria and crystals being retained in the outer boundaries of the sample.

To validate this claim, it would be necessary to gain higher resolution insight into the pore space of the samples, as discussed in section 3.2. Although there is a possibility that this effect could be due to boundary effects of the filtering, this case is unlikely since boundary effects influence a zone not larger than twice the particle diameter [45]. The effect of the larger amount of individual pores is observable further into the sample than this effected zone would occur, especially for particle sizes of 63 µm and 125 µm. Micro-CT measurements offer valuable insight and enable a deeper investigation into the differences between various cementation protocols. For future research, it could be interesting to investigate e.g. the effects of the contact flexible mold on the distribution of calcium carbonate crystals in the biosandstone [46]. During this cementation protocol, the sand is loaded with bacteria suspension and the sample is immersed in a bath of calcination solution. Micro-CT could help to detect how strongly pronounced a cementation gradient from the outer layers to the internal parts of the biosandstone is. Also, it helps to detect defects and large pore systems. These large pore systems can form channels and have a bigger impact on the permeability of sandstone than just the porosity [47]. Also, possible weak points in the sandstone in the form of large pore systems that impact the UCS of biosandstone can be detected by micro-CT. Although it was not possible for us to find

a correlation between large pore systems and breaking points of biosandstone due to the destructive nature of UCS testing, a coupled measurement of UCS and CT scans could be possible to detect initial crack forming. The location of these cracks in the biosandstone would help greatly to improve our understanding of cementation protocols. Whereas the individual pores have also an influence on the biosandstone strength, their influence depends on the pore volume and their number. This is especially important in the context of the correlation of calcium carbonate content, permeability and strength of the biocemented sample.

While this study and various research results [19, 48–50] showed that there is a correlation between compressive strength and calcium carbonate content observing the bulk calcium carbonate content will not be enough to describe or reliably predict strength parameters. It is necessary to also include intrinsic information about the efficiency of the bonding of calcium carbonate crystals as described by Dadda et al. [51] or Roy et al. [22]. Dadda et al. [51] focused on differentiating between different types of contact between sand particles (frictional contact, mixed contact and cemented contact) and concluded that for degrees of calcium carbonate most crystals form mixed contacts. Roy et al. [22] on the other hand differentiated between active and inactive bonds of calcium carbonate with a focus of the effects of both bonding types on the result of the MICP. Both studies conclude that there is a necessity to study intrinsic properties of MICP samples which will help to better understand the impact of different MICP treatment strategies on macroscale parameters after treatment. The nature of bonding and non-bonding particles can also be observed through microscopy as shown in section 3.1 but the use of microscopy is not suitable to determine larger amounts of bonding types through a whole sample compared to CT analysis which allows to compute large amounts of images and data from a single sample. With a resolution of 6.79 µm/pixel during this study a visualization of the bonding crystals was not possible. Although this resolution is sufficient to observe pores (average sizes of 91.7 µm in this study which results in an average of 13.5 pixels per pore diameter) or the sand particles (63 to 500 µm in this study which results in 9.3 to 73.6 pixel per average particle diameter) the resolution is not suitable to detect smaller calcium carbonate crystals of only a few micrometre. In follow-up studies higher resolution must be achieved, for example

by reducing the sample size even further or by diving the smaller samples in subsamples to be able to determine the amount of efficient bonding of the precipitated calcium carbonate. As the understanding of MICP increases it will become more necessary to include information about intrinsic pore systems and the type of calcium carbonate bonds for example through CT or even synchrotron [52] images in studies concerning the optimization of MICP protocols to be able to reliable differentiate between bonding and non-bonding calcium carbonate deposits. Therefore standardized protocols have to be developed to achieve high comparability of these results. This also includes a recommendation on the use of filters for preprocessing the gray value images. Because depending on the filter, changes are made to the gray values by weighting. As soon as the threshold is set, this results in different quantities of voxels that represent the object to be analyzed (sandstone or pore network) as can be seen in Table 4 for individual pores.

Table 4: Number of individual pores

	Without filter	***Gauss filter***	***NLM filter***
Sample Label	Number of individual pores	Number of individual pores	Number of individual pores
SP0063	581 020	456 481	468 219
SP0125	398 861	277 628	305 105
SP0250	380 962	171 691	142 371
SP0500	420 214	136 188	100 691

Here, without a filter a lot of noise is recognized as a pore network, so the use of a sufficient filter is quite useful. The resolution of the images should also be taken into account, especially with small sand grain sizes. Because it is more difficult to distinguish whether there are pores or noise is changing the results. Furthermore, Figure 6 shows the individual pores as pore volume distributions. There it can be seen, especially for SP0063 and SP0125, that without the use of a filter, the distribution is shifted towards small pore diameters. Additionally, with consideration of the other curve profiles, which show fewer small pores, it can be estimated, that without a filter there is noise in the ROI images, especially for SP0125. It is also noticeable in Figure 6 that with increasing sand grain size the amount of pores

towards higher pore diameters increases. SP0250 and SP0500 show higher pore diameter differences about the used filter. Based on this data, no trends can be seen but to be sure, a higher sample size has to be analyzed. Also, it has to be kept in mind that pore volumina are calculated as spheres and the influence of the pore diameter is high. Therefore, small differences in the filtering process can lead to bigger pores and are shown as peaks in Figure 6. While the pores of biosandstone are mostly not in the shape of a sphere due to the shape of sand grains and their packing, the assumption of a spherical shape is a simplification to create a working model. The representation as pore distribution curves provides good possibilities for comparison over the entire sample height. In contrast, Minto et al. [21] chose to display the porosity per image along the z-axis to provide an insight into the pore structure in the biosandstone. In SP0063 there is, regardless of whether a filter was used in the image analysis, the highest proportion of individual pores with about 8.76 % (NLM filter) up to 10 % (without filter or Gauss filter) of total pore volume. Towards larger sand grains, the proportions become smaller and smaller until it is only 1.39 % (NLM filter), 1.48 % (Gauss filter), or 2.87 % (without filter) for SP0500.

If the entire pore system is considered, it can be seen that the volume of connected pores is lower after using the NLM filter than without the filter (see Table 3), despite otherwise identical treatment of the images. This illustrates the effect of the NLM filter very clearly, as the gray values are averaged here as described above. Some areas that would be counted as pores without the filter are probably influenced by NLM in such a way that they are included at a threshold of 50-255 and counted as sandstone. The use of filters in image analysis and characterization of pore systems has an impact on the results which is shown in Figure 6. The influence of the filter method varies for different analysis results like the amount of individual pores, volume of connected pores, or total porosity as well as sandstone volume. It is important to mention the filtering method in investigations and consider its effects on calculations. Filters are necessary to reduce visible noise in micro-CT images. The Gauss filter visually reduces noise by smoothing but still retains a high proportion of very fine pores and speckles. On the other hand, the NLM filter performs well, particularly for fractions with larger sand grains. However, it should be noted that the NLM filter produces a noticeable difference from the original image due to the way it

changes the gray values, which affects the results when setting the threshold for image analysis.

All in all, the use of a filter for our data is necessary to remove noise. The comparison of Gauss filter and non-local means filter showed differences in resulting images. Thresholding of this images led to different amounts of sandstone volume or pore network volume. By using the non-local means filter, a more uniform grey value distribution within the sand grains could be achieved and therefore less speckles within image analysis. It has to be kept in mind, that the sigma parameter must be adjusted to the size of the sand grains depicted so that even the smallest grains of sand and pores are still sharply depicted and are not removed by blurring, if sigma is too large. We recommend using the NLM filter for the application on biosandstone, taking into account the problems and limitations mentioned above.

Further steps in image analysis of the pore network are the determination of pore throats, particle contacts or pores connecting to each other, that are not part of the biggest connected pore network. This analysis is necessary, as research results showed that pore throats play an important role in the efficiency of MICP. This is due to bacteria movement through soil being dependent on the ratio of bacteria size to pore throat size [53, 9, 54] and the fact that formation of calcium carbonate crystals at pore throats seem to correspond to effective $CaCO_3$ cementation [55, 56]. Furthermore, calcium carbonate forming at pore throat has a significant impact on the permeability of the treated samples [57]. Knowledge about pore throats before and after certain treatment cycles during MICP could therefore lead to valuable insights into phenomena like blocking of the samples at the injection point, which is a common phenomenon during MICP treatment and most likely leading to inhomogeneous treated samples. Therefore, algorithms like Delaunay Tessellation [58], Maximal Ball method [59], Watershed [60] or Medial Axis [61] can be used. Each method has advantages or limitations, which have to be considered for the image analysis process:

- Maximal Ball (MB): Here, spheres are constructed at each voxel of the void until they touch the solid boundaries of the next void. A sphere is a maximal ball, if it is entirely within the material and not contained in another sphere. The spheres of the MB are considered as pores while the minimal balls between

the pores are considered as pore throats [62]. This method often leads to an underestimation of throat sizes and also produces tiny and incorrect throats [63].

- Medial Axis (MA): In this method the pore space is transformed into a reduced axis resulting in a topological skeleton along the middle of pore channels [64]. This reduction can be achieved through pore space burning algorithms [65]. After the creation of the skeleton, pore bodies (clusters of void voxels, that are bounded by solid voxels and necks) can be determined [62]. They build the pore space with the constituent pores. A disadvantage of this method is the requirement of a clean-up process afterwards, because noise leads to false positive identification as pores [66]. But MA method allows the preservation of morphological or topological parameters of the pore network [64, 62].
- Delaunay Tessellation (DT): For this method, starting with a packed bed, the pore space is subdivided into a set of tetrahedral volumes with the vertices as the centres of four neighbouring spheres with the void space inside the tetrahedron representing a pore [67]. Then the tetrahedra are merged into larger polyhedrons if single voids were unnecessarily subdivided into multiple ones [68]. To mention hereby is, that the merging of the Delaunay tetrahedra is a subjective criterion and therefore prone to errors, but the throat size can be clearly defined [63].
- Watershed (WA): Here grayscale images are considered as topographic surface based on pixel intensity. Starting from local minima the space is “flooded” until floods coming from two minima come into contact [69]. Because of the “flooding-mechanism", many different pore geometries can be analysed, but often over-segmentation is archived with this method [62].

Further analysis of the pore throats with these algorithms would be suitable to explain some of the observations from section 3.1, especially the stronger reduction of pore size with a smaller particle size of the sand and the higher calcium carbonate content, possibly due to in pore throats retained microorganisms forming more calcium carbonate. Future research on this topic will therefore require CT data with higher resolution to be able to gain further insight into these correlations which will allow researchers to develop new MICP application strategies.

5 Conclusion

In this study, different sand fractions from a local sandstone quarry were consolidated using MICP. The resulting biosandstones were analyzed for unconfined compressive strength, water permeability, and calcium carbonate content. Additionally, the samples were visualized by micro-CT, and the resulting pore system was analyzed. From the results, the following conclusions can be drawn:

- Sand fractions ranging from 63 µm to 500 µm as well as ungraded sands could effectively be treated with MICP which resulted in a reduction of permeability coefficient and measurable unconfined compressive strengths (UCS) of biosandstone
- Smaller particle size of sand was better suited for MICP than larger particle size. For smaller sand particles higher UCS, calcium carbonate content and reduction of permeability coefficient could be observed
- Particle size distribution is not the only parameter of sand affecting the efficiency of MICP. Particle shape likely impacts the MICP, as well which became apparent by the different results of industrial sand and a reconstruction of the particle size distribution of industrial sand with local quarry sand
- When using locally available sand resources it is necessary to investigate particle size distribution before MICP treatment and eventually reconstruct a more suitable particle size distribution by recombining sand fractions
- X-ray microcomputed tomography (micro-CT) is suitable for visualization of biosandstone and its pore space but appears to be limited for small particle sizes due to difficulties in differentiating between pore space and noise for certain resolutions. With increasing resolution of the CT there will be more possibilities to switch from visualization of large pores and uneven areas in the samples towards detailed information about the efficiency of calcium carbonate crystals towards bonding of the sand or the total bonding surface area
- The necessity to include micro-CT visualization and computing in MICP optimization studies will increase. Therefore, suitable protocols for reproducible and comparable data acquisition must be established.

- The choice of filter is important to consider for processing the micro-CT data. Without filtering, noise is apparent in the particle size distribution curves and different filtering changes the results of the observed pore space and porosity
- Inhomogeneous areas of biosandstone can be visualized destruction free by micro-CT. This could help to characterize homogeneity of biosandstone in addition to segmented calcium carbonate measurements. In future studies, it could be interesting to investigate if these areas act as breaking points by combining compressive tests with micro-CT measurements

Compliance with Ethical Standards

Funding

This project was financially supported by the Deutsche Forschungsgemeinschaft (DFG. German Research Foundation) – Project-ID 172116086 – SFB 926 and the “Landespotentialbereich NanoKat”.

Acknowledgment

We thank Martin Picard and the staff of Carl Picard Natursteinwerk GmbH for providing the sand necessary to conduct this research.

We would also like to thank Prof. Dr. Christos Vrettos for the opportunity to use the equipment at the department for Soil Mechanics and Foundation Engineering and for his expert input on several occasions.

Data availability

The data that support the findings of this study are available from the corresponding author upon reasonable request.

Code availability

Not applicable

Conflict of Interest

The authors have no relevant financial or non-financial interests to disclose

Author Contributions

S.S. and N.E.conceived and,planned the experiments. Material preparation, data collection, and analysis were performed by S.S, N.E. and T.S.. The manuscript was written by S.S. and N.E. equally. All authors provided critical feedback and input for the manuscript. All authors read and approved the final manuscript.

Ethical approval

This article does not contain any studies with human participants or animals performed by any of the authors.

6 References

1. Erdmann N, Strieth D (2022) Influencing factors on ureolytic microbiologically induced calcium carbonate precipitation for biocementation. World journal of microbiology & biotechnology 39:61. https://doi.org/10.1007/s11274-022-03499-8
2. Liufu Z, Yuan J, Shan Y et al. (2023) Effect of particle size and gradation on compressive strength of MICP-treated calcareous sand. Applied Ocean Research 140:103723. https://doi.org/10.1016/j.apor.2023.103723
3. Yuan J, Li Y, Shan Y et al. (2023) Effect of Magnesium Ions on the Mechanical Properties of Soil Reinforced by Microbially Induced Carbonate Precipitation. J Mater Civ Eng 35. https://doi.org/10.1061/JMCEE7.MTENG-15080
4. Sharma M, Satyam N, Reddy KR (2022) Liquefaction Resistance of Biotreated Sand Before and After Exposing to Weathering Conditions. Indian Geotech J 52:328–340. https://doi.org/10.1007/s40098-021-00576-x
5. Shan Y, Zhao J, Tong H et al. (2022) Effects of activated carbon on liquefaction resistance of calcareous sand treated with microbially induced calcium carbonate precipitation. Soil Dynamics and Earthquake Engineering 161:107419. https://doi.org/10.1016/j.soildyn.2022.107419
6. Dagliya M, Satyam N, Sharma M et al. (2022) Experimental study on mitigating wind erosion of calcareous desert sand using spray method for microbially induced calcium carbonate precipitation. Journal of Rock Mechanics and Geotechnical Engineering. https://doi.org/10.1016/j.jrmge.2021.12.008
7. Nasser AA, Sorour NM, Saafan MA et al. (2022) Microbially-Induced-Calcite-Precipitation (MICP): A biotechnological approach to enhance the durability of concrete using Bacillus pasteurii and Bacillus sphaericus. Heliyon 8:e09879. https://doi.org/10.1016/j.heliyon.2022.e09879
8. Chahal N, Siddique R, Rajor A (2012) Influence of bacteria on the compressive strength, water absorption and rapid chloride permeability of fly ash concrete. Construction and Building Materials 28:351–356. https://doi.org/10.1016/j.conbuildmat.2011.07.042
9. Konstantinou C, Biscontin G, Jiang N et al. (2021) Application of microbially induced carbonate precipitation to form bio-cemented artificial sandstone. Journal of Rock Mechanics and Geotechnical Engineering 13:579–592. https://doi.org/10.1016/j.jrmge.2021.01.010
10. Xiao Y, Wang Y, Wang S et al. (2021) Homogeneity and mechanical behaviors of sands improved by a temperature-controlled one-phase MICP method. Acta Geotech 16:1417–1427. https://doi.org/10.1007/s11440-020-01122-4
11. Cheng L, Cord-Ruwisch R (2012) In situ soil cementation with ureolytic bacteria by surface percolation. Ecological Engineering 42:64–72. https://doi.org/10.1016/j.ecoleng.2012.01.013

12. Yang D, Xu G, Duan Y (2020) Effect of Particle Size on Mechanical Property of Bio-Treated Sand Foundation. Applied Sciences 10:8294. https://doi.org/10.3390/app10228294
13. Chu J, Ivanov V, Naeimi M et al. (2014) Optimization of calcium-based bioclogging and biocementation of sand. Acta Geotech 9:277–285. https://doi.org/10.1007/s11440-013-0278-8
14. Zhao Q, Li L, Li C et al. (2014) Factors Affecting Improvement of Engineering Properties of MICP-Treated Soil Catalyzed by Bacteria and Urease. Journal of Materials in Civil Engineering, 26(12), 04014094. https://doi.org/10.1061/(ASCE)MT.1943-5533.0001013
15. Al Qabany A, Soga K, Santamarina C (2012) Factors Affecting Efficiency of Microbially Induced Calcite Precipitation. J Geotech Geoenviron Eng 138:992–1001. https://doi.org/10.1061/(ASCE)GT.1943-5606.0000666
16. Saenger EH, Lebedev M, Uribe D et al. (2016) Analysis of high-resolution X-ray computed tomography images of Bentheim sandstone under elevated confining pressures. Geophysical Prospecting 64:848–859. https://doi.org/10.1111/1365-2478.12400
17. Gong L, Nie L, Xu Y (2020) Geometrical and Topological Analysis of Pore Space in Sandstones Based on X-ray Computed Tomography. Energies 13:3774. https://doi.org/10.3390/en13153774
18. Schmitt M, Halisch M, Müller C et al. (2016) Classification and quantification of pore shapes in sandstone reservoir rocks with 3-D X-ray micro-computed tomography. Solid Earth 7:285–300. https://doi.org/10.5194/se-7-285-2016
19. Terzis D, Laloui L (2019) Cell-free soil bio-cementation with strength, dilatancy and fabric characterization. Acta Geotech 14:639–656. https://doi.org/10.1007/s11440-019-00764-3
20. Akimana RM, Seo Y, Li L et al. (2016) Exploring X-Ray Computed Tomography Characterization and Reactive Transport Modelling of Microbially-Induced Calcite Precipitation in Sandy Soils. American Society of Civil Engineers
21. Minto JM, Hingerl FF, Benson SM et al. (2017) X-ray CT and multiphase flow characterization of a 'bio-grouted' sandstone core: The effect of dissolution on seal longevity. International Journal of Greenhouse Gas Control 64:152–162. https://doi.org/10.1016/j.ijggc.2017.07.007
22. Roy N, Frost JD, Terzis D (2023) 3-D contact and pore network analysis of MICP cemented sands. Granular Matter:62. https://doi.org/10.1007/s10035-023-01347-6
23. Zhou B, Zhang X, Wang J et al. (2022) Insight into the mechanism of microbially induced carbonate precipitation treatment of bio-improved calcareous sand particles. Acta Geotech:1–15. https://doi.org/10.1007/s11440-022-01625-2
24. Wang B, Guo L, Luo X et al. (2024) Identification and extraction of cementation patterns in sand modified by MICP: New insights at the pore scale. PLoS ONE 19:e0296437. https://doi.org/10.1371/journal.pone.0296437

25. Terzis D, Laloui L (2018) 3-D micro-architecture and mechanical response of soil cemented via microbial-induced calcite precipitation. Sci Rep 8:1416. https://doi.org/10.1038/s41598-018-19895-w
26. Kirkland CM, Norton D, Firth O et al. (2019) Visualizing MICP with X-ray µ-CT to enhance cement defect sealing. International Journal of Greenhouse Gas Control 86:93–100. https://doi.org/10.1016/j.ijggc.2019.04.019
27. Huang M, Xu K, Liu Z et al. (2023) Effect of drying-wetting cycles on pore characteristics and mechanical properties of enzyme-induced carbonate precipitation-reinforced sea sand. Journal of Rock Mechanics and Geotechnical Engineering. https://doi.org/10.1016/j.jrmge.2022.12.032
28. Zhao H, Zhao T, Ning Z et al. (2019) Petrophysical characterization of tight oil sandstones by microscale X-ray computed tomography. Marine and Petroleum Geology 102:604–614. https://doi.org/10.1016/j.marpetgeo.2019.01.029
29. Schlüter S, Sheppard A, Brown K et al. (2014) Image processing of multiphase images obtained via X-ray microtomography: A review. Water Resour Res 50:3615–3639. https://doi.org/10.1002/2014WR015256
30. Thomson P-R, Ellis R, Chiarella D et al. (2020) Microstructural Analysis From X-Ray CT Images of the Brae Formation Sandstone, North Sea. Front Earth Sci 8. https://doi.org/10.3389/feart.2020.00246
31. Sun B, Hou S-S, Zeng S et al. (2020) 3D characterization of porosity and minerals of low-permeability uranium-bearing sandstone based on multi-resolution image fusion. NUCL SCI TECH 31. https://doi.org/10.1007/s41365-020-00810-w
32. Jacob A, Peltz M, Hale S et al. (2021) Simulating permeability reduction by clay mineral nanopores in a tight sandstone by combining computer X-ray microtomography and focussed ion beam scanning electron microscopy imaging. Solid Earth 12:1–14. https://doi.org/10.5194/se-12-1-2021
33. Su Y, Zha M, Jiang L et al. (2022) Pore structure and fluid distribution of tight sandstone by the combined use of SEM, MICP and X-ray micro-CT. Journal of Petroleum Science and Engineering 208:109241. https://doi.org/10.1016/j.petrol.2021.109241
34. Whiffin VS (2004) Microbial CaCO3 Precipitation for the Production of Biocement. PhD Thesis, Murdoch University
35. Erdmann N, Payrebrune KM de, Ulber R et al. (2022) Optimizing compressive strength of sand treated with MICP using response surface methodology. SN Appl Sci 4. https://doi.org/10.1007/s42452-022-05169-8
36. Deutsches Institut für Normung e. V. DIN EN ISO 17892-11:2021-03: Geotechnical investigation and testing - Laboratory testing of soil - Part 11: Permeability tests (ISO 17892-11:2019); German version EN ISO 17892-11:2019
37. Buades A, Coll B, Morel J-M (2011) Non-Local Means Denoising. Image Processing On Line 1:208–212. https://doi.org/10.5201/ipol.2011.bcm_nlm

38. Darbon J, Cunha A, Chan TF et al. (2008) Fast nonlocal filtering applied to electron cryomicroscopy. In: 2008 5th IEEE International Symposium on Biomedical Imaging: From Nano to Macro. IEEE, pp 1331–1334
39. Lorensen WE, Cline HE (1998) Marching cubes. In: Wolfe R (ed) Seminal graphics: Pioneering efforts that shaped the field ; [SIGGRAPH 98 ; celebrating 25 years of discovery ; a publication of ACM SIGGRAPH]. ACM Press, New York, NY, pp 347–353
40. AlHomadhi ES (2014) New correlations of permeability and porosity versus confining pressure, cementation, and grain size and new quantitatively correlation relates permeability to porosity. Arab J Geosci 7:2871–2879. https://doi.org/10.1007/s12517-013-0928-z
41. Cheshomi A, Mansouri S (2020) Study the grain size and infiltration method effects for sand soil improvement using the microbial method. Geomicrobiology Journal 37:355–365. https://doi.org/10.1080/01490451.2019.1705437
42. Song C, Wang C, Elsworth D et al. (2022) Compressive Strength of MICP-Treated Silica Sand with Different Particle Morphologies and Gradings. Geomicrobiology Journal 39:148–154. https://doi.org/10.1080/01490451.2021.2020936
43. Gowthaman S, Iki T, Nakashima K et al. (2019) Feasibility study for slope soil stabilization by microbial induced carbonate precipitation (MICP) using indigenous bacteria isolated from cold subarctic region. SN Appl Sci 1. https://doi.org/10.1007/s42452-019-1508-y
44. Zhao Y, Wang Q, Yuan M et al. (2022) The Effect of MICP on Physical and Mechanical Properties of Silt with Different Fine Particle Content and Pore Ratio. Applied Sciences 12:139. https://doi.org/10.3390/app12010139
45. I. Koval, M. Roozbahani & D. Frost (2014) Comparison between geometrical and dynamic particle packing. CRC Press
46. Zhao Q, Li L, Li C et al. (2014) A Full Contact Flexible Mold for Preparing Samples Based on Microbial-Induced Calcite Precipitation Technology. Geotech Test J 37:20130090. https://doi.org/10.1520/GTJ20130090
47. Sun S, Shu L, Zeng Y et al. (2007) Porosity–permeability and textural heterogeneity of reservoir sandstones from the Lower Cretaceous Putaohua Member Of Yaojia Formation, Weixing Oilfield, Songliao Basin, Northeast China. Marine and Petroleum Geology 24:109–127. https://doi.org/10.1016/j.marpetgeo.2006.10.006
48. Mahawish A, Bouazza A, Gates WP (2019) Unconfined Compressive Strength and Visualization of the Microstructure of Coarse Sand Subjected to Different Biocementation Levels. J Geotech Geoenviron Eng 145. https://doi.org/10.1061/(ASCE)GT.1943-5606.0002066
49. Hoang T, Alleman J, Cetin B et al. (2020) Engineering Properties of Biocementation Coarse- and Fine-Grained Sand Catalyzed By Bacterial Cells

and Bacterial Enzyme. J Mater Civ Eng 32. https://doi.org/10.1061/(ASCE)MT.1943-5533.0003083
50. Liu L, Liu H, Stuedlein AW et al. (2019) Strength, stiffness, and microstructure characteristics of biocemented calcareous sand. Can Geotech J 56:1502–1513. https://doi.org/10.1139/cgj-2018-0007
51. Dadda A, Geindreau C, Emeriault F et al. (2019) Characterization of contact properties in biocemented sand using 3D X-ray micro-tomography. Acta Geotech 14:597–613. https://doi.org/10.1007/s11440-018-0744-4
52. Dadda A, Geindreau C, Emeriault F et al. (2017) Characterization of microstructural and physical properties changes in biocemented sand using 3D X-ray microtomography. Acta Geotech 12:955–970. https://doi.org/10.1007/s11440-017-0578-5
53. Wei-Soon Ng, Min-Lee Lee, Siew-Ling Hii (2012) An Overview Of The Factors Affecting Microbial-Induced Calcite Precipitation And Its Potential Application In Soil Improvement. Zenodo
54. Maleki Kakelar M, Yavari M, Yousefi MR et al. (2020) The Influential Factors in the Effectiveness of Microbial Induced Carbonate Precipitation (MICP) for Soil Consolidation. J Hum Environ Health Promot 6:40–46. https://doi.org/10.29252/jhehp.6.1.8
55. Wang Y, Soga K, DeJong JT et al. (2019) A microfluidic chip and its use in characterising the particle-scale behaviour of microbial-induced calcium carbonate precipitation (MICP). Géotechnique 69:1086–1094. https://doi.org/10.1680/jgeot.18.P.031
56. Wang Y, Soga K, DeJong JT et al. (2019) Microscale Visualization of Microbial-Induced Calcium Carbonate Precipitation Processes. J Geotech Geoenviron Eng 145:4019045. https://doi.org/10.1061/(ASCE)GT.1943-5606.0002079
57. Almajed A, Lateef MA, Moghal AAB et al. (2021) State-of-the-Art Review of the Applicability and Challenges of Microbial-Induced Calcite Precipitation (MICP) and Enzyme-Induced Calcite Precipitation (EICP) Techniques for Geotechnical and Geoenvironmental Applications. Crystals 11:370. https://doi.org/10.3390/cryst11040370
58. Shenton D, Cendes Z (1985) Three-Dimensional finite element mesh generation using delaunay tesselation. IEEE Trans Magn 21:2535–2538. https://doi.org/10.1109/TMAG.1985.1064165
59. Dong H, Blunt MJ (2009) Pore-network extraction from micro-computerized-tomography images. Phys Rev E Stat Nonlin Soft Matter Phys 80:36307. https://doi.org/10.1103/PhysRevE.80.036307
60. Meyer F, Beucher S (1990) Morphological segmentation. Journal of Visual Communication and Image Representation 1:21–46. https://doi.org/10.1016/1047-3203(90)90014-M

61. Liang Y, Hu P, Wang S et al. (2019) Medial axis extraction algorithm specializing in porous media. Powder Technology 343:512–520. https://doi.org/10.1016/j.powtec.2018.11.061
62. Ben-Noah I, Hidalgo JJ, Dentz M (2024) Efficient pore space characterization based on the curvature of the distance map. arXiv
63. Li Z, Wang YH, Chow JK et al. (2018) 3D pore network extraction in granular media by unifying the Delaunay tessellation and maximal ball methods. Journal of Petroleum Science and Engineering 167:692–701. https://doi.org/10.1016/j.petrol.2018.04.058
64. Alatrash H, Velledits F (2024) Comparing petrophysical properties and pore network characteristics of carbonate reservoir rocks using micro X-ray tomography imaging and microfacies analyses. Int J Geomath 15:1–29. https://doi.org/10.1007/s13137-023-00243-8
65. Lindquist WB, Lee S-M, Coker DA et al. (1996) Medial axis analysis of void structure in three-dimensional tomographic images of porous media. J Geophys Res 101:8297–8310. https://doi.org/10.1029/95jb03039
66. Lindquist WB, Venkatarangan A (1999) Investigating 3D geometry of porous media from high resolution images. Physics and Chemistry of the Earth, Part A: Solid Earth and Geodesy 24:593–599. https://doi.org/10.1016/S1464-1895(99)00085-X
67. Gao S, Meegoda JN, Hu L (2012) Two methods for pore network of porous media. Num Anal Meth Geomechanics 36:1954–1970. https://doi.org/10.1002/nag.1134
68. Al-Raoush R, Thompson K, Willson CS (2003) Comparison of Network Generation Techniques for Unconsolidated Porous Media. Soil Science Soc of Amer J 67:1687–1700. https://doi.org/10.2136/sssaj2003.1687
69. Serge Beucher (1992) The Watershed Transformation Applied to Image Segmentation. Scanning Microscopy

7 Supplementary Data

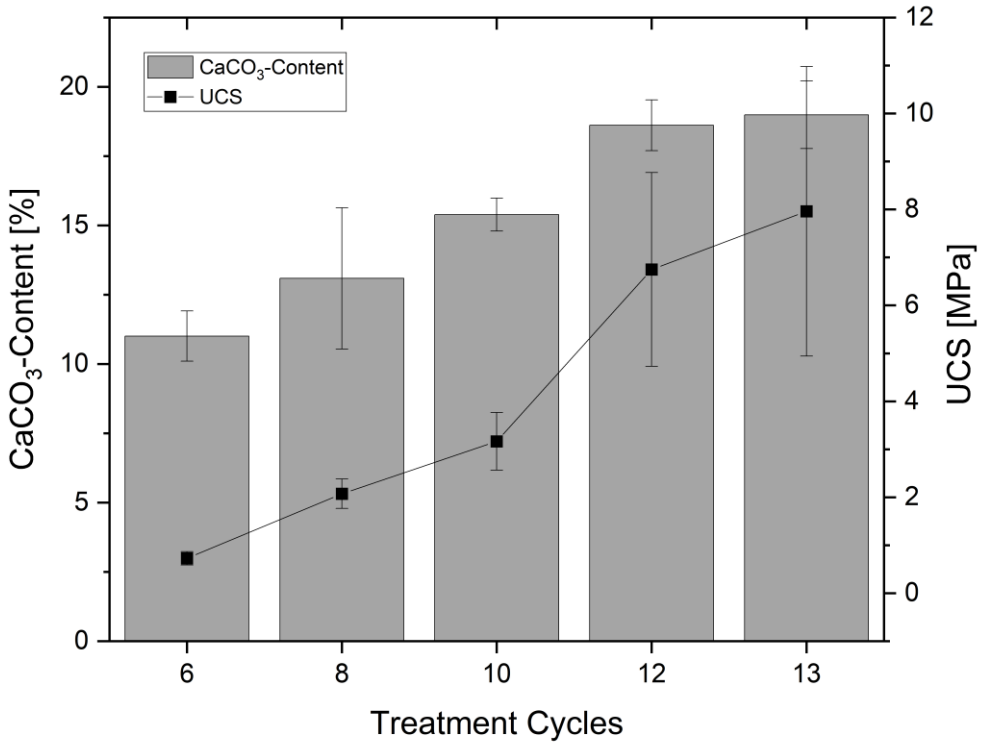

Supplement 7: Calcium carbonate content and UCS of sand SH treated with MICP

Supplement 8: Tasklist 1 - without filter

Step	Plug-in	Parameters
1	Reload image	
2	Reload Region of Interest	
3	Reload Clipboard	
4	Comment: Sand and calcite material	
5	Filtering	Contrast enhancement (3D space)
6	Threshold	Lower grey threshold: 50; upper grey threshold: 255
7	Despeckle	Sweep (3D Space); Remove all except the largest object
8	Despeckle	Remove black spackles (3D space); volume: less than 16 voxels; apply to: image
9	Despeckle	Remove black speckles (2D space); area: less than 2 pixels); apply to: image
10	Save bitmaps	
11	3D analysis	
12	Comment: extract pore system	
13	Bitwise operations	Image = NOT Image
14	Mode: Shrink-wrap (3D space)	
15	Save bitmaps	

Supplement 9: Tasklist 1 – gauss filter

Step	Plug-in	Parameters
1	Reload image	
2	Reload Region of Interest	
3	Reload Clipboard	
4	Comment: Sand and calcite material	
5	Filtering	Gaussian blur (3D space); Kernel: round; radius 1.0
6	Filtering	Contrast enhancement (3D space)
7	Threshold	Lower grey threshold: 50; upper grey threshold: 255
8	Despeckle	Sweep (3D Space); Remove all except the largest object
9	Despeckle	Remove black spackles (3D space); volume: less than 16 voxels; apply to: image
10	Despeckle	Remove black speckles (2D space); area: less than 2 pixels); apply to: image
11	Save bitmaps	
12	3D analysis	
13	Comment: extract pore system	
14	Bitwise operations	Image = NOT Image
15	Mode: Shrink-wrap (3D space)	
16	Save bitmaps	

Supplement 10: Tasklist 1 – non local means filter. non-local means filtering was applied before use in CTAn by using Fiji and NLM plug-in. There sigma=15 was applied

Step	Plug-in	Parameters
1	Reload image	
2	Reload Region of Interest	
3	Reload Clipboard	
4	Comment: Sand and calcite material	
5	Filtering	Contrast enhancement (3D space)
6	Threshold	Lower grey threshold: 50; upper grey threshold: 255
7	Despeckle	Sweep (3D Space); Remove all except the largest object
8	Despeckle	Remove black spackles (3D space); volume: less than 16 voxels; apply to: image
9	Despeckle	Remove black speckles (2D space); area: less than 2 pixels); apply to: image
10	Save bitmaps	
11	3D analysis	
12	Comment: extract pore system	
13	Bitwise operations	Image = NOT Image
14	Mode: Shrink-wrap (3D space)	
15	Save bitmaps	

Supplement 11: Tasklist 2- all samples

Step	Plug-in	Parameters
1	Comment: Analysis pore system	
2	Thresholding: global	Lower grey threshold: 1; Upper grey threshold: 255
3	Despeckle	Remove white speckles (2D space); Area: more than 350 000 pixels; apply to: image
4	Despekle	Remove white speckles (3D); Volume: less than 50 voxels; Apply to: image
5	Save bitmaps	
6	Comment: Conneced ore system	
7	Bitwise operations	Clipboard = COPY Image
8	Despeckle	Sweep (3D Space); Remove: all exept the largest object; Apply to: Image
9	3D-Analysis	
10	Save bitmaps	
11	Comment: Analysis not connected pores	
12	Bitwise operations	Image = COPY Clipboard
13	Despeckle	Sweep (3D Space); Remove: the largest object; Apply to: image
14	Save bitmaps	
15	Individual object analysis	

V Optimizing compressive strength of sand treated with MICP using response surface methodology

N. Erdmann[1], K.M. de Payrebrune[2], R. Ulber[1], D. Strieth[1]

[1]Technical University of Kaiserslautern, Chair of Bioprocess Engineering, Kaiserslautern, Germany

[1]Technical University of Kaiserslautern, Chair for Computional Physics in Engineering, Kaiserslautern, Germany

SN Applied Sciences 4, 282 (2022).
DOI:10.1007/s42452-022-05169-8

Author Contribution:

N. Erdmann*	Methodology, project administration, visualization, writing, data acquisition, data curation and analysis
K.M. de Payrebrune	Supervision, review&editing
R. Ulber	Supervision, review&editing
D. Strieth	Funding acquisition, supervision, review&editing

Keywords: microbiologically induced calcium carbonate precipitation (MICP); Sporosarcina pasteurii, response surface methodology; central composite design; biosandstone;

Abstract

In the present study, the optimization of the microbiologically induced calcium carbonate precipitation (MICP) to produce biosandstone regarding the compressive strength is shown. For the biosandstone production, quartz sand was treated sequentially with the ureolytic microorganism *Sporosarcina pasteurii* (ATCC 11859) and a reagent containing urea and calcium chloride. Response surface methodology (RSM) was applied to investigate the influence of urea concentration, calcium chloride concentration and the volume of cell suspension on the compressive strength of produced biosandstone. A central composite design (CCD) was employed, and the resulting experimental data applied to a quadratic model. The statistical significance of the model was verified by experimental data (R^2=0.9305). Optimized values for the concentration of urea and calcium chloride were 1492 mM and 1391 mM. For the volume of cell suspension during treatment 7.47 mL was determined as the optimum. Specimen treated under these conditions achieved a compressive strength of 1877 ± 240 kPa. This is an improvement of 144 % over specimen treated with a reagent that is commonly used in literature (1000 mM urea/1000 mM $CaCl_2$). This protocol allows for a more efficient production of biosandstone in future research regarding MICP.

Article highlights

- Microbially induced calcium carbonate precipitation can be used to produce artificial sandstone
- Compressive strength of artificial sandstone is dependent on urea and calcium-ion concentration. An optimum exists for nearly equimolar concentrations of urea und calcium-ions
- High concentration of calcium-ions inhibits calcium carbonate precipitation and therefore compressive strength of sandstone

1 Introduction

With over 10^{10} m³ per year, concrete is the most widely used construction material [1]. A main component of concrete is cement which is produced from Limestone [2]. During this process, high temperatures of 1450 °C [3] are used and the energy required for this process accounts for about 2.6 % of the global energy demand [4]. Microbial induced calcium carbonate precipitation (MICP) is a process in which calcium carbonate is produced by microbiological activity. If the calcium carbonate is produced in the cavities of mineral particles it can form bridges between particles and solidify them. With 20-50 °C the optimal temperatures for MICP are lower than the temperatures for producing cement. Because of that, MICP has the potential to produce construction material that has a lower energy demand than concrete. Previous studies showed that MICP can improve the strength of construction material like sandstone and cement mortar [5, 6], to repair cracks in these materials [7, 8] and to produce construction material like concrete [9–11]. Furthermore, MICP can be used to improve the resistance of soils to earthquake-induced liquefaction [12, 13] and can be utilized for the mitigation of wind erosion of soil [14]. The ureolytic hydrolysation of urea is the most common used mechanism for MICP [15, 16] because it is easy to control [17]. During this mechanism one mol of ammonia is hydrolysed by urease (EC 3.5.1.5) [18] into two mol ammonia and one mol carbonic acid (Equation 1 and 2). Both products hydrolyse which results in a pH increase and the formation of carbonate ions (Equation 3 and 4). In the presence of soluble calcium ions, the carbonate ions are precipitated as calcium carbonate (Equation 5).

$$CO(NH_2)_2 + H_2O \rightarrow NH_2COOH + NH_3 \quad (1)$$

$$NH_2COOH + H_2O \rightarrow H_2CO_3 + NH_3 \quad (2)$$

$$2NH_3 + 2H_2O \leftrightarrow 2NH^{4+} + 2OH^- \quad (3)$$

$$2OH^- + H_2CO_3 \leftrightarrow CO_3^{2-} + 2H_2O \quad (4)$$

$$Ca^{2+} + CO_3^{2-} \rightarrow CaCO_3 \quad (5)$$

Besides the production of carbonate ions, the ureolytic microorganisms are discussed to have a further effect on the precipitation of carbonate. Positive charged

calcium ions are attracted by negative charged carboxy- and phosphoryl-groups on the cell surface through electrostatic interactions [19–21]. The negatively charged cell walls act as nucleation sites for the formation of calcium carbonate crystals. For the consolidation of sand using ureolytic MICP, specimens are treated sequentially with cell suspension and a cementation solution containing urea and a calcium source. Previous studies have often used a solution with equimolar concentrations of urea (1 M) and a calcium salt (1 M) [22–25]. However, some studies have shown that MICP is more efficient for different ratios of urea and calcium [26–29].

These results suggest that there is an optimal ratio between urea and calcium ions which provides the highest consolidation of quartz sand for a given amount of cells in the specimen. The one factor at a time method is a time consuming process for the optimization of a system with multiple variables and often ignores the alternative effects between components based on the literature MICP is a process that is dependent on a lot of factors that can also influence each other. For example the concentration of urea and calcium in the cementation solution, the concentration of cells, urease activity, pH, temperature, and more [30]. During RSM the required number of experiments is reduced by proper experimental design. Furthermore it allows to investigate the interactions of the variables [31]. Therefore RSM can help to mitigate the disadvantages of the one factor at a time method for MICP. The optimization of MICP in terms of compressive strength was studied by Sotoudehfar et al. [29]. They described optimal concentrations of 3000 mM urea and 1500 mM calcium for MICP. This optimum was based on a study using the Taguchi method, in which three concentration levels were investigated. Due to the nature of the method, concentrations between these levels were not considered. Up to now, no study has investigated the efficiency of MICP in terms of compressive strength of consolidated sand using response surface methodology (RSM). For this reason, a central composite design (CCD) was used in this study to determine the optimum concentrations of urea and calcium chloride and volume of cell suspension that maximize the compressive strength of consolidated sand. The next section explains the experimental setup of the optimization process. In section 3.1 the results of the CCD are shown and discussed in detail. In section 3.2 a comparison of the optimized

protocol and common literature protocols is given. Section 4 is a short summary and conclusion of the study.

2 Material and Methods

2.1 Bacteria and cultivation procedure

Sporosarcina pasteurii (ATCC 11859) has been used as urease producing organism during this study. NH_4-YE medium was used as culture medium according to ATCC recommendation. The medium contained 15.75 g TRIS-Buffer, 10 g ammonium sulfate and 20 g of yeast extract. For media preparation the TRIS-Buffer solution was adjusted to pH 9.2 and divided into two portions. Ammonium sulfate and yeast extract were then added in each part. The solutions were autoclaved separately at 121 °C for 20 min. After cooling, the parts were combined under aseptically conditions. For the preculture, 100 mL of NH_4-YE medium was placed in 250 mL Erlenmeyer flasks and inoculated with 20 µL of a cryo-culture (15 v/v % glycerol) and incubated to an optical density at 600 nm (OD_{600}) of 0.3 at 120 rpm at 30 °C (Multitron S-000115689, Infors HT, Swiss). For the main culture 200 mL of NH_4-YE medium was placed in 500 mL Erlenmeyer flasks and inoculated with 3 v/v % of the preculture and incubated at 120 rpm at 30 °C until an OD_{600} of 1.6 was reached.

2.2 Determination of urease activity

For the determination of urease activity the conductivity method was used [9, 32]. 1 mL of cell suspension was added to 19 mL of a solution containing 1.053 M urea and 10 mM Tris buffer. The change in conductivity was recorded for 5 min with a conductivity probe (Qcond 2200, VWR International GmbH, Germany). To correlate the change in conductivity (mS/cm/min) with the degraded urea, urea standards (50-250 mM) were hydrolysed with urease from Jackbean (Carl Roth GmbH) and the change in conductivity was measured after complete degradation of urea.

2.3 Preparation of sand columns

The sand used in this study was quartz sand from a deposit in Haltern, Germany. It consists of 98 % quartz and the particle size ranges from 125 to 500 µm (see Table 1). 50 mL reaction tubes (Greiner centrifuge tubes, Sigma-Aldrich) were used as moulds. For this, they were cut off at the bottom and split in half. A hole (6 mm)

was drilled into the cap to allow suspended effluent to exit the mould. Before packing the mould, the hole was covered with a sheet of cellulose fibres. 42 g of sand were packed loosely into the tubes which resulted in a height of the specimen of 50 mm and a diameter of 27 mm.

Table 1. Particle size distribution of Quartz sand H33.

Sieve size (mm)	Mass fraction (%)
0.063	0
0.125	1
0.25	44
0.5	100

The top part of the packed sand was also covered with a sheet of cellulose fibres to prevent a dislocation of the upper particles during treatment (see Figure 1)

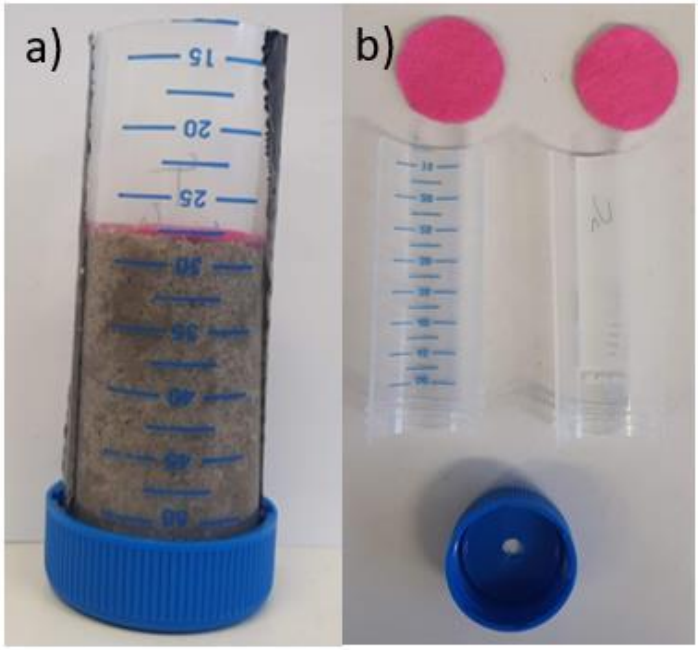

Figure 1. a) packed mould for the MICP b) components of the mould before assembly

2.4 MICP treatment

For the MICP treatment the sand columns were injected sequentially with cell suspension and a cementation solution. Cell suspension of *S. pasteurii* was used directly after cultivation (OD_{600} = 1.6, 10.6 mM urea/min). Between each cycle of the

treatment the suspension was stored at 7 °C to prevent further growth. The cementation solution contained various concentrations of urea and calcium chloride (see Table 2). Each solution had its pH adjusted to pH 7. For treatment, a defined volume of cell suspension was injected into the column by a peristaltic pump with a constant flow of 1 mL/min (see Figure 2).

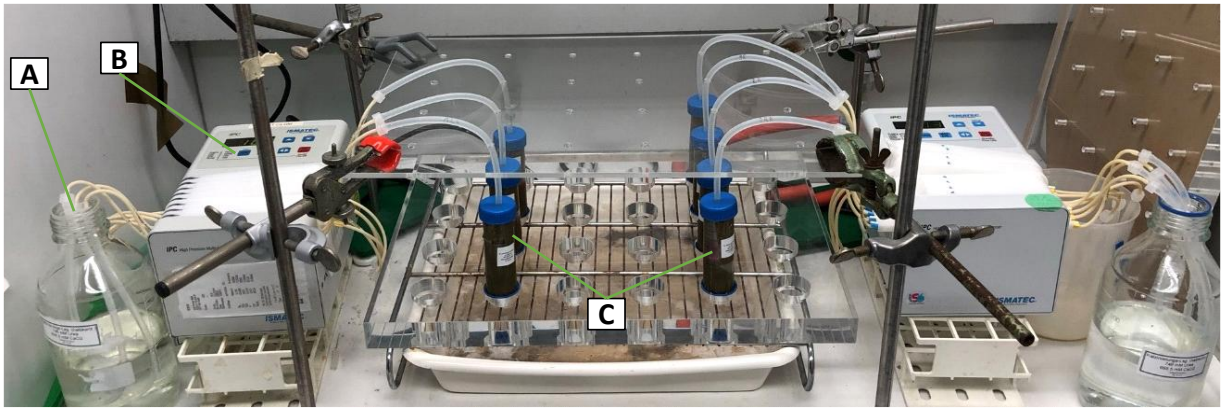

Figure 2. Experimental setup during MICP. A: Storage of cell suspension/calcination solution, B: Peristaltic pump, C: Moulds for MICP as described in Figure 1

After a period of 30 min the cementation solution was injected into the column to achieve a total volume of cell suspension and cementation solution of 15 mL which corresponds to an injection pore volume of 1. The specimens were incubated for 24 hours at 30 °C. This procedure was repeated twice for a total of three treatment cycles. After the third incubation period the specimen was oven dried at 60 °C for 72 h and, after cooling at room temperature for 24 hours, the compressive strength was measured.

2.5 Experimental design

The software ‘Design Expert´ (Version 12.0.12.0, Stat-Ease, Minneapolis, USA) was used to determine a CCD. The variables utilized in the design were concentration of urea (A), concentration of calcium chloride (B) and the volume of cell suspension during treatment (C) (see Table 2 and 3). These variables were chosen based on a previous screening experiment (Data not shown). The design had a total of 20 experiments, containing 6 center points and 14 non-center points. Five levels of variables were considered for the design: negative star (-α), minimum (-1), center (0), maximum (+1) and positive star (+α). The compressive strength was considered as the main response.

Table 2. Experimental range and levels of independent variables.

Level	Urea concentration (mM)	calcium chloride concentration (mM)	Volume of cell suspension (mL)
+α	2341	2341	11,7
+1	2000	2000	10
0	1500	1500	7,5
-1	1000	1000	5
-α	659	659	3,3

2.6 Determination of compressive strength

The compressive strength was measured by means of a concrete penetrometer (B19082, Form+Test Prüfsysteme, Germany) with a measuring range of 0-5000 kPa as suggested by Al-Thawadi [33]. The penetrometer was fixed with a tripod clamp and a lifting platform was positioned underneath, on which the specimen was measured. If there were any unevenness's in the surface of the specimen, these were ground off with a file so that the measuring head of the penetrometer rested even on the specimen. For the measurement itself, the specimen was positioned so that the measuring head of the penetrometer rested centrally on the specimen. The lifting platform was then moved upwards consistently (200 kPa per 5 s). As soon as the specimen broke, the applied force was read on the penetrometer.

3 Results and Discussion

3.1 Optimization of compressive strength

In this study an experimental design was conducted to optimize the compressive strength of quartz sand treated with MICP. Concentrations of urea (A), calcium chloride (B) and volume of cell suspension (C) were chosen as the variables for the CCD. The observed compressive strengths (Y) ranged from 0 to 3300 kPa (see Table 3).

Table 3. Design matrix of the CCD used in this study.

	Coded variables			Response		
Run No.	Urea Concentration (mM)(A)	Calcium chloride concentration (mM)(B)	Volume cell suspension (mL)(C)	Sqrt (Compressive strength)		Com-pressive strength (kPa) (Y)
				observed	predicted	
1	0	0	-α	10	5.38	100
2	1	-1	1	24.49	23.31	600
3	-α	0	0	33.17	33.57	1100
4	0	0	0	52.92	48.45	2800
5	0	0	0	42.43	48.45	1800
6	0	0	0	46.9	48.45	2200
7	α	0	0	37.42	33.19	1400
8	0	0	α	17.32	18.12	300
9	0	0	0	57.45	48.45	3300
10	-1	-1	1	N/A	N/A	N/A
11	-1	1	1	34.64	33.11	1200
12	-1	-1	-1	37.42	36.56	1400
13	1	1	1	28.28	31.84	800
14	-1	1	-1	0	3.88	0
15	0	0	0	37.42	48.45	1400
16	0	- α	0	N/A	N/A	N/A
17	1	-1	-1	33.17	37.39	1100
18	1	1	-1	0	2.7	0
19	0	α	0	24.49	20.68	600
20	0	0	0	52.92	48.45	2800

R^2=0.9185, adj. R^2=0.8269, α=1.682

Experiment number 14 and 18 could be removed from the moulds but showed no measurable consolidation. Further, these specimens showed signs of humidity after cooling to room temperature. All broken samples, as well as samples for which no measurable consolidation was achieved, have in common that they were treated with low amounts of cell suspension (<5 mL) and high $CaCl_2$ concentrations (>1500 mM). These findings are probably due to unreacted calcium chloride. The poor solidification of the samples could be attributed to a limitation of urease activity due to

the high calcium concentrations. Various studies have demonstrated an inhibitory effect of calcium salts on the activity of ureases from different sources. For example, Ferrer et al. describe an inhibition of calcium carbonate precipitation by *Deleya Halophila* above a calcium concentration of 10 mM [34]. Gorospe et al. observed inhibition of *S. pasteurii* urease activity for different calcium salts, including calcium chloride, for a concentration of 50 mM. [35]. However, while these studies only investigated the effect of a low concentration of calcium ions, Whiffin demonstrated a steady decrease in the urease activity of *S. pasteurii* by increasing the concentration of calcium nitrate [36]. She found that at a concentration of 2000 mM the urease activity of *S. pasteurii* stopped completely.

By substituting a solution containing pure calcium nitrate to a mixture of calcium nitrate and calcium chloride (1:1) she found that the inhibition of urease activity was lower for this mixture than a solution of pure calcium nitrate. Therefore, it is not clear that the inhibition of urease activity was due to calcium or nitrate ions. In addition to a decrease in urease activity, the restriction of various other metabolic pathways of *S. pasteurii* could also result in the absence of calcium carbonate precipitation at high calcium concentrations.

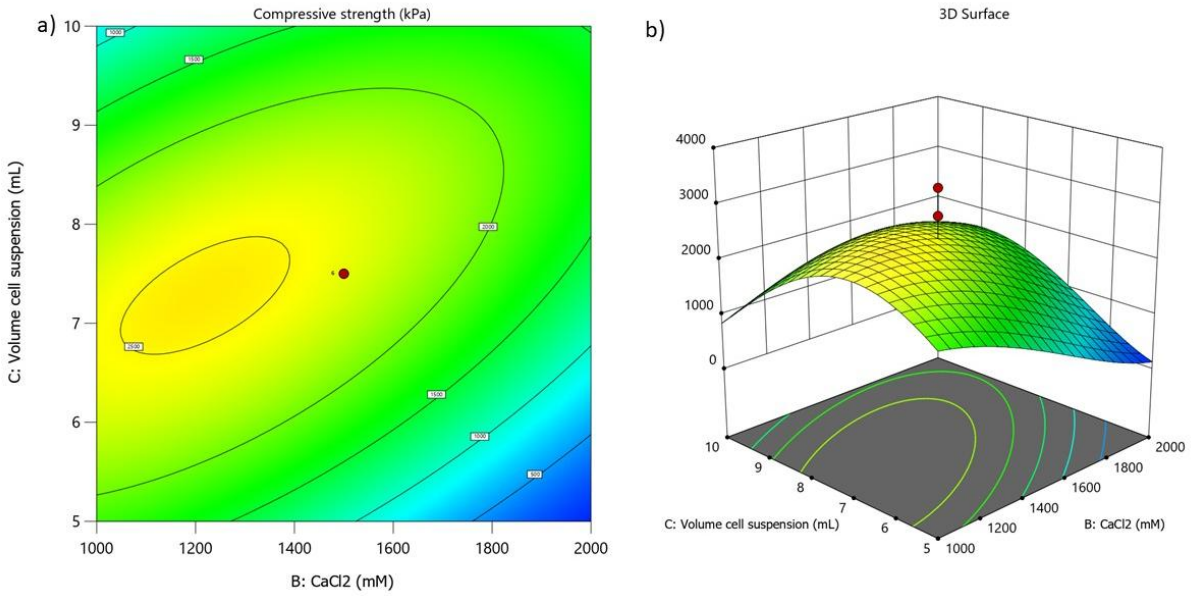

Figure 3. a) contour plot and b) 3D-Surface plot of the interactive effects of calcium chloride concentration (B) and cell suspension (OD 1.6, 10.6 mM urea/min) (C) on the compressive strength of consolidated sand at constant urea concentration of 1500 mM.

The highest strength was calculated for $CaCl_2$ concentrations of 1000 to 1600 mM and a cell suspension fraction of 5.5-8 mL (see Figure 3, Supplement 1 and Supplement 2). These results are consistent with expectations that there must be an optimal ratio between the reactants available in the specimen and the cells. If cell concentrations are too low, limitation of calcium carbonate precipitation may occur due to cell encapsulation during the process of MICP. The calcium carbonate precipitaded in close proximity of the cell surface forms a layer around the cell which limitates mass transfer of urea into the cell. Once the cell is fully encapsulated, the cell dies and MICP comes to a halt [16].

Muynck and Verbeken investigated the influence of different concentrations of urea and $CaCl_2$ on the improvement of strength parameters of sandstone [26]. They also describe that for a certain number of cells in the system, there must be an optimum level of urea and $CaCl_2$, above which the nutrients are not further degraded and negative effects, such as the accumulation of salt in the sample, occur. For a fixed volume of cell suspension (C) of 7.5 mL calcium chloride concentration (B) and urea concentration (A) are more likely independent influence factors on the compressive strength (S1). The same seems to be the case for the factors volume of cell suspension (C) and urea concentration (A) at a constant calcium chloride concentration (C) of 1500 mM (Supplement 2). This is supported by the fact that the only statistically significant model term containing two independent factors for Equation 6 is “AB” (see Table 4). The regression analysis of the experimental data found that the response and the test variables are related using the following second order polynomial equation:

$$\sqrt{Y} = +48.45 - 0.1128A - 6.04B + 3.79C - 0.503AB - 0.0235AC + 10.80BC - 5.33A^2 - 6.23B^2 - 12.97C^2 \quad (6)$$

R^2 should be above 0.6 and the larger this value, the higher the statistical significance of the model. The R^2 (0.9815) and adj. R^2 (0.8269) of Equation 6 indicate a high correlation between the observed and predicted values of compressive strength by Design Expert. The F-value of the model of 10.02 implies that the model is significant and that there is only a 0.18 % chance that an F-value this large could occur due to noise (see Table 4). A p-value < 0.0500 indicates that the model term is

significant for a 5 % significance level. P-values > 0.1000 indicate the model term is not significant.

Table 4. Design analysis for the predictive equation by the Design expert software.

Source	Sum of Squares	df	Mean Square	F-value	p-value	
Model	4430.14	9	492.24	10.02	0.0018	(s)
A-Urea	0.1325	1	0.1325	0.0027	0.9599	(ns)
B-CaCl2	193.66	1	193.66	3.94	0.0823	(ns)
C-Volume cell suspension	149.32	1	149.32	3.04	0.1194	(ns)
AB	1.32	1	1.32	0.0269	0.8738	(ns)
AC	0.0029	1	0.0029	0.0001	0.9941	(ns)
BC	609.34	1	609.34	12.40	0.0078	(s)
A^2	387.41	1	387.41	7.89	0.0229	(s)
B^2	246.08	1	246.08	5.01	0.0556	(ns)
C^2	2299.08	1	2299.08	46.80	0.0001	(s)
Residual	392.99	8	49.12			
Lack of Fit	111.86	3	37.29	0.6632	0.6095	(ns)
Pure Error	281.13	5	56.23			
Cor Total	4823.13	17				

(s)= significant, (ns)=not significant

The p-value of the model was 0.0018 and therefore found to be adequate for prediction. In this case BC, A^2 and C^2 are significant model terms (see Table 4). The mutual effects of the three variables urea concentration, calcium chloride concentration and volume of cell suspension were analysed by Design Expert software. The model predicted that the optimal urea concentration is 1492 mM, calcium chloride concentration is 1391 mM and the volume of cell suspension is 7.47 mL. For both concentrations, this optimum is above the values described in the literature for optimum calcium carbonate precipitation in terms of enzymatic activity

and calcium carbonate precipitation rate [27, 28]. In order to validate the model created to optimize the compressive strength, 5-10 verification specimens must be examined (Jensen 2016). For this purpose, the cementation was performed according to the determined optimum and the results were used to validate the model by Design Expert. The PIMean (Prediction Interval Mean) approach is used as the method of validation. In this approach, the mean value of the validation runs is compared with the prediction interval in a 95 % confidence interval [37]. A total of 6 experimental runs were conducted using the optimized parameters from the mathematical model. The obtained mean value of 1876.85 kPa lies within the 95 % confidence interval (see Table 5).

Table 5. Results of the validation runs at urea concentration 1492 mM, calcium chloride concentration 1391 mM and volume of cell suspension 7.47 mL.

Response	Predicted Mean	Predicted Median*	Std Dev	n	95% PI low	Data Mean	95% PI high
Compressive strength (kPa)	2495.58	2446,46	696,81	6	1603	1876,85	3467,55

Thus, it can be assumed that the model is valid. These results indicate that calcium chloride is the limiting component in the cementation solution in terms of compressive strength and that for a given amount of cells, an optimum amount of urea and calcium chloride exists for the MICP. Muynck et al. also describe that for a certain amount of cells an optimum urea and calcium dosage exists [16]. Some studies have investigated the MICP regarding the concentration of urea, calcium ions and the cell concentration. However, the target parameters considered varied, as MICP has a wide range of applications and the same target parameters are not considered optimal for every application (see Table 6).

While studies optimizing MICP for the rate of calcium carbonate formation use a significant excess of urea [27, 28] optimization for the rate of MICP is not a useful parameter for sand consolidation because low concentrations of calcium-ions stoichiometrically result in low amounts of calcium carbonate (see Eq. 5). Various

studies have shown that the strength of sand after MICP treatment correlates with the mass fraction of precipitated calcium carbonate [39,40].

Table 6. Overview of studies on the optimization of MICP by variation of the concentration of urea and $CaCl_2$.

Strain	Investigated parameters	Target parameter	Optimum	Reference
S. pasteurii	[Urea]; [$CaCl_2$]; [$NiCl_2$]	Precipitation rate of calcium carbonate (h^{-1})	63 mM $CaCl_2$; 700 mM urea; 6.9 mM NiCl2	[28]
S. pasteurii	[Urea]; [$CaCl_2$]; Reaction time; flow rate; cell concentration	Unconfined compressive strength	3000 mM Urea; 1500 mM CaCl2; 20 mL/min; OD_{600} 4	[29]
S. pasteurii	[Urea]; [$CaCl_2$]	Rate of ureolysis (h^{-1})	666 mM Urea; 250 mM $CaCl_2$	[27]
Bacillus sphaericus	[Urea]; [$CaCl_2$]	Mass gain Permeability	333 mM Urea; 450 mM $CaCl_2$	[26]
Bacillus megaterium	[Urea]; [$CaCl_2$]	Shear strength; Calcite content	500 mM Urea; 500 mM $CaCl_2$	[38]
S. pasteurii	[Urea]; [$CaCl_2$] Cell concentration	Unconfined compressive strength	1500 mM Urea; 1500 mM $CaCl_2$; OD_{600} 1.5	[39]

A high concentration of calcium-ions in cementation solution and therefore also a high resulting mass fraction of calcium carbonate is desirable. Studies that investigated MICP for a post MICP strength parameter achieved optimum results for nearly equimolar ratios of urea and $CaCl_2$ [26, 38, 39]. Only Sotoudehfar et al. [29] found an optimum for a ratio of 2:1 urea:$CaCl_2$. Since a comparability of these studies is difficult due to different experimental setups and bacterial strains, the protocol optimized by RSM was compared with two literature protocols in this study under the same treatment conditions to ensure a comparable comparison with literature values.

3.2 Comparison of three cementation solutions

The optimized and validated model was additionally compared with two protocols from the literature (see Table 7). Cementation solution 1 was chosen because it is utilized in many studies concerning MICP and solution 3 is based on the optimized protocol by Sotoudehfar et al. [29]. In addition to the absolute compressive strength, the efficiency of cementation in relation to the nutrients used was investigated. For this purpose, the quotient of the compressive strength and the total concentration of nutrients was formed.

Table 7. Overview of cementation solutions from this study in comparison to chosen references.

Cementation solution	Urea concentration (mM)	$CaCl_2$ concentration (mM)	References
1	1000	1000	[23, 25, 42, 43]
2	1492	1391	This study
3	3000	1500	[29]

For this comparison, cementation was performed with 7.47 mL portion of cell suspension for all protocols in order to limit the comparison of the methods to the composition of the cementation solution. The lowest compressive strength (771 ± 149 kPa) and compressive strength per mol (0,39 ± 0,08 kPa/mM) was obtained with cementation solution 1 (see Figure 4). The second highest compressive strength (1877 ± 240 kPa) was achieved with cementation solution 2, which was optimized in this work. Thus, by increasing the amount of urea and $CaCl_2$ used by 49 % and 39 %, respectively, an increase in the compressive strength of cementation solution 1 to 2 of 144.1 ± 34.5 % was achieved. The cementation solution 1, which is frequently used in the literature, is consequently not optimal for consolidating quartz sand under the conditions carried out in this study. The highest absolute compressive strength was achieved with solution 3 (2471 ± 368 kPa) according to Sotoudehfar et al. [29]. However, solution 2 obtained a higher compressive strength per mol (0,65 ± 0,08 kPa/mM) than

solution 3 (0,55 ± 0,08 kPa/mM). Due to the use of 101 % more urea and 7.8 % more $CaCl_2$ which results in a 15,9 % lower compressive strength per mol cementation solution. Although solution 3 achieved a higher absolute compressive strength the efficiency of the consolidation regarding the nutrients is lower. Therefore, the efficiency for MICP using solution 2 is higher.

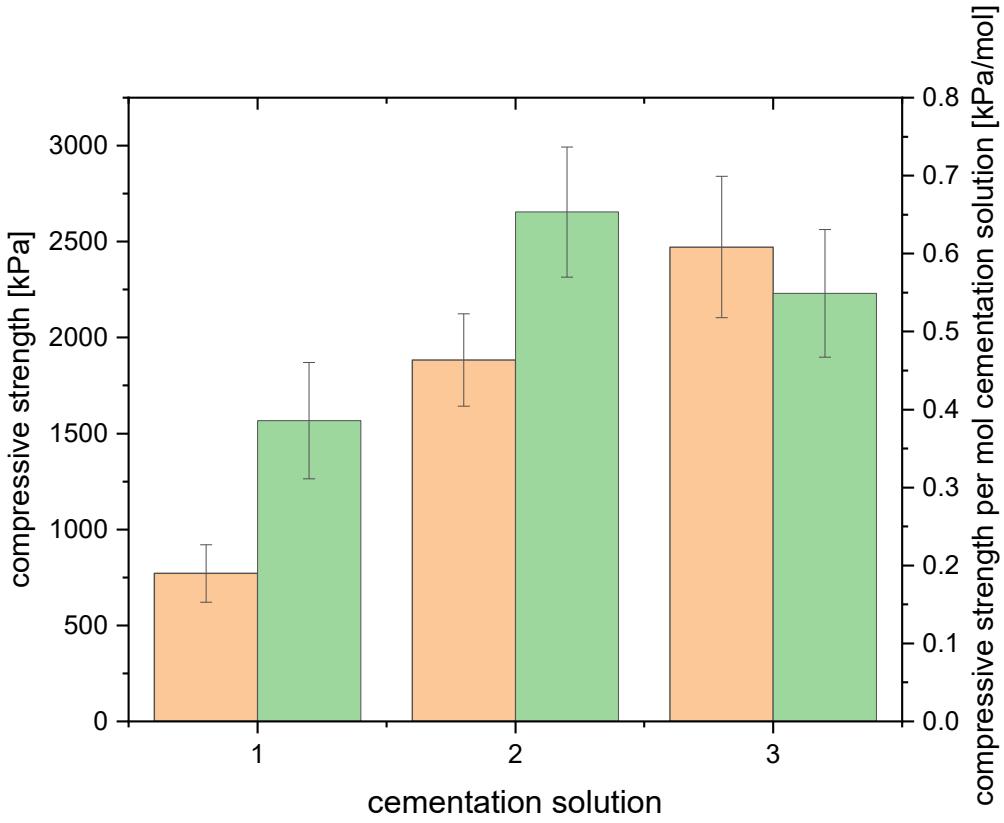

Figure 4. Comparison of three cementation protocols from this study and with literature values. Proportion of cell suspension 7.47 mL, reaction temperature: 30 °C, reaction time 24 h, measurement with penetrometer, n = 6.

It should be stressed that while solution 3 achieved a high compressive strength the borders of the CCD used in this study were lower than the urea concentration used in solution 3. Thus, the model could not find an optimum concentration in the range of the concentrations used in solution 3. The use of the high urea concentrations in solution 3 should be considered critically. Due to the stoichiometric ratios in calcium carbonate formation (Equation 1-5), a maximum of 1500 mM $CaCO_3$ could be formed at concentrations of 3000 mM urea and 1500 mM $CaCl_2$. Excess urea could only be metabolized by *S. pasteurii* for growth. Regardless of whether the excess urea is

completely degraded, or metabolized by *S. pasteurii* in the samples, additional use of urea is associated with additional costs and additional CO_2 emissions during production, due to the energy costs in urea production [43]. However, if urea was to be completely degraded, this would cause a significantly higher concentration of ammonium ions in the samples, which is harmful due to its toxicity especially to water organisms. Any excess urea leads to the formation of extra ammonium, which can outgas as toxic ammonia under high pH conditions. By knowing the optimum ratio of urea to calcium ions, an excess of urea can be avoided.

There are also various approaches in the literature for handling the ammonium formed. For example, the efflux after MICP in the Basarov reaction can be converted to urea after MICP in the Basarov reaction [45, 46] or the ammonium oxidized during wastewater treatment [45, 46]. Also, studies have been conducted to precipitate ammonium from MICP as struvite [47]. The use of zeolites [48] in MICP has also been discussed to solve this problem. Hence, a ratio of urea and $CaCl_2$ close to equimolar is desirable, while obtaining a high compressive strength and to avoid the production of more excess ammonia than necessary. The optimized solution shown in this study is a helpful approach to identify the optimal concentrations in cementation solution for the consolidation of sand. This optimized protocol might help to improve the results of research investigating MICP for production of novel construction materials based on MICP. The results could also be of interest for other fields of application of MICP like the granulometric stabilization of soil for unsealed road construction [49] or the improvement of liquefaction resistance [12, 13]. For that, further parameter like stiffness, erosion resistance, permeability and shear strength after treatment with this optimized protocol need to be evaluated and compared to literature protocols.

4 Conclusion

In this study the response surface methodology was used to optimize the compressive strength of quartz sand treated with MICP. It could be shown that the concentrations of urea and calcium chloride as well as the volume of cell suspension have the greatest impact on consolidation of quartz sand. Finally, the model predicted that the optimal urea concentration is 1492 mM, calcium chloride concentration is 1391 mM and the volume of cell suspension is 7.47 ml (OD_{600} 1.6,

10.6 mM urea/min) with a predicted compressive strength of 2.495 kPa. The predicted compressive strength could be verified (n = 6). Thus, it can be assumed that the model is valid. Additionally, the achieved results were compared to standard methods used in literature (Solution 1: 1000 mM Urea, 1000 mM $CaCl_2$) as well to another optimized protocol (Solution 3: 3000 mM Urea, 1500 mM $CaCl_2$). The compressive strength could be increased by 2.5 times compared to standard methods. Although solution 3 achieved a higher absolute compressive strength the efficiency of the consolidation regarding the nutrients is lower. Therefore, the efficiency for MICP using the method optimized in this study is higher and less excess ammonium is produced. Further research is necessary to optimize the conditions for MICP regarding compressive strength of consolidated sand.

Short summary:

- Calcium concentration has negative impact on MICP
- Amounts of Urea, Calcium and cell suspension have the highest impact on compressive strength of quartz sand
- Predicted compressive strength could be verified
- Compressive strength could be increased 2.5 times compared to standard methods described in literature using the optimal concentrations predicted by the model

Compliance with Ethical Standards

Funding

This project was financially supported by the Deutsche Forschungsgemeinschaft (DFG, German Research Foundation) – Project-ID 172116086 – SFB 926, the TU Nachwuchsring and the “Landespotentialbereich NanoKat”.

Data availability

The data that support the findings of this study are available from the corresponding author upon reasonable request.

Conflict of Interest

The authors have no relevant financial or non-financial interests to disclose

Author Contributions

All authors contributed to the study conception and design. Material preparation, data collection and analysis were performed by Niklas Erdmann and Felix Kästner. The first draft of the manuscript was written by Niklas Erdmann and all authors commented on previous versions of the manuscript. All authors read and approved the final manuscript.

Ethical approval

This article does not contain any studies with human participants or animals performed by any of the authors.

5 References

1. Gartner EM, Macphee DE (2011) A physico-chemical basis for novel cementitious binders. Cement and Concrete Research 41:736–749. https://doi.org/10.1016/j.cemconres.2011.03.006
2. Røyne A, Phua YJ, Balzer Le S et al. (2019) Towards a low CO2 emission building material employing bacterial metabolism (1/2): The bacterial system and prototype production. PLoS ONE 14. https://doi.org/10.1371/journal.pone.0212990
3. Husillos Rodríguez N, Martínez-Ramírez S, Blanco-Varela MT et al. (2013) The effect of using thermally dried sewage sludge as an alternative fuel on Portland cement clinker production. Journal of Cleaner Production 52:94–102. https://doi.org/10.1016/j.jclepro.2013.02.026
4. Miller SA, Horvath A, Monteiro PJM (2018) Impacts of booming concrete production on water resources worldwide. Nat Sustain 1:69–76. https://doi.org/10.1038/s41893-017-0009-5
5. Ghosh P, Mandal S, Chattopadhyay BD et al. (2005) Use of microorganism to improve the strength of cement mortar. Cement and Concrete Research 35:1980–1983. https://doi.org/10.1016/j.cemconres.2005.03.005
6. Muynck W de, Cox K, Belie N de et al. (2008) Bacterial carbonate precipitation as an alternative surface treatment for concrete. Construction and Building Materials 22:875–885. https://doi.org/10.1016/j.conbuildmat.2006.12.011
7. Achal V, Mukerjee A, Sudhakara Reddy M (2013) Biogenic treatment improves the durability and remediates the cracks of concrete structures. Construction and Building Materials 48:1–5. https://doi.org/10.1016/j.conbuildmat.2013.06.061
8. Dhami NK, Reddy MS, Mukherjee A (2014) Application of calcifying bacteria for remediation of stones and cultural heritages. Front Microbiol 5:304. https://doi.org/10.3389/fmicb.2014.00304
9. Whiffin VS, van Paassen LA, Harkes MP (2007) Microbial Carbonate Precipitation as a Soil Improvement Technique. Geomicrobiology Journal 24:417–423. https://doi.org/10.1080/01490450701436505
10. Mondal S, Ghosh A (2018) Microbial Concrete as a Sustainable Option for Infrastructural Development in Emerging Economies:413–423. https://doi.org/10.1061/9780784482032.042
11. Mondal S, Ghosh A (2019) Review on microbial induced calcite precipitation mechanisms leading to bacterial selection for microbial concrete. Construction and Building Materials 225:67–75. https://doi.org/10.1016/j.conbuildmat.2019.07.122
12. Sharma M, Satyam N, Reddy KR (2022) Liquefaction Resistance of Biotreated Sand Before and After Exposing to Weathering Conditions. Indian Geotech J 52:328–340. https://doi.org/10.1007/s40098-021-00576-x

13. Sharma M, Satyam N (2021) Strength and durability of biocemented sands: Wetting-drying cycles, ageing effects, and liquefaction resistance. Geoderma 402:115359. https://doi.org/10.1016/j.geoderma.2021.115359
14. Dagliya M, Satyam N, Sharma M et al. (2022) Experimental study on mitigating wind erosion of calcareous desert sand using spray method for microbially induced calcium carbonate precipitation. Journal of Rock Mechanics and Geotechnical Engineering. https://doi.org/10.1016/j.jrmge.2021.12.008
15. Hammes F, Verstraete W (2002) Key roles of pH and calcium metabolism in microbial carbonate precipitation. Reviews in Environmental Science and Bio/Technology 1:3–7. https://doi.org/10.1023/a:1015135629155
16. Muynck W de, Belie N de, Verstraete W (2010) Microbial carbonate precipitation in construction materials: A review. Ecological Engineering 36:118–136. https://doi.org/10.1016/j.ecoleng.2009.02.006
17. Stocks-Fischer S, Galinat JK, Bang SS (1999) Microbiological precipitation of CaCO3. Soil Biology and Biochemistry 31:1563–1571. https://doi.org/10.1016/s0038-0717(99)00082-6
18. Anbu P, Kang C-H, Shin Y-J et al. (2016) Formations of calcium carbonate minerals by bacteria and its multiple applications. Springerplus 5:250. https://doi.org/10.1186/s40064-016-1869-2
19. Douglas S, Beveridge TJ (1998) Mineral formation by bacteria in natural microbial communities. FEMS Microbiology Ecology 26:79–88. https://doi.org/10.1111/j.1574-6941.1998.tb00494.x
20. Bäuerlein E (2003) Biomineralization of unicellular organisms: an unusual membrane biochemistry for the production of inorganic nano- and microstructures. Angew Chem Int Ed Engl 42:614–641. https://doi.org/10.1002/anie.200390176
21. Seifan M, Samani AK, Berenjian A (2016) Bioconcrete: next generation of self-healing concrete. Appl Microbiol Biotechnol 100:2591–2602. https://doi.org/10.1007/s00253-016-7316-z
22. Cheng L, Cord-Ruwisch R, Shahin MA (2013) Cementation of sand soil by microbially induced calcite precipitation at various degrees of saturation. Can Geotech J 50:81–90. https://doi.org/10.1139/cgj-2012-0023
23. Cheng L, Shahin MA, Mujah D (2017) Influence of Key Environmental Conditions on Microbially Induced Cementation for Soil Stabilization. J Geotech Geoenviron Eng 143:4016083. https://doi.org/10.1061/(ASCE)GT.1943-5606.0001586
24. Omoregie AI, Khoshdelnezamiha G, Senian N et al. (2017) Experimental optimisation of various cultural conditions on urease activity for isolated Sporosarcina pasteurii strains and evaluation of their biocement potentials. Ecological Engineering 109:65–75. https://doi.org/10.1016/j.ecoleng.2017.09.012
25. Zhao Y, Xiao Z, Lv J et al. (2019) A Novel Approach to Enhance the Urease Activity of Sporosarcina pasteurii and its Application on Microbial-Induced

Calcium Carbonate Precipitation for Sand. Geomicrobiology Journal 36:819–825. https://doi.org/10.1080/01490451.2019.1631911
26. Muynck W de, Verbeken K, Belie N de et al. (2010) Influence of urea and calcium dosage on the effectiveness of bacterially induced carbonate precipitation on limestone. Ecological Engineering 36:99–111. https://doi.org/10.1016/j.ecoleng.2009.03.025
27. Okwadha GD, Li J (2010) Optimum conditions for microbial carbonate precipitation. Chemosphere 81:1143–1148. https://doi.org/10.1016/j.chemosphere.2010.09.066
28. Onal Okyay T, Frigi Rodrigues D (2014) Optimized carbonate micro-particle production by Sporosarcina pasteurii using response surface methodology. Ecological Engineering 62:168–174. https://doi.org/10.1016/j.ecoleng.2013.10.024
29. Sotoudehfar AR, Mirmohammad sadeghi M, Mokhtari E et al. (2016) Assessment of the Parameters Influencing Microbial Calcite Precipitation in Injection Experiments Using Taguchi Methodology. Geomicrobiology Journal 33:163–172. https://doi.org/10.1080/01490451.2015.1025316
30. Zhang J, Shi X, Chen X et al. (2021) Microbial-Induced Carbonate Precipitation: A Review on Influencing Factors and Applications. Advances in Civil Engineering 2021:1–16. https://doi.org/10.1155/2021/9974027
31. Aydar AY (2018) Utilization of Response Surface Methodology in Optimization of Extraction of Plant Materials. In: Silva V (ed) Statistical Approaches With Emphasis on Design of Experiments Applied to Chemical Processes. InTech
32. Erdmann N, Kästner F, Payrebrune K de et al. (2022) Sporosarcina pasteurii can be used to print a layer of calcium carbonate. Eng Life Sci. https://doi.org/10.1002/elsc.202100074
33. Salwa Al-Thawadi (2008) High strength in-situ biocementation of soil by calcite precipitating locally isolated ureolytic bacteria. Dissertation, Murdoch University
34. Ferrer MR, Quevedo-Sarmiento J, Bejar V et al. (1988) Calcium carbonate formation byDeleya halophila:Effect of salt concentration and incubation temperature. Geomicrobiology Journal 6:49–57. https://doi.org/10.1080/01490458809377821
35. Gorospe CM, Han S-H, Kim S-G et al. (2013) Effects of different calcium salts on calcium carbonate crystal formation by Sporosarcina pasteurii KCTC 3558. Biotechnol Bioproc E 18:903–908. https://doi.org/10.1007/s12257-013-0030-0
36. Whiffin (2004) High strength in-situ biocementation of soil by calcite precipitating locally isolated ureolytic bacteria, Murdoch University
37. Jensen WA (2016) Confirmation Runs in Design of Experiments. Journal of Quality Technology 48:162–177. https://doi.org/10.1080/00224065.2016.11918157

38. Lee LM, Ng WS, Tan CK et al. (2012) Bio-Mediated Soil Improvement under Various Concentrations of Cementation Reagent. AMM 204-208:326–329. https://doi.org/10.4028/www.scientific.net/AMM.204-208.326
39. Zhao Q, Li L, Li C et al. (2014) Factors Affecting Improvement of Engineering Properties of MICP-Treated Soil Catalyzed by Bacteria and Urease. Journal of Materials in Civil Engineering, 26(12), 04014094. https://doi.org/10.1061/(ASCE)MT.1943-5533.0001013
40. Chu J, Ivanov V, Naeimi M et al. (2014) Optimization of calcium-based bioclogging and biocementation of sand. Acta Geotech 9:277–285. https://doi.org/10.1007/s11440-013-0278-8
41. Al Qabany A, Soga K, Santamarina C (2012) Factors Affecting Efficiency of Microbially Induced Calcite Precipitation. J Geotech Geoenviron Eng 138:992–1001. https://doi.org/10.1061/(ASCE)GT.1943-5606.0000666
42. Omoregie AI, Ngu LH, Ong DEL et al. (2019) Low-cost cultivation of Sporosarcina pasteurii strain in food-grade yeast extract medium for microbially induced carbonate precipitation (MICP) application. Biocatalysis and Agricultural Biotechnology 17:247–255. https://doi.org/10.1016/j.bcab.2018.11.030
43. Brentrup F, Hoxha A, Christensen B (2016) Carbon footprint analysis of mineral fertilizer production in Europe and other world regions. https://irees.de/wp-content/uploads/2020/04/180716_IREES_AP4_Prozessemissionen.pdf. Accessed 27 May 2022
44. Meessen J (2014) Urea synthesis. Chemie Ingenieur Technik 86:2180–2189. https://doi.org/10.1002/cite.201400064
45. Torres-Aravena Á, Duarte-Nass C, Azócar L et al. (2018) Can Microbially Induced Calcite Precipitation (MICP) through a Ureolytic Pathway Be Successfully Applied for Removing Heavy Metals from Wastewaters? Crystals 8:438. https://doi.org/10.3390/cryst8110438
46. Mao N, Ren H, Geng J et al. (2017) Engineering application of anaerobic ammonium oxidation process in wastewater treatment. World journal of microbiology & biotechnology 33:153. https://doi.org/10.1007/s11274-017-2313-7
47. Gowthaman S, Mohsenzadeh A, Nakashima K et al. (2022) Removal of ammonium by-products from the effluent of bio-cementation system through struvite precipitation. Materials Today: Proceedings 61:243–249. https://doi.org/10.1016/j.matpr.2021.09.013
48. Su F, Yang Y, Qi Y et al. (2022) Combining microbially induced calcite precipitation (MICP) with zeolite: A new technique to reduce ammonia emission and enhance soil treatment ability of MICP technology. Journal of Environmental Chemical Engineering 10:107770. https://doi.org/10.1016/j.jece.2022.107770
49. Portugal CRMe, Fonyo C, Machado CC et al. (2020) Microbiologically Induced Calcite Precipitation biocementation, green alternative for roads – is this the breakthrough? A critical review. Journal of Cleaner Production 262:121372. https://doi.org/10.1016/j.jclepro.2020.121372

VI Sporosarcina pasteurii can be used to print a layer of calcium carbonate

N. Erdmann[1], F. Kästner[2], K.M. de Payrebrune[2], D. Strieth[1]

[1]*Technical University of Kaiserslautern, Chair of Bioprocess Engineering, Kaiserslautern, Germany*

[2]*Technical University of Kaiserslautern, Chair for Computional Physics in Engineering, Kaiserslautern, Germany*

Engineering in Life Sciences (2022) Jun16;22(12):760-768,
DOI: 10.1002/elsc.202100074

Author Contribution:

N. Erdmann*	Methodology, project administration, visualization, writing, data acquisition (all figures), data curation and analysis
F. Kästner	Methodology, project administration, visualization, writing, data acquisition: figure 1
K.M. de Payrebrune	Supervision, review&editing
D. Strieth	Funding acquisition, supervision, review&editing

Keywords: microbially induced calcium carbonate precipitation (MICP), Sporosarcina pasteurii, ureolytic activity, 3D printing

Practical application

Microbiologically induced calcium carbonate precipitation (MICP) has the potential to produce an ecological alternative to conventional cement in building materials through the formation of calcium carbonate. These materials often lack homogeneity of carbonate in the produced samples and therefore consolidation is poor. A possible way to achieve a more uniform sample could be an application of MICP in layers during 3D printing. We demonstrate that printing of a calcium carbonate layer utilizing MICP is possible. In further research this concept can be expanded to achieve true 3D printing with MICP. *Sporosarcina pasteurii* is able to maintain its ability to induce calcium carbonate precipitation during storage at low temperatures as well as during its passage through the printer nozzle. The application of this technology in 3D printing processes could offer the potential to address the issue of unevenly consolidated samples. It also offers the potential to provide artificial sandstone in suitable shapes for the restoration of historic sandstone, for example.

Abstract

When using microbiologically induced calcium carbonate precipitation (MICP) to produce calcium carbonate crystals in the cavities between mineral particles to consolidate them, the inhomogeneous distribution of the precipitated calcium carbonate poses a problem for the production of construction materials with consistent parameters. Various approaches have been investigated in the literature to increase the homogeneity of consolidated samples. One approach can be the targeted application of ureolytic organisms by 3D printing. However, to date, this possibility has been little explored in the literature. In this study, the potential to use MICP to print calcium carbonate layers on mineral particles will be investigated. For this purpose, a dispensing unit was modified to apply both a suspension of *Sporosarcina pasteurii* and a calcination solution containing urea and calcium chloride onto quartz sand. The study showed that after passing through the nozzle, *S. pasteurii* preserved consistent cell vitality and therefore its potential of MICP. Applying cell suspension and calcination solution through a printing nozzle resulted in a layer of calcium carbonate crystals on quartz sand. This observation demonstrated the proof of concept of printing calcium carbonate by MICP through the nozzle of a dispensing unit. Furthermore, it was shown that cell suspensions of *S. pasteurii* can be stored at 4 °C for a period of 17 days while maintaining its optical density, urease activity and cell vitality and therefore the potential for MICP. This initial concept could be extended in further research to printing three-dimensional objects to solve the problem of homogeneity in consolidated mineral particles.

1 Introduction

The production of concrete, the most widely used building material worldwide, accounts for 8.6 % of anthropogenic CO_2 emissions [1]. The reason for this is the high energy requirement for the production of cement, the main binding agent of concrete since cement is produced from limestone at a temperature of 1450 °C [2]. Various microorganisms can produce calcium carbonate. This process is called microbiologically induced calcium carbonate precipitation (MICP). The calcium carbonate formed in this process can form bridges between mineral particles, similar to classical binders such as cement, and thus consolidate them. Since the optimal temperature for MICP is 20-50 °C, MICP has the potential to produce a building material with a lower energy demand. Past studies have already shown that MICP can be used to increase strength [3, 4] and repair cracks in concrete and sandstone [5, 6]. The production of novel building materials by MICP has also been described in various studies [7–10]. The mechanism most commonly used for this purpose is ureolysis [11, 12]. This mechanism is easy to control and the necessary reagents are readily available [13]. During ureolytic hydrolysis, one mole of urea is hydrolyzed by urease (EC 3.5.1.5) [14] into two moles of ammonia and one mole of carbonic acid (Equation 1 and 2). Both products hydrolyze (equation 3 and 4) forming carbonate ions and increasing the pH. In the presence of soluble calcium ions, the carbonate ions formed are precipitated as calcium carbonate (equation 5).

$$CO(NH_2)_2 + H_2O \rightarrow NH_2COOH + NH_3 \quad (1)$$

$$NH_2COOH + H_2O \rightarrow H_2CO_3 + NH_3 \quad (2)$$

$$2NH_3 + 2H_2O \leftrightarrow 2NH^{4+} + 2OH^- \quad (3)$$

$$2OH^- + H_2CO_3 \leftrightarrow CO_3^{2-} + 2H_2O \quad (4)$$

$$Ca^{2+} + CO_3^{2-} \rightarrow CaCO_3 \quad (5)$$

$$CO(NH_2)_2 + 2\,H_2O + Ca^{2+} \rightarrow 2NH_4^+ + CaCO_3 \quad (6)$$

An important factor for the formation of calcium carbonate is the presence of nucleation sites, which serve as initial nucleation cells for the formation of calcium carbonate ions [11, 12]. The negatively charged cell walls of the microorganisms play

a supporting role in this process. Positively charged calcium ions in the environment of the microorganisms are attracted to carboxy and phosphoryl groups on the cell surface by electrostatic interactions [15–17]. This increases the calcium concentration near the cells. Calcium carbonate precipitation subsequently occurs at this nucleation site in the liquid phase around the cell. The influence of cells as nucleation sites is also reflected in the fact that MICP is more efficient compared to enzymatically induced calcium carbonate precipitation (EICP). For example, Zhao et al. showed that when free urease was used instead of *S. pasteurii*, a lower amount of calcium carbonate was precipitated from a solution of urea and calcium chloride. In addition, samples treated by EICP had a lower unconfined compressive strength in relation to the calcium carbonate content than samples treated by MICP [18]. To consolidate mineral particles using ureolytic organisms, various methods have been used in the literature. The three main components of these processes are mineral particles, cell suspension of ureolytic microorganisms, for example *S. pasteurii, Bacillus megaterium* or *Lysinibacillus sphaericus*, and a calcination solution containing urea and a calcium source. Since calcium carbonate precipitation starts immediately after mixing of cell suspension and calcination solution, mixing of the components before application to the sand leads to clogging of the pores in the upper part of the samples, resulting in an inhomogeneous distribution of calcium carbonate in the samples. Various methods have been investigated to circumvent this effect.

A commonly used method to consolidate sand is two-phase injection. After the addition of cell suspension, a curing time is applied to achieve a better fixation of the cells on the sand [19, 20]. This reduced the accumulation of calcium carbonate at the injection point and achieved a more uniform distribution of calcium carbonate. However, the distribution of calcium carbonate in samples produced with two-phase injection is not completely homogeneous [21].

Another way to increase the homogeneity of the samples is to use a one-phase injection. To avoid direct precipitation of calcium carbonate during injection, a lag-phase was achieved by Cheng et al. [22] by adjusting the biomass concentration, urease activity, and pH after mixing the components, which delays the begin of calcium carbonate precipitation [22]. Since in these methods the distribution of the cell suspension is achieved by flushing the sample, there is a filtering effect by the

particles, which causes the cells to be distributed unevenly in the sample [23]. Furthermore, these methods result in non-uniform transport of calcination reagents [24]. This makes it difficult to obtain a homogeneous distribution of calcium carbonate crystals. A more uniform distribution of calcium carbonate in the samples was achieved by Zhao et al. [18] using a method of immersion. For this purpose, sand was first mixed with cell suspension, which initially distributed the cells evenly in the sample. Then, this mixture was placed in geotextile molds and immersed in the calcination solution. The high number of pores allows nutrients to pass through the geotextile into the sample, where the MICP occurs, and the samples are consolidated. A uniform distribution of microorganisms was achieved by Cheng et al [24] by developing a so-called bioslurry. For this purpose, ureolytic organisms were mixed with a urea and calcium source after cultivation, causing the cells to encapsulate in calcium carbonate. The precipitated calcium carbonate was then harvested and lyophilized. This resulted in a powder with ureolytic activity. By mixing this powder with sand a homogeneous distribution of the cells in the sand can be achieved [24]. The samples were then consolidated by injecting a calcination solution. Through this method, Cheng et al. [24] were able to achieve a nearly homogeneous distribution of calcium carbonate along a 275 mm long sample. Thus, the immersion and bioslurry methods can solve the problem of sample homogeneity. However, the strength of the samples in both methods is limited by the initial number of cells in the sample. Once all cells are encapsulated, no further consolidation of the samples is achieved.

A possible approach to provide both a homogeneous distribution of the calcination solution and a sufficient number of cells and thus nucleation sites could be 3D printing. In fact, the method of bioslurry and the method of immersion have already been combined by Nething et al. [25] to enable a 3D printing process by powder printing. For this purpose, silica sand was mixed with bioslurry in the areas that would later be consolidated, while the outer bed consisted of untreated sand. After printing these layers, the printed bed was immersed in a calcination solution, thus consolidating the structure. In this study, the possibilities of printing cell suspension and cementation solution directly on a surface for MICP are explored. For this purpose, it was first investigated whether *S. pasteurii* can survive passing through

different nozzle sizes of a dispensing system. In addition, it was investigated how long a cell suspension of *S. pasteurii* can maintain its potential for MICP during sterile storage at different temperatures. Subsequently, as a proof of concept, a layer of quartz sand was consolidated using MICP. If it is possible to print one layer of calcium carbonate on mineral particles the findings could lead to the development of a 3D printer that is able to produce samples with uniform consolidation without the drawbacks of a fixed number of cells in the sample or the necessity of an immersion of the sample in calcination solution.

2 Materials and Methods

2.1 Cultivation method

Sporosarcina pasteurii (ATTC 11859) was used as ureolytic microorganism as this strain has a very high specific ureolytic activity, its urease synthesis is not repressed by ammonium, has no known pathogenicity [26] and is therefore the most common used strain for MICP. The strain was cultured in NH4-YE medium as recommended by ATTC. The medium contained 15.75 g Tris buffer (Carl Roth GmbH), 10 g ammonium sulfate (Sigma Aldrich) and 20 g yeast extract (Carl Roth GmbH) per liter. For preparation of the medium, Tris buffer was adjusted to pH 9.2 and divided into two equal parts. Yeast extract and ammonium sulfate were dissolved separately each in one part. The solutions were autoclaved at 121 °C for 20 minutes. After cooling, the solutions were combined under sterile conditions to obtain the final medium. For cultivation, 200 mL of NH4-YE medium was placed in 500 mL Erlenmeyer flasks and inoculated with 1 v/v % of a pre-culture that was grown overnight. Cultivation was performed at 120 rpm at 30 °C. During the cultivation samples were taken under sterile conditions and the optical density (OD_{600}) was measured at a wavelength of 600 nm (Cary 60 UV-Vis, Agilent Technologies, USA).

2.2 Measurement of urease activity

Urease activity was measured using the conductivity method [7]. For this purpose, 1 mL of cell suspension was added to 19 mL of a solution containing a concentration of 1.053 M urea and 10 mM Tris buffer. The change in conductivity was recorded over 5 minutes. To correlate the change in conductivity with the amount of urea degraded, urea standards were completely hydrolyzed with urease (50 mM -

250 mM) from Jackbean (Carl Roth GmbH) and the change in conductivity after complete degradation was measured.

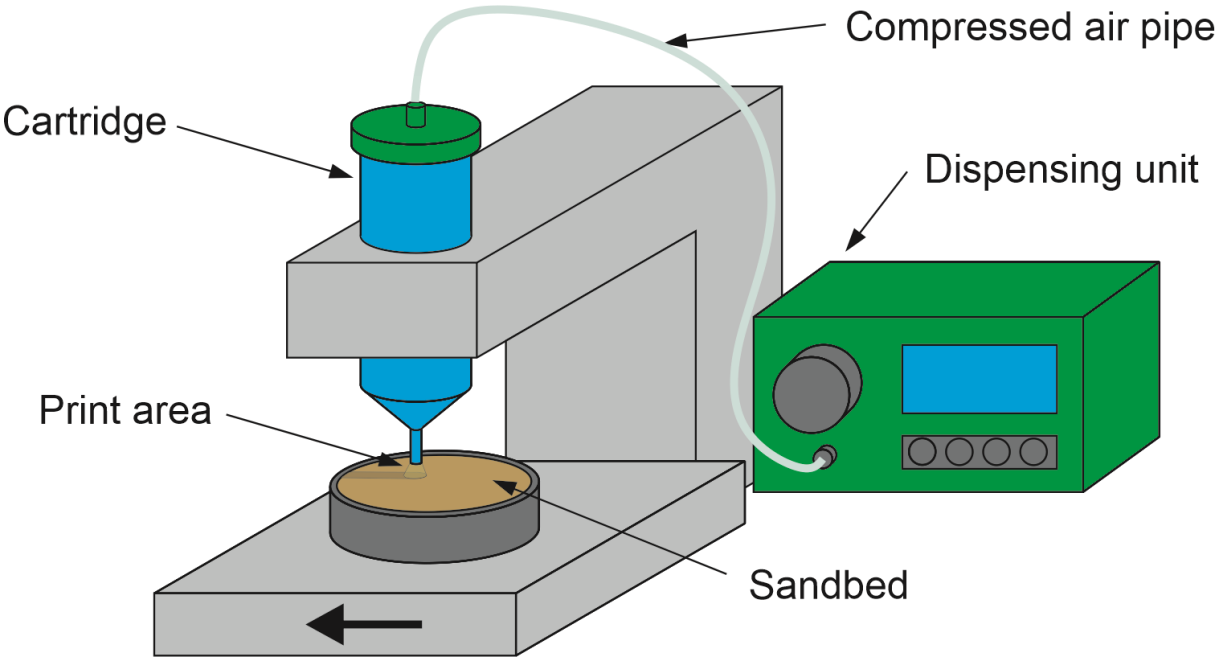

Figure 1: Prototype printer based on an dispensing unit for applying the cell suspension and the calcination solution.

2.3 Measurement of cell vitality

Cell vitality was determined by resazurin assay according to the method of Mehring et al. [27]. For this purpose, the cell suspension was diluted to an OD of 0.2 with Sorensen buffer (pH 7.4). For each 20 µL of cell suspension, another 180 µL of Sorensen buffer and 20 µL of a resazurin solution (2 mg/mL) (Sigma Aldrich) were added to a 96 well plate. Fluorescence was measured at 540 nm excitation and 590 nm emission (2030 Multilable Reader VICTOR X3, PerkinElmer, USA). Calibration was performed using standards that contained 0 - 100% live cells of *S. pasteurii*.

2.4 Storage of cell suspension

To investigate storage stability, a culture of *S. pasteurii* was harvested in exponential phase (OD 2.0) and transferred as aliquots to sterile 2 ml reaction tubes. The aliquots were stored in a drying oven (25 °C), in a refrigerator (4 °C) and in a freezer (-18 °C) to obtain different storage conditions. The optical density, urease activity, and cell viability of the stored aliquots were checked at regular intervals.

2.5 MICP printer

A printer (see Figure 1) based on a dispensing unit (DC 1000 series, Vieweg) was used to apply the cell suspension and the calcination solution. The use of this dispensing unit makes it possible to use a variety of different dispensing tips for the application of the respective solutions. This makes it possible to test different flow rates and identify the optimal configuration for printing the calcium carbonate layer. Initial tests were carried out with dispensing tips with diameters of 150 µm, 200 µm and 250 µm. The device is pressure driven and allows the use of pressure up to 2.76 bar. In order to print directly on a sand bed, it has been necessary to build a printer that can accommodate the cartridge with the dispensing tip. To provide a prototype that can be easily modified and quickly implemented, this is made from interlocking bricks (Lego Technic, The Lego Group). With this motor-controlled prototype the sand bed can be moved the cartridge while applying the respective solution. For the time being, the printer is designed to reliably print wide bars on sand in one layer.

2.6 MICP treatment

A calcination solution of urea (Carl Roth GmbH) and calcium chloride of various concentrations (Carl Roth GmbH) was prepared for MICP. The cell suspension of *S. pasteurii* was harvested after cultivation to an optical density of 2.0 and stored sterile at 4°C. Quartz sand from Haltern, Germany with a quartz content of 98 % was used for this study. Particle sizes ranged from 125 µm to 500 µm with the largest percentage of particles (43 %) having a size between 125 µm and 250 µm. For consolidation of silica sand, cell suspension was first added by the printer to the sand through a nozzle with a diameter of 200 µm under a pressure of 0.69 bar. For the negative control NH4-YE medium was added instead of cell suspension under the same conditions. Then, after 15 minutes, an equivalent volume of calcination solution was added. This was followed by a period of 3.5 h during which the calcination solution used was allowed to react. Before each cycle the solution was washed with deionized water to wash off excess salts from the previous cycle. Between the intervals the container was closed with a layer of plastic film to prevent the sample from drying out. Following the sixth printing interval, the sand bed was oven dried for 48 h at 55 °C. Subsequently, the sand bed was treated with Resazurin Red S for staining the calcium carbonate.

2.7 Staining of calcium carbonate

Alizarin Red S was used to stain calcium carbonate. The yellow dye changes to red in the presence of calcium carbonate. 10 mg Alizarin Red S (Carl Roth GmbH) was dissolved in 100 mL 0.2 % HCl (Carl Roth GmbH). The solution was sprayed with a spray flask on the entire sand bed after printing.

2.8 Microscopic imaging

Microscopic images were taken using a digital reflected light microscope (Digital microscope VHX 7000, KEYENCE, Japan). Images were taken with bright field illumination and a polarizing filter to reduce reflective effects.

3 Results and Discussion

3.1 Storage stability of *S. pasteurii*

To obtain uniform results during MICP the cell suspension used during each cycle of MICP should have similar cell density, urease activity and cell vitality. In order to determine for which period of time a cell suspension of *S. pasteurii* can be used for MICP, the cell suspension was investigated with regard to these parameters. This should give an indication of how long the cells can be stored under different conditions after fermentation while maintaining their potential for MICP. For this purpose, *S. pasteurii* was harvested in the exponential growth phase and stored sterilely as aliquots at various temperatures (-18 °C, 4 °C and 25 °C). Over the storage period, the cell density initially shows a decrease for all temperatures, presumably as a shock response (see Figure 2 C). Subsequently, the cell densities remain constant at about OD_{600} 1.5 over a period of 16 days when stored at -18 °C and 4 °C. At a storage temperature of 25 °C, the cell density drops constantly to a value of OD_{600} 0.53 ± 0.02. The decrease in cell density and thus nucleation sites may ensure that the formation of new crystals at nucleation sites decreases, increasing the growth of pre-existing calcium carbonate crystals, leading to the formation of larger calcium carbonate crystals [28, 29]. Since larger calcium carbonate crystals allow higher consolidation of silica sand than smaller crystals [30], a decrease in cell density can thus lead to higher calcination efficiency.

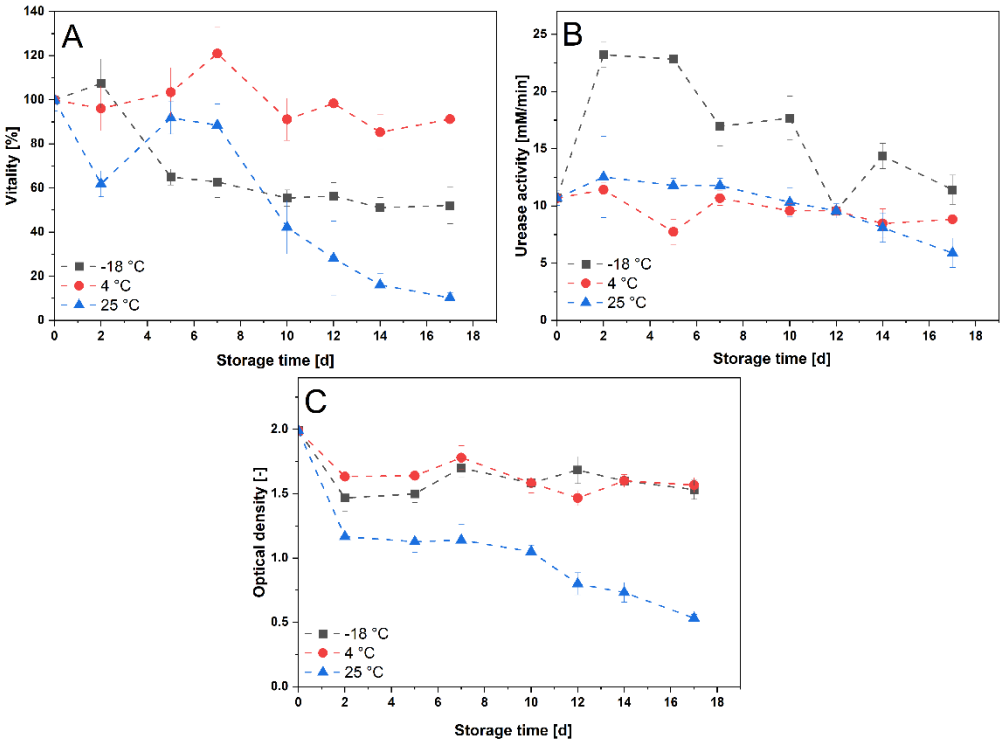

Figure 2: Storage stability of *S. pasteurii* in sterile reaction vials at -18 °C, 4 °C and 25 °C. A: cell vitality B: urease activity, C: OD_{600}. The error bars represent the ± standard deviation for n=3 replicates

At the same time, a sufficient amount of biomass and thus nucleation sites must be present to allow the growth of new crystals. A strong decrease of the biomass concentration could lead to a decrease of the calcination efficiency. Storage at -18 °C and 4 °C thus seems uncritical with regard to cell density, while storage at 25 °C could lead to problems with MICP. However, the function of the cells as nucleation sites depends, among other things, on whether the cell excretes ammonium ions to obtain ATP [26]. An indicator of whether cells are maintaining their metabolic processes can be obtained by measuring cell vitality. While the cell vitality remains almost constant over the storage period at 4 °C, the vitality decreases to 52.2 ± 8.4 % within 17 days when stored at -18 °C, while at 25 °C the vitality decreases to 10.3 ± 2.3 % (see Figure 2 A). The decrease in vitality during storage at 25 °C is most likely due to the fact that the cells continue to grow at this temperature and enter the death phase, which is also reflected in the decrease in cell density. The decrease in cell viability during storage at -18 °C, on the other hand, can be attributed to damage to the cells due to freeze-thaw stress, since no protective agent

against ice crystal formation was added for storage. In addition to their function as nucleation sites, the cells need to maintain their ureolytic activity for MICP. Storage at -18 °C shows a strong increase in ureolytic activity in the first days of storage (see Figure 2 B). Since urease from *S. pasteurii* is intracellularly, this increase is most likely due to damage to the cells during freezing, whereby urease is released from the cells and is present as free urease which declines in its activity over the following storage time. Since free urease is not limited by mass transport of the substrate urea into the cell, the observed urease activity increases. During storage at 4 °C and 25 °C, the urease appears to remain present intracellularly and is thus protected from loss of activity. The findings of Bachmeier et al [31] support this thesis. They describe that free urease isolated from *S. pasteurii*, dropped to an activity of 10 % within a few days of storage at 30 °C. In a similar experiment, Konstantinou et al. [32] found that the urease activity of a culture of *S. pasteurii* which was grown in NH4-YE medium increased after day 14 of storage at 4 °C. They attribute this increase to a slow growth of *S. pasteurii* during storage. However, in the study by Konstantinou et al. [32] the initial cell density during the experiment was OD_{600} 1.0. This suggests that the cells have grown less dense and therefore consumed a different amount of nutrients which might lead to different results in the stability of the urease activity. The results of cell density, vitality and ureolytic activity suggest that it is appropriate to store cells of *S. pasteurii* at -18 °C or 4 °C for a period of 17 days and use them for subsequent MICP. Storage at 25 °C should be avoided, as the vitality of the cells and thus their function as nucleation sites is not guaranteed. For use in a printer, however, storage at 4 °C would be more appropriate, as the cell suspension can then be applied directly from a cooled storage vessel via a nozzle, whereas a frozen suspension would first have to be thawed.

3.2 Stability of cells through printing nozzle

Since the printer is based on a dispensing unit that is operated with pressure it is necessary to evaluate if *S. pasteurii* cells can pass through different nozzles unharmed. For this purpose, cell vitality was investigated. Nozzle sizes of 150, 200 and 250 µm were chosen, while three pressure levels were tested (0.69, 1.38 and 2.76 bar). The Mann-Whitney U test was performed to determine whether the cell vitality drops significantly after passing through the printing nozzle. Null hypothesis:

The difference in the position under the sample is zero. If the p value was higher than 0.05, the hypothesis was discarded. No parameter combination tested resulted in a significant decrease in cell viability compared to the negative control that did not pass a nozzle (see Figure 3). Also, no significant differences were found for optical density and urease activity after nozzle passage to the negative control (see supplement 1, 2). These results suggest that *S. pasteurii* retained its potential for MICP after passing through nozzles of sizes 150, 200 and 250 µm at pressure up to 2.76 bar.

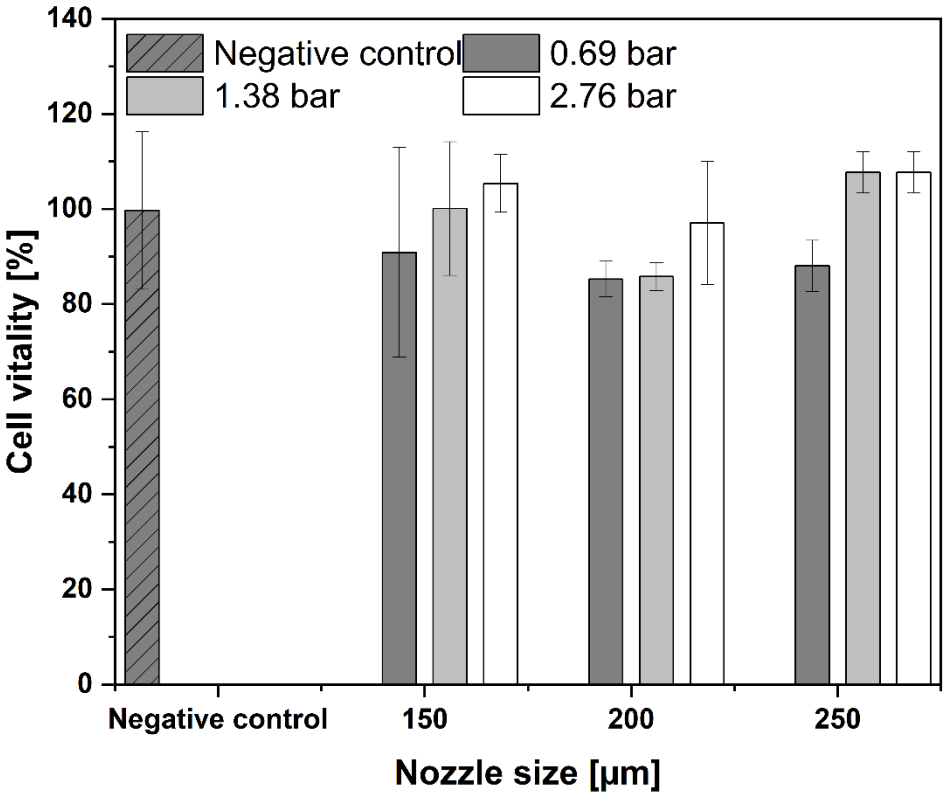

Figure 3: Comparison of cell vitality of *S. pasteurii* before and after passing through nozzles of various sizes (150-250 µm) at different pressure levels (0.69-2.76 bar). The error bars represent the ± standard deviation for n=5 replicates.

The findings also indicate that there are no shear forces high enough to damage the cells and reduce their potential for MICP. Each of the parameter combinations studied is thus suitable for printing layers of biocemented sand using MICP. Further selection can therefore be based on the required flow rate and the result of uniform application of the fluids. For the proof of concept, a nozzle diameter of 200 µm and a pressure of 0.68 bar were used. This parameter combination showed subjectively the

least disturbance of the sand bed when one cycle of cell suspension and calcination solution was applied.

3.3 Proof of concept

To demonstrate a proof of concept for printing a layer of calcium carbonate, quartz sand was placed in a container under the printer. The sand was smoothed out with a plastic card in order to obtain a homogenous surface. Now the cell suspension and the calcination solution were alternately applied by the printer. For the first tests, six printing intervals were run with a curing time of 3.5 hours between each interval. Since only a limited amount of calcium carbonate can be precipitated when cells and calcination solution are added [7], up to twelve printing intervals are necessary to generate enough calcium carbonate to achieve a good detectability via microscopy. Three different equimolar concentrations of the calcination solution have been tested for printing (500 mM, 250 mM and 100 mM). For concentrations of 500 and 250 mM urea and $CaCl_2$ the samples were consolidated after the printing process and could be taken out of the printing bed (see Figure 4) while the samples treated with 100 mM calcination solution could not be separated from the unconsolidated sand bed without breaking apart.

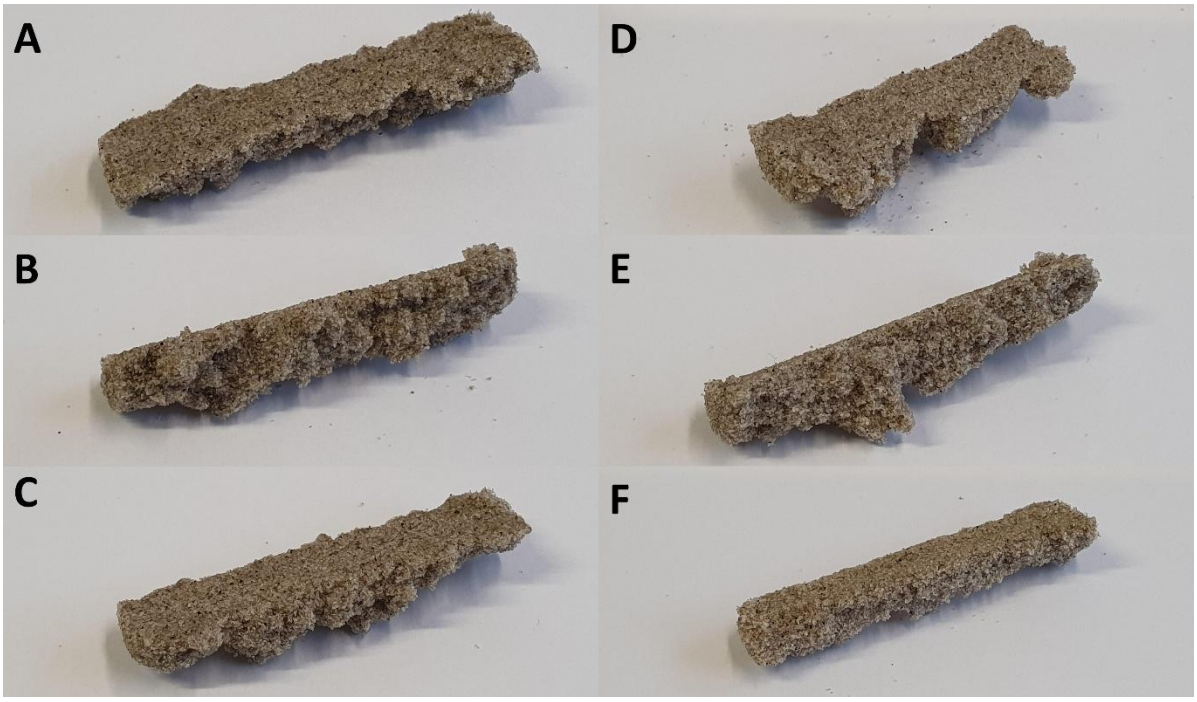

Figure 4: Biocemented samples after six cycles of printing with MICP. A,B,C: Treatment with 250 mM calcination solution D,E,F: Treatment with 500 mM calcination solution

On microscopic examination, individual calcium carbonate crystals are visible on the sand grains, reaching a diameter of up to 26.8 respective 45.9 µm for samples treated with 250 mM and 500 mM calcination solution (see Figure 5). These crystals can act as bridges between individual sand grains and thus consolidate the samples. No calcium carbonate crystals were observed at a concentration of 100 mM. This is probably due to the fact that the crystals do not reach a sufficient size during a cycle of MICP and are flushed out by rinsing deionized water.

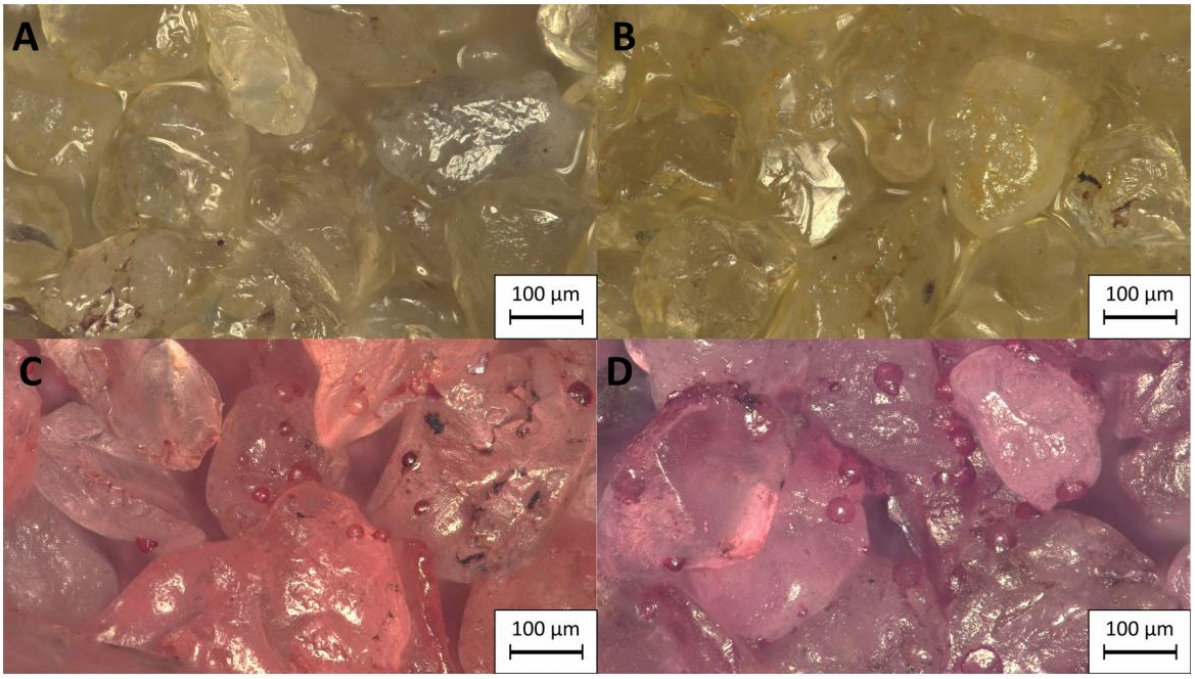

Figure 5: Microscopic images of the printed calcium carbonate layer on top of silica sand after six cyles of MICP and after staining with Alizarin Red S. A: Negative control B: Treatment with cell suspension of *S. pasteurii* (OD_{600} 2.0) and 100 mM Urea/$CaCl_2$ C: Treatment with (OD_{600} 2.0) and 250 mM Urea/$CaCl_2$ D: Treatment with (OD_{600} 2.0) and 500 mM Urea/$CaCl_2$

Since no measurements of the compressive strength can be made due to the non-uniform structure of the specimens, the size of the calcium carbonate crystals can give an indication of the degree of consolidation of the specimens since the compressive strength of biocemented sand increases with the size of the calcium carbonate crystals [30, 33]. The formation of the calcium carbonate crystals does not occur uniformly over the entire surface of the sand. This could be due to the fact, that the cells are flushed from the upper areas of the sand grains into depressions by the

application of the cementing solution and remain there during MICP. Furthermore, cells of *S. pasteurii* agglomerate in the presence of high calcium chloride concentrations, which could lead to an uneven distribution of the cells on the sand surface. However, since the formation of bridges between particles is crucial for particle consolidation, the formation of a uniform calcium carbonate layer on the surface of the layer is not desirable [33].

So far, the possibilities of printing with MICP have been demonstrated on one layer. In further studies, the printer will be extended to print three-dimensional objects. This will allow measurements of parameters like compressive strength and to evaluate the homogeneity of the calcium carbonate distribution in the samples in comparison to different methods of MICP. For this purpose, it is necessary to investigate under which conditions individual printed layers can be bonded together and how the cells and solutions applied to the sand are distributed in adjacent sand. Therefore, parameters such as the volume added through the nozzle during each cycle, the concentration of $CaCl_2$ and urea in the calcination solution, the cell density and the number of treatments must be studied and optimized to print a 3D object. This would allow to make measurements of the compressive strength of the samples and to obtain additional data on the homogeneity in comparison to samples produced with different MICP methods.

4 Concluding remarks

The potential of MICP as a technology to create sustainable construction material is limited by the necessity to create materials with a homogenous distribution of calcium carbonate. Over the last years many studies have investigated different technologies to achieve this goal. A possible solution to this problem could be 3D printing with MICP. In this study, possibilities and potential for printing calcium carbonate layers using MICP were investigated. This can be a first step to develop a 3D printing system for MICP. It was found that *S. pasteurii* can be stored at 4 °C for at least 17 days after batch cultivation without major losses in optical density, ureolytic activity or cell vitality. This storage capability of the cells is important for achieving a uniform result during each treatment of MICP. Furthermore, the cells of *S. pasteurii* retain their urease activity, optical density, and cell vitality after passing through printer nozzles of various sizes (150-250 µm) and at different pressure levels (0.69-

2.76 bar). That *S. pasteurii* maintains its potential of MICP after passing through the nozzles was also shown by printing a layer of calcium carbonate crystals by applying *S. pasteurii* cells and calcination solution on a bed of sand through a printer nozzle (200 µm). This technology offers the potential to enable the printing of 3D three-dimensional objects using MICP. Further research is still necessary to develop this application of MICP into a functional technology that can be used to create homogenous construction material.

Compliance with Ethical Standards

This project was financially supported by the Deutsche Forschungsgemeinschaft (DFG, German Research Foundation) – Project-ID 172116086 – SFB 926 and the “Landespotentialbereich NanoKat”.

The authors have declared no conflicts of interest

The data that support the findings of this study are available from the corresponding author upon reasonable request.

5 References

1. Miller, S. A., Horvath, A., Monteiro, P. J. M., Impacts of booming concrete production on water resources worldwide. *Nat Sustain* 2018, *1*, 69–76.
2. Husillos Rodríguez, N., Martínez-Ramírez, S., Blanco-Varela, M. T., Donatello, S. et al., The effect of using thermally dried sewage sludge as an alternative fuel on Portland cement clinker production. *Journal of Cleaner Production* 2013, *52*, 94–102.
3. Ghosh, P., Mandal, S., Chattopadhyay, B. D., Pal, S., Use of microorganism to improve the strength of cement mortar. *Cement and Concrete Research* 2005, *35*, 1980–1983.
4. Muynck, W. de, Cox, K., Belie, N. de, Verstraete, W., Bacterial carbonate precipitation as an alternative surface treatment for concrete. *Construction and Building Materials* 2008, *22*, 875–885.
5. Achal, V., Mukerjee, A., Sudhakara Reddy, M., Biogenic treatment improves the durability and remediates the cracks of concrete structures. *Construction and Building Materials* 2013, *48*, 1–5.
6. Dhami, N. K., Reddy, M. S., Mukherjee, A., Synergistic Role of Bacterial Urease and Carbonic Anhydrase in Carbonate Mineralization. *Applied Biochemistry and Biotechnology* 2014, *172*, 2552–2561.
7. Whiffin, V. S., van Paassen, L. A., Harkes, M. P., Microbial Carbonate Precipitation as a Soil Improvement Technique. *Geomicrobiology Journal* 2007, *24*, 417–423.
8. Mondal, S., Ghosh, A., Microbial Concrete as a Sustainable Option for Infrastructural Development in Emerging Economies 2018, 413–423.
9. L.A. van Paassen M.P. Harkes, Scale up of BioGrout: a biological ground reinforcement method. *Proceedings of the 17th International Conference on Soil Mechanics and Geotechnical Engineering* 2009, *2009*, 2328–2333.
10. Omoregie, A. I., Palombo, E. A., Ong, D. E., Nissom, P. M., A feasible scale-up production of Sporosarcina pasteurii using custom-built stirred tank reactor for in-situ soil biocementation. *Biocatalysis and Agricultural Biotechnology* 2020, *24*, 101544.
11. Hammes, F., Verstraete*, W., Key roles of pH and calcium metabolism in microbial carbonate precipitation. *Reviews in Environmental Science and Bio/Technology* 2002, *1*, 3–7.
12. Muynck, W. de, Belie, N. de, Verstraete, W., Microbial carbonate precipitation in construction materials: A review. *Ecological Engineering* 2010, *36*, 118–136.
13. Stocks-Fischer, S., Galinat, J. K., Bang, S. S., Microbiological precipitation of CaCO3. *Soil Biology and Biochemistry* 1999, *31*, 1563–1571.
14. Anbu, P., Kang, C.-H., Shin, Y.-J., So, J.-S., Formations of calcium carbonate minerals by bacteria and its multiple applications. *SpringerPlus* 2016, *5*, 250.

15. Bäuerlein, E., Biomineralization of unicellular organisms: an unusual membrane biochemistry for the production of inorganic nano- and microstructures. *Angewandte Chemie (International ed. in English)* 2003, *42*, 614–641.
16. Douglas, S., Beveridge, T. J., Mineral formation by bacteria in natural microbial communities. *FEMS Microbiology Ecology* 1998, *26*, 79–88.
17. Seifan, M., Samani, A. K., Berenjian, A., Bioconcrete: next generation of self-healing concrete. *Applied microbiology and biotechnology* 2016, *100*, 2591–2602.
18. Zhao, Q., Li, L., Li, C., Zhang, H. et al., A Full Contact Flexible Mold for Preparing Samples Based on Microbial-Induced Calcite Precipitation Technology. *Geotech. Test. J.* 2014, *37*, 20130090.
19. Cheng, L., Cord-Ruwisch, R., In situ soil cementation with ureolytic bacteria by surface percolation. *Ecological Engineering* 2012, *42*, 64–72.
20. Tobler, D. J., Maclachlan, E., Phoenix, V. R., Microbially mediated plugging of porous media and the impact of differing injection strategies. *Ecological Engineering* 2012, *42*, 270–278.
21. Shahrokhi-Shahraki, R., Zomorodian, S. M. A., Niazi, A., O'Kelly, B. C., Improving sand with microbial-induced carbonate precipitation. *Proceedings of the Institution of Civil Engineers - Ground Improvement* 2015, *168*, 217–230.
22. Cheng, L., Shahin, M. A., Chu, J., Soil bio-cementation using a new one-phase low-pH injection method. *Acta Geotech.* 2019, *14*, 615–626.
23. Ginn, T. R., Wood, B. D., Nelson, K. E., Scheibe, T. D. et al., Processes in microbial transport in the natural subsurface. *Advances in Water Resources* 2002, *25*, 1017–1042.
24. Cheng, L., Shahin, M. A., Urease active bioslurry: a novel soil improvement approach based on microbially induced carbonate precipitation. *Can. Geotech. J.* 2016, *53*, 1376–1385.
25. Zhao, Q., Li, L., Li, C., Zhang, H. et al., Factors Affecting Improvement of Engineering Properties of MICP-Treated Soil Catalyzed by Bacteria and Urease. *Journal of Materials in Civil Engineering,* 2014,26 (12), 04014094
26. Cheng L, Shahin MA, Cord-Ruwisch R. Bio-cementation of sandy soil using microbially induced carbonate precipitation for marine environments. Géotechnique. 2014;64:1010-1013.
27. Nething, C., Smirnova, M., Gröning, J. A., Haase, W. et al., A method for 3D printing bio-cemented spatial structures using sand and urease active calcium carbonate powder. *Materials & Design* 2020, *195*, 109032.
28. Mehring, A., Erdmann, N., Walther, J., Stiefelmaier, J. et al., A simple and low-cost resazurin assay for vitality assessment across species. *Journal of Biotechnology* 2021, *333*, 63–66.

29. Gandhi, K. S., Kumar, R., Ramkrishna, D., Some Basic Aspects of Reaction Engineering of Precipitation Processes. *Ind. Eng. Chem. Res.* 1995, *34*, 3223–3230.
30. Al-Thawadi, Calcium Carbonate Crystals Formation by Ureolytic Bacteria Isolated from Australian Soil and Sludge. *Journa of Advanced Science and Engineering Research* 2012, *2012*.
31. Whiffin, High strength in-situ biocementation of soil by calcite precipitating locally isolated ureolytic bacteria, Perth, Western Australia 2004.
32. Bachmeier, K. L., Williams, A. E., Warmington, J. R., Bang, S. S., Urease activity in microbiologically-induced calcite precipitation. *Journal of Biotechnology* 2002, *93*, 171–181.
33. Konstantinou, C., Wang, Y., Biscontin, G., Soga, K., The role of bacterial urease activity on the uniformity of carbonate precipitation profiles of bio-treated coarse sand specimens. *Scientific reports* 2021, *11*, 6161.
34. Cheng, L., Shahin, M. A., Mujah, D., Influence of Key Environmental Conditions on Microbially Induced Cementation for Soil Stabilization. *J. Geotech. Geoenviron. Eng.* 2017, *143*, 4016083.

6 Supplement

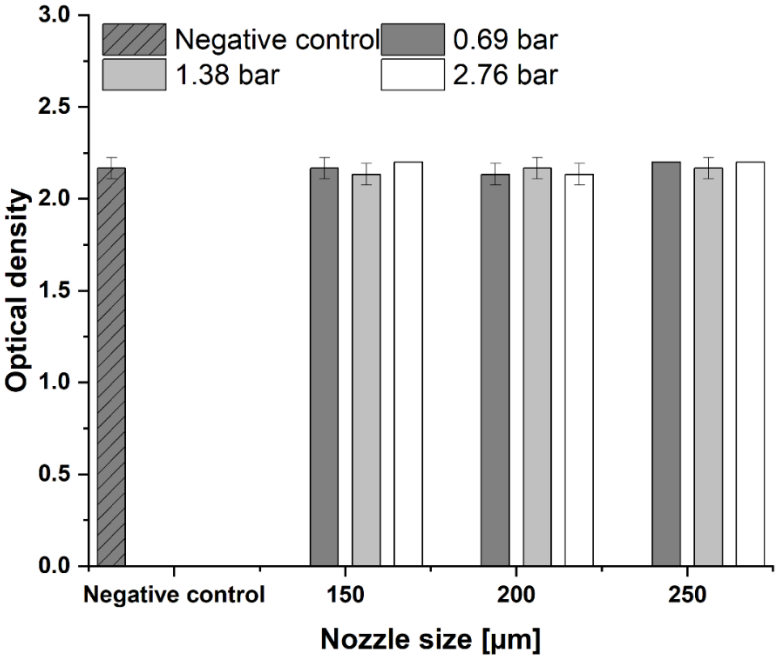

Supplement 1: Comparison of optical density of *S. pasteurii* before and after passing through nozzles of various sizes (150-250 µm) at different pressure levels (0.69-2.76 bar). The error bars represent the ± standard deviation for n=5 replicates.

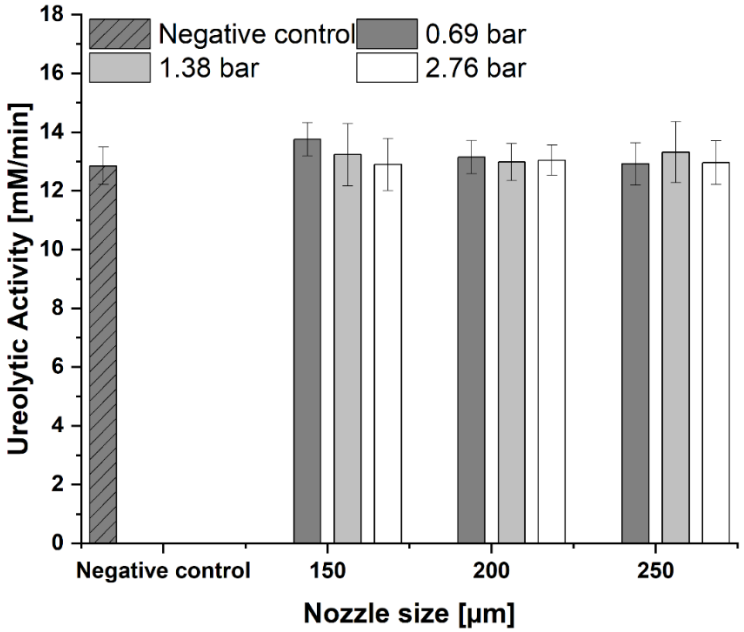

Supplement 2: Comparison of ureolytic activity of *S. pasteurii* before and after passing through nozzles of various sizes (150-250 µm) at different pressure levels (0.69-2.76 bar). The error bars represent the ± standard deviation for n=5 replicates.

VII Concluding Remarks

1 Summary and Outlook

The aim of this work was to investigate the MICP process for biosandstone production and to improve the resource and time efficiency of ureolytic MICP. Based on these findings, two application cases of MICP were considered: (1) The optimization of the compressive strength of biosandstone, produced using surface percolation methods. (2) The potential application of MICP in 3D printing as proof-of-concept. The main results of the scientific publications written as part of this thesis are summarized and discussed in this chapter. Additionally, an outlook on possible future research fields for ureolytic MICP is provided.

Chapter 2 provided an overview of the main factors influencing the MICP. The critical discussion of these parameters and the current state of research highlights the complexity of MICP in the consolidation of particles. The outcome of MICP in terms of compressive strength is primarily dependent on the mass and morphology of the formed calcium carbonate crystals. However, these are influenced by a multitude of biological, chemical, and physical factors as well as the applied application methods. Therefore, a classic optimization of MICP by a one factor at a time approach is not always suitable. Furthermore, different application areas of MICP have varying requirements for the outcome. While rapid production and strength are paramount in biosandstone production, in soil stabilization the focus might be more on the balance between water permeability and consolidation. The efficiency of MICP is primarily measured by mechanical parameters, especially uniaxial compressive strength, which depends on the calcium carbonate content after MICP. Regardless of scaling, the core factors of MICP are the time between application cycles and the amount of precipitated calcium carbonate per cycle.

In Chapter 3 the most important parameters of MICP (temperature, calcium concentration and cell density of ureaolytic bacteria) were selected and further studied. The results show that the reaction time of MICP primarily depends on the temperature and cell density of the cell suspension. An increase in temperature from 40 to 45 °C led to a tenfold increase in reaction rate, which, however, decreased

significantly at temperatures above 65 °C. Another important temporal factor was cell concentration, and thus the concentration of the catalyst. In the investigated range, a linear relationship was observed. The maximum tested OD_{600} of 30 is significantly higher than the values considered optimal in the literature, which range from OD_{600}=0.4 to 3 [1-3]. A linear relationship between cell density and reaction rate of the MICP can therefore be assumed for all common applications of the MICP. Also, the calcium concentration influenced the reaction rate of the MICP. Contrary to expectations, the reaction rate initially doubled between 0 M and 2 M calcium chloride. However, further increases in calcium concentration inhibited the reaction rate. While temperature and cell density are parameters that influence the reaction rate of MICP in practical applications, the amount of calcium carbonate formed is crucial. The results showed that a calcium concentration between 2 and 3 M is suitable for MICP concerning reaction time and possible calcium carbonate precipitation per cycle. Higher calcium concentrations can only be used during MICP by using higher cell densities (OD_{600} > 6). The balance between the amount of calcium carbonate per cycle and the amount of cell suspension used must be decided based on the specific application.

Regardless of these considerations, the results of this study close the knowledge gap regarding the impact of high cell and calcium concentrations on MICP and provide a basis for better estimating the reaction rate of MICP under given conditions in future studies. However, the investigations into reaction kinetics in shaken reaction vessels do not consider the static conditions and poor mixing ratios during MICP. However, the approach of this study, as well as all previous studies dealing with the kinetics of cell activity during MICP [4–16], remains overall phenomenological and limited to observing ammonium/urea and calcium concentrations during the reaction. A detailed consideration of the individual steps of MICP – such as substance transport into the cell, intracellular ureolysis, substance transport out of the cell, and precipitation reaction – could deepen our understanding of MICP and provide new approaches, possibly also for modeling the process. The results from Chapter 3 could be repeated in the future using identical parameters for MICP in a sand bed to verify how well the laboratory results translate to real applications.

The results from Chapter 4 illustrate that merely considering the reaction rates and the amount of precipitated calcium carbonate is insufficient to fully describe the production of biosandstone. When treating sand with different average particle diameters (between 0.063 mm and 0.500 mm) using the same MICP protocol (cell density, composition of calcination solution, and temperature), significant differences in the uniaxial compressive strength, permeability, and calcium carbonate content of the biosandstone were observed. It was shown that smaller particle diameters resulted in higher compressive strengths and calcium carbonate contents. At the same time, this resulted in a stronger decrease in the soil's permeability. This effect is due to the distribution and filling of voids in the sand by calcium carbonate crystals. Only crystals that form bridges between the sand particles contribute to the material's strength, while crystals that grow into the voids between the particles do not provide any strength and thus represent wasted resources. In addition to particle size, the shape of the sand grains is also discussed as a factor influencing the outcome of MICP [17]. Although our understanding of the complex mechanisms by which sand size and shape affect the MICP outcome is still limited [18], it is important to consider this aspect when planning biosandstone production.

The optimization of MICP using design of experiments (DoE), as described in Chapter 5, can help optimize the mechanical parameters of MICP for specific applications. The results from Chapter 3 helped define the limits of this optimization regarding Urea and calcium concentrations. Thus, the boundaries for urea and calcium concentration were set between 0.659 M and 2.341 M, which lies within the optimal concentration ranges discussed in Chapter 3. The described optimum of the calcining solution was at 1.492 M urea and 1.391 M calcium chloride. Compared to the most used protocol from the literature (1 M equimolar urea/calcium [19–21]), a 143 % increase in compressive strength was achieved, with 49 and 39 % more resources being used, respectively. This led to an increase in resource efficiency by 60 %, from 0.38 ± 0.08 kPa/mol to 0.65 ± 0.08 kPa/mol.

However, the optimization of biosandstone production using the infiltration method encounters a limiting phenomenon already described in Chapter 4: the decrease in permeability. It was observed that from about 10 MICP application cycles, the infiltration rate significantly decreased. Between the 12th and 13th cycle, the

infiltration came to a complete halt with the protocols used. This effect is also observed in literature, leading to the compressive strength of biosandstone produced by the infiltration method reaching its maximum at about 15 MPa [22]. In contrast, the start-up Biomason reports a maximum compressive strength of 27.6 to 41.4 MPa for their biosandstone tiles, with a calcium carbonate content of 15 % [23]. However, it remains unclear how such high compressive strengths are achieved with these low calcium carbonate contents. Higher compressive strengths could be achieved by different application methods of bacteria and nutrients during MICP into the sand matrix to overcome the loss of permeability due to pore blocking (see Chapter 4). Chapter 2 already described various alternative methods for the application of MICP during biosandstone production and soil stabilization. The application of cell suspension and calcination solution under pressure could be combined in the future with the already optimized parameters to further increase the compressive strength of the biosandstone.

In Chapter 6, the printing of a calcium carbonate layer with a nozzle of 150 µm diameter and a pressure of 2.76 bar was demonstrated. The cells maintained their cell viability and ureolytic activity. A calcium carbonate layer could be formed, and an unquantified strength was observed. However, further experiments showed that as applications progressed, the cell suspension and calcination solution did not infiltrate the already treated layers quickly enough, causing the layer to widen. Thus, clear demarcations of a printed biosandstone structure are not realizable at the present scale. Based on the findings from Chapter 6, future studies should examine whether the idea of an MICP 3D printer can be scaled up to consolidate soil surfaces, for example, to protect against soil erosion. In this case, only a layer of calcium carbonate would be applied to the surface. This approach is not new, but the literature mainly discusses widespread application [24]. Ghasemi and Montoya (2022) demonstrated using a 100 m^3 large sand basin that MICP is suitable for protecting sandy soils extensively and long-term (over a year) from erosion by wind and rain [25]. The targeted application of MICP through a nozzle would open the possibility of ”printing” various MICP structures onto sandy soils. Synthetic geogrids and geocells, which are already used for soil stabilization, could serve as models

[26]. This precise application could save resources, particularly by reducing the formation and application of ammonium.

Regardless of the findings of this work and the potential success of future studies on the application of MICP, the technology still faces significant challenges. These need to be addressed before a larger industrial application of MICP becomes feasible. These challenges are discussed in the following chapter.

2 Future Challenges

Despite intensive research over the past two decades, MICP remains in an early development stage for many applications. Numerous studies have demonstrated the potential of MICP for soil stabilization and the production of novel building materials on a laboratory scale. Some of these applications have been optimized and, in some cases, brought to market readiness. Successfully implemented products include Biozement Biotiles® [23] (Biomason, USA), the self-healing cement SITREN® [27] (Evonik, Germany), and a product for soil stabilization, BCEM [28] (MeduSoil, Switzerland). However, the application of MICP remains niche at present. The two main reasons for this are (1) the large amounts of byproduct ammonium produced and (2) the high energy costs of urea production. If MICP relies primarily on ureolysis, 2 moles of ammonium will always be produced per mole of urea used (approximately 0.6 tons of ammonium per ton of urea). Although efforts are being made to mitigate the impact of the ammonium load through measures such as controlled washing [29], the potential for eutrophication remains high with ureolytic MICP due to the introduction of high amounts of ammonium [30].

MICP applications in the environment should always aim to achieve the highest possible consolidation with minimal use of urea and calcium salts. In the controlled production of biosandstone, wastewater treatment would also be required, which would incur additional costs but would not pose an additional environmental burden. In addition to the negative ecological effects of ammonium, urea production is associated with high energy consumption. In large-scale urea production, ammonia is first synthesized via the Haber-Bosch process, and then urea is produced. In Europe, approximately 890 kg of CO_2 equivalents are generated per ton of urea [31]. Therefore, the production of one ton of calcium carbonate via ureolytic MICP is

associated with 534.07 kg of CO_2 solely from urea production (assuming an ideal yield of 100%, as described in Chapter 3). Current life cycle analyses that consider the total CO_2 burden of an MICP application for soil production estimate the CO_2 emissions to produce one ton of calcium carbonate at 3.4 tons of CO_2 equivalents [32] and 1.51 tons of CO_2 equivalents [30]. The production of one ton of biosandstone with a mass fraction of 15 % calcium carbonate (as marketed by Biomason with a compressive strength of 27.6-41.4 MPa) is associated with 0.23 to 0.51 tons of CO_2 equivalents. In comparison, Portland cement-based concrete (with 1/6 mass fraction of cement) produces 129 kg of CO2 equivalents per ton of concrete (based on a CO_2 equivalent of 0.776 kg per ton of cement) [33]. Therefore, the term "environmentally friendly alternative to cement" cannot currently be used for biocement based on MICP. An estimated 80 % of the greenhouse gas emissions of MICP are related to raw materials [32]. It will therefore be necessary to optimize MICP efficiency per mass fraction of calcium carbonate while also finding alternative raw material sources. A promising approach could be using urine as an alternative to industrial urea. This approach has already been demonstrated in the literature for pig urine [34], cow urine [35], and human urine [36]. Whether these hurdles of ureolytic MICP can be overcome in the future cannot be conclusively determined at present. As of this work, research interest in MICP continues to grow (based on published works on the topic in Scopus). Evonik's (Germany) interest in the technology [37] also shows that MICP could potentially lead to industrial applications in the future. However, the MICP project for self-healing concrete is currently on hold due to regulatory hurdles in the construction industry, and it remains to be seen whether promising business opportunities will arise in the field of MICP [37].

Until then, research in these areas will need to continue to advance and develop creative solutions. Whether or not these solutions are found, it is unlikely that MICP will bring about the "green revolution" in the construction industry by becoming a competitive alternative to conventional cement. However, a niche existence in soil consolidation, decorative building materials with a sandstone look, or as a component in self-healing cement is certainly possible.

3 References

1. Chen F, Deng C, Song W et al. (2016) Biostabilization of Desert Sands Using Bacterially Induced Calcite Precipitation. Geomicrobiology Journal 33:243–249. https://doi.org/10.1080/01490451.2015.1053584
2. Shannoon LK, Ibrahim MA (2020) Bio-Cementation of Sandy Soil through Bacterial Processing to Precipitate Carbonate. NJES 23:225–231. https://doi.org/10.29194/NJES.23030225
3. CHENG L, SHAHIN MA, CORD-RUWISCH R (2014) Bio-cementation of sandy soil using microbially induced carbonate precipitation for marine environments. Géotechnique 64:1010–1013. https://doi.org/10.1680/geot.14.T.025
4. Jain S (2024) Influence of biomass and chemicals on kinetics of ureolysis-based carbonate biomineral precipitation. Environ Earth Sci 83. https://doi.org/10.1007/s12665-023-11355-7
5. Wang Y, Wang Y, Soga K et al. (2022) Microscale investigations of temperature-dependent microbially induced carbonate precipitation (MICP) in the temperature range 4–50 °C. Acta Geotech. https://doi.org/10.1007/s11440-022-01664-9
6. Murugan R, Suraishkumar GK, Mukherjee A et al. (2021) Insights into the influence of cell concentration in design and development of microbially induced calcium carbonate precipitation (MICP) process. PLoS ONE 16:e0254536. https://doi.org/10.1371/journal.pone.0254536
7. Sridhar S, Bhatt N, Suraishkumar GK (2021) Mechanistic insights into ureolysis mediated calcite precipitation. Biochemical Engineering Journal 176:108214. https://doi.org/10.1016/j.bej.2021.108214
8. Zhang P, Liu X-Q, Yang L-Y et al. (2023) Immobilization of Cd2+ and Pb2+ by biomineralization of the carbonate mineralized bacterial consortium JZ1. Environ Sci Pollut Res Int 30:22471–22482. https://doi.org/10.1007/s11356-022-23587-4
9. Wen K, Li Y, Amini F et al. (2020) Impact of bacteria and urease concentration on precipitation kinetics and crystal morphology of calcium carbonate. Acta Geotech 15:17–27. https://doi.org/10.1007/s11440-019-00899-3
10. Mitchell AC, Espinosa-Ortiz EJ, Parks SL et al. (2019) Kinetics of calcite precipitation by ureolytic bacteria under aerobic and anaerobic conditions. Biogeosciences, 16(10), 2147-2161. https://doi.org/10.5194/BG-16-2147-2019
11. Lauchnor EG, Topp DM, Parker AE et al. (2015) Whole cell kinetics of ureolysis by Sporosarcina pasteurii. Journal of Applied Microbiology 118:1321–1332. https://doi.org/10.1111/jam.12804
12. Cuthbert MO, Riley MS, Handley-Sidhu S et al. (2012) Controls on the rate of ureolysis and the morphology of carbonate precipitated by S. Pasteurii biofilms and limits due to bacterial encapsulation. Ecological Engineering 41:32–40. https://doi.org/10.1016/j.ecoleng.2012.01.008
13. Tobler DJ, Cuthbert MO, Greswell RB et al. (2011) Comparison of rates of ureolysis between Sporosarcina pasteurii and an indigenous groundwater

community under conditions required to precipitate large volumes of calcite. Geochimica et Cosmochimica Acta 75:3290–3301. https://doi.org/10.1016/j.gca.2011.03.023
14. Okwadha GD, Li J (2010) Optimum conditions for microbial carbonate precipitation. Chemosphere 81:1143–1148. https://doi.org/10.1016/j.chemosphere.2010.09.066
15. Dupraz S, Parmentier M, Ménez B et al. (2009) Experimental and numerical modeling of bacterially induced pH increase and calcite precipitation in saline aquifers. Chemical Geology 265:44–53. https://doi.org/10.1016/j.chemgeo.2009.05.003
16. Ferris FG, Phoenix V, Fujita Y et al. (2004) Kinetics of calcite precipitation induced by ureolytic bacteria at 10 to 20°C in artificial groundwater. Geochimica et Cosmochimica Acta 68:1701–1710. https://doi.org/10.1016/S0016-7037(03)00503-9
17. Song C, Wang C, Elsworth D et al. (2022) Compressive Strength of MICP-Treated Silica Sand with Different Particle Morphologies and Gradings. Geomicrobiology Journal 39:148–154. https://doi.org/10.1080/01490451.2021.2020936
18. Konstantinou C, Biscontin G, Jiang N et al. (2021) Application of microbially induced carbonate precipitation to form bio-cemented artificial sandstone. Journal of Rock Mechanics and Geotechnical Engineering 13:579–592. https://doi.org/10.1016/j.jrmge.2021.01.010
19. Cheng L, Shahin MA, Mujah D (2017) Influence of Key Environmental Conditions on Microbially Induced Cementation for Soil Stabilization. J Geotech Geoenviron Eng 143:4016083. https://doi.org/10.1061/(ASCE)GT.1943-5606.0001586
20. Zhao Y, Xiao Z, Lv J et al. (2019) A Novel Approach to Enhance the Urease Activity of Sporosarcina pasteurii and its Application on Microbial-Induced Calcium Carbonate Precipitation for Sand. Geomicrobiology Journal 36:819–825. https://doi.org/10.1080/01490451.2019.1631911
21. Omoregie AI, Ngu LH, Ong DEL et al. (2019) Low-cost cultivation of Sporosarcina pasteurii strain in food-grade yeast extract medium for microbially induced carbonate precipitation (MICP) application. Biocatalysis and Agricultural Biotechnology 17:247–255. https://doi.org/10.1016/j.bcab.2018.11.030
22. Rahman MM, Hora RN, Ahenkorah I et al. (2020) State-of-the-Art Review of Microbial-Induced Calcite Precipitation and Its Sustainability in Engineering Applications. Sustainability 12:6281. https://doi.org/10.3390/su12156281
23. bioMASON (2020) Home - bioMASON. https://www.biomason.com/. Accessed 10 Nov 2020
24. Portugal CRMe, Fonyo C, Machado CC et al. (2020) Microbiologically Induced Calcite Precipitation biocementation, green alternative for roads – is this the breakthrough? A critical review. Journal of Cleaner Production 262:121372. https://doi.org/10.1016/j.jclepro.2020.121372

25. Ghasemi P, Montoya BM (2022) Field Implementation of Microbially Induced Calcium Carbonate Precipitation for Surface Erosion Reduction of a Coastal Plain Sandy Slope. J Geotech Geoenviron Eng 148. https://doi.org/10.1061/(ASCE)GT.1943-5606.0002836
26. Vibhoosha MP, Bhasi A, Nayak S (2021) A Review on the Design, Applications and Numerical Modeling of Geocell Reinforced Soil. Geotech Geol Eng 39:4035–4057. https://doi.org/10.1007/s10706-021-01774-3
27. Evonik Industries AG (2021) Grauer Star - Wie Beton nachhaltiger wird. ELEMENTS Forschen. Wissen. Zukunft 2021
28. MEDUSOIL SA (2024) A new class of organic binder products designed to serve earthworks & building applications. https://622wh4bifqy.preview.infomaniak.website/wp-content/uploads/2024/08/Medusoil_flyer_A4_technique.pdf
29. Raymond AJ, DeJong JT, Gomez MG et al. (2025) Life Cycle Sustainability Assessment of Microbially Induced Calcium Carbonate Precipitation (MICP) Soil Improvement Techniques. Applied Sciences 15:1059. https://doi.org/10.3390/app15031059
30. Porter H, Mukherjee A, Tuladhar R et al. (2021) Life Cycle Assessment of Biocement: An Emerging Sustainable Solution? Sustainability 13:13878. https://doi.org/10.3390/su132413878
31. Brentrup F, Hoxha A, Christensen B (2016) Carbon footprint analysis of mineral fertilizer production in Europe and other world regions. https://irees.de/wp-content/uploads/2020/04/180716_IREES_AP4_Prozessemissionen.pdf. Accessed 27 May 2022
32. Deng X, Li Y, Liu H et al. (2021) Examining Energy Consumption and Carbon Emissions of Microbial Induced Carbonate Precipitation Using the Life Cycle Assessment Method. Sustainability 13:4856. https://doi.org/10.3390/su13094856
33. United States Environmental Protection Agency (2021) U.S. Cement Industry Carbon Intensities; EPA 430-F-21-004
34. Chen H-J, Huang Y-H, Chen C-C et al. (2019) Microbial Induced Calcium Carbonate Precipitation (MICP) Using Pig Urine as an Alternative to Industrial Urea. Waste Biomass Valor 10:2887–2895. https://doi.org/10.1007/s12649-018-0324-8
35. Comadran-Casas C, Schaschke CJ, Akunna JC et al. (2022) Cow urine as a source of nutrients for Microbial-Induced Calcite Precipitation in sandy soil. Journal of Environmental Management 304:114307. https://doi.org/10.1016/j.jenvman.2021.114307
36. Lambert SE, Randall DG (2019) Manufacturing bio-bricks using microbial induced calcium carbonate precipitation and human urine. Water Research 160:158–166. https://doi.org/10.1016/j.watres.2019.05.069
37. Manfred Nagel (Evonik Operations GmbH) und Alina Gawel (2024) „Bodenverfestigung mittels MICP. Persönliches gespräch

VIII Supplementary material

1 Student theses

Bachelor Theses

- Kalisch Jan Konstruktion eines modularen Photobioreaktorsystems
- Lorenz Michaela Untersuchung der Kinetik der Calciumcarbonatfällung durch ureolytische Mikroorganismen

Master Theses

- Ebel Christian Kultivierung von *Sporosarcina pasteurii* für die mikrobiologisch induzierte Calciumcarbonatfällung
- Weisbrodt Martin Kultivierung von *Sporosarcina pasteurii* mit Kulturmedien auf Basis nachwachsender Rohstoffe
- Estebanez Marta Erasmus Growth of cyanobacteria on soils stabilized with microbial-induced carbonate precipitation (MICP)

Team Work (Bachelor)

- Wagner Max, Sivagunarajah Vaishnavan, Noll Marc-André, Feise Peter Untersuchung der Lagerungsstabilität ureolytischer Mikroorganismen

Research Work (Bachelor)

- Marcel Cwienczek Kultivierung ureolytischer Organismen für die mikrobiologisch induzierte Calciumcarbonatfällung
- Kharik Eduard Immobilisierung ureolytischer Mikroorganismen für die mikrobiologisch induzierte Calciumcarbonat Fällung

Research work (Master)

- Aldabbousi Karim Untersuchung von Einflusfaktoren auf die mikrobiologisch induzierte Calciumcarbonatfällung
- Ebel Christian Kultivierung und Stammanpassung von *Sporosarcina pasteurii*
- Oeztas Taner Einsatz von mikrobiologisch induzierter Calciumcarbonatfällung zur Verfestigung mineralischer Partikel

Study Project (Master)

- Calvin-Brown Marces Untersuchung der Ureolyse von *Sporosarcina pasteurii*

2 List of publications

Peer-Review publications

- **N. Erdmann**, K. Aldabbousi, D. Strieth: Investigating the influential factors on microbially induced calcium carbonate precipitation: effects of cell density, temperature, and calcium concentration, Discov Appl Sci 7, 696 2025, https://doi.org/10.1007/s42452-025-06881-x
- **N. Erdmann**, S. Schaefer, T. Simon, A. Becker, B. Brökel, D. Strieth: MICP treated sand: insights into the impact of particle size on mechanical parameters and pore network after biocementation. Discov Mater 4, 45 2024. https://doi.org/10.1007/s43939-024-00108-3
- S. Wallrath, A. Engl, **N. Erdmann**, J. Kollmen, D. Strieth, B. Risch.: Mikrocontroller als Low-Cost Technologie: Monitoring von Wachstumsparametern bei Mikroalgen in einem 3D-gedruckten IoT-Photobioreaktor, MNU Journal - Ausgabe 05/2023
- **N. Erdmann**, D. Strieth: Influencing factors on ureolytic microbiologically induced calcium carbonate precipitation for biocementation. World J Microbiol Biotechnol; 2023, https://doi.org/10.1007/s11274-022-03499-8
- L. Geuer, **N. Erdmann**, M. Lorenz, H. Albrecht, T. Schanne, M. Cwienczek, D. Geib, D. Strieth, R. Ulber; Colourful diversity – Modified methods for extraction and quantification of photopigments and phycobiliproteins isolated from phototrophic micro- and macroalgae; The Journal for Chemical Education; 2022; https://doi.org/10.1021/acs.jchemed.2c00899
- **N. Erdmann**, K.M. de Payrebrune, R. Ulber, D. Strieth; Optimizing compressive strength of sand treated with MICP using response surface methodology; SN Applied Sciences, 2022; https://doi.org/10.1007/s42452-022-05169-8
- **N. Erdmann**, F. Kästner, K.M. de Payrebrune, D. Strieth; *Sporosarcina pasteurii* can be used to print a layer of calcium carbonate; Engineering in Life Sciences; 2022; https://doi.org/10.1002/elsc.202100074
- J. Walther, **N. Erdmann**, M. Stoffel, K. Wastian, A. Schwarz, D. Strieth, K. Muffler, R. Ulber, Passively immobilized cyanobacteria *Nostoc* species BB 92.2 in a moving bed photobioreactor (MBPBR): design, cultivation and characterization; Journal Biotechnology and Bioengineering; 2022; https://doi.org/10.1002/bit.28072
- A. Mehring, **N. Erdmann**, J. Walther, D. Strieth, R. Ulber, A fast, simple and low-cost resazurin assay for vitality assessment across species; Journal of Biotechnology; 2021; https://doi.org/10.1016/j.jbiotec.2021.04.010
- D. Strieth, A. Schwarz, J. Stiefelmaier, **N. Erdmann**, K. Muffler, R. Ulber, New procedure for separation and analysis of the main components of cyanobacterial EPS; Journal of Biotechnology; 2020; https://doi.org/10.1016/j.jbiotec.2021.01.007

- J. Stiefelmaier, D. Strieth, S. Di Nonno, **N. Erdmann**, K. Muffler, R. Ulber; Characterization of terrestrial phototrophic biofilms of cyanobacterial species; Algal Research; 2020; https://doi.org/10.1016/j.algal.2020.101996

Presentations at national and international conferences

- **N. Erdmann**, M. Lorenz, K. de Payrebrune,D. Strieth: Investigation of the rate of ureolytisduring microbially induced calcium carbonateprecipitation under high concentrations of ureaand calcium salts; (Bio)Process Engineering – a Key to Sustainable Development (2022), Aachen, Germany
- **N. Erdmann**, M. Lorenz, K. de Payrebrune, D. Strieth; Investigation of the efficiency of microbiologically induced Calcium carbonate precipitation; Himmelfahrtstagung on Bio process Engineering (2022), Mainz, Germany
- **N. Erdmann**, S. Schaefer, K. Nicolaus, U. Bröckel, D. Strieth, Efficiency of microbiologically induced calcium carbonate precipitation under high urea and calcium ion concentrations; 16th Annual International Conference on Porous Media (2024); Qingdao, China (online)
- **N. Erdmann**, D. Strieth Enhancing Biosandstone production time by incorporating whole cell kinetics of Sporosarcina pasteurii; Dechema Forum (2024), Friedrichshafen, Germany
- L. Geuer, **N. Erdmann**, J. Kollmen, S. Wallrath, A. Engl, J. Stiefelmaier, D. Strieth, B. Risch, R. Ulber (2023), Biotechnological approaches for science outreach - Cultivation of microalgae in photobioreactors and extraction of their natural dyes, Himmelfahrtstagung on Bioprocess Engineering 2023- Novel production routes and processes for bio-pharmaceuticals and industrial bioeconomy; Weimar, Deutschland
- D. Strieth, J. Stiefelmaier, J. Kollmen, **N. Erdmann**, A. Mehring; Phototrophe Biofilme: Invasive und nicht-invasive Methoden zur Charakterisierung; 13. Bundesalgenstammtisch, Frankfurt, Deutschland
- D. Strieth, J. Kollmen, **N. Erdmann**: Phototrophic biofilms: Invasive and non-invasive tools for characterization; (Bio)Process Engineering – a Key to Sustainable Development (2022), Aachen, Germany

Poster contributions at national and international conferences

- **N. Erdmann**, S. Schaefer, U. Bröckel, D. Strieth, Investigation of reaction rates during microbiologically induced calcium carbonate precipitation; 15th Annual International Conference on Porous Media (2023); Edinburgh, United Kingdoms
- **N. Erdmann**, L. Geuer, J. Kalisch, B. Risch, D. Strieth; Mikroalgen gegen den Klimawandel – ein Science Outreach Projekt; 13. Bundesalgenstammtisch (2022); Frankfurt, Deutschland

- **N. Erdmann**, L. Geuer, J. Kalisch, B. Risch, D. Strieth; Microalgae against climate change – a science outreach project; Biofilms 10 (2022); Leipzig, Deutschland
- **N. Erdmann**, K.M. de Payrebrune, R. Ulber, D. Strieth, Optimization of the microbial induced calcium carbonate precipitation for the production of biocement, Himmelfahrtstagung on Bioprocess Engineering 2021 - New Bioprocesses, New Bioproducts (2021) Digital
- **N. Erdmann**, K.M. de Payrebrune, E. Kharik, D. Strieth, Enhancement of the strength of sand treated with microbial induced calcium carbonate precipitation, 13th European Congress of Chemical Engineering and 6th European Congress of Applied Biotechnology (2021), Digital
- S. Wallrath, A. Engl, **N. Erdmann**, J. Kollmen, D. Strieth, Björn Risch; Establishment of two low-cost do-it-yourself photobioreactors for cultivation and monitoring of cyanobacterial growth (2023); International Conference on Algal Biomass, Biofuels & Bioproducts; Waikoloa Beach, Hawaii, USA
- D. Strieth, **N. Erdmann**, S. Schäfer, E. Hagen, U. Bröckel; An innoviative methode for the utilization of quarry sand; 15th Annual International Conference on Porous Media (2023); Edinburgh, United Kingdoms
- L. Geuer, **N. Erdmann**, M. Roth, G. Liese, J. Stiefelmaier, D. Strieth, R. Ulber; „Die Kiste macht´s einfach“ – Entdecke die Vielfalt bei Mikroorganismen im naturwissenschaftlichen Unterricht mit forschungsbasierten Experimenten aus der Kiste; Abschlussveranstaltung "Die Zukunft des MINT-Lernens“, Deutsche Telekom-Stiftung (2022); Berlin, Deutschland
- D. Strieth, J. Stiefelmaier, J. Kollmen, **N. Erdmann**, A. Mehring; Phototrophe Biofilme: Invasive und nicht-invasive Methoden zur Charakterisierung; 13. Bundesalgenstammtisch (2022), Frankfurt, Deutschland
- D. Strieth, **N. Erdmann**, J. Kollmen, J. Kalisch, B. Risch; Development of a plug-in system for photobioreactors; Himmelfahrtstagung on Bioprocess Engineering 2022 – Future Bioprocesses for a Sustainable Industry (2022) Mainz, Deutschland
- J. Walther, **N. Erdmann**, K. Wastian, D. Strieth, R. Ulber; Novel photobioreactor for moving bed biofilm cultivation of terrestrial cyanobacteria; 2020; Biofilms 9, Digital, Deutschland
- J. Walther, **N. Erdmann**, K. Wastian, D. Strieth, R. Ulber; Kultivierung von terrestrischen Cyanobakterien in Moving-Bed-Photobioreaktoren; 2020; ProcessNet-Jahrestagung; Digital, Deutschland

3 Curriculum vitae

Personal information

Name	Niklas Julian Erdmann
Place of birth	Cologne, Germany
Nationality	German

Education

Since 01/2021	**PhD candidate** Chair of Bioprocess Engineering, University of Kaiserslautern-Landau
04/2018-12/2020	**Biochemical and Chemical Engineering Sciences (Master of Science)** Technical University of Kaiserslautern
09/2013-07/2018	**Biochemical and Chemical Engineering Sciences (Bachelor of Science)** Technical University of Kaiserslautern
03/2012	**General University Entrance Qualification (“Abitur”)** Gymnasium Birkenfeld

Declaration in lieu of an oath

I, Niklas Julian Erdmann, hereby confirm that I have prepared this thesis independently, have not used any aids other than those permitted and have marked all verbatim or analogous references as such. I also confirm that this thesis has not been the basis for any other examination procedure in this or a similar form.

_____	_____
Place, Date	Signature